

Imperial College London



2407239064

CARBON FORMATION ON

STEAM REFORMING CATALYSTS

by

JOSÉ LUÍS CABRAL DA CONCEIÇÃO FIGUEIREDO

A thesis submitted for
the Degree of Doctor of Philosophy
in the Faculty of Engineering of
the University of London

ABSTRACT

Studies of carbon formation from propylene on nickel catalysts have been completed under both pyrolysis and steam-reforming conditions, and the effect of hydrogen on the reactions was investigated. Gasification of the carbon deposited on the catalysts was also studied. The kinetic features of all of these reactions were followed by continuous weighing of catalyst samples suspended from a microbalance in a differential flow reactor, and by gas-chromatographic analysis of the reaction products.

Carbon formation on nickel foil and on supported nickel was examined as a function of reaction conditions. At low temperatures (below 800K), the specific rate of carbon deposition was found to be the same over both foils and supported catalysts. Nickel crystallites were found to be carried with the growing carbon, and the results have been explained in terms of the diffusion of carbon through nickel being rate-determining.

Differences in behaviour during gasification were explained in terms of the amount of nickel available in the carbon formed on foils and on supported catalysts. Nickel was found to be an efficient gasification catalyst, and the kinetics of gasification by steam and by hydrogen have been established. Under certain conditions, it appears that gasification may also be rate-controlled by the diffusion of carbon through nickel. Experimental observations obtained for carbon formation and gasification are found to be consistent and to throw light upon the processes involved in both reactions.

The reaction of propylene with steam was usually accompanied by carbon deposition on the catalyst, but these deposits did not cause any significant loss of catalytic activity. The main products of the reaction were found to be hydrogen and carbon dioxide. The measured reaction orders suggest that the rate controlling step may be a surface reaction in which an associatively adsorbed olefin reacts with steam adsorbed on different sites.

A detailed survey of the literature on catalyst deactivation, steam-reforming, carbon formation on metals and carbon gasification is presented in the introduction.

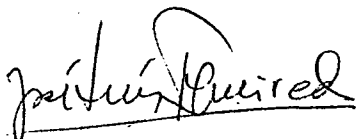
ACKNOWLEDGEMENTS

I would like to express my gratitude to Dr D.L. Trimm for his supervision and interest in this project; to Professor R. Guedes de Carvalho and to the Faculty of Engineering of the University of Oporto for a generous leave of absence; and to Instituto de Alta Cultura for the award of a scholarship covering the entire period of study.

Valuable assistance from the technical staff of the Department is gratefully acknowledged. My thanks are also due to all my colleagues in the Department for their pleasant and helpful companionship. In particular, I am indebted to Luís Sousa Lobo for his advice in the initial stages of this project, to Manuel Jerónimo and José Romão de Sousa for their help with computing and for their most stimulating discussions, and to Massoud Moayeri for his advice and friendship.

Finally, I wish to thank all my family, especially my wife Maria Emilia, for their understanding and support during this long period of study.

December, 1974

A handwritten signature in cursive script, which appears to read 'António Pereira', is written over a horizontal line.

Department of Chemical Engineering and

Chemical Technology

Imperial College

London S W 7

A meus Pais .

CONTENTS

	Page
CHAPTER 1 INTRODUCTION	7
CHAPTER 2 EXPERIMENTAL	71
CHAPTER 3 RESULTS	101
CHAPTER 4 DISCUSSION	209
CONCLUSIONS	251
APPENDICES	255
REFERENCES	262

CHAPTER 1

INTRODUCTION

	Page
1.1 <u>Deactivation</u>	9
1.1.1 Classification	9
1.1.2 Quantitative Aspects of Catalyst Deactivation	11
1.1.3 Regeneration of Coked Catalysts	15
1.2 <u>The Steam-Reforming Process</u>	16
1.2.1. Description	16
1.2.2 Thermodynamics	18
1.2.3 Catalyst Formulation	20
1.2.4 Deactivation	24
1.2.5 The Kinetics and Mechanism of Steam-Reforming	29
1.2.5.1 Methane Reforming	29
1.2.5.2 Reforming of Higher Hydrocarbons	33
1.3 <u>Carbon Formation</u>	43
1.3.1 Thermodynamics of the Carbon-Hydrogen System	43
1.3.2 The Structure and Deposition of Carbon	46
1.3.3 Catalytic Carbon Formation	50
1.3.3.1 Substrate Orientation and Pretreatment	52
1.3.3.2 Kinetics and Mechanism	53

1.4	<u>Carbon Gasification</u>	62
	1.4.1 Uncatalysed Gasification	62
	1.4.2 . Catalysed Gasification	64
1.5	<u>Present Work</u>	69

1. INTRODUCTION

The work described in this thesis is concerned with the study of the processes that lead to carbon deposition on metal catalysts used for the steam-reforming of hydrocarbons. This is a form of deactivation very common in hydrocarbon processing, and usually leads to changes in activity and/or selectivity.

This introductory chapter is intended to provide a background for the various processes involved. A short discussion of the different types of catalyst deactivation is presented initially, followed by a description of the steam-reforming process. Carbon formation and carbon gasification reactions are discussed next, with the emphasis on metal catalysed systems. A review of the pertinent literature is included in the introduction.

1.1 DEACTIVATION

1.1.1 Classification

In most catalytic processes the activity of the catalyst is found to decrease gradually as the reaction proceeds.

Catalyst deactivation can be divided into three main groups:

a) Poisoning The catalyst surface is slowly modified by chemisorption on the active sites by materials which are usually present as impurities in the feedstocks. A good example of this type of deactivation is sulphur poisoning of nickel catalysts. In this particular case, the poisoning is reversible and the activity can be recovered by operating with feedstocks of lower sulphur concentration (1). If the adsorption is not reversible, permanent poisoning results. In general, a high degree of susceptibility to poisoning is limited to metals, especially those

of groups VIII and IB. This subject has been reviewed by Maxted (2), who has grouped the common poisons of these catalysts under three major headings:

- i) Compounds of elements in group Vb or VIb;
- ii) Compounds of a large number of catalytically toxic metals;
- iii) Multiple bond molecules.

b) Sintering This type of catalyst decay is typical of supported metal catalysts, and is associated with the growth of crystallites and with a decrease of active surface area: permanent deactivation results. Sintering can occur by the loss in stability of the refractory support (e.g. by the action of steam on alumina (3)) or by increased mobility of the metal, which may be enhanced by small concentrations of impurities (e.g. transition metals can be transported as volatile carbonyls, halides or oxides (1)). Temperature has a marked effect upon sintering, and mobility is expected to become appreciable above the so-called "Tammann temperature" ($0.4 \times$ melting point, in degrees K). The rate of decay of the exposed metal surface area, S , caused by thermal sintering has been found to obey an equation of the form

$$dS / dt = -kS^n$$

where the range of the exponent n is between 2 and 8 (4,5).

c) Fouling This type of deactivation is caused by deposition of "coke", formed by side reactions, physically blocking the surface of the catalyst and/or plugging the pore entrances. The accumulation of coke on the catalyst will also increase the pressure drop through the reactor, and this is the factor that frequently determines when the catalyst must be regenerated (1). Regeneration is usually possible, by burning-

off the coke with air or steam. Severe catalyst disintegration may also be caused as a result of carbon lay-down within the catalyst pellets, making a complete change of catalyst necessary. Some examples of industrially important processes affected by fouling are presented in Table 1.1. The work described in this thesis is primarily focused on the fouling of catalysts by carbon.

1.1.2 Quantitative Aspects of Catalyst Deactivation

Extensive reviews on this subject can be found in the literature (6, 7, 8, 9, 10). In general, catalyst decay can be described in terms of four kinetic schemes, as summarized in Table 1.2. The main difference between them is to be found in the concentration term of the deactivation equation (7). With porous catalysts the progress of catalyst deactivation depends not only on the type of decay reaction, but also on the importance of pore diffusion, as shown in Table 1.3. The fouling mechanism can be identified from the knowledge of the carbon profile inside the pellet, as shown by Masamune and Smith (11) and others (12, 13). The experimental determination of carbon profiles and diffusivities in fouled catalysts has been described by Richardson (14). The effect of coke on the surface area and effective diffusivity of the catalyst may be negligible for low coke contents (15), unless blockage of the pore mouths occurs (16).

The rate equations that describe deactivating porous catalysts have been considered by Levenspiel (7, 17, 18). In particular, it has been found that a simple form of equation, $-da/dt = k(T) a^d$, represents and generalizes many of the previously proposed decay equations (10). The experimental

PROCESS	FEED	CATALYST	PRESSURE (atm)	TEMPERATURE (°C)
Steam- -Reforming	H ₂ O + CH ₄ or naphthas	Ni on Al ₂ O ₃ , MgO or mixtures thereof	3 - 40	450 - 1000
Reforming	Naphthas	Pt/Al ₂ O ₃ or MoO ₃ /Al ₂ O ₃	10 - 40	450 - 530
Cracking	Petroleum Fractions	SiO ₂ -Al ₂ O ₃ or zeolites	2 - 4	450 - 530
Dehydro- genation	Light hy- drocarbons	Ca ₈ Ni(PO ₄) ₆ , Al ₂ O ₃ -Cr ₂ O ₃ , Fe ₂ O ₃	1 - 3	550 - 650
Fischer- -Tropsch	CO + H ₂	Fe ₂ C/Fe ₃ O ₄ /Fe ; also Co or Ni based	17 - 25	220 - 350
Desulphur- isation	Naphthas	CoO+MoO ₃ /Al ₂ O ₃	30 - 40	300 - 400
Methana- tion	CO or CO ₂ + H ₂	Ni/Al ₂ O ₃	1 - 30	230 - 450
Dehydra- tion	Alcohols	Al ₂ O ₃ , SiO ₂ -Al ₂ O ₃	1	250 - 350
Water-gas Shift	CO + H ₂ O	Fe ₃ O ₄ -Cr ₂ O ₃	1 - 30	315 - 485

Table 1.1 Industrial Processes Affected by Fouling Problems

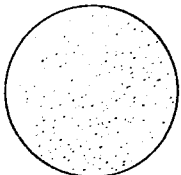
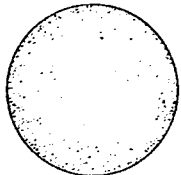
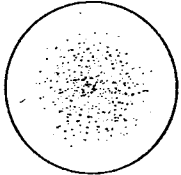
, Table 1.2 Deactivation Mechanisms

Type of Decay Reaction	Deactivation Law
Parallel : $A \rightarrow R + P\downarrow$ or $ \begin{array}{l} \nearrow R \\ A \\ \searrow P\downarrow \end{array} $	$-\frac{da}{dt} = k.C_A^n.a^d$
Series : $A \rightarrow R \rightarrow P\downarrow$	$-\frac{da}{dt} = k.C_R^n.a^d$
Concurrent : $\begin{cases} A \rightarrow R \\ P \rightarrow P\downarrow \end{cases}$	$-\frac{da}{dt} = k.C_P^n.a^d$
Independent : Sintering or: $ \begin{cases} A \rightarrow R \\ A \rightarrow P\downarrow \\ R \rightarrow P\downarrow \end{cases} $	$-\frac{da}{dt} = k.a^d$

LEGEND : A = reactant ; R = product ; P = poison
 P↓ = deposited or adsorbed poison
 a = activity ; t = time ; n, d = constants
 k = rate constant for deactivation
 C_i = gas-phase concentration of species i
 d = order of deactivation

(Compiled from Levenspiel, 1972)

Table 1.3 Effect of Resistance to Pore Diffusion
on the Distribution of Poison

Pore Resistance	Distribution of Poison	Decay Reaction
Negligible	Uniform 	Any type
Strong	Shrinking core model 	Parallel or Concurrent
	Growing core model 	Series

(Compiled from Levenspiel, 1972)

determination of orders of reaction and deactivation has also been discussed (17).

The effect of fouling on selectivity has been reviewed by Satterfield (8) and some chemical engineering aspects of the operation with deactivating catalysts have been discussed by Levenspiel (7).

1.1.3 Regeneration of Coked Catalysts

Regeneration is accomplished by burning-off the coke, generally with air, steam, a mixture of air and nitrogen, or a mixture of air and steam. Most of the literature on regeneration refers to the burn-off with oxygen of coke deposited on catalysts such as SiO_2 , Al_2O_3 or MgO , which do not catalyse carbon gasification. The subject has been reviewed by Satterfield (8) and Thomas (20).

If the carbon is assumed to be uniformly distributed through the catalyst, two extreme regimes may be considered for the burn-off:

a) Reaction control - At sufficiently low temperature, the concentration of reactant will be constant within the pellet, and uniform burning results.

b) Diffusion Control - At higher temperatures the rate of burn-off will be fast so that the process will be solely controlled by diffusion of the reactant through a shell of carbon free solid. This leads to a "shell-progressive" burn-off, as studied by Weisz and Goodwin (19).

When the burn-off is carried out in fixed-bed reactors, the burning takes place largely within a burning zone which moves slowly through the reactor, and it is important to keep the moving maximum temperature as low as possible, to avoid sintering.

1.2 THE STEAM-REFORMING PROCESS

1.2.1 Description

The reaction of steam with hydrocarbons over a catalyst has found considerable use in industry, providing the starting gas for the manufacture of ammonia, town gas, substitute natural gas, methanol, C₄/C₈ alcohols (Oxo Synthesis) and for the Fischer-Tropsch synthesis. A detailed description of the process can be found in the Catalyst Handbook (1).

Natural gas or petroleum fractions are used as feed-stocks, and nickel is the active component of most catalyst formulations. The process conditions can be chosen to give a variety of gas compositions suitable for the ultimate use of the product gas. Fig. 1.1 shows a simplified flow diagram for a steam-reforming plant as used for the production of ammonia synthesis gas (21). The hydro-desulphurisation stage is essential, sulphur compounds poisoning the nickel catalyst. Since a gas of low methane content is required, high temperatures are used and the process is endothermic (See 1.2.2). The temperature at the exit of the primary reformer will be in the range 750-850°C. In the secondary reformer, air is admitted and temperatures of 1000-1300°C are reached, so that the methane content will be further reduced, and nitrogen, needed for ammonia synthesis, will be produced from the air. In the shift converter the CO concentration is reduced by conversion into CO₂ ($\text{CO} + \text{H}_2\text{O} = \text{CO}_2 + \text{H}_2$) and the latter gas is subsequently eliminated (for example, by absorption). Subsequent methanation ($\text{CO} + 3\text{H}_2 = \text{CH}_4 + \text{H}_2\text{O}$; $\text{CO}_2 + 4\text{H}_2 = \text{CH}_4 + 2\text{H}_2\text{O}$) removes residual carbon oxides.

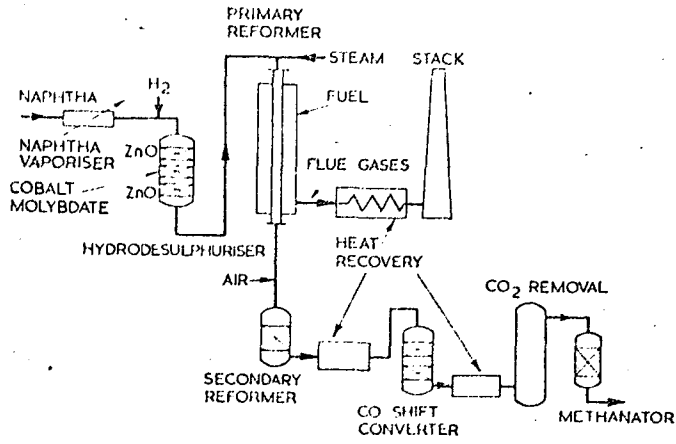


Fig. 1.1 Diagram of a Steam-Reforming Plant (21)

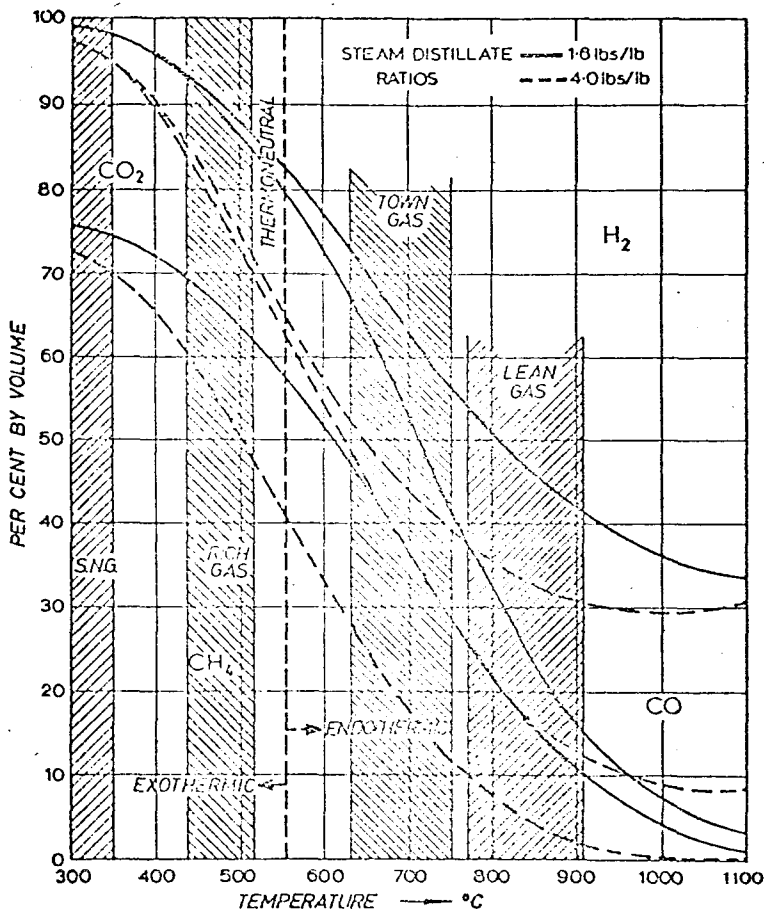
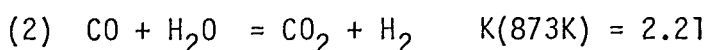
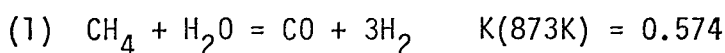


Fig. 1.2 EQUILIBRIUM GAS COMPOSITIONS - (DRY) (25)
 DISTILLATE - STEAM 25 ATMOSPHERES

1.2.2 Thermodynamics

Under normal steam-reforming conditions, methane is the only hydrocarbon thermodynamically stable to any appreciable extent, so that in determining the equilibrium composition only two reactions need be considered:



The factors which affect the equilibrium are pressure, temperature, C : H₂ ratio of the feed and the steam-ratio, defined as:

$$\text{Steam ratio} = \frac{\text{moles of steam in feed}}{\text{atoms g of carbon in feed}}$$

Examples of thermodynamic calculations in steam-reforming can be found in the literature (1, 22, 23, 24) and the Catalyst Handbook (1) presents graphs of equilibrium concentrations as a function of the operating variables for the steam reforming of methane and naphtha. Two limiting possibilities may be considered:

a) No methane present in the product gas - favoured by high temperatures, low pressure and high steam ratios, the reaction being endothermic;

b) No hydrogen present in the product gas - favoured at low temperatures, high pressures and low steam ratios, the reaction being exothermic. It is to be noted here, however, that the choice of operating pressure is usually not governed by thermodynamic considerations. For instance, in the case of gas for ammonia synthesis, since the whole process works at high pressures, it is more economical to operate the steam-reforming stage at high pressure (25-40 atm) as well. Fig. 1.2 gives an idea of the product distribution to be expected if equilibrium

is reached in the steam-reforming of a high petroleum distillate at 25 atm (25). Calculations are also presented in the Appendix for the partial reforming of C_3H_6 at various conversion levels.

One of the major problems in the steam-reforming process is carbon deposition on the catalyst. Carbon can be formed either from decomposition of higher hydrocarbons or from any of the following reactions:



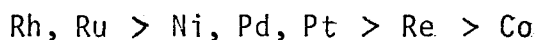
Coke originating from these reactions can usually be prevented by operating with excess steam, so that these equilibria are displaced to the left. The minimum steam-ratio required for freedom from carbon can be calculated thermodynamically (22), and minimum steam-ratios have been plotted as a function of temperature and pressure (1). At $600^\circ C$ and 1 atm, the minimum steam ratio for methane reforming is 1.38 (22). However, if the system is not at equilibrium, the conditions may be such that thermodynamics favour carbon formation by one reaction and its removal by another. Whether there is a net build-up of carbon deposit is then a kinetic question.

Carbon formation by direct decomposition of higher hydrocarbons may be prevented by using excessive amounts of steam, but this procedure is uneconomic. This has led to the development of suitable catalysts, capable of operating near the thermodynamic minimum steam ratio without serious carbon formation. This has been possible, to a certain extent, by suitable choice

of the support materials.

1.2.3 Catalyst Formulation

All commercial catalysts are based on nickel (20) which combines good activity for steam-reforming with low cost. Cobalt and the precious metals could also be used (1) but are more expensive. Rostrup-Nielsen (26) investigated the activity of metals supported on alumina and magnesia for ethane reforming, and reported the following activity pattern:



The main problems with nickel catalysts are carbon formation and sintering. The Gas Council C.R.G. catalyst, for example, has a very high nickel content (75%) to compensate for its initial loss of activity, due to sintering (3).

Recently, the use of ruthenium has been suggested as an alternative to nickel catalysts (143) in connection with the methanation process, and the same conclusions might apply for steam-reforming. Basically, the idea is to use highly dispersed, low-metal content supported catalysts to diminish the possibility of sintering. A more active metal is needed to compensate for the lower metal content, thus the choice of ruthenium. Although this metal is much more expensive than nickel, the lower metal contents would partly level off the difference, and an extra advantage would be the lower activity of ruthenium for carbon formation (16). However, present industrial practice has been concentrated on nickel based catalysts.

The catalyst must operate under severe conditions, so that the metal crystallites must be supported in a refractory

material to keep sintering to a minimum. Suitable supports are Al_2O_3 , MgO or their mixtures. A calcium aluminate cement is usually added to increase the physical strength of the catalyst. In the case of naphtha-reforming, a further problem is the greater ease of carbon deposition on the catalyst, by cracking of the hydrocarbons - either homogeneously or catalytically. Not only is nickel a catalyst for carbon formation, but also acidic materials, such as aluminosilicates, can catalyse hydrocarbon cracking. This has led to the use of basic support materials for steam-reforming, such as MgO or MgAl_2O_4 (Spinel). Andrew (29) has reported some studies in this context. Minimum steam-ratios (i.e. the lowest possible operating value before coking occurs) were measured for naphtha reforming at 30 atm, using nickel catalysts supported on china clay (plus calcium aluminate cement), alumina, magnesia and lime (supported on α -alumina). The results are shown in Table 1.4, and show that the ease of carbon formation increases with the acidity of the support. However, the change from Al_2O_3 to MgO to CaO brings little improvement. Another series of experiments (Table 1.5) has shown the importance of homogeneous processes in promoting carbon formation. From the results in the absence of nickel, it can be concluded that massive carbon formation requires (under normal steam-reforming conditions and in the absence of an acid catalyst) the presence of both a high amount of voids and of a nickel catalyst. Summarizing then, Andrew suggests that olefins, produced by hydrocarbon cracking, could be the first stage of carbon formation, according to the scheme shown in Fig. 1.3.

One way of minimizing carbon formation is to add an alkali, as with various ICI catalysts (1). This will, in part, neutralise

Table 1.4 Minimum Steam-Ratios for Nickel Catalysts
Supported on Materials of Decreasing Acidity

Naphtha reforming, 30 atm, exit temperature 750°C

Support material	SiO ₂	Al ₂ O ₃	MgO	CaO
Minimum steam- -ratio	10	4.3	3.7	3.7

(Compiled from Andrew, 1969)

Table 1.5 Minimum Steam-Ratios for Fixed-Beds of
Decreasing Nickel Content

Naphtha reforming, 30 atm, exit temperature 750°C

Bed composition	Ni/SiO ₂	3/4 Ni/SiO ₂ 1/4 α-Al ₂ O ₃	1/5 Ni/SiO ₂ 4/5 α-Al ₂ O ₃	Al ₂ O ₃
Minimum steam- -ratio	5.0	8.0	10.5	*

* In this case there is no steam-reforming, but operation at low steam-ratios is possible without massive carbon formation.

(Compiled from Andrew, 1969)

acidity by forming compounds such as KAlSiO_4 (29). Under steam-reforming conditions these decompose slowly, releasing potash, which is a catalyst for carbon gasification by steam (30). Al_2O_3 and SiO_2 produced by decomposition of the potassium complexes react with magnesia added to the catalyst for that purpose, forming spinels of lower acidity. In practice, the effect of adding alkali is to allow the operation near the thermodynamic minimum steam ratio. A reduction in minimum steam ratio from 10 to 1.5 by adding 7% alkali to a $\text{Ni/SiO}_2\text{-MgO}$ catalyst has been reported (29).

Recently, a nickel/urania/ α -alumina catalyst has been developed by the Gas Council (31, 32, 33) which seems to provide an alternative mechanism to prevent the accumulation of carbonaceous deposits. Lower rates of carbon deposition were observed with catalysts of increasing U:Ni ratio (33) and, in addition, kinetic studies on the reforming of butane (34) led to the conclusion that the surface of urania containing catalysts is fully saturated with adsorbed water. This preferential adsorption is probably the key factor in decreasing carbon formation, since UO_2 has been reported to have negligible activity for carbon gasification (35). By contrast, on a simple nickel/alumina catalyst the kinetic results suggest that the surface is covered with adsorbed hydrocarbon species (36). Furthermore, the presence of non-stoichiometric oxides in the urania catalyst (ranging from UO_2 to U_2O_8) can lead to enhanced dissociation of steam, as discussed by Dowden et. al. (27). This will tend to favour hydrogenation rather than dehydrogenation reactions.

Mention should also be made of the use of WO_3 supported nickel catalysts (37) for the low temperature production of gases

suitable for the Oxo, Fischer-Tropsch and methanol syntheses, i.e. gases consisting mainly of hydrogen and carbon monoxide. With conventional catalysts, this is favoured by high temperature operation (See Fig. 1.2). The higher selectivity of the Ni/WO₃ catalyst for CO formation has been explained on the basis that the catalyst does not promote the water-gas-shift reaction (37).

Recently, high-activity nickel and cobalt catalysts for steam-reforming have been prepared by ion exchange from synthetic zeolites. The activity for n-hexane at 400-500°C was found to be 8-30 times higher than the conventional Ni/Al₂O₃ catalyst (38). No data are yet available on the long-term stability and activity of such catalysts.

Finally, the theoretical design of steam reforming catalysts has been discussed by Dowden et. al. (27). The chemical functions that the catalyst must perform were examined on the basis of a virtual mechanism (28), and activity patterns for the different catalyst components were presented:

- a) Metals: Precious metals > Ni ≥ Co > Fe
- b) Supports: MgAl₂O₄ > β-Al₂O₃ > α-Al₂O₃ > ZrO₂
- c) Promoters: UO₂ > Pr₂O₃(CeO₂) > MoO₂ > CaO ≥ MgO ≥ Al₂O₃

1.2.4 Deactivation

Deactivation of steam-reforming catalysts may occur by poisoning, sintering and fouling.

The tendency of nickel catalysts to sulphur poisoning is well known, but other elements may cause deactivation, such as halogens and some metals. Sulphur and halogens are reversible poisons, but arsenic causes permanent deactivation (1). In

full scale operation, poisoning of the catalyst will become apparent as an increase in the concentration of aromatics at the reformer exit.

The chemisorption of hydrogen sulfide on supported nickel catalysts was shown to be reversible (39), coverage being a function of the ratio $P(\text{H}_2\text{S})/P(\text{H}_2)$. A saturation layer was observed even when the concentration of H_2S was not large enough to cause the formation of a bulk nickel sulphide. Its structure can be regarded as a two-dimensional sulphide phase, as discussed by McCarroll et al (40). As a result, the poisoning effect of H_2S on nickel catalysts may be ascribed to a reversible blocking of the metallic surface. The regeneration of sulphur poisoned nickel catalysts has also been considered (41).

The main cause of sintering of steam-reforming catalysts is probably the thermal instability of the Al_2O_3 support. Studies on the sintering of $\text{Ni}/\text{Al}_2\text{O}_3$ have been reported (3), showing that steam plays an important role in this context. It is thought that the loss in nickel surface area is caused by coalescence of the nickel particles when they are brought together by the sintering of the alumina, accelerated under the hydrothermal conditions. Pore size distributions obtained for fresh catalyst and sintered catalyst show that, under steam treatment at 600°C , the fine pore structure of the fresh catalyst gradually disappears with time. This is most probably associated with the transformation of $\gamma\text{-Al}_2\text{O}_3$ into $\alpha\text{-Al}_2\text{O}_3$.

Recent studies of the sintering behaviour of nickel films supported on various substrates (42) at $400\text{-}600^\circ\text{C}$, have shown that hydrogen induces massive surface reorganisation in the nickel, grain boundary grooving controlling the early stages of

the process. A peculiar sintering pattern emerged, which was attributed to the formation of two f.c.c. nickel hydrides: a β -phase (lattice constant $a = 3.8 \text{ \AA}$) was formed at low partial pressures (< 100 torr) and a new phase, X, (lattice constant $a = 4.2 \text{ \AA}$) was important at higher hydrogen pressures. At low hydrogen pressures a fast rate of nickel sintering was observed, but at high hydrogen pressures, sintering rates were decreased as the result of phase X hydride stabilising the surface. Under steam-reforming conditions, nickel sintering was hampered as a result of hydride and carbide formation (which stabilised the surface) and played only a minor role in catalyst deactivation. In practice, then, sintering causes an initially fast loss of activity (3), and further deactivation can be attributed to carbon deposition on the catalyst (43).

Several studies have been reported on the coking of steam-reforming catalysts (16, 35, 42-45) and the inter-relationship between carbon formation and catalyst formulation has already been discussed (See section 1.2.3.). Coking on the support material alone is negligible below 650°C (16).

Moseley et al (43) and Bhatta et al (36) explained the deactivation of a $\text{Ni}/\text{Al}_2\text{O}_3$ catalyst at temperatures between 400 and 500°C by formation of a film of polymers blocking the nickel surface, and high molecular weight hydrocarbons were identified in an extract of the deactivated catalyst (36). The deactivation was found to decrease with increasing steam ratio and temperature (43) and was found to be independent of the partial pressure of the hydrocarbon. The accumulated amounts of carbon during deactivation appeared to be negligible. Reaction of the gaseous

hydrocarbon with some surface species was suggested to be the poisoning reaction (43). However, Macak et al (35) suggested that the carbonaceous deposits block the nickel surface and that the reactants have to diffuse through the coke layer to react on the nickel surface. At low temperatures, the coke layer is permeable to reactants and products, but above about 600°C, graphitization causes increased diffusion restrictions, thereby reducing the reaction rate. This explanation is in conflict with the lower temperature observations of Moseley et al (43) showing formation of a polymer film blocking the surface, and also with the results of Rostrup-Nielsen (16) who found no deactivation effects, at 500°C, as a result of coking. The presence of carbon may not necessarily deactivate the catalyst. Thus, for example, in studying the reaction of steam with propylene on supported nickel films Moayeri (42) observed increased activity after coking, and attributed this result to the presence of nickel particles in the carbon.

Maxima in coking rates with temperature were observed by Macak et al (35), by Saito et al (44) and by Rostrup-Nielsen (16) under steam-reforming conditions, and also by Lobo (131) for carbon formation from olefins on nickel foils.

It becomes apparent, then, that the nature of coking in steam-reforming varies with temperature: At low temperatures, a significant deactivation of steam-reforming reaction occurs, while the accumulated amounts of coke remain small. When the temperature is increased, the deactivation rate decreases and coking increases, a maximum being observed at around 550°C. At even higher temperatures, thermal pyrolysis and cracking on the support material may contribute to the formation of coke.

Fig. 1.3 Proposed Scheme for Carbon Formation in the Steam-Reforming of Naphthas (29)

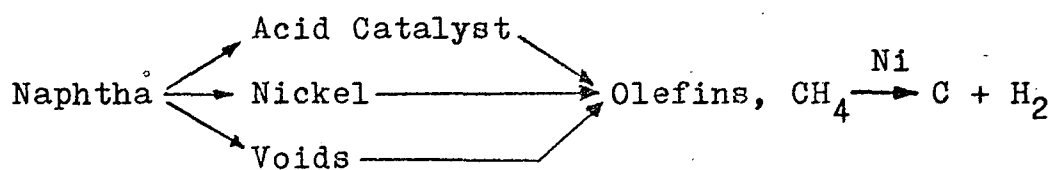
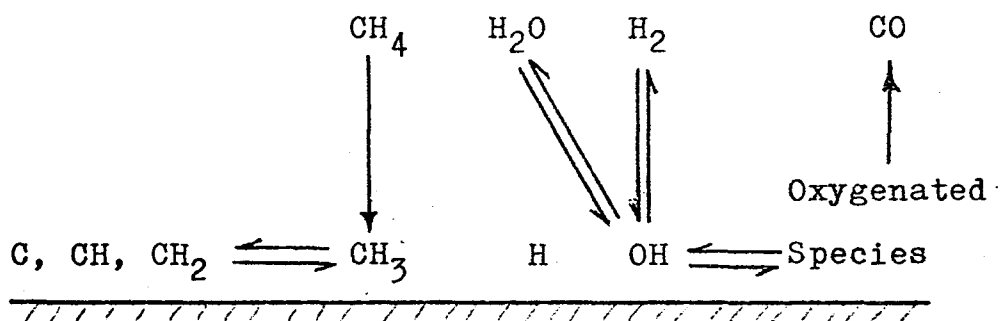


Fig. 1.4 Proposed Mechanism for Methane Steam-Reforming (53)



1.2.5 The Kinetics and Mechanism of Steam-Reforming

Because of the increased tendency to form carbon, the reforming of naphthas requires special catalyst formulation (see 1.2.3) which in turn affects the kinetics of the process. Therefore, this review will be subdivided, and methane reforming considered separately.

1.2.5.1 Methane Reforming

The reaction between methane and steam was studied by Gordon (47) at 1000-1100°C in the absence of a solid catalyst. A reaction mechanism was proposed, based on the initial decomposition of methane and subsequent reaction of the carbon formed with steam to produce carbon oxides.

Bodrov et al (48) studied the reaction on nickel foil at 800-900°C and 1 atm, and came to the following conclusions:

- a) The decomposition of methane and the reaction of methane with steam or CO₂ were negligible in the absence of catalyst;
- b) The water gas shift equilibrium was always established;
- c) The results could be described by the equation

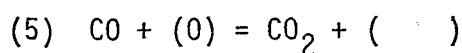
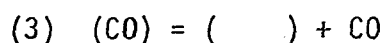
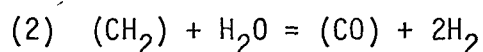
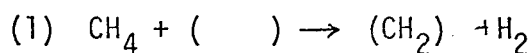
$$r = \frac{k \cdot P(\text{CH}_4)}{1 + a \cdot \frac{P(\text{H}_2\text{O})}{P(\text{H}_2)} + b \cdot P(\text{CO})}$$

and at 900°C the inhibition by CO was negligible;

- d) The activity of the catalyst was affected by its previous history, and this was explained in terms of oxidation-reduction disrupting the surface;

- e) In the temperature range 800-900°C, the activation energy determined was 31 kcal/mole;

f) The decomposition of methane to carbon on the nickel surface was much slower than the reaction of methane with steam, making any mechanism based on initial decomposition of methane to carbon and hydrogen improbable. The role of chemisorbed CH_2^* and CH_3^* species was established by Kemball (49) in studying the exchange of methane with deuterium on nickel films, and an activation energy of 31 kcal/mole was associated with a mechanism involving formation of CH_2 radicals. From these observations, the following mechanism was proposed:



where (\quad) is an active site on the nickel surface (assumed to be homogeneous) and (X) represents adsorbed species; step (1) is assumed rate determining. The same rate determining step was also postulated by Akers et al (50) in their study of the reaction over nickel/kieselguhr catalyst at 335-638°C, although their experimental activation energy was only 9 kcal/mole, reflecting possible diffusion limitations. Bodrov et al have also reported results with supported nickel catalysts. At 700-900°C they met with diffusion problems (51) but at 400-600°C the reaction was found to proceed in the kinetic regime (52). They obtained an activation energy of 36 kcal/mole and found that the reaction was inhibited by hydrogen, although this became negligible at higher temperatures. The equation

$$r = k.P(\text{CH}_4)/P(\text{H}_2)$$

was found to describe their results well. Here, the rate limiting step was assumed to be the surface reaction involving adsorbed CH_2 radicals.

Ross et al (53) used a static vacuum system to study the methane-steam reaction at 500-600°C over a coprecipitated nickel-alumina catalyst. On the carbided catalyst, they observed 1st. order dependency both in methane and water, but on the fresh catalyst the experimental order of reaction in H_2O was -0.5. An activation energy of 7 kcal/mole was found. Their main conclusions are as follows:

a) Decomposition of CH_4 in the absence of steam at 600°C produced only hydrogen;

b) The rate of this reaction was greater than the steam-reforming of methane and showed 1st. order dependency on the methane partial pressure;

c) Carbon gasification by steam over "carbided" catalyst at 600°C produced CO and H_2 and there was no sign of methane formation;

d) Carbon gasification by steam was faster than the rate of the steam-reforming reaction of methane over both the carbided catalyst and the reduced fresh catalyst. They proposed the mechanism shown in Fig. 1.4, where, again, the rate determining step was assumed to be the dissociative adsorption of CH_4 to form adsorbed CH_3^* and CH_2^* radicals, water competing with methane for the active sites. Consideration of the determined rates for gasification and for the methane-steam reaction explains why carbon deposition does not occur during the reforming reaction, because, even if carbon atoms are formed, they are immediately

Ref.	Catalyst	Temp. °C	Pressure (atm)	Reaction orders		E _A kcal/mole	Observations
				CH ₄	H ₂ O		
(50)	Ni/kies- elguhr	335-638	1	1	0	9	CO and CO ₂ are primary products. Rate determining step is CH ₄ decomposition
(48)	Ni foil	800-900	1	*	*	31	Idem, to form CH ₂ * chemisorbed species
(51)	Ni/Al ₂ O ₃	700-900	1	1	0	19	Pore diffusion
(52)	"	400-600	1	1	0	36	r = k.P _{meth.} /P _{hydr.} but H ₂ inhibition disappears at high T
(53)	"	500-680	≤.013	1	-0.5	7	Dissociative adsorption of CH ₄ is rate determining
(53)	"carbided	"	"	1	1		
(26)	Ni/MgO	500	1			26	

* Kinetic equation : $r = kP_{CH_4} / (1 + aP_{H_2O} / P_{H_2} + bP_{CO})$

Table 1.6 Methane Steam-Reforming

removed by reaction with water vapour. In the course of their studies, Ross et al (53) also observed that the catalyst freshly reduced in hydrogen was further reduced by the reaction mixture, implying that reduction of some phase like NiAl_2O_4 was occurring. The activity for steam-reforming over various catalysts was also tentatively correlated with the amount of spinel present (54) after failure to correlate activity with nickel area, although this contradicts the findings of Takemura et al (55), who attributed the observed initial deactivation of steam-reforming catalysts to spinel formation.

A summary of these kinetic studies is shown in Table 1.6.

1.2.5.2 Reforming of Higher Hydrocarbons

The obvious difference between methane reforming and reforming of higher hydrocarbons is that rupture of C-C bonds is required in the latter case. Three different mechanisms may be postulated:

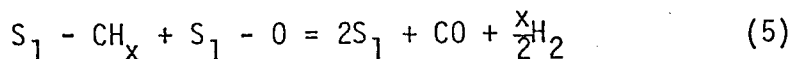
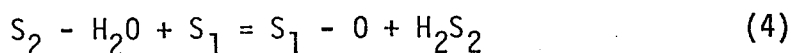
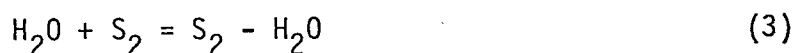
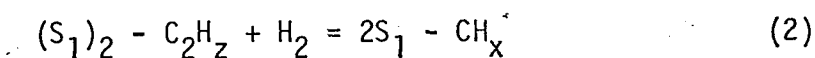
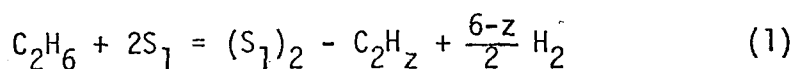
- a) Initial decomposition of the hydrocarbons to carbon and hydrogen, followed by reaction of carbon with steam (47);
- b) Stepwise breakdown of the hydrocarbons and direct reaction of steam with hydrocarbon fragments on the catalyst surface (56);
- c) Direct reaction of hydrocarbons with steam, giving oxygen-containing intermediates, possibly in the form of surface compounds on the catalyst (57).

A large amount of literature aimed at the elucidation of the mechanism of steam-reforming has appeared in recent years. The emphasis has been placed either on low nickel content, alkalised catalysts as pioneered by ICI (21, 29, 58) for production of hydrogen rich gases at high temperatures, or on high nickel content catalysts, such as developed by the Gas Council (32, 43, 59, 60)

for the production of methane rich gases at lower temperatures (400-500°C).

Balashova et al (56) studied steam-reforming of cyclohexane and concluded that the rate determining step in the process was the rupture of C-C bonds, producing adsorbed hydrocarbon radicals on the nickel surface.

Rostrup-Nielsen has reported comprehensive studies on steam-reforming (26) and a strong influence of the support on activity and on the kinetics was observed. The major differences in kinetics were found in the influence of steam partial pressure, in direct relation to the ability of the support material towards steam adsorption. At temperatures near 500°C, the results indicated multiple fission (on the nickel surface) of C-C bonds for most nonaromatic hydrocarbons. The results were qualitatively discussed in terms of a simple speculative sequence. Chemisorption of the hydrocarbon on nickel was assumed to follow the pattern usually proposed in hydrogenolysis studies. An initial chemisorption step on a dual site involving dehydrogenation is followed by C-C bond rupture and formation of surface radicals CH_x^* . For ethane:



where S_1 and S_2 represent empty sites on the surface of nickel and the support, respectively. Since the dissociative chemisorption of ethane is most probably irreversible (62) in the temperature range considered, and since the surface reaction step can also be considered as irreversible, $r_1 = r_2 = \frac{1}{2} r_5$, while steps (3) and (4) are considered in equilibrium. The surface species S_1-O and S_1-CH_x are considered the most abundant, the concentrations of other intermediates being negligible. Using Langmuir equations, the following rate expression was obtained:

$$r = \frac{k \cdot P(C_2H_6)}{\left[1 + a \cdot P(C_2H_6) \cdot P(H_2)/P(H_2O) + b \cdot P(H_2O)/P(H_2) \right]^2}$$

From this expression it can be seen that the experimental order of reaction in steam may become positive or negative depending on the magnitude of the equilibrium constant for steam adsorption \underline{b} , and the relative sizes of the rate constants for hydrocarbon adsorption and surface reaction. The value of \underline{b} is strongly influenced by the adsorption properties of the support material, since it is the product of the equilibrium constants of steps (3) and (4). It is difficult to determine whether CH_x or the initially formed radicals participate in carbon forming reactions. A point in favour of the latter is the difference in coking rates obtained with various hydrocarbons (16).

Results obtained in the steam reforming of propane, butane, heptane and benzene over ICI catalyst 46-1 have been reported (21, 58). For heptane at 750°C at long contact time (contact time = catalyst volume/gas flow rate at NTP) the exit gas composition approached that corresponding to the methane-steam and water gas shift equilibria. At short contact times, significant

concentrations of saturated and unsaturated compounds were observed (Fig. 1.5). At 500°C, however, these lower hydrocarbons were not detected (Fig. 1.6). Comparison runs in the absence of catalyst helped to establish the importance of thermal decomposition of hydrocarbon: at 750°C, the pyrolysis gases contained about 50% unsaturated compounds and 20% saturated compounds, but at 500°C no decomposition was observed. The activation energy for the reaction was found to be 14 kcal/mole at low temperatures, but increased with temperature to become 54 kcal/mole above 800°C, very close to the activation energy reported (61) for the thermal pyrolysis of heptane (58 kcal/mole). It was therefore concluded that at low temperatures (around 500°C) the steam-reforming of heptane was essentially a catalytic process, with thermal cracking becoming important only at higher temperatures. On the other hand, no thermal cracking was observed in the steam-reforming of benzene even at 800°C.

The reactions of propane and butane with steam were investigated at even shorter contact times ($< 10^{-3}$ s). The gas produced was found to contain large amounts of saturated and unsaturated compounds (CH_4 , C_2H_4 , C_3H_6) and little CO , CO_2 and H_2 , as shown in Fig. 1.7. Since the thermal reaction is very slow at 600°C, the conclusion emerged that these hydrocarbons were produced by catalytic cracking and subsequently reformed to CO , CO_2 and H_2 which eventually would come to equilibrium with methane and steam. The fact that the methane concentrations are higher at these shorter contact times than the methane-steam equilibrium would predict supports this view. The process thus produces olefins and methane selectively at short contact times and hydrogen plus carbon oxides at long contact times.

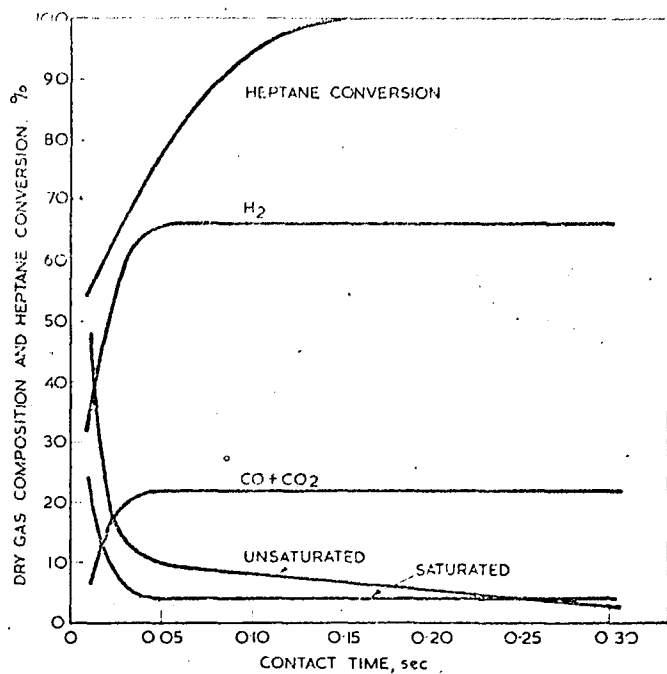


Fig. 1.5 Steam-Reforming of Heptane at 750°C (21)

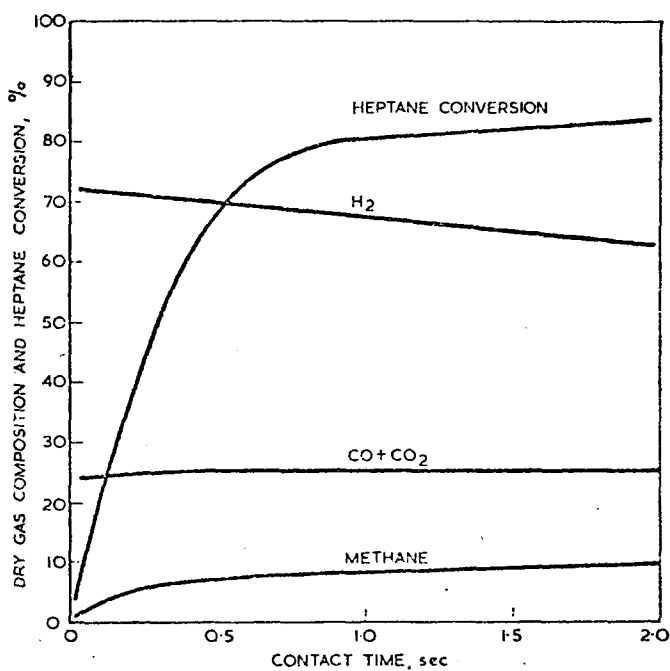


Fig. 1.6 Steam-Reforming of Heptane at 500°C (21)

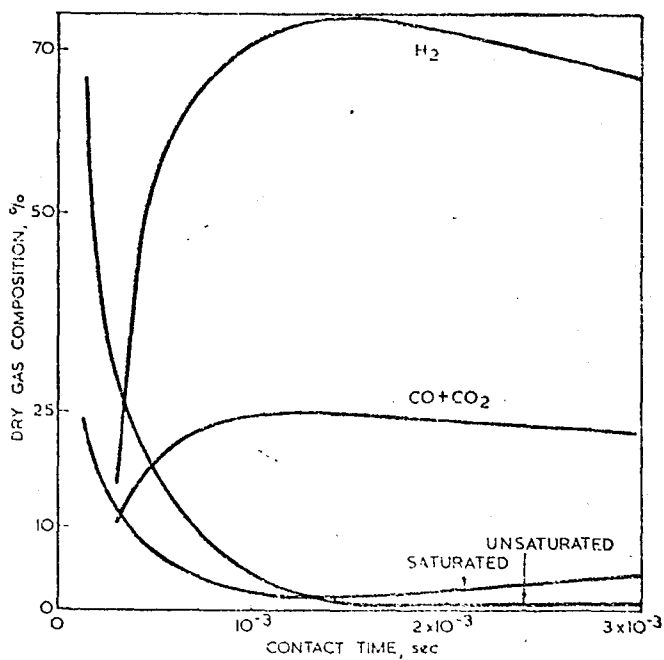


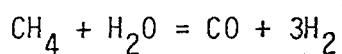
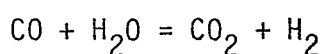
Fig. 1.7 Steam-Reforming of Butane at 600°C (21)

Carbon dioxide was found to be the first formed oxide of carbon, carbon monoxide being formed later by the water-gas shift reaction. At any time, the product gas was found to contain more CO_2 than would be present if the water-gas shift equilibrium were established, showing that this reaction was slower than the reaction of steam with unsaturated intermediates, which produces the carbon dioxide. On the basis of the above results, the scheme shown in Fig. 1.8 was proposed for the reaction of steam with hydrocarbons, three major stages being considered:

a) Catalytic cracking and dehydrogenation (and, above 650°C , also thermal cracking) leading mainly to olefins of low molecular weight, methane and some hydrogen;

b) Reaction of the primary intermediates (olefins and methane) with steam, leading initially to hydrogen and carbon dioxide;

c) Equilibration reactions between hydrogen, steam, carbon dioxide, carbon monoxide and methane, so that the composition of the final gas is approximately defined by these equilibria at the pressure and temperature of the catalyst bed exit:



In addition, the reaction of olefins with steam competes with reactions leading to coke on the surface of the catalyst. Steam and hydrogen react also with these carbonaceous deposits, but too slowly to provide a major route for the main reaction (44). Aromatic compounds in the feed are decomposed by the catalytic reaction alone (21) forming CO , CO_2 and H_2 from which methane is then produced.

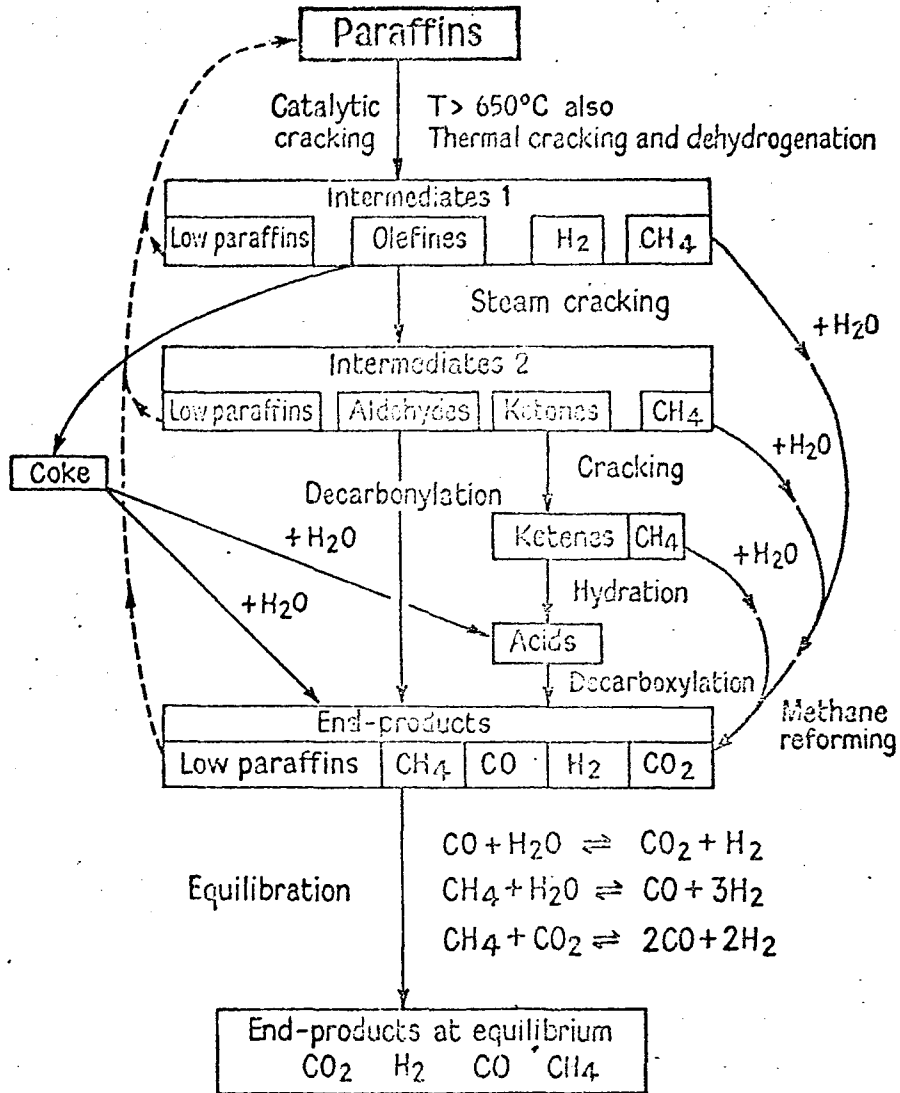


Fig. 1.8. Proposed Mechanism for the Steam-Reforming of Paraffins (1, 58)

In contrast with these findings, Phillips et al (59, 60) suggest that the primary products of reaction of n-heptane and n-hexane over a nickel-alumina catalyst in the temperature range 350-500°C at 13 atm are hydrogen and carbon monoxide, and that methane is formed from carbon oxides and hydrogen. They propose a Langmuir-type mechanism involving adsorption of the hydrocarbon followed by its rapid decomposition to produce CH_x species on the surface; these react with steam strongly adsorbed on different sites to produce hydrogen and carbon oxides which desorb and subsequently interact to form equilibrium gas mixtures (Fig. 1.9). The surface reaction between CH_x and adsorbed water species was considered rate controlling, explaining the similarity of reaction rates and activation energies (21 ± 1 kcal/mole) obtained with n-hexane and n-heptane.

Bhatta and Dixon (34, 36) studied the reaction of butane with steam over nickel-alumina and nickel-urania-alumina catalysts. Different kinetic expressions were found, establishing the role of the support as a supplier of oxygenated species (resulting from adsorption of water) to the surface of the nickel (Fig. 1.10). The steam-reforming of cyclohexane and ethane was also studied on similar catalysts (35). Once again, the results were explained in terms of adsorbed CH_2^* radicals reacting with adsorbed water species:

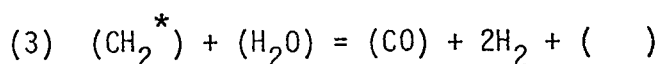
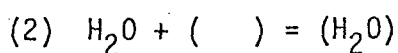
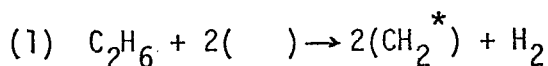


Fig. 1.9 Steam-Reforming Mechanism Proposed by Phillips et. al. (59)

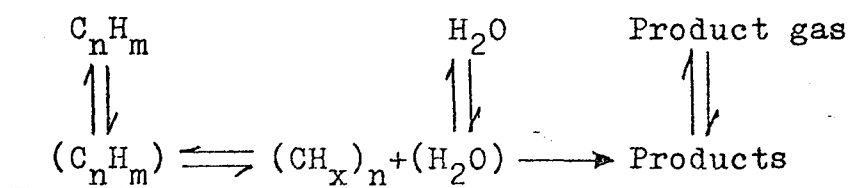


Fig. 1.10 Steam-Reforming Mechanism Proposed by Bhatta et. al. (34)

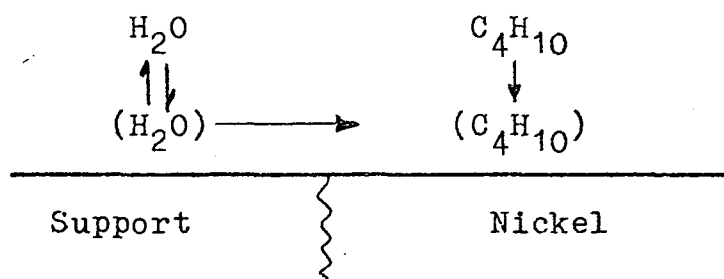
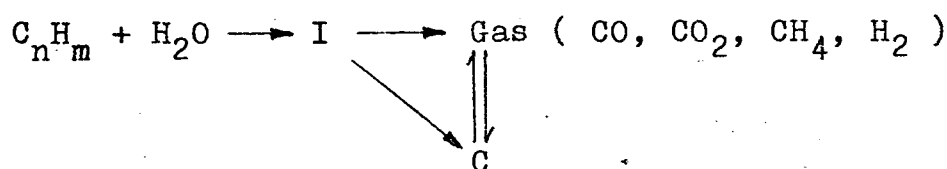


Fig. 1.11 Simplified Scheme of the Steam-Reforming Process



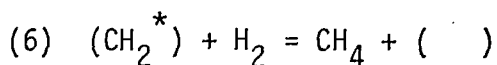
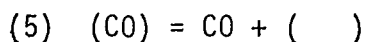
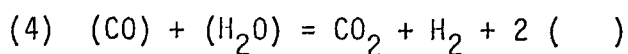
(I = Intermediate products and hydrocarbon radicals)

Table 1.7 Steam-Reforming of Higher Hydrocarbons

Ref.	Catalyst	Hydrocarbon	Temp. °C	P atm	Reaction orders Hydroc.	steam	E_A kcal/mole
(56)	Ni/SiO ₂ Ni/C	cyclo-C ₆ H ₁₂ "	400-460	1	0	0-1	22-24
					no activity		
(36)	Ni/γ-Al ₂ O ₃	n-C ₄ H ₁₀	425-475	30	0	1	13
(34)	Ni/α-Al ₂ O ₃ / /UO ₂ (.3%K)	"	404-491	30	1	-.6	24
(59)	Ni/γ-Al ₂ O ₃	n-C ₆ H ₁₄ n-C ₇ H ₁₆	360-450	15	.3	0	21±1
(145)	Ni/SiO ₂	n-C ₄ H ₁₀	370-450	1	0	1	
(44)	"	n-C ₆ H ₁₄	500-750	1	0	1	(14)
(35)	Ni/α-Al ₂ O ₃ Ni/α-Al ₂ O ₃ / /UO ₂	C ₂ H ₆ " "	550 " "	1 " "	* @ @	* @ @	
(42)	Ni/SiO ₂	C ₃ H ₆	536-710	1	.75	.6	15
(26)	Ni/MgO Ni/MgAl ₂ O ₄ Ni/Al ₂ O ₃	C ₂ H ₆ " "	500 " "	1 " "	.5 .4 .6	-.3 -1.1 .13	18
(139)	Ni/kieselguhr	C ₂ H ₆					15
(140)	"	cyclo-C ₆ H ₁₂					19
(141)	Ni/Al ₂ O ₃	C ₃ H ₈	500-700	1			12
(146)	"	cyclo-C ₆ H ₁₂	250-350				19
(147)	Ni/Cr ₂ O ₃	"	310-360				21

* $r = 19.7 P(C_2H_6)/(1+0.49 P(H_2O))$

@ $r = 41.9 P(C_2H_6)/(1+1.41 P(H_2O))$



Step (1) was considered rate determining and, at the same time, carbon formation was possible by dehydrogenative polymerisation of the species (CH_2^*) .

This variety of kinetic results has been summarized in Table 1.7, and reflects mainly the effects of different operating conditions and catalyst formulations. On the other hand, there is general agreement that the simplified scheme of Fig. 1.11 represents the steam reforming process well.

1.3 CARBON FORMATION

1.3.1 Thermodynamics of the Carbon-Hydrogen System

Standard free energies of formation of some hydrocarbons are represented in Fig 1.12 as a function of temperature, showing the relative stabilities of the different compounds. Possible conversions of hydrocarbons can be predicted from an analysis of this diagram, as summarised by Germain (79):

- At low temperatures, hydrogenation of olefins to the corresponding paraffins is favoured, while the reverse reaction takes over at higher temperatures;

- High temperatures favour hydrogenolysis and cracking of high paraffins to low molecular weight products and favour the cracking of aromatic side chains;

- Alkylations and olefin polymerization are favoured by low temperatures. Under a given set of conditions multiple conversion paths are open for each system, the actual products being

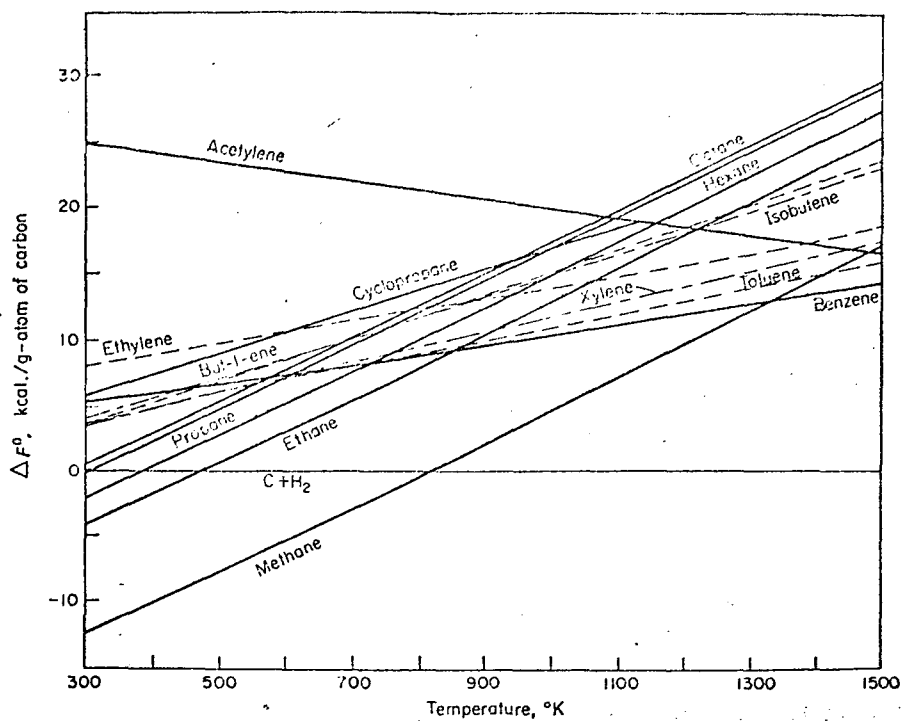


Fig. 1.12 Free energy of formation of hydrocarbons
(From Parks and Huffman, ref.80)

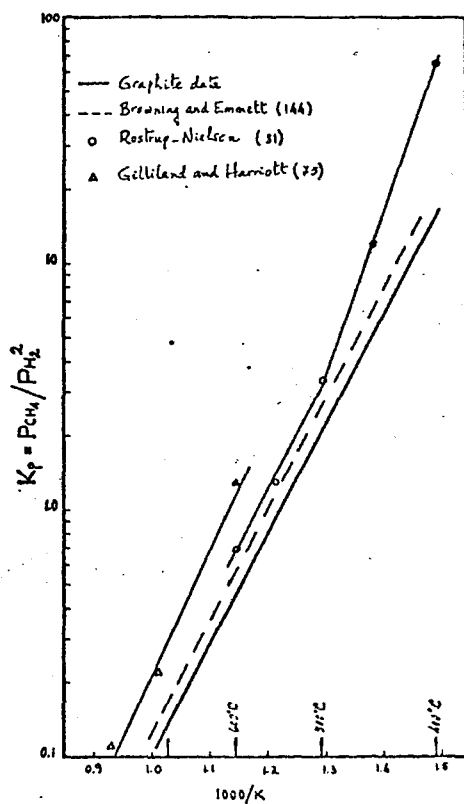


Fig. 1.13 Carbon-Hydrogen-Methane equilibrium

determined by the relative reaction rates. As a result, specific hydrocarbon conversions are dependent on the use of highly selective catalysts, so that one of the numerous thermodynamically possible paths is favoured.

Inspection of Fig 1.12 also shows that acetylene is thermodynamically unstable over the whole temperature range, and tends to decompose to an equilibrium mixture containing large proportions of carbon and hydrogen. Methane is the most stable of the paraffins, and should decompose spontaneously to carbon and hydrogen only above 570°C . Above room temperature all olefins, acetylenic and aromatic hydrocarbons, as well as paraffins higher than C_3 , should dissociate to carbon and hydrogen. However, direct equilibria between hydrocarbons and carbon are not experimentally feasible, except for the case of methane. This equilibrium has been approached from both sides in the presence of metal catalysts (Fe, Co, Ni), as shown in Fig. 1.13, and several studies on these systems have been published recently (81, 82). It has been consistently observed, however, that equilibrium constants experimentally determined in the presence of nickel catalysts, deviate from those based on graphite data (75, 81, 83). The subject was investigated by Rostrup-Nielsen (81) and a good correlation between these deviations and the maximum crystallite size of the catalysts was found. Greater deviations were observed on catalysts with small nickel crystallites. Still higher deviations were observed in the case of the Boudouard reaction (81), these results indicating formation of nonideal graphite.

Another effect to consider when metal catalysts are used is the possible presence of other solid phases. Thus, for example, oxide formation has been observed on iron, nickel, and cobalt under

apparently reducing conditions (99) and two f.c.c. hydride phases ($a = 0.38$ and $a = 0.42$ nm) have been identified after hydrogen treatment of nickel films (42). In addition, the possibility of carbide formation is always present with reactions involving hydrocarbons on transition metal catalysts (46, 99).

1.3.2. The Structure and Deposition of Carbon

Carbon deposits can present a variety of structures ranging from the near amorphous to a highly crystalline graphitic state, depending on the mechanisms by which they are formed. The stable allotropic form of carbon at normal temperatures and pressures is graphite. The ideal lattice consists of planes of hexagons in a stacking sequence ABAB..., and the unit cell has dimensions $a = 0.246$ nm and $c = 0.671$ nm, with an interlayer spacing of 0.335 nm (84, 85). A metastable rhombohedral form with the layer stacking ABCABC... has also been shown to exist, but only in association with the hexagonal form.

The so-called "amorphous carbons" actually consist of small crystallites with their hexagonal layers arranged roughly parallel and equidistant, but with random orientation with respect to each other. This structure is known as "turbostratic" (86) and results in weaker bonding between the layer planes, the interlayer spacing increasing to 0.344 nm when the stacking sequence is completely random. As a consequence of this structure, diffraction patterns show diffuse rings.

The interlayer spacing, d , is the parameter most frequently used in the characterization of carbons, and has been correlated with the degree of three dimensional order and with the crystallite dimensions (L_a = crystallite diameter, L_c = crystallite

height), as reviewed by Bokros (88), Ergun (87) and Ruland (85).

Pyrolytic carbons are formed from carbon containing gases at high temperatures, either homogeneously or heterogeneously, giving two distinct types of carbon (gas phase and surface carbon). Gas phase carbon is a microcrystalline form of carbon, produced in spherical particles with crystallites oriented approximately parallel to the surface. Surface carbons are obtained as films with well ordered crystallites deposited on solid substrates. This type of carbon is nearer to graphite than gas-phase carbon, having bigger crystallites, higher density and lower interlayer spacings (Table 1.8). The formation of both types of carbon is largely determined by the conditions of pyrolysis rather than by the structure of the starting gas (89). The structure of gas-phase carbons is little affected by the temperature of reaction, in contrast with surface carbons (89), in which a high degree of order is obtained when the deposition temperature approaches 2000°C .

Carbons of much higher crystallinity are obtained at lower temperatures on catalytic surfaces, particularly on transition metals. Nickel, cobalt and iron have been found to be particularly active catalysts at low temperatures ($350\text{-}750^{\circ}\text{C}$) and have been the subject of numerous studies (cf. Table 1.9). A good example of the distinction between inert and catalytic surfaces is found in the work of Banerjee et al (90), who studied carbon formation from carbon suboxide on porcelain, nickel, copper and platinum at 713°C . Electron diffraction of the deposits obtained on nickel revealed extensive three dimensional ordering and substantial crystallite size, turbostratic carbons being found on the other substrates; they produced similar diffraction patterns to those of nickel only after heating to 2000°C .

Table 1.8 Typical Values of Properties of Pyrolytic Carbons

Type of Carbon	Temp. °C	d nm	Lc nm	La nm	C/H atomic	Density g/cc
Gas-phase	1000	.361-.370	1.22	4.2	8	
Surface	1000	.346-.354	2.8	5.1	>80	2.00
Catalytic	600	.337	20.	40.	20	
Graphite		.335	∞	∞	∞	2.26

Compiled from : Palmer and Cullis (1965)

Cullis et.al. (1965)

Walker et.al. (1959)

Typical values of some parameters of pyrolytic carbons are presented in Table 1.8.

Three distinct types of carbon deposits have been obtained on catalytic surfaces: laminar graphite, non-oriented carbon and fibrous carbon. Laminar graphite, consisting of numerous single crystals oriented with their basal planes parallel to the substrate surface, has been obtained between 600-1200°C under conditions which favour low deposition rates (93-100). Non-oriented graphite, also described as "polycrystalline", is formed together with laminar graphite at higher rates of carbon deposition (94, 96-100). The crystallite size is usually small and the crystallites lack orientation with the substrate. The formation of non-oriented and laminar graphite appears to be complementary (101), the nature of the deposit being changed from laminar to non-oriented by increasing the reactant pressure at fixed temperature (94) while a rise in temperature at fixed pressure results in the formation of laminar graphite from a non-oriented deposit. In addition, carbon flakes formed on nickel and cobalt at high temperatures and pressures have been found to exhibit similar appearance to the non-oriented deposits in their upper surface, while the lower surface shows features normally associated with laminar graphite. Electron probe analysis has shown the presence of significant concentrations of metal on the lower surface of the flakes, but very little on their upper surface (101). Filamentary carbon has been obtained in many pyrolytic systems (81, 92, 102-112), and the structure of carbon fibres formed over iron, cobalt and nickel has been investigated (102, 103). They are turbostratic, with a preferred orientation of the basal planes parallel to the fibre axis. They

are long and thin, sometimes up to 7 μm long and 0.1 μm wide, and have a hollow tubular core. The fibre tip contains a particle of metal or carbide, whose size appears related to the fibre and core diameters. Metal or metal carbide particles are also found distributed in the hollow core along the fibre length (81, 92, 102-110).

Metal carbides have also been identified in systems where laminar and fibrous carbons are formed (45, 99, 107, 109, 110, 113) and they are thought to play an important role in the mechanism of carbon formation, as discussed below.

1.3.3 Catalytic Carbon Formation

Certain metals, especially iron, cobalt and nickel, exhibit high catalytic activity for carbon formation. They not only accelerate the rate of carbon formation but also affect the structure of the carbons formed, as discussed in 1.3.2.

Most of the earlier literature on the subject was devoted to the study of carbon deposition from carbon monoxide on iron, and has been reviewed by Renshaw et al (109). Interest in this system was related with the study of the Fisher-Tropsch process (115, 116) and also with the need to minimize carbon formation in the brickwork of blast furnaces (117). More recently, the use of supported metal catalysts in reforming and steam-reforming processes and the interest in avoiding carbon deposition on reactor walls and heat exchangers has directed more attention to the study of carbon formation from hydrocarbons on metals. A summary of the pertinent literature is shown in Table 1.9 and some features of the process are now considered in more detail.

Table 1.9 Studies of Carbon Formation on Metals

Author & reference	Reactants	Metals	Temp. °K	Observations
Cimino (126)	C_6H_{14}	Ni	520-670	
Cunningham (120)	C_2H_4	Ni	720	Effect of crystal face
Karu (124)	CH_4	Ni	1175-1375	Graphite growth
Lafitau (127)	CH_4	Ni	1270	C diffusion controls, $E=37$ kcal/mole
Lecoanet (82)	CH_4	Ni	670-1220	$E=20-35$ kcal/mole
Escoubes (126)	$CH_4, C_2H_2,$ C_2H_4, C_2H_6	Ni	460-580	$E=22.5$ kcal/mole, C diffusion controls
Patrikeev (148)	C_2H_4	Ni	570-820	Main gas products: C_2H_6 (700K), CH_4 (700-820K), H_2 (820K)
Patrikeev (149)	C_2H_4	Co		
Tamai (113)	$CH_4, C_2H_4,$ C_2H_6	Fe, Ni	1140-1300	Kinetic study
Tamai (114)	idem	Fe, Ni	1170-1270	Effect of hydrogen; mechanism
Presland (95)	C_2H_2	Pt, Ni	1270	Mechanism proposed
Robertson (96)	CH_4	Fe, Co, Ni	920-1020	Growth of graphite
Robertson (103)	CH_4	Fe, Co, Ni	920-1020	Flake and polycrystalline carbon; metal found in carbon
Tesner (108)	C_2H_2	Ni-Cr	720-970	Carbon fibres. Kinetics. Metal in carbon
Moayeri (100)	CH_4	Ni, Co	1070-1370	Growth of graphite. Ni(111) Ni(110)
Presland (93)	C_2H_2	Ni	1270	Effect of crystal face on epitaxial growth
Blau (94)	C_2H_2	Ni	1070-1470	Effect of pressure and temperature on crystallinity
Saito (129)	C_2H_2	Ni, Fe	870	
Lobo (130)	C_2H_2	Ni	670-970	Complex temperature dependency. Gas-phase above 870K
Baird (102)	CH_4, C_3H_8	Ni	970	Structure of carbon fibres. Suggests atomic Ni in Carbon
Tomita (125)	Benzene	Ni	870-1240	Flake and sooty carbon. Metal in carbon
Baker (98)	$CH_4/CO/CO_2$	Fe	725-1225	Mechanisms for amorphous C & graphite formation
Baker (105)	C_2H_2	Ni	870-1300	Mechanism for fibrous C formation. C diffusion in Ni
Rostrup-Nielsen(81)	CH_4	Ni	720-970	Equilibrium studies. Correlation with crystallite size
Robertson (104)	CH_4	Fe, Co, Ni	920-1020	Factors affecting flake or polycrystalline C formation
Lobo (131)	C_2H_2, C_2H_4, C_3H_6 C_4H_6, C_4H_8	Fe, Co, Ni Pd, Pt, Cu Ag, Au	570-1070	Pd, Pt, Cu, Ag, Au, inactive. Mechanism: C diffusion in Ni, Ni crystallites transported
Lobo (132)	idem, plus CH_4, C_2H_6, C_3H_8	Ni	670-870	Autocatalytic deposition from olefins, very slow with paraffins Effect of pretreatment
Baker (112)	C_2H_2	Fe, Co, Cr	785-1270	Mechanism of fibre growth: C diffusion in metal
Fryer (111)	C_6H_{12}	Pt	630	C fibres of graphitic nature
Lobo (133)	C_2H_4, C_4H_8	Ni	740-820	Nucleation and growth models
Nishiyama (134)	Benzene	Ni/Cu	850-1170	Diffusion of C in metal
Derbyshire (101)	CH_4, C_2H_4, C_2H_2 C_2H_6 , benzene	Fe, Co, Ni	770-1370	Conditions of formation of laminar, non-oriented and fibrous carbon and metal carbides
Moayeri (42)	C_3H_6	Ni	870	Graphite formed initially, then soot

1.3.3.1 Substrate Orientation and Pretreatment

The catalytic activity of the metal has been shown to depend on the crystal faces presented to the gas phase (118-121). Different faces show different activities and only certain faces may be stable in a particular reaction environment; on occasions, the surface will rearrange to expose these faces (42, 122). Thus, for example, for carbon deposition from CO over nickel single crystal spheres (118) and monocrystalline thin films (123), the activity pattern observed was $[321] > [111] > [110] > [100]$ and similar results were found for the low temperature hydrogenation of ethylene (120). Presland (93) and Moayeri (100) also found that the rate of carbon formation from hydrocarbons was greater over the Ni $[111]$ face than the $[110]$ face and, as a result, a more crystalline deposit was obtained over the latter. However, in the case of ethylene decomposition, Cunningham and Gwathmey (120) found that the Ni $[111]$ face was less active, and pretreatment with argon completely inhibited carbon deposition on the $[111]$ and $[100]$ faces. Thus, the geometry of the surface seems to play an important role in carbon formation and, in this context, reference should also be made to the work of McCarroll et al (40), who reported that the Ni $[111]$ face develops $[100]$ orientation in the presence of H_2S , C_2H_4 and benzene. This rearrangement seems to be caused by surface diffusion, the rates of this process being increased by one or two orders of magnitude in the presence of such adsorbed species (122).

Substrate pretreatment is also an important factor. Vacuum annealing has been found to lead to more crystalline deposits (93, 124) and freedom from surface oxide is an essential requirement if well ordered graphite is desired (93). On the other hand,

higher rates of carbon formation were obtained after preheating nickel foils in air (125), while untreated foils and those reduced in hydrogen gave similar rates of deposition (113). One of the possible effects of these annealing procedures may be to induce particular crystalline rearrangements (42) which, in turn, may assist or retard the catalytic action of the metal.

1.3.3.2 Kinetics and Mechanism

A survey of the literature on catalytic carbon formation (Table 1.9) reveals several common features in a large number of different systems:

I Rates of deposition remain constant for extended periods of time (125, 132, 134, 135);

II The inclusion of metal in carbon deposits has been reported for deposition from hydrocarbons (81, 102, 103, 105, 108, 125, 132, 134) as well as in the case of CO disproportionation (106, 107, 110, 135);

III The presence of carbides has been reported under similar circumstances (46, 99, 107, 109, 113);

IV A maximum rate of carbon formation has been observed at temperatures in the region 550-600°C (99, 108, 110, 130, 135, 136) and approximately zero order kinetics have been determined for the low temperature region (99, 127, 131, 135);

V Hydrogen has been generally found to increase the rates of deposition (108, 131, 134, 135, 136);

VI The rate determining step has been associated with a solid-state diffusion mechanism by a large number of researchers,

both at low temperatures ($< 350^{\circ}\text{C}$) where carbides are the final solid products (126, 128, 137), and at higher temperatures where carbon is formed (112, 127, 131, 134, 136).

These observations suggest that a general mechanism for carbon formation must apply under a variety of circumstances.

The formation of pyrolytic graphite on nickel, cobalt and iron foils was studied by Derbyshire (99). One of the features of the kinetic data obtained with nickel was the coincidence of laminar graphite formation with a particular type of curve of uptake vs. time, the rate of growth falling to zero after a significant reaction time. In every case, the final weight corresponded closely to the solubility of carbon in nickel at the deposition temperature (Fig. 1.14). In addition, amorphous carbon evaporated onto nickel foils could be dissolved by increasing the temperature and then reprecipitated as a graphite film upon cooling (138). The same behaviour was observed with deposits of non-oriented graphite, which precipitated on cooling as a laminar graphite film, similar to those films directly formed by pyrolysis. These results show that, under certain conditions of pyrolysis, the uptake of carbon by the nickel foil is limited by the carbon solubility, and demonstrates that a diffusion precipitation process must play a major role in the formation of laminar graphite films on nickel.

Studies of carbon deposition from light hydrocarbons on metal foils were also carried out by Lobo (46); only nickel, cobalt and iron showed catalytic activity below 600°C , as shown in Table 1.10. For nickel, a complex temperature dependency was observed for the rates of deposition, with a maximum at $500\text{-}550^{\circ}\text{C}$ and a minimum at

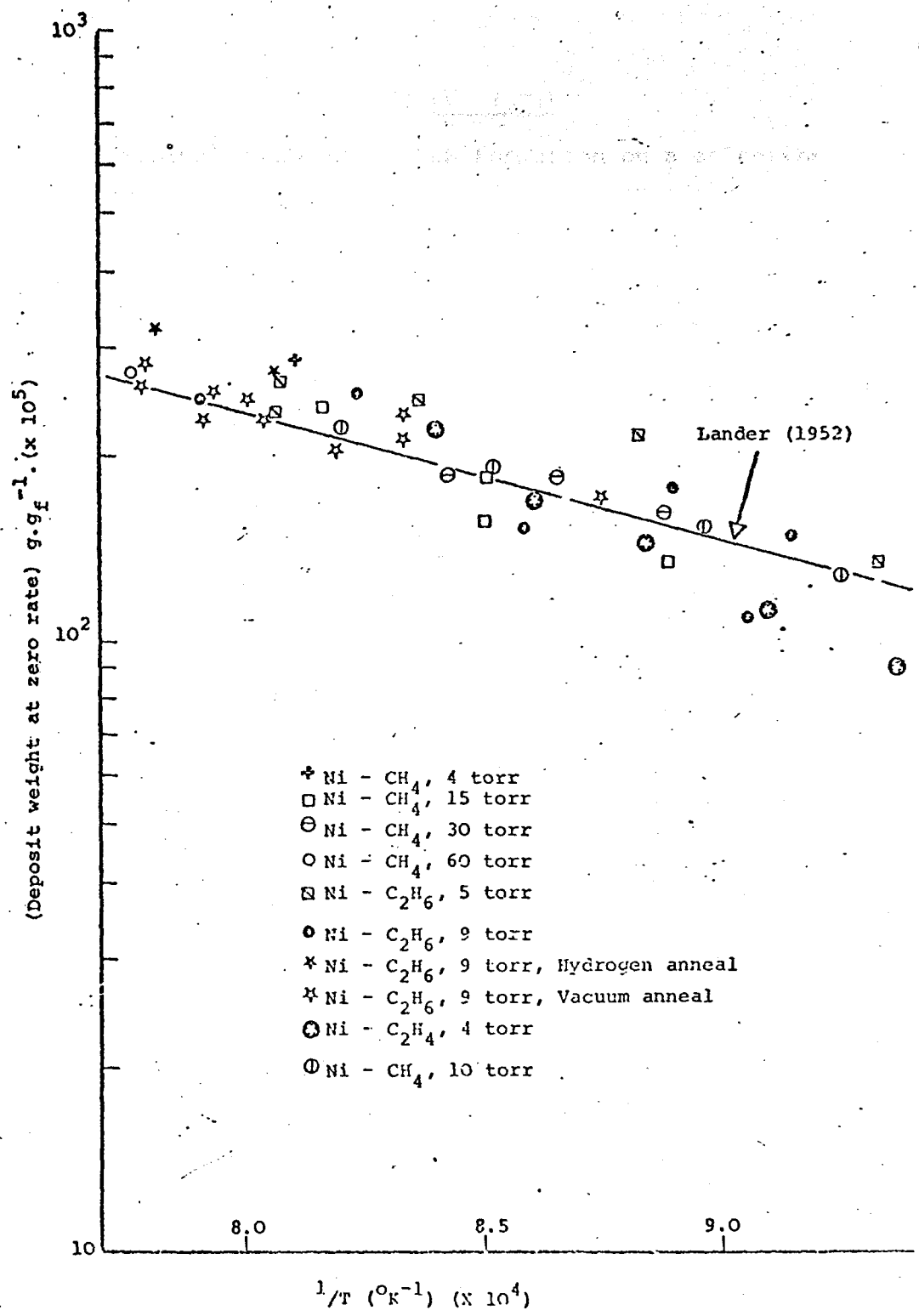


Fig. 1.14 Correlation between carbon uptake and solubility of carbon in nickel (99)

TABLE 1.10

Typical rates of carbon formation on a selection of metals. Conditions: 100 torr cis-2-butene, 50 torr hydrogen, 550°C.

GROUP VIII			GROUP IB
Fe 3	Co 5	Ni 150	Cu 0.00
Ru -	Rh -	Pd 0	Ag 0.00
Os -	Ir -	Pt 0.0	Au 0.00

The rates are expressed in $\mu\text{g}/\text{cm}^2 \text{ min.}$

600-650°C, defining three regions in the Arrhenius plot. At the lower temperatures, deposition rates were found to be independent of the nature and pressure of the unsaturated hydrocarbon used, with activation energies in the range 29-34 kcal/mole. Above 600-650°C, the carbon forming reaction has been identified as gas-phase pyrolysis in the case of acetylene (130), the order of reaction (2nd) and activation energy (50 kcal/mole) being in agreement with reported values for the pyrolysis. This is probably true for olefins as well, carbon forming on all the metals used at similar rates above 600°C (131). In the intermediate temperature region, negative temperature dependencies were observed and the rates were dependent on the partial pressures of hydrocarbon and hydrogen. Hydrogen did not affect deposition from acetylene, but some minimum ratio hydrogen: olefin was found to be necessary for a fast deposition from C₃-C₄ olefins. The following mechanism of carbon formation on nickel foils was proposed (131):

The adsorption of olefins on the surface is followed by dehydrogenation and hydrogenolysis reactions to produce carbon atoms; these then migrate through the nickel to active growth regions. Disruption of the nickel takes place and crystallites, detached from the surface, are carried with the growing carbon (Fig. 1.15) and catalyse further production of carbon. Induction periods, observed under certain conditions, are accounted for in terms of the nucleation of a new solid phase presenting an initial energy barrier. The rate determining step at low temperatures is considered to be the diffusion of carbon through the nickel. Lobo suggested that the overall process may involve the formation of

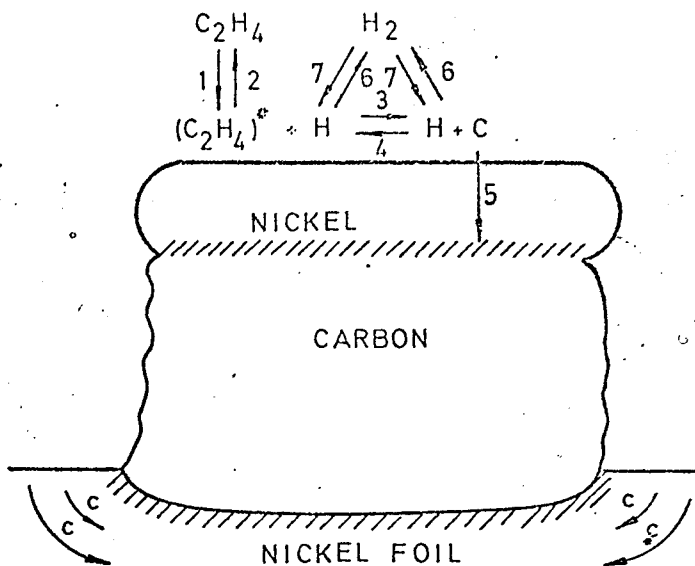


Fig. 1.15 Proposed model for carbon formation on nickel (131)

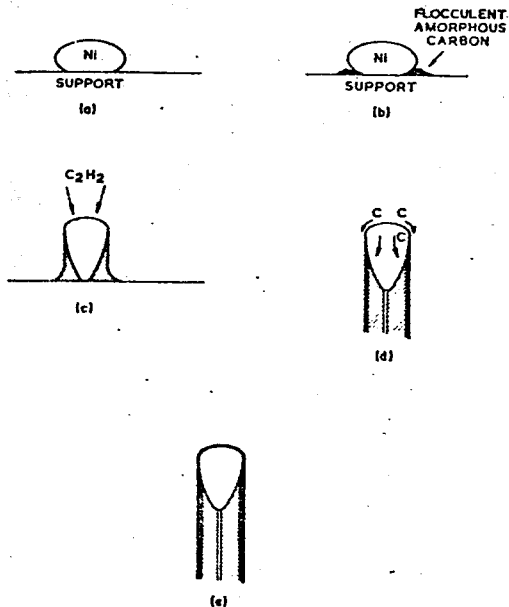


Fig. 1.16 Stages in the growth of carbon filaments (From Baker et.al., ref.105)

Table 1.11 Solid Phases Detected in Carbon Deposits
on Nickel (46)

Phase	Symmetry	a (nm)	d (nm)	L (nm)	Conditions
P	Cubic	.71-.74		30	Late stages Low temperatures (*)
Q	FCC	1.86-1.96		150	Late stages High temperatures (*)
Graphite			$d_c = .333-.342$ $d_a = .210-.211$	$L_c = 50$ $L_a = 130$	Late stages (*)
L	FCC, or Cubic or HCP	.446 .223 .184			Early stages only after annealing (@)

(*) - By X-ray diffraction

(@) - By electron diffraction

carbides, and X-ray and electron diffraction studies of the solid products of reaction (46) revealed the presence of several new phases, as shown in Table 1.11. Carbide L was identified at the early stages of reaction, while carbides P and Q, together with graphite, were found at the later stages. The fast deposition of carbon did not occur on foils with carbide Q alone, so that all the available evidence supported the sequence:

Nickel \rightarrow phase L \rightarrow phase P \rightarrow graphite

Baker et.al. (98, 105, 112) studied pyrolysis over metal films evaporated onto silica and graphite substrates. The metal nucleated into particles upon heating, and graphite platelets were observed to grow from the edges of larger particles which had lost their mobility. It was proposed that the metal particles were immobilized when the concentration of dissolved carbon reached the solubility limit. The platelets were then formed by surface diffusion and crystallization of carbon. For the growth of carbon fibres from pyrolysis of acetylene, they proposed the following mechanism (Fig. 1.16):

- The formation of a flocculent amorphous deposit around the nickel particles is attributed to the gas phase polymerization of the hydrocarbon. The heat released by acetylene decomposition on the exposed surfaces then sets up a temperature gradient across the particles. Carbon from decomposed acetylene is taken into solution, diffuses in and is deposited from the particle in the cooler regions protected by the amorphous deposit. This precipitation of carbon at the rear of the particle builds up a deposit which forces it away from the support. From then on, the nickel particles will be carried on top of the growing fibre, accounting for the observed

constant rate kinetics. Diffusion of carbon through the metal is the proposed rate determining step, since the activation energies for the process agree well with published values for carbon diffusion, in the cases of iron, nickel, chromium and cobalt (112). Excess carbon will thus be deposited at the exposed surface of the particle, and this can migrate by surface diffusion, accounting for the different structure of the fibre skin (105). Eventually, the surface of the metal particle will become encapsulated and the fibre will cease to grow. This has been observed experimentally (105, 112).

The incorporation of atomically dispersed metal in the carbon layers was suggested by Baird et.al. (102) and confirmed by oxidation studies, these fine dispersions becoming visible upon agglomeration. They based their mechanism of carbon growth (97) on the catalytic activity of these metal atoms (or small clusters of atoms) that diffuse into the carbon.

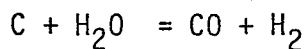
Carbon formation from benzene on Cu-Ni alloys has been recently studied by Nishiyama et.al. (134). They reported the formation of two different types of carbon, a thin film formed at high temperatures and a black powder, similar to carbon black, formed at low temperatures. Alloys of 40-80% Ni showed higher catalytic activity than pure nickel. Preferential nucleation at grain boundaries was suggested to explain the presence of metal grains in the carbon deposits, while nucleation on the surface was suggested to be responsible for encapsulation of the metal and inhibition of further deposition. The observed enhancement of deposition by hydrogen was ascribed to the elimination of carbon nuclei at the surface, preventing encapsulation.

1.4 CARBON GASIFICATION

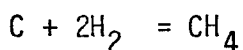
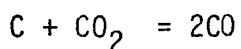
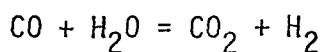
1.4.1 Uncatalysed Gasification

The uncatalysed gasification of carbon has been the subject of numerous studies and reviews (63, 64, 65, 66). However, the greatest interest has been centered around gasification by oxygen or carbon dioxide. The former reaction is of significant practical importance, mainly in the context of combustion processes, while the latter has been recently studied in the context of gas-cooled nuclear reactors. Relatively little work has been published on gasification by steam or hydrogen.

The relative rates of gas-carbon reactions have been compared at 800°C and 0.1 atm pressure (63), as shown in Table 1.12. A summary of thermodynamic considerations relevant to carbon gasification is presented in (63). Carbon gasification by oxygen and hydrogen is exothermic, and by steam and carbon dioxide is endothermic. The carbon-steam reaction



is accompanied by the secondary reactions:



Thermodynamic considerations (63) show that the oxidation of carbon to carbon monoxide and carbon dioxide is not restricted by equilibrium at normal working temperatures, but, in the case of $\text{C} + 2\text{H}_2 = \text{CH}_4$, the production of methane is seriously limited at 1 atm.

Table 1.12 Approximate Relative Rates of Gas-Carbon
Reactions at 800°C and 0.1 atm Pressure

<u>Reaction</u>	<u>Rate</u>
C - O ₂	1 x 10 ⁵
C - H ₂ O	3
C - CO ₂	1
C - H ₂	3 x 10 ⁻³

(From Walker et.al., ref. 63)

The uncatalysed reaction of carbon with steam has been described successfully by the equation:

$$r = \frac{K_1 P(H_2O)}{1 + K_2 P(H_2) + k_3 P(H_2O)} \quad (67, 68)$$

from which orders of reaction w.r.t. H₂O ranging from 0 to 1 are expected. At low temperatures and atmospheric pressure, the reaction is of zero order, and is expected to become 1st order only above 1640 K (65). Activation energies in the range 60-80 kcal/mole have been reported (63).

Zielke and Gorin (69) studied the gasification of a low-temperature char with hydrogen and proposed the rate equation:

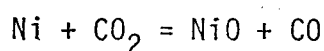
$$\frac{a.P(H_2)^2}{1 + b.P(H_2)}$$

from which reaction orders between 1 and 2 are expected. These authors report an activation energy of about 50 kcal/mole for the later stages of burn-off, when the structure of the carbon residue is thought to approach that of graphite.

1.4.2 Catalysed Gasification

The catalysis of carbon gasification has been reviewed by Walker et.al. (70) and results are reported for the catalytic effects of Fe, Co and Ni on the gasification of carbon with carbon dioxide (at 800-1000°C). In most cases, the gasification rate increased initially (up to ca. 15% burn-off) and the rate then remained constant over a considerable burn-off range. The initial increase in rate was attributed to some initial increase in surface

area of the sample. With Fe and, to a lower extent with Co, the rates of gasification were found to level off after a period of constant rate. With increasing temperature this effect occurred at shorter times, but, due to the faster rate, the burn-off achieved was higher. This was caused by deactivation (by oxidation) of the catalyst, and activity could be restored by H₂, by CO or by thermal treatment. Subsequent investigation showed that Fe₃O₄ and Fe₂O₃ were not catalysts for the reaction; FeO increased the rate of gasification by a factor of 6 and metallic Fe by a factor of 180-240. The catalytic activities followed the order Fe > Co > Ni and any of these metals succeeded in lowering the activation energy for gasification by CO₂ (87 kcal/mole for the pure graphite samples). However, the interpretation of the Arrhenius plots was complicated by catalyst deactivation and by diffusion effects. Deactivation of nickel was not observed, as expected from thermodynamic considerations, since the equilibrium



was well to the left under reaction conditions, with about 1% of CO in the gas mixture being enough to maintain Ni in the metallic state. In this case, an activation energy of 76 kcal/mole was determined in the range 860-960°C, which was considered to correspond to chemical control. The presence of Ni (300 ppm) was found to increase the gasification rate by 200-fold over the uncatalysed rate.

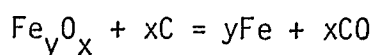
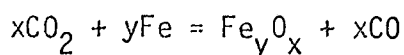
The effect of the products in the C-CO₂ and C-H₂O reactions on the gasification rate is dependent upon whether the reactions are being catalysed or not. In the uncatalysed reaction, CO and H₂ are inhibitors of the gasification (63), while in the catalysed reaction, their presence in sufficient amounts helps to maintain the catalyst

in the reduced (active) state (70). The uncatalysed combustion of carbon usually produces some CO, the ratio of CO to CO₂ increasing with temperature. Gasification catalysts change the nature of the reaction in that the CO:CO₂ ratio is reduced and is usually zero (20, 63). A similar effect has been reported by Tuddenham and Hill (71) for gasification of carbon with steam, catalysed by nickel. It has been questioned as to whether the catalyst changes the ratio of CO to CO₂. Heuchamps et al (72) concluded that the primary ratio itself is affected.

Two general theories of catalysis of the gasification of carbon have been proposed (70), the oxygen-transfer and the electron-transfer mechanisms. These will be summarised below, for the particular case of catalysis by transition metals.

The electron-transfer mechanism supposes that the transition metal has unpaired electrons in its d-band and, when in contact with graphite, π electrons in the graphite will pair up with these electrons. As a result, π electrons are localised, and the number of mobile π electrons in the graphite decreases, weakening the average strength of the bonds between peripheral carbon atoms and carbon-oxygen complexes. As a result, gasification of the latter will be enhanced. On the basis of thermoelectric power studies Walker et al (73) concluded that the mechanism of catalysis by Fe in their investigation could not be primarily attributed to such a process.

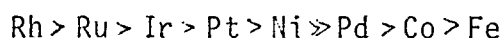
The essential features of the oxygen-transfer mechanism involve the assumption that the catalyst undergoes a cycle between two oxidation states, such as metal-oxide or lower oxide-higher oxide. For the case of the C-CO₂ reaction catalysed by Fe, the mechanism can be represented by the equations (74):



Experimental evidence has been presented (70) to support the contention that the metal acts as a dissociation center, thereby producing active species - oxygen atoms. These can diffuse across the metal surface to the metal-graphite-interface and react there to form CO. Walker et al (70) explain their results on the basis of this mechanism. The marked reduction in catalytic activity when the Fe is oxidised appears consistent with this view, since the dissociative chemisorption of CO₂ on metal oxides has not been reported. Similar considerations can be applied to the catalysed gasification of carbon with steam.

The reaction of hydrogen with carbon deposited on a nickel-silica gel catalyst, was investigated by Gilliland et al (75). The carbon was deposited on the catalyst from decomposition of methane, carbon monoxide and butane. Gasification with hydrogen produced methane with only occasional traces of higher hydrocarbons, and an activation energy of 36 ± 6 kcal/mole was measured. More recently, Tomita et al (76, 77) reported studies of the hydrogenation of carbons catalysed by transition metals. Three kinds of carbon were used, an active carbon (1230 m²/g), a carbon black (78 m²/g) and a natural graphite scale. These were impregnated with aqueous solutions of the group VIII transition metal salts, so that the resulting materials contained about 4.8 wt% of metal. Thermogravimetric studies (76) revealed the presence of two or three stages in the hydrogenation of carbon. The pattern of methane formation was dependent on the metal catalyst present, the type of carbon and the preparative method of the metal-carbon system. With nickel/active carbon, about 50% of the carbon was gasified in the region 500-700°C. A plateau was then observed

in the thermogram, followed by further hydrogenation above 800°C. Maximum methane concentration was observed at 550°C; a second (but lower) peak occurred at 950°C. The behaviour of Ru and Rh was quite similar to that of nickel. Maxima in the methane concentration curve were found at 605-610°C and 880-890°C. Fe, Co and Pd showed low activity and the first stage of hydrogenation was absent. Iridium and platinum showed unique patterns: Three maxima (590, 650, 780°C) were observed with the former, whereas the first stage of the platinum-catalysed reaction was observed only at about 770°C. The order of activities determined was:



The reaction kinetics at constant temperature was also investigated in the case of nickel and platinum (77). Rates of gasification in the presence of nickel were 6 orders of magnitude higher than for the uncatalysed reaction, and a complex dependency of the rate on temperature was observed, with maxima at 540°C and 683°C. At higher temperatures, the rates of gasification were found to decrease with increasing temperature, paralleling the decrease in methane content at equilibrium. The activation energy determined for the second stage of gasification was 25 kcal/mole, whereas the noncatalytic initial rates were associated with an activation energy of 41 kcal/mole. The same authors (76) reported activation energies for the first stage of hydrogenation only in the case of Rh (30-34 kcal/mole) and Pt (36 kcal/mole). The reactivities of the various carbons followed the pattern: active carbon > carbon black > graphite. The first stage of gasification was found to be specific for the catalytic process, whereas the

second stage was found to occur in the same temperature region as the uncatalysed reaction. The role of the catalyst, however, does not explain the presence of two stages, since the hydrogenation of graphite was found to proceed only in a single stage, even if an active catalyst was added. The structure of carbon was recognised therefore as an important factor and the following explanation was proposed (77):

- The first stage reaction is considered to be the hydrogenation of the amorphous fraction of the carbon, and the second stage the gasification of the crystalline carbon. When the starting material is perfectly amorphous, graphitization in the presence of the metal catalyst may account for the development of a crystalline carbon during the course of the reaction, as evidenced by X-ray studies. The metal catalyst provides the active sites for hydrogen chemisorption, producing hydrogen atoms which then migrate across the interface to react with the carbon (76). The transport of hydrogen from the metal to the carbon may involve a spill-over phenomenon, as discussed by Boudart (78).

1.5 PRESENT WORK

The literature review presented in the previous sections reveals the need for more quantitative information on the carbon formation processes occurring in the steam-reforming of hydrocarbons. The present work was initiated in order to provide such kinetic data and to help in elucidating the mechanism of carbon deposition on metal catalysts. The following reactions were thus investigated:

a) carbon formation on nickel catalysts from propylene in the absence of steam;

b) gasification (by hydrogen and by steam) of the carbon deposits obtained;

c) carbon formation in the presence of steam, as a side reaction of the steam-reforming process.

Previous investigations (58) had revealed that olefins were likely intermediates in carbon formation from other hydrocarbons. Since propylene is one of the major products from the cracking of naphthas (142), attention was focussed on the reactions of this olefin.

CHAPTER 2

EXPERIMENTAL

	Page
2.1 <u>Introduction</u>	72
2.2 <u>Equipment</u>	72
2.2.1 The Microbalance and Reactor	72
2.2.2 The Fixed-Bed Reactor	78
2.2.3 Furnace and Temperature Control	79
2.2.4 Feed System for Reactants	80
2.2.5 Gas Chromatograph	84
2.2.6 Gravimetric Adsorption Apparatus	86
2.2.7 Carbon Monoxide Chemisorption Apparatus	87
2.3 <u>Materials</u>	87
2.4 <u>Procedure</u>	91
2.4.1 Catalyst Preparation	91
2.4.2 Kinetic Experiments	93
2.4.3 Measurement of Total Surface Areas	94
2.4.4 Measurement of Metal Surface Areas	98
2.5 <u>On the Planning of Experiments</u>	98

2.1 INTRODUCTION

The main reaction system consisted of a microbalance and associated flow reactor, furnace and temperature controller, feed system for reactants and a gas chromatograph on line, as shown in Fig. 2.1. The sample of catalyst was suspended from the microbalance arm, the system was flushed with nitrogen, or evacuated with a rotary pump, and brought to the reaction temperature. The reactants were then admitted to the reactor and the weight change of the catalyst sample was continuously recorded. The amounts of reactants delivered were controlled by needle-valves and measured by calibrated rotameters. Gas products were analysed gas chromatographically.

Surface areas of catalysts and carbons were determined from nitrogen adsorption isotherms by the B.E.T. method. A gravimetric technique was adopted, using the vacuum microbalance and associated vacuum line (Fig. 2.7). Metal surface areas of supported catalysts were measured by carbon monoxide chemisorption in a chromatographic flow system (Fig. 2.10).

A more detailed description of the experimental set-up follows.

2.2 EQUIPMENT

2.2.1 The Microbalance and Reactor

A C.I. Electronics MK.2B vacuum microbalance head was used in a pyrex glass vacuum bottle with B34 conical glass connection. The balance head was connected to the electrical control cabinet and to a Honeywell recorder (1 mV) via a matching unit (C.I. Electronics); damping and range extending facilities were provided in the matching unit.

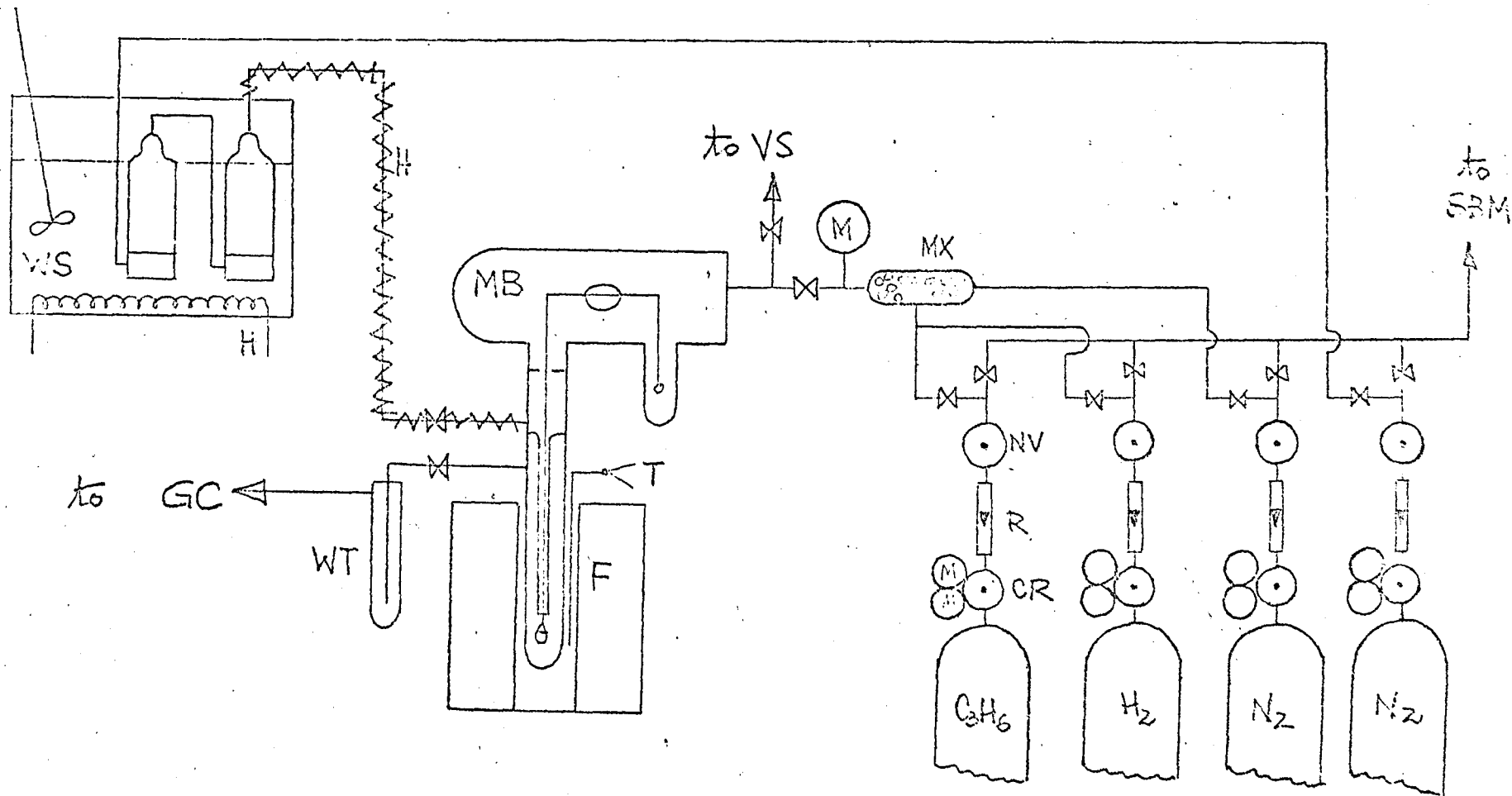


Fig. 2.1 Reaction System

Key to Fig. 2.1

MB	Microbalance
WS	Water saturator
F	Furnace
H	Heater
WT	Water trap
GC	Gas chromatograph
VS	Vacuum system
T	Thermocouple
M	Manometer
MX	Mixer
NV	Needle valve
R	Rotameter
CR	Two-stage pressure regulator
SBM	Bubble meter

The microbalance had the following characteristics:

Capacity	1 gram sample, 1 gram counterweight
Sensitivity	0.5%
Reproducibility	$\pm 0.5 \mu\text{g}$
Ranges	0 - 25 μg 0 - 250 μg 0 - 2.5 mg 0 - 10 mg 0 - 100 mg
Electrical tare	up to 12 mg

The volume of the vacuum bottle with counterweight flask was approximately 660 cm^3 .

The microbalance was suspended from a metal bar mounted in a concrete block standing on the floor. A flexible coupling (Edwards) was used between the balance and the vacuum line, in order to minimize vibrations.

Pieces of Ni wire were used as counterweight and suspended from the balance arm by means of a glass fibre, 10 cm long. Three silica fibres (10-15 cm) were hooked together and used to suspend the sample. The use of small segments instead of a long suspension fibre was preferred, in that a better positioning of the sample in the centre of the reactor tube could be achieved. Long suspension fibres were more fragile and very difficult to make straight. Better damping of oscillations could also be achieved by using segments. The only problem encountered with these fibres was the need for extra care to avoid electrostatic charges between the fibres and the reactor walls. Metal suspensions would have been better in this respect, but this would increase the suspended load, causing more noise (which is proportional to the load). The weight of the 3 hangdown fibres was about 100 mg.

Powdered catalysts were placed in small silica baskets (0.1 - 0.3 mg and 0.3 - 1.5 cm³). Metal foils were suspended from the hangdown wire hook through a hole. Pellets could be suspended by fastening a small piece of tungsten wire (0.13 cm diameter) around them.

The flow of gases along the sample was found to cause a small deflection on the microbalance reading, but this was of no consequence, the deflection being of constant magnitude for each value of the total flow rate. Noise was not greatly affected by flow, and rates of carbon formation were usually so high that there was no need to use the more sensitive ranges of the balance.

No shielding or painting of the microbalance bottle was found to be necessary in the present system. Changes in the level of luminosity of the room, which could affect the balance stability, were prevented merely by keeping the lights on at all times. Electrostatic charges between the suspension fibres and the walls of the reactor were only induced by friction, usually when cleaning the conical connections; and this could be avoided by using a damp cloth. No charging was found to develop in the operation of the flow system.

The flow reactor used in association with the microbalance is shown in Fig. 2.2. It is a modification of the "Universal Attachment" available from C.I. Electronics, and was designed to minimize flow effects on the sample and to avoid condensation in the balance head. The main body was made of Pyrex glass, and the inner tube and reactor tube were made of silica. The lower cone connection was provided with a cooling jacket. The gas could flow in through the inner tube, passing over the sample and then emerging through the annular space

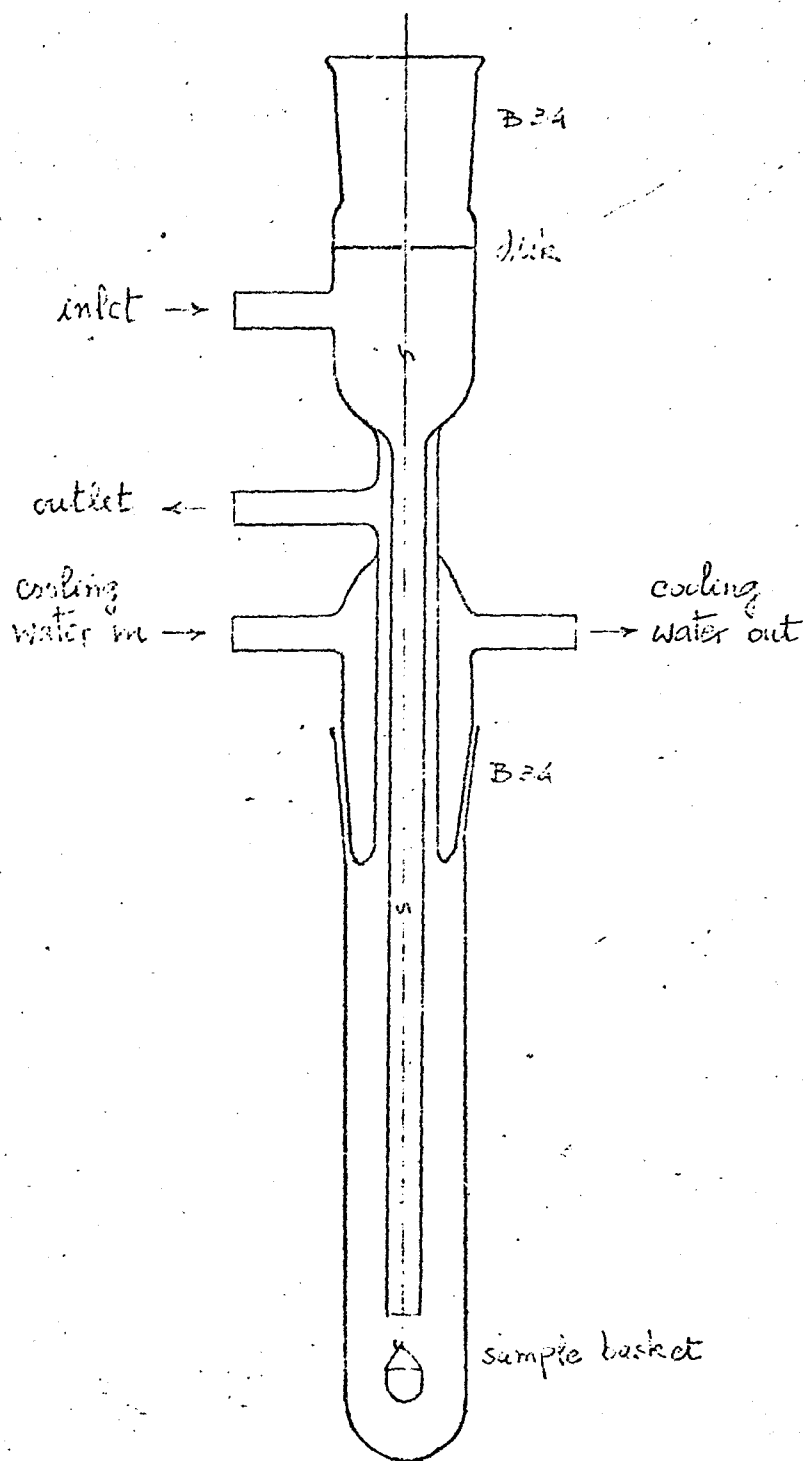


Fig. 2.2 Microbalance Flow Reactor

between the inner tube and the outer walls. The balance head could be kept flushed with N_2 or other gas. A metallic disk with a small hole was built in just above the reactor inlet in order to prevent back diffusion of water vapour into the balance mechanism. Without this disk some condensation was observed in the balance head, even when it was being flushed with a large excess of nitrogen.

The cone and socket connections were sealed with silicone grease (Edwards) which is leak tight at temperatures of up to $200^{\circ}C$. The temperature in the reactor connection was kept below this limit by the flow of cooling water through the jacket. However, this procedure could not be used in runs where water vapour was a reactant. In these cases the cooling water was turned off, but some water was left inside the jacket. After some time this would start boiling, thereby keeping the temperature constant at about $100^{\circ}C$.

The design of the reactor proved very effective for moderate flow rates (up to $500\text{ cm}^3/\text{min}$) because a counterflow path of gas was established which provided effective preheating via heat transfer from the hot gas leaving the reaction zone to the cold inlet gas.

The total volume of the reactor was 180 cm^3 . Since it operated at low conversions (dilute feed and small loads of catalyst) the reactor could be treated as differential.

2.2.2 The Fixed-bed Reactor

The majority of runs were performed using the microbalance flow reactor described in 2.2.1. However, under certain conditions, film diffusion limitations were encountered when using the more active catalysts. Increasing the gas flow rates, within the limits imposed by the equipment used, did not solve the problem, as a result of the method used for suspending the catalyst, i.e., inside a basket. As a result,

the gas did not in fact pass through the catalyst bed, but rather impinged on the top surface.

In order to obtain a complete picture of the reactions under study, a tubular reactor was designed for use with very fast reactions. This reactor was made of silica tube, 7 mm diameter and 41.5 cm long, provided with a porous silica disk in the middle, to act as a support for the catalyst bed. This disk was supplied by Thermal Syndicate and had a maximum pore diameter of 0.150 mm. The catalyst bed was made of equal amounts of catalyst and pumice stone with the same particle size.

An ice trap was placed at the outlet of the reactor. Product gases were passed through the chromatograph sampling valve and carbon lay down was estimated by a mass balance. The formation of carbon was accompanied by an increase in the pressure drop through the reactor, and this could also serve as a measure of carbon deposition if the deposit was assumed to have constant porosity.

2.2.3 Furnace and Temperature Control

The furnace was constructed by winding about 10 metres of nichrome tape around a porcelain tube 20.5 cm long and 4.6 cm in diameter. The furnace winding had an electrical resistance of 33 ohm and the furnace could operate at temperatures up to 1000°C. In an attempt to get a good temperature profile, the nichrome tape was wound more closely at both ends of the furnace tube. The winding was covered with a layer of alumina cement (Thermal Syndicate type C60) and the tube was placed in a case made up of asbestos slab in a Dexion frame. The interior of this case was filled with vermiculite.

Temperature profiles and other calibrations of the furnace are shown in Fig. 2.3, 2.4, 2.5.

A three mode (proportional, derivative, integral) temperature controller was designed and built in the departmental Electronic Workshop; details are given in the Appendix. The controller worked in conjunction with a chromel-alumel thermocouple, and was fitted with a digital display to show the temperature in the furnace. However, this indicated temperature had to be corrected, since no compensation for the temperature of the cold junction was provided. Usually another thermocouple connected to a portable potentiometer was used (Croydon Precision Instruments, type P.6).

The three mode controller proved to be a very reliable unit and was claimed to keep the temperature constant within $\pm 0.5^{\circ}\text{C}$. The controller settings (gain, reset rate and time constant) were adjusted in order to give a fast rate of heating coupled with a fast approach to the set point. The furnace could be brought up from room temperature to control at 500°C in 15 minutes.

The temperature measured just outside the reactor wall was found to be nearly the same as that measured inside the reactor for moderate flow rates, as shown in Table 2.1.

2.2.4 Feed System for Reactants

Gases were supplied from cylinders, through two-stage pressure regulators, calibrated rotameters and fine control needle valves (Edwards, model LB2B). The rotameters were calibrated by bubble-meters.

Water vapour was produced in a pick-up system consisting of two Drechsel bottles (500 cm^3 each) in series, immersed in a water

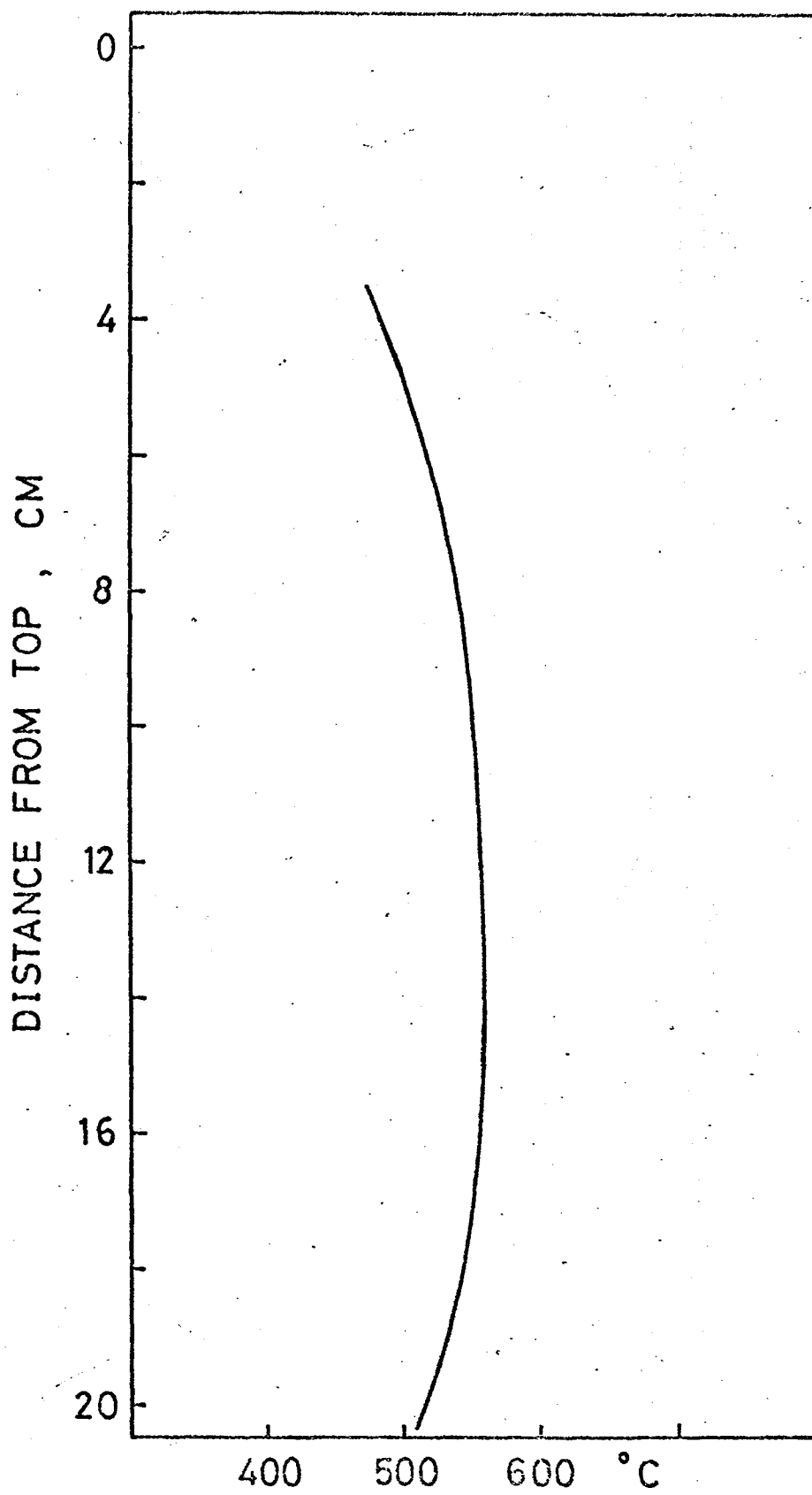


Fig. 2.3 Temperature Profile of the Furnace

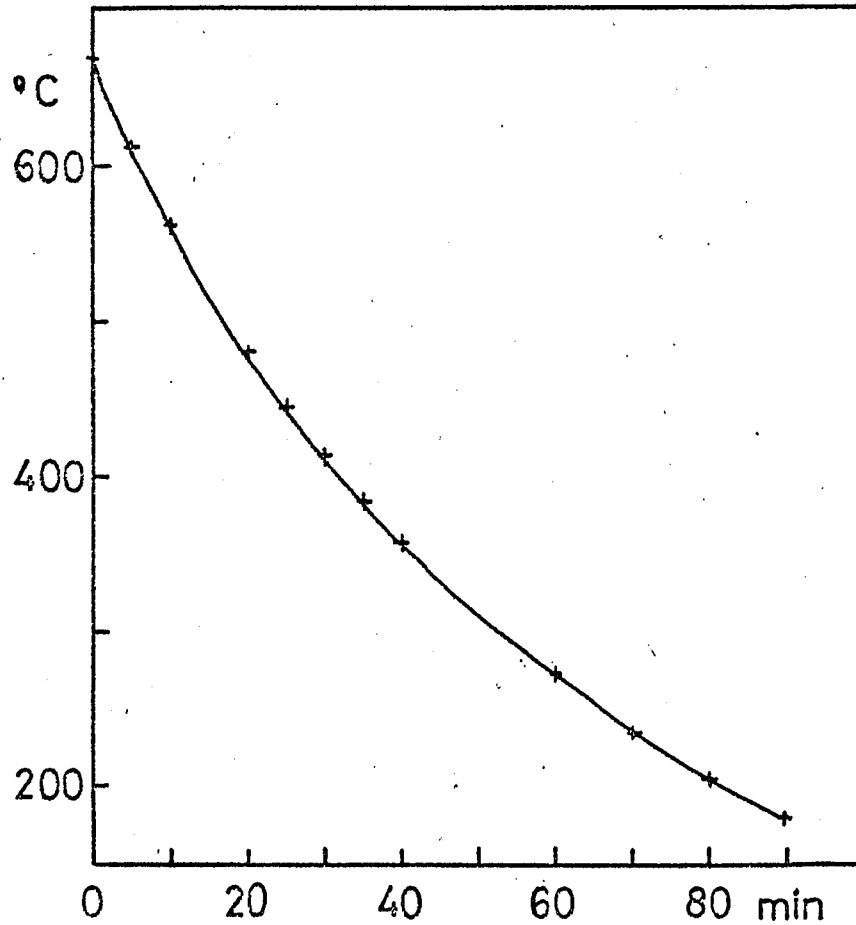


Fig. 2.4 Cooling curve of the furnace

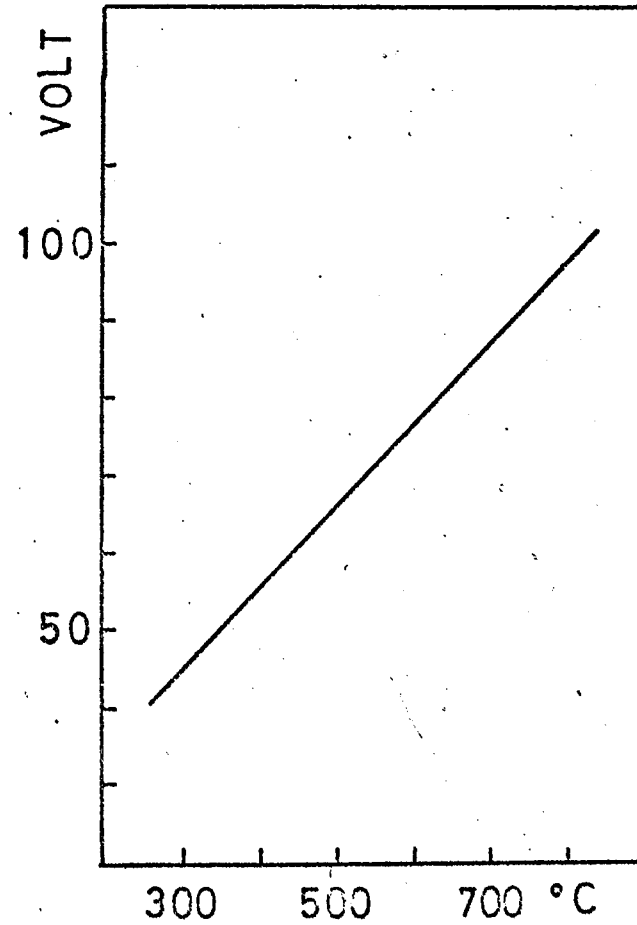


Fig. 2.5 Maximum temperature in the furnace

Table 2.1 Temperature Differences across the
Reactor Wall in the Reaction Zone

N_2 Flow Rate (cm^3/min)	Temperature ($^{\circ}C$)	ΔT ($^{\circ}C$)
240	480	0
240	527	0
500	526	+1
500	575	0
500	443	+1
230	444	0

Table 2.2 Calibration Factors and Retention
Times for Gas Chromatography

Component	Retention time (sec)	Calibration factors
H_2	35	0.00028
N_2	53	0.00292
CO	68	0.00364
CH_4	90	0.00083
* CO_2	65	0.00316
* C_3H_6	170	0.00087

* At $150^{\circ}C$

bath kept at constant temperature as shown in Fig. 2.1. Nitrogen bubbling through distilled water in the bottles carried the vapour to the reactor via a heated glass line. A former system, consisting of a boiler and a set of condensers placed inside the thermostatic bath, was found to be unsatisfactory, causing large pulsations which disturbed the microbalance readings.

The amount of water delivered could be varied by changing the flow rate of pick-up gas or by setting the thermostat at different temperatures. The pick-up system was calibrated by condensation of the water delivered in a fixed time (Fig. 2.6). The calibration was checked eventually by gas-chromatography, using a "Porapak Q" column.

The temperature of the water bath was controlled by a Gallenkamp's "Thermostirrer", this unit comprising a 1 kW heater, stirrer, contact thermometer and solid state relay. This was claimed to control the temperature within $\pm 0.05^{\circ}\text{C}$, with a maximum variation of 0.3°C over the whole bath volume.

2.25 Gas Chromatograph

Gases were analysed in a PYE Panchromatograph fitted with a microkatharometer detector (Servomex Mk.158). A silica gel column (80/100 mesh) of 4 mm diameter and 1.5m long was used to separate H_2 , N_2 , CO and CH_4 when operating at room temperature, and CO_2 and C_3H_6 when operating at 150°C . Argon (flow rate = $75 \text{ cm}^3/\text{min}$) was used as carrier gas after purification by passage through a molecular sieve column (Linde Air Products 5A). The detector operated at 150°C with a constant current of 95 mA, and its signal was attenuated and recorded on a Vitatron UR 402M linear integrating recorder. The

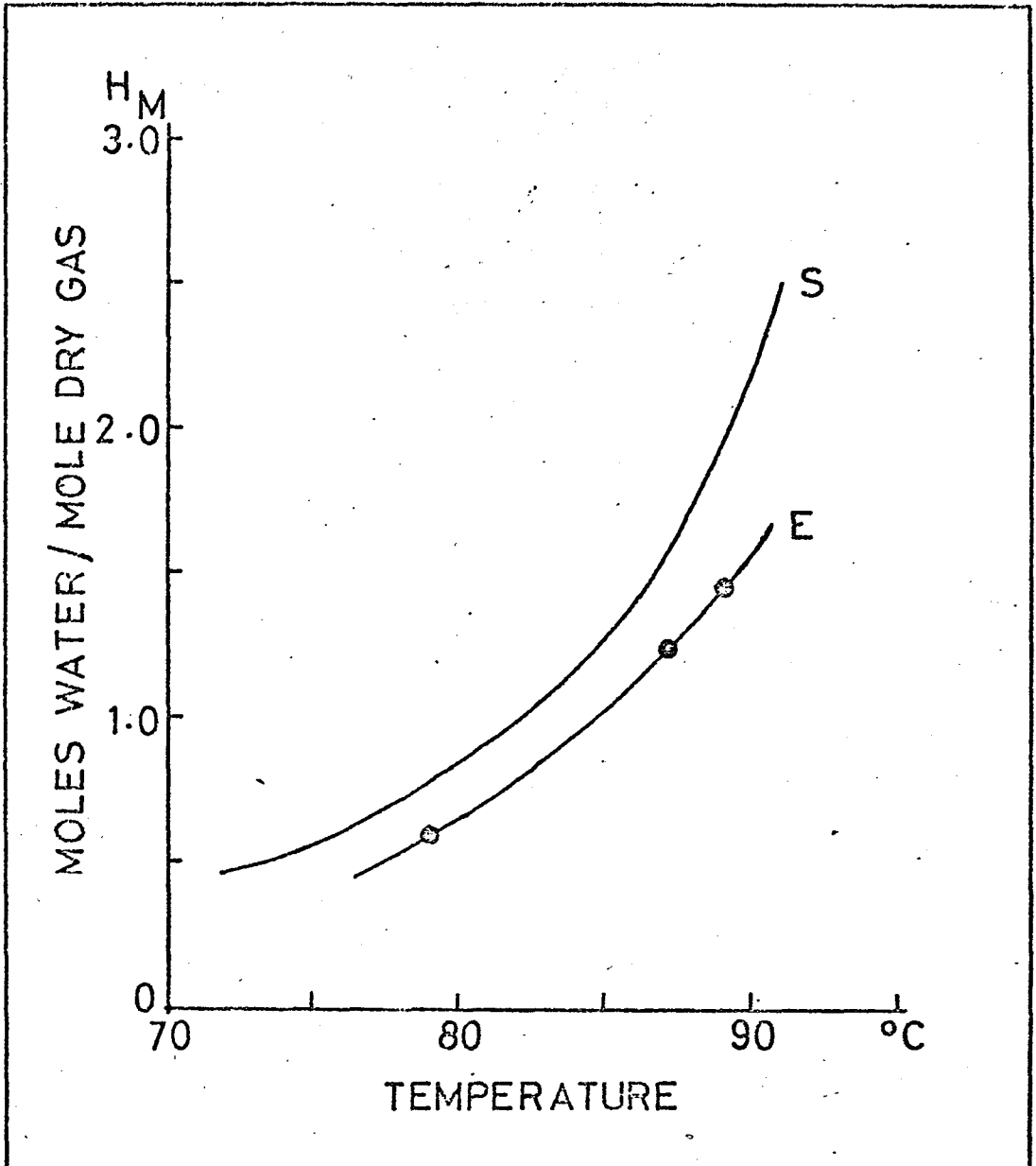


Fig. 2.6 Calibration of the Pick-up System
 S = Saturation curve : $H_M = P/(760-P)$
 E = Experimental curve
 (P = vapour pressure of water, torr)

sample was taken at a six-port gas sampling valve (PYE), usually fitted with a 2 cm³ sample loop.

Calibration charts were obtained by injection of known amounts of pure gas and plotting the volume injected as a function of peak area. In the ranges of interest, all calibrations were linear.

The standard calculations were as follows:

$$\begin{aligned} X &= u.A/r \\ v &= K.X \quad (\text{calibration charts}) \\ x &= v/S \end{aligned}$$

where:

u = number of counts in the integrator (6 counts = 1 cm²)

A = attenuation factor

r = counting rate (integrator)

S = calibrated volume of the sample loop

X = area units

x = mole fraction of each component

v = volume of pure gas

K = calibration factors

Calibration factors and retention times are given in Table 2.2.

2.2.6 Gravimetric Adsorption Apparatus

A vacuum line was originally built in association with the microbalance so that the system could operate under batch conditions. In the present work, this association was only used for the gravimetric determination of adsorption isotherms, kinetic experiments being performed under flow conditions as described.

The vacuum system, represented in Fig.2.7, consisted of an Edwards Speedivac rotary pump and a two-stage mercury diffusion pump (Thermal Syndicate), giving an ultimate vacuum of about 10^{-5} torr. To measure the pressure, a Leybold "Combitron" unit was used, with a combination of two Thermotron and one Penning gauge heads. A mercury manometer was also included in the system. All taps in the high vacuum line were greaseless (O-ring type, from J. Young).

An oxygen vapour thermometer (Fig.2.8), designed as in reference (153), was used to measure the temperature of the bath to determine the saturation vapour pressure of nitrogen: values of P_o were usually in the range 760-780 torr. Calibrations for the oxygen thermometer are given in Fig. 2.9, calculated with values from Table 2.3.

2.2.7 Carbon Monoxide Chemisorption Apparatus

Metal surface areas of supported catalysts were determined by carbon monoxide chemisorption in a chromatographic flow system available in the department. The apparatus (Fig.2.10) consisted of a katharometer and three sampling valves, together with gas lines for the carrier gas (helium), carbon monoxide and hydrogen. The system was operated inside an air thermostat.

2.3 MATERIALS

Nickel foils, as well as supported nickel catalysts, were used in this work.

Polycrystalline nickel foils were obtained from Metals Research Ltd., and were of 99.7% purity, 0.1mm thickness and about $23 \text{ cm}^2/\text{g}$ geometric surface area.

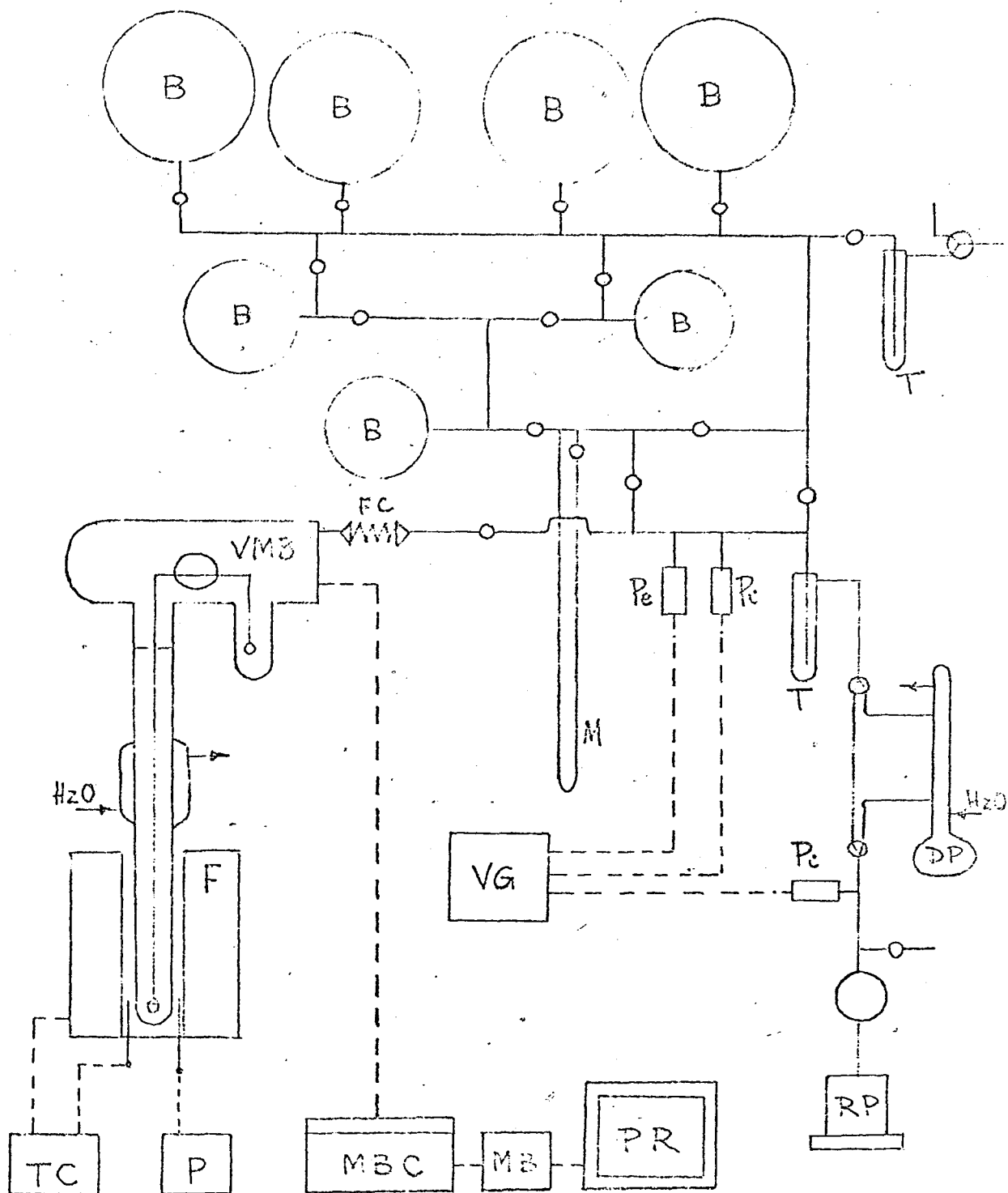


Fig. 2.7 The Vacuum System

F = furnace ; VMB = microbalance ; B = bulbs
MBC = microbalance cabinet ; MB = matching box
PR = recorder ; TC = temperature controller
P = potentiometer ; RP, DP = pumps ; T = traps
Pe, Pi = vacuum gauge heads, VG = vacuum gauge
M = manometer ; FC = flexible coupling

Table 2.3 Vapour Pressure Data for Vapour Pressure
Thermometers (torr)

Temp. (K)	$100 \times 1/T$	Oxygen	Nitrogen
83	1.205	340.7	1428
82	1.219	300.2	1289
81	1.235	263.6	1162
80	1.250	230.6	1043
79	1.266	200.9	933
78	1.282	174.4	833
77	1.299	150.9	741
76	1.316	129.9	657
75	1.333	111.3	581
74	1.351	95.0	511
73	1.370	80.7	459

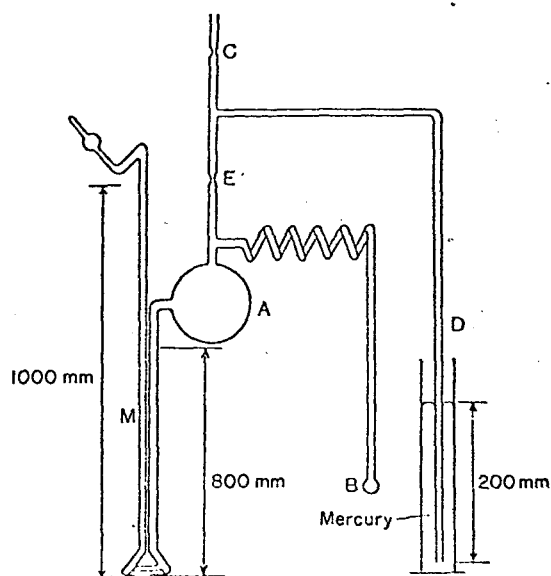


Fig. 2.8 Oxygen-vapour Thermometer (153)

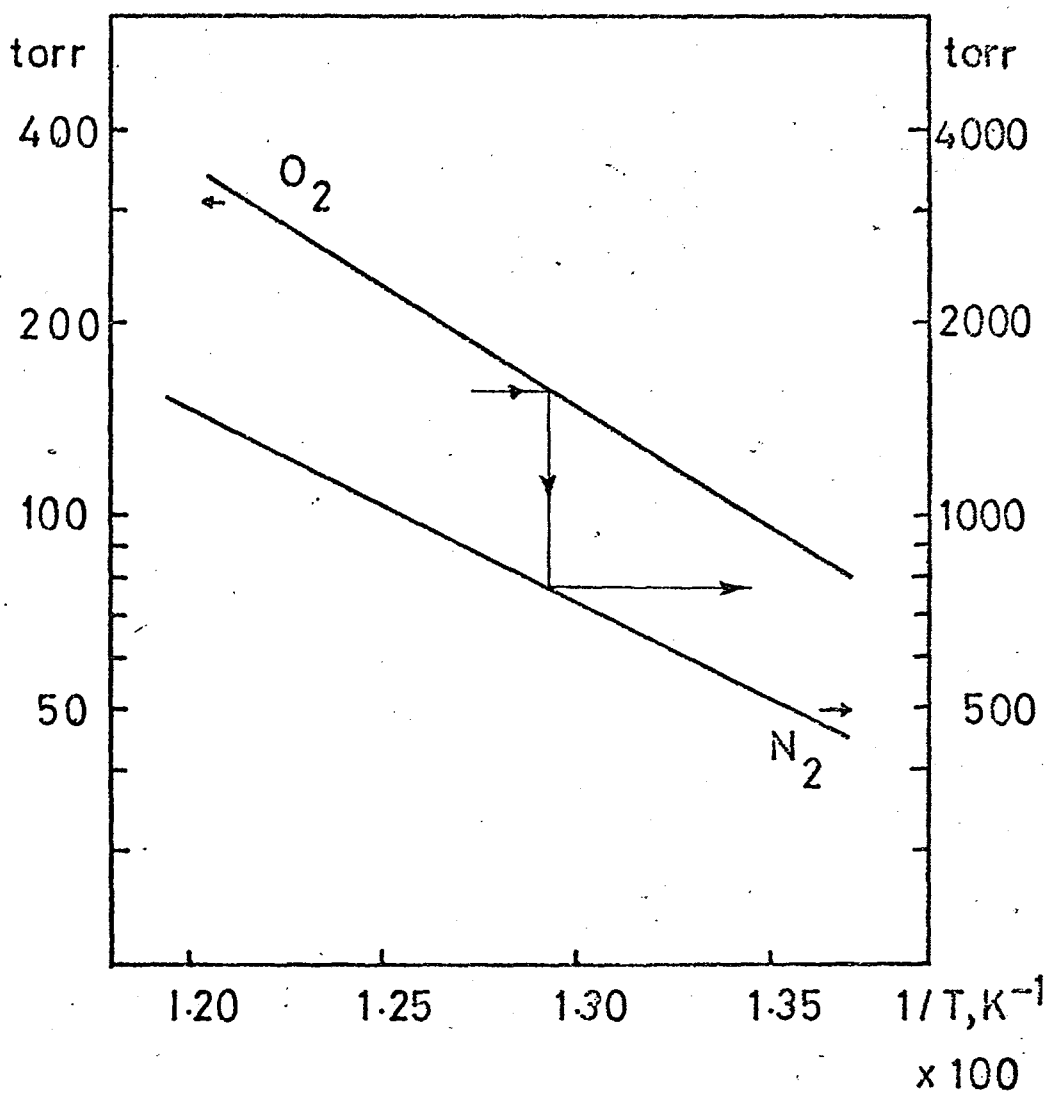


Fig. 2.9 Calibration of the Oxygen Vapour
Thermometer

Nickel on alumina catalysts were kindly supplied by ICI Agricultural Division, their composition and method of preparation being described in Table 2.4. A nickel on kieselguhr catalyst (40 % NiO) was obtained from Peter Spence & Sons. Some properties of these catalysts were determined and are given in Table 2.5.

Gases were supplied by the British Oxygen Company and by Air Products, and were of technical grade.

2.4 PROCEDURE

2.4.1 Catalyst Preparation

Nickel foils and supported nickel catalysts were used in carbon formation experiments, coked catalyst samples were used in gasification studies.

Nickel foils were cut from a large metal sheet and their geometric area determined by weighing, with an accuracy better than 0.1%. They were cleaned with acetone and suspended from the balance. Foils of about 3 cm² were used in most cases. One of the following procedures was then used:

- a) The microbalance was evacuated, the furnace heated up and the whole system degassed at reaction temperature; or
- b) The microbalance was flushed with nitrogen and the furnace heated up to reaction temperature; or
- c) The microbalance was flushed with nitrogen, the furnace heated up to reaction temperature and the sample reduced under flow with H₂/N₂ mixture.

Supported catalysts were usually crushed and sieved, and the fraction corresponding to B.S.S. 40-60 used (0.235 to 0.360mm). A portion of catalyst powder was weighed and suspended in a basket from the microbalance. The reactor was flushed with nitrogen and

Table 2.4 Ni/Al₂O₃ Catalysts : Composition (*)
and Preparation

Component	46-1	Ni/Al ₂ O ₃
NiO	22.8 %	21.9 %
Al ₂ O ₃	24.9	78.1
CaO	13.5	
MgO	12.0	
SiO ₂	14.8	
Fe ₂ O ₃	5.0	
K ₂ O	7.0	
Preparation	I	II

* Analyses in the loss-free basis and for catalysts in the oxidized form.

Preparation methods :

I - Commercially available (I.C.I.)

II- 1) α -Al₂O₃ pellets soaked in Al(NO₃)₃·9H₂O melt, then calcined at 450 °C

2) Pellets soaked in Ni nitrate melt, then calcined at 450 °C

Table 2.5 Properties of the Nickel Catalysts

Catalysts	Ni %	Total Surface Area (m ² /g)	Metal Surface Area (m ² /g)	Density (g/cm ³)
46-1	18	22	0.6	2.25
Ni/Al ₂ O ₃	18	14	0.4	2.15
Ni/kieselguhr	45	37	1.7	1.85

the catalyst was then reduced at 600°C with H₂ (4.5 l/hr.). The reduction was completed when no further weight loss could be detected. The reactor was then flushed with nitrogen and brought to the reaction temperature. A similar procedure was adopted for runs carried out in the tubular fixed bed reactor, but the catalyst was mixed with an equal amount of pumice stone of the same particle size. Whole catalyst pellets were used in some cases. They were weighed and suspended from the balance with a small piece of tungsten wire. The reduction procedure was similar to that of powdered catalysts.

In gasification studies, coked foils or coked samples of catalyst from previous carbon deposition runs were kept in the microbalance. The reactor was flushed with nitrogen and brought to the gasification temperature. The sample was heated in nitrogen flow for at least 1 hour prior to gasification, in order to desorb any remaining gases from the deposition run.

2.4.2 Kinetic Experiments

After the pre-treatment, reaction was initiated by allowing the flow of reactants through the microbalance. Water vapour, when used, was introduced in the reactor by the side inlet and all other gases through the top inlet, in order to keep the microbalance head flushed and to prevent condensation. The pick-up system was usually operated at 89°C, and the flow rate of pick-up gas varied whenever it was desired to change the amount of water vapour delivered. The flow rate of diluent nitrogen flushing the balance head was varied accordingly in order to keep total flow rate constant. The hydrocarbon inlet valve was always opened before the water vapour was admitted, in an attempt to prevent catalyst oxidation. Water was condensed in an ice trap at the reactor outlet.

A record of the amount of carbon deposited (or gasified) with time was obtained, and rates of carbon deposition (or gasification) were calculated from the slopes of the plots. Gas analyses were obtained when necessary, in terms of mole fraction of each component. The following mass balances were then established:

$$\text{Nitrogen balance: } E = N/x(N_2)$$

$$\text{Oxygen balance: } A = E.(x(\text{CO})+2x(\text{CO}_2))$$

$$\text{Hydrogen balance: } 3P+A = E.(x(\text{H}_2)+2x(\text{CH}_4)+3x(\text{C}_3\text{H}_6))$$

$$\text{Carbon balance: } 3P = C+E.(x(\text{CO})+x(\text{CH}_4)+x(\text{CO}_2)+3x(\text{C}_3\text{H}_6))$$

where

$x(i)$ = mole fraction of component i in the dry effluent

P = propylene flow rate, mole/hr

N = nitrogen flow rate, mole/hr

C = rate of carbon formation, mole/hr

A = rate of water consumption, mole/hr

E = effluent flow rate after water condensation, mole/hr

W = weight of catalyst, g

Individual rates of reaction were obtained by multiplying E and the mole fraction of each product formed. The overall rate of reaction could be expressed as:

$$\text{(moles of reactant consumed)/}W.\text{hr}$$

and the % conversion as

$$100 \cdot \frac{\text{(moles of reactant consumed)}}{\text{(moles of reactant fed)}}$$

2.4.3 Measurement of Total Surface Areas

Catalyst samples were placed in small silica baskets and

suspended from the microbalance. The balance was evacuated and the sample degassed at 250-300°C until no further loss in weight was recorded. This was found to take 3-5 hours. The reactor was allowed to cool down to room temperature and then placed in a liquid nitrogen bath. Small amounts of nitrogen were admitted successively into the microbalance, the change in weight and final equilibrium pressure being recorded. When the saturation pressure was reached, a desorption isotherm was obtained similarly by successive partial evacuations of the balance. Buoyancy effects, caused by differences in volume and temperature between sample and counterweight, were corrected for by calculation:

$$\Delta w = (M \cdot p / R) \cdot (V_c / T_c - V_s / T_s)$$

where:

Δw = buoyancy correction

M = molecular weight of adsorbate

R = gas law constant

V_c, T_c = volume and temperature of counterweight

V_s, T_s = volume and temperature of sample

p = pressure

Specific surface areas were calculated by the B.E.T. equation:

$$\frac{p}{m(P_0 - p)} = \frac{1}{m_0 c} + \frac{c-1}{m_0 c} \cdot \frac{p}{P_0}$$

where

m = amount adsorbed (corrected)

p = equilibrium pressure

P_0 = saturation vapour pressure of N_2

m_0 = weight of monomolecular layer of adsorbate

c = constant

A plot of $p/m(P_0-p)$ vs. p/P_0 yields a straight line up to relative pressures of 0.3 - 0.4. From the values of the slope and intercept the weight of a monolayer of adsorbate, m_0 , was calculated:

$$\text{intercept} = I = 1/m_0 c$$

$$\text{slope} = S = (c-1)/m_0 c$$

$$m_0 = 1/(I+S)$$

The total surface area of the sample was then:

$$\text{S.A.} = m_0 \cdot N \cdot s / M$$

where:

N = Avogadro's Number = 6.02×10^{23} molecules/mole

M = molecular weight of adsorbate (N_2)

s = cross section of adsorbate molecule

(for N_2 , $s = 16 \times 10^{-20}$ m²/molecule)

The treatment of Pierce (151) could then be applied to the desorption branch of the isotherm in order to derive the pore size distribution. The total pore volume of the solid could be obtained from the cumulative pore volume calculated for the pore size distribution or by application of the Gurvitsch rule, based on the weight of adsorbate taken up at saturation (152). The apparent density and porosity of the solid could then be obtained from the pore volume and the true density of the material by use of the relationships:

$$V_p = (1/d_a - 1/d_t) = e/d_a$$

V_p = pore volume; cm³/g

e = porosity

d_a = apparent density

d_t = true density

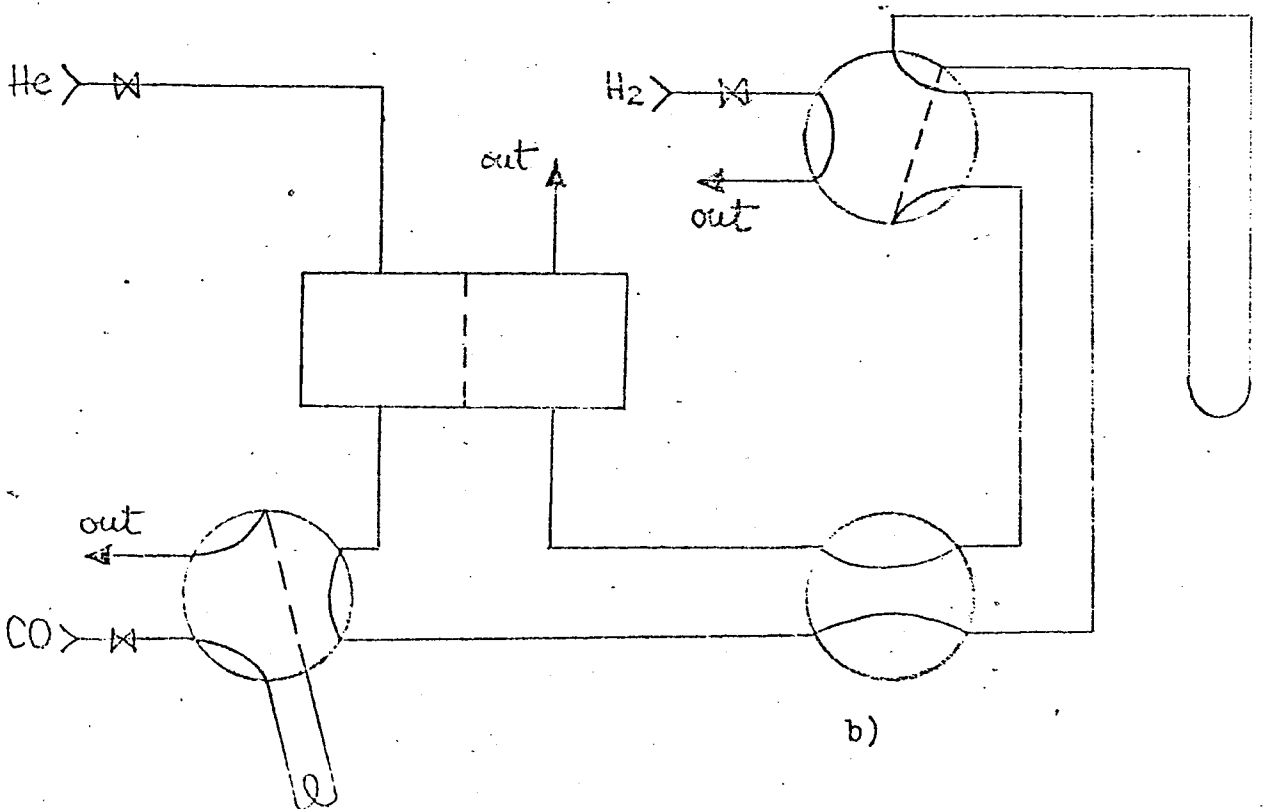
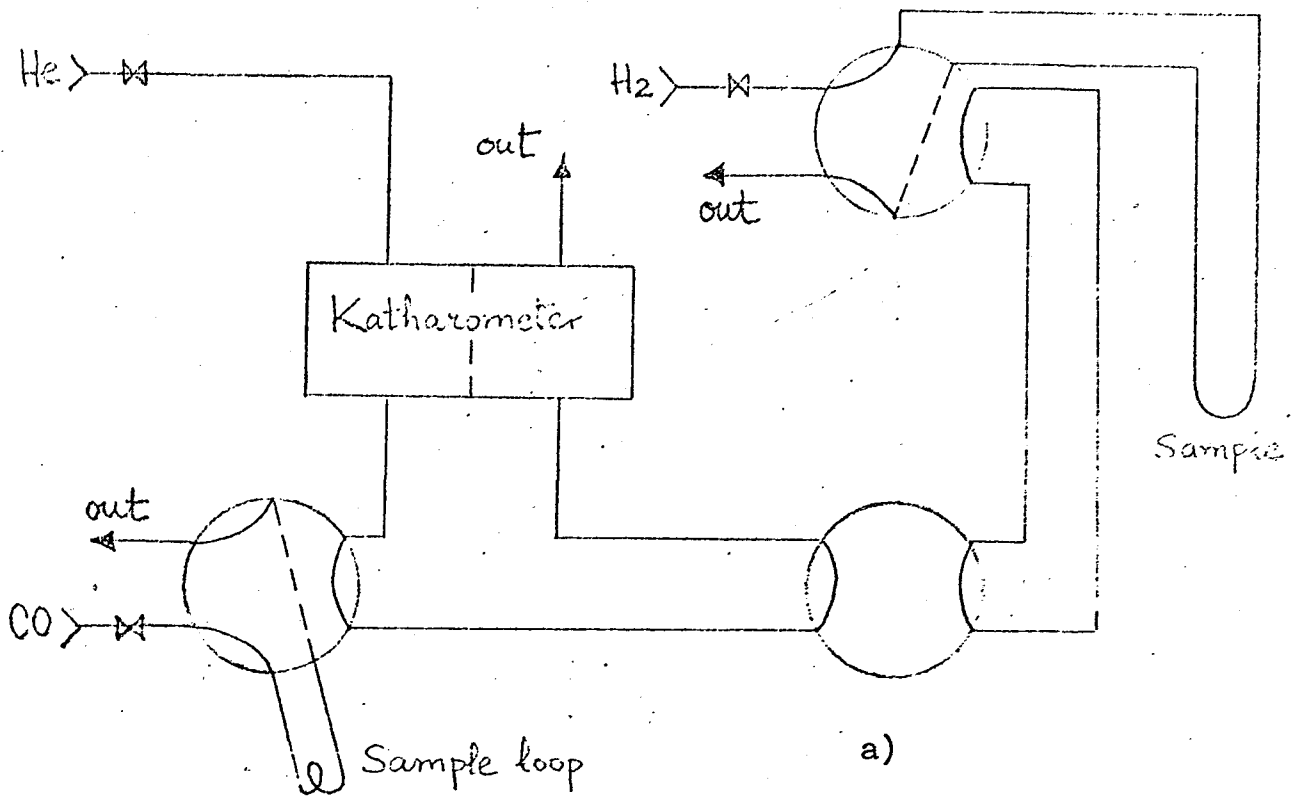


Fig. 2.10 CO chemisorption apparatus

2.4.4 Measurement of Metal Surface Areas

The sample of catalyst was placed in a glass U-tube and attached to the apparatus (Fig.2.10). The catalyst could be reduced with hydrogen in situ, by placing the sample tube in a small fluidised bed furnace, and by setting the position of the sampling valves as shown in Fig.2.10(a). By switching the valves to the position shown in Fig.2.10(b), helium was passed through the sample. This was allowed to cool down to room temperature before starting the chemisorption of CO. Successive amounts of CO were then injected, using a 0.1 cm³ sample loop, and the peaks obtained were recorded and integrated, the procedure being stopped when two successive injections produced peaks of the same area. These latter peaks were used to obtain a calibration factor. All the amounts adsorbed were added and the metal surface area calculated as follows:

$$\text{Ni area of the sample} = V.N.s/V_M$$

where:

V = total volume of CO chemisorbed by the sample

N = Avogadro's Number = 6.02×10^{23} molecules/mole

V_M = molar volume at room temperature and pressure

s = coverage area for CO molecule chemisorbed on Ni
 = 13×10^{-20} m²/molecule. (154).

2.5 ON THE PLANNING OF EXPERIMENTS

Considerable experimental difficulties with reproducibility were observed, and considerable care was taken to obtain more reliable comparisons.

The decomposition of propylene on nickel catalysts was

characterized by constant rates of carbon deposition after some initial stages which were dependent on the pretreatment followed. Advantage was taken of these steady-state rates of reaction by obtaining most kinetic data in single runs. Under isothermal conditions, the partial pressures of the reactants were changed and orders of reaction were obtained from their effect upon reaction rates. The effect of temperature on carbon deposition was investigated by keeping reactants concentrations constant and recording the steady state rates at different stationary temperatures. This procedure could be used in the present work because of the large range of the Mk2 microbalance (100mg) and the fast response of the temperature controlling facilities. In a previous study of similar reactions under batch conditions (46), a dynamic method was used by establishing a constant cooling or heating rate and taking the slopes of the carbon deposition curves at each temperature. This did not take into consideration the possibility of temperature gradients between the sample and the furnace, but the method was imposed by the shorter range (10mg) of the balance used.

Gasification of carbon deposits was also characterized by constant rates of weight loss which were found to last for about 60-70% burn-off. In some circumstances, the length of the period of constant rate of gasification was enough for data to be obtained from single runs. When the gasification reaction was fast (high temperatures, gasification by H_2O) this method could not be used and reproducibility was impaired by difficulties in obtaining carbon deposits of exactly the same properties.

Coking of the catalyst in the steam-reforming of the hydrocarbon was found to have no deactivation effects. In fact, some loss of activity occurred at the very beginning of the reaction,

but the level of activity changed very little thereafter. This meant that after a short initial period the rate of reaction could be considered constant, and kinetic parameters could be obtained in the same run. After the lay-down of large coke deposits the catalyst could be regenerated by burning-off the carbon, followed by reduction, and the reaction started again.

CHAPTER 3

RESULTS

	Page
3.1 <u>Introduction</u>	103
3.2 <u>Carbon Formation from Propylene</u>	103
3.2.1 Carbon Deposition on Nickel Foil	103
3.2.1.1 Description	103
3.2.1.2 Preliminary Experiments	104
3.2.1.3 Kinetic Results	114
3.2.1.4 Effect of Hydrogen	120
3.2.2 Carbon Deposition on Supported Nickel Catalysts	129
3.2.2.1 Description	129
3.2.2.2 Kinetic Results	129
3.2.2.3 Film Diffusion	134
3.2.2.4 Fixed-Bed Experiments	140
3.2.2.5 Surface Area Measurements	140
3.2.3 Other Carbon Deposition Studies	142
3.2.4 Characterization of the Carbon Deposits	146
3.2.4.1 Carbon from Nickel Foils	146
3.2.4.2 Carbon from Supported Catalysts	148
3.3. <u>Gasification of Carbon Deposits by Water Vapour</u>	156
3.3.1 Carbon Gasification from Nickel Foil	156
3.3.1.1 Description	156
3.3.1.2 Kinetic Results	159
3.3.1.3 Test of Diffusion Limitations	163

3.3.1.4	Stoichiometry	164
3.3.1.5	Catalysed vs. Uncatalysed Gasification	165
3.3.2	Carbon Gasification from Supported Catalysts	167
3.3.3	Surface Area Measurements	173
3.4	<u>Gasification of Carbon Deposits by Hydrogen</u>	173
3.4.1	Carbon Gasification from Nickel Foil	173
3.4.1.1	Description	173
3.4.1.2	Kinetic Results	173
3.4.1.3	Catalysed vs. Uncatalysed Gasification	177
3.4.2	Carbon Gasification from Supported Catalysts	178
3.5	<u>Steam-Reforming of Propylene</u>	183
3.5.1	Carbon Formation on Nickel Foil	183
3.5.2	Steam-Reforming on Supported Nickel Catalysts	188
3.5.2.1	Preliminary Experiments	188
3.5.2.2	Carbon Formation	191
3.5.2.3	The Steam-Reforming Reaction	198
3.6	<u>Kinetic Results : Summary</u>	208

3.1 INTRODUCTION

Studies of carbon formation from propylene on nickel foils, with and without hydrogen were carried out initially, extending the range of conditions used in a previous study (46). Water vapour was then added to the system and the picture completed by studying the gasification of carbon deposits by water vapour and hydrogen.

Supported nickel catalysts were then used for the study of the same reaction systems. Higher conversions were obtained and gas analysis was possible, so that the steam-reforming reaction could also be followed. A differential analysis of results was employed, since conversions were low enough (less than 10%) and steady rates were usually observed.

3.2 CARBON FORMATION FROM PROPYLENE

3.2.1 Carbon Deposition on Nickel Foil

3.2.1.1 Description

Carbon formation from propylene on Ni starts to become appreciable at temperatures above 400°C. The results obtained in the present flow system show a general agreement with the observations reported by Lobo (46):

- Carbon deposition is autocatalytic, showing an acceleration in rate until a steady-state is reached which lasts for a long period; for heavy deposits, this can be followed by a drop in rate. Induction periods are observed under certain conditions. Although the initial stages are dependent on the type of pretreatment given to the catalyst, steady-state rates are not much affected.

Studies of the steady-state region show a complex dependency of rates on temperature, and three regions can be defined in an Arrhenius-type plot: A low temperature region (up to 550°C) where

rates are not much affected by reactant concentration with an activation energy of $33 \pm 5\%$ kcal/mole; an intermediate region where the reaction becomes of 2nd order overall and rates decrease when temperature is increased; and a third region, above 650°C , where rates increase again with temperature. This latter has been shown (130) to correspond to the gas-phase homogeneous pyrolysis for the case of C_2H_2 , and will not be considered in detail in the present study. As a rule, specific rates measured in the present system were found to be about 50% higher than those reported by Lobo.

The effects of temperature, partial pressure and presence of hydrogen were studied in detail. Temperatures in the range 350°C - 700°C and partial pressures of 0.033 to 0.528 atm were scanned. The total pressure was always 1 atm. Conditions used in all experimental runs are given in Table 3.1, together with the rate of deposition obtained under steady-state.

3.2.1.2 Preliminary Experiments

Reproducibility was poor, even when care was taken to follow exactly the same pretreatment of the foils. Initial stages were very much dependent on annealing procedures, but these did not seem to affect the steady rate of deposition eventually obtained. To test the reproducibility of carbon deposition, two series of runs were performed at about 494°C . The measured rates of deposition were corrected to their values at the average temperature (494°C) by using an activation energy of 33 kcal/mole. The results, presented in Table 3.2, show the uncertainty involved when comparing data from different runs.

In order to check for the absence of mass transfer limitations, total flow rates were changed after a steady rate of deposition was

Table 3.1 Carbon Formation on Nickel Foils
Experimental Conditions and Results

Run	Pre-treatment	Temp °C	P _{H₂} atm	P _{C₃H₆} atm	Rate μg/min.cm ²	Obs. (*)
1	Reduction	525	.066	.066	200	
2	"	494	.066	.066	65	T
3	"	494	.066	.066	68	T
4	"	494	.066	.066	68	T
5	"	496	.066	.132	87	
6	"	494	.066	.132	102	T
7	"	496	.066	.132	98	T
8	"	492	.066	.132	102	T
9	"	494	.066	.066	72	P
10	"	494	.066	.132	104	H
11	"	494	.0	.066	37	H
12	"	494	.132	.132	85	
13	"	495	.066	.132	80	
14	"	494	.066	.132	92	T
15	"	494	.066	.132	93	T
16	"	494	.066	.132	84	T
17	"	502	.066	.132	98	T
18	"	497	.066	.066	74	P
19	"	496	.066	.066		S
20	"	494	.066	.066	67	
21	"	494	.066	.066	75	P
22	"	492	0	.132		S
23	"	492	0	.132		S,H
24	"	490	.066	.132		S
25	"	492	.066	.066	72	P

Table 3.1 (Continued)

Run	Pre-treatment	Temp °C	P _{H₂} atm	P _{C₃H₆} atm	Rate μg/min.cm ²	Obs. (*)
26	Reduction	489	.066	.066	72	P
27	"	493	.066	.066	89	P
28	"	495	.066	.264	126	
29	"	494	.066	.198	112	
30	"	495	.066	.066	63	P
31	"	498	.066	.066	74	P
32	"	400	.066	.066	-	
33	"	450	.066	.066	28	
34	"	452	.066	.066	24	
35	"	520	.066	.066	110	P
36.	Nitrogen	492	0	.066	37	T,H
37	"	496	.066	.066	61	P
38	"	495	.066	.043	49	P
42	"	494	.032	.021	18	P
45	"	600	.066	.066	variable	
46	"	495	.066	.066	62	
48	"	542	.066	.066	120	CR
49	"	542	.058	.116	147	OR
50	"	490	.062	.122	64	CR
51	"	490	.062	.122	75	CR
52	"	490	.062	.122	74	CR
53	"	490	.062	.122	69	CR
54	"	490	.062	.122	69	CR
55	"	490	.066	.122	81	CR
56	Vacuum	486	.066	.122	82	CR
57	"	540	.062	.122	172	CR
58	"	564	.058	.174	224	CR

Table 3.1 (Continued)

Run	Pre-treatment	Temp °C	P _{H₂} atm	P _{C₃H₆} atm	Rate μg/min.cm ²	Obs. (*)
59	Vacuum	485	.058	.174	67	T
60	"	572	.058	.174	170	CR
61	"	490	.080	.120	88	FR
62	"	548	.080	.120	184	FR
63	"	493	.066	.198	99	
64	"	515	.066	.198	130	
65	"	490	.062	.174	95	
66	"	492	.066	.168	93	T
67	"	564	.046	.046	41	P
70	"	585	.046	.046	41	
74	"	589	.053	.159	174	CR
76	"	525	.053	.159	157	CR
77	"	514	.053	.159	138	CR
78	"	549	.053	.159	192	CR
79	"	512	.053	.159	139	CR
80	"	527	.053	.159	186	CR
81	"	518	.053	.159	135	CR
82	"	538	.053	.159	124	CR
83	"	527	.053	.159	163	CR
84	"	535	.053	.159	191	CR
86	Nitrogen	527	.053	.159	140	CR
87	"	532	.053	.159	137	CR
88	"	510	.053	.159	115	CR
89	"	514	.053	.159	109	CR, SA
90	"	524	.053	.159	105	CR
92	Vacuum	512	.053	.159	110	CR
93	"	510	.053	.159	125	CR

Table 3.1 (Continued)

Run	Pre-treatment	Temp °C	P _{H₂} atm	P _{C₃H₆} atm	Rate μg/min.cm ²	Obs. (*)
94	Vacuum	510	.053	.159	104	CR
95	"	490	.066	.198	121	T, CR
96	"	493	.198	.198	146	T, CR
97	"	490	.132	.132	80	T, CR
98	"	486	.066	.066	64	T
99	"	490	.132	.198	115	T
100	"	490	.132	.066	78	T
101	"	460	.043	.086	31	P
102	"	500	.043	.086	74	P
103	"	490	.172	.086	62	P
104	"	490	.132	.132	77	P
105	"	490	.132	.132	76	P
106	"	445	.132	.132	32	P
107	"	494	.132	.132	76	T
108	"	470	.198	.132	64	T
109	"	490	.198	.132	114	T
110	"	490	.066	.066	47	P
111	"	490	.066	.066	58	P
112	"	550	.066	.066	116	P
113	"	550	.066	.066	106	P
114	"	540	.132	.132	223	CR
115	"	550	.132	.132	250	CR
116	"	560	.132	.132	278	CR
117	"	545	.132	.132	246	CR
118	"	542	.132	.132	238	CR
119	"	580	.132	.132	254	CR
120	"	584	.132	.132	233	T

Table 3.1 (Continued)

Run	Pre-treatment	Temp °C	P _{H₂} atm	P _{C₃H₆} atm	Rate µg/min.cm ²	Obs. (*)
121	Vacuum	590	.132	.132	263	CR
122	"	595	.132	.132	264	CR
123	"	603	.132	.132	233	T
125	"	560	.066	.066	97	
127	"	560	.042	.042	43	P
135	"	540	.132	.132	280	CR
136	"	554	.132	.132	297	T
137	"	600	.132	.132	220	T
138	"	604	.132	.132	255	T
144	"	745	.066	.066	variable	T
145	"	597	.066	.066	108	H
148	Vacuum+steam	640	.042	.042	1	P,T
149	Vacuum	640	.042	.042	2	P,T
150	"	590	.042	.042	45	T
151	"	595	.042	.042	20	T
152	"	595	.042	.084	62	T
157	"	650	.066	.066	2	T
158	"	630	.066	.066	5.6	T
263	Nitrogen	550	.132	.132	290	TH
264	"	550	.132	.132	284	TH
269	"	500	.066	.066	87	TH
270	"	500	.066	.066	85	TH
275	"	600	0	.132	-	
276	Vacuum	600	0	.132	-	
278	Nitrogen	590	.066	.066	variable	P,H
279	"	640	.132	.066	18	P,H
280	"	595	.132	.066	121	P,H

Table 3.1 (Continued)

Run	Pre-treatment	Temp °C	P _{H₂} atm	P _{C₃H₆} atm	Rate μg/min.cm ²	Obs. (*)
281	Nitrogen	592	.528	.132	905	P,H
288	"	655	.867	.132	934	T
289	"	500	.934	.066	68	T
290	"	650	.934	.066	374	T
291	Reduction	600	0	.132	-	H
292	"	600	0	.132	-	T,H
293	Vacuum	520	0	.132	65	H
297	Nitrogen	600	0	.132	-	
298	"	550	0	.132		
299	"	500	0	.132	56	T
300	"	550	.132	.132	263	SA,CR
306	"	550	.923	.077	302	CR
307	"	550	.923	.077	343	CR
308	"	550	.923	.077	290	CR
309	"	550	.923	.077	350	CR
314	"	600	.137	.070	33	H,T
318	"	746	0	.132	.2	T,H
320	"	548	.132	.132	262	TH
322	"	550	.132	.132	240	CR
336	"	550	.132	.132	327	A
337	"	550	.132	.132	292	A
338	"	550	.938	.062	298	A
339	"	550	.938	.062	277	A
340	"	550	.132	.132	326	A
341	"	550	.528	.132	420	A
342	"	590	.528	.132	780	SA
345	"	550	.132	.132	330	SA

Table 3.1 (Continued)LEGEND

(*) The following code refers to the particular type of study undertaken after the attainment of a steady-state rate of deposition in each run :

P	Effect of pressure
T	Effect of temperature
H	Effect of hydrogen
FR	Effect of flow rate
S	Examination of the structure of the deposit
SA	Surface area determination
A	Analysis of the deposit
CR	Gasification by water vapour
TH	Gasification by hydrogen

Table 3.2 Reproducibility of Carbon Deposition Rates

1st. series: $P_{H_2} = .066$ atm
 $P_{C_3H_6} = .066$ atm

2nd. series: $P_{H_2} = .066$ atm
 $P_{C_3H_6} = .132$ atm

Run	T°C	Rate _T	Rate ₄₉₄	Run	T°C	Rate _T	Rate ₄₉₄
2	494	65	65	5	496	87	82
3	494	68	68	6	494	102	102
4	494	68	68	7	496	98	93
9	494	72	72	8	492	102	108
18	497	74	68	9	494	100	100
20	494	67	67	10	494	104	104
21	494	75	75	14	494	92	92
25	492	72	76	15	494	93	93
26	489	72	83	16	494	84	84
27	493	89	92	17	502	98	78
30	495	63	61	18	497	89	82
31	498	74	66	21	494	90	90
				25	492	79	84
				26	489	97	112
				27	493	125	129
				30	495	94	91
				31	498	94	84

No. of runs = 12

Range of rates: 61 - 92

Average rate = $72 \mu\text{g}/\text{min}\cdot\text{cm}^2$

Std. deviation = 8.7

Probable rate(99%) = 72 ± 8

$\mu\text{g}/\text{min}\cdot\text{cm}^2$

No. of runs = 17

Range of rates: 78 - 129

Average rate = $95 \mu\text{g}/\text{min}\cdot\text{cm}^2$

Std. deviation = 13.3

Probable rate(99%) = 95 ± 10

$\mu\text{g}/\text{min}\cdot\text{cm}^2$

Table 3.3 Effect of Total Flow Rate on Rates of Carbon Formation

Run	$P_{C_3H_6}$ atm	P_{H_2} atm	T °C	Deposition Rates for Flow Rates of		
				125 cc/min	250 cc/min	500 cc/min
61	.12	.08	490	88	84	88
62	.12	.08	548	174	192	186

(*) Flow rates measured at room temperature and pressure
Deposition rates in $\mu\text{g}/\text{min}\cdot\text{cm}^2$

Table 3.4 Effect of Nickel Area (Geometric) on Rates of Deposition

Run	Area cm^2	$P_{C_3H_6}$ atm	P_{H_2} atm	T °C	Rate $\mu\text{g}/\text{min}$	Specific Rate $\mu\text{g}/\text{min}\cdot\text{cm}^2$
89	1.53	.053	.159	514	167	109
92	2.85	.053	.159	512	313	110
336	3.06	.132	.132	550	1000	327
340	4.20	.132	.132	550	1370	326

obtained in runs 61 and 62. Reactants' partial pressures were kept constant throughout. Results are presented in Table 3.3, and show that the effect is negligible. Most runs were carried out with a total flow rate of $250 \text{ cm}^3/\text{min}$ (measured at room temperature and pressure).

3.2.1.3 Kinetic Results

Rates of carbon formation were found to be proportional to the geometric area of the Ni foil used as substrate, as can be seen in Table 3.4.

Orders of reaction (in propylene and hydrogen) were found to be near zero at low temperatures, increasing with temperature and approaching unity above 550°C . Orders were determined at four temperature levels for a wide range of hydrogen and propylene pressures, as seen in Figures 3.1 and 3.2.

Activations energies at low temperatures (up to 530°C) were determined for several $\text{C}_3\text{H}_6 : \text{H}_2$ feed ratios, as shown in Fig. 3.3. In every case the values found for the activation energies were within 5% of 33 kcal/mole. However, above 530°C - 560°C there was an inversion in the Arrhenius plot and rates of carbon formation were found to decrease as temperature increased (Fig.3.4). Activation energies were then apparently negative. Inversion temperatures moved upwards as pressures increased.

When hydrogen pressures were low, steady rates were difficult to be maintained at high temperatures; in many such cases, partial deactivation was observed and an Arrhenius plot would not give a straight line. The deactivation was easily recognized by the impossibility of returning to the original rate, i.e. reversibility was lost (Fig.3.5). However, in most cases where $P(\text{H}_2) > 0.13 \text{ atm}$,

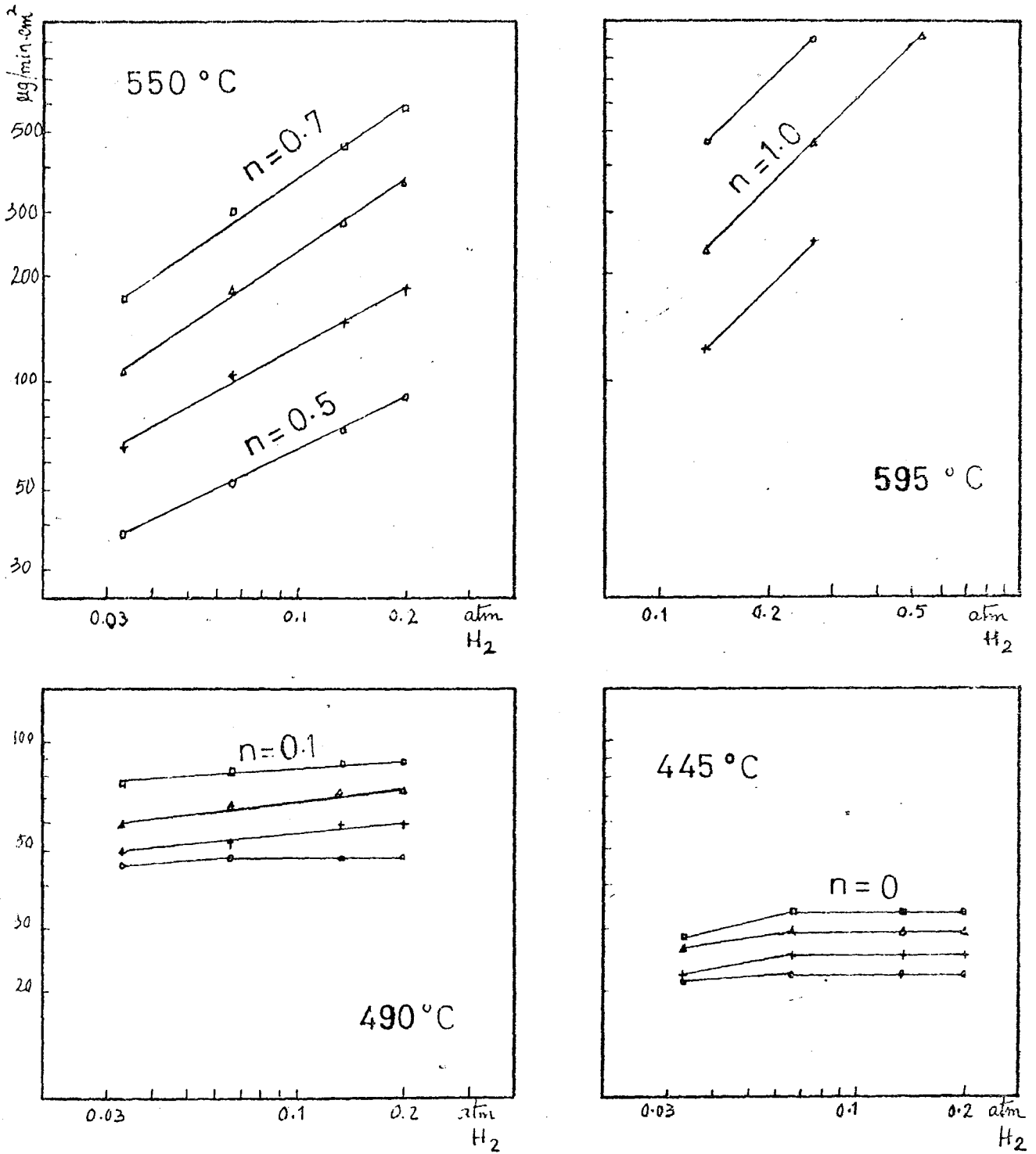


Fig. 3.1 Carbon deposition on nickel foils .

Orders of reaction in hydrogen.

$\circ P_{\text{C}_3\text{H}_6} = .033 \text{ atm} ; + P_{\text{C}_3\text{H}_6} = .066 \text{ atm}$

$\Delta P_{\text{C}_3\text{H}_6} = .132 \text{ atm} ; \square P_{\text{C}_3\text{H}_6} = .264 \text{ atm}$

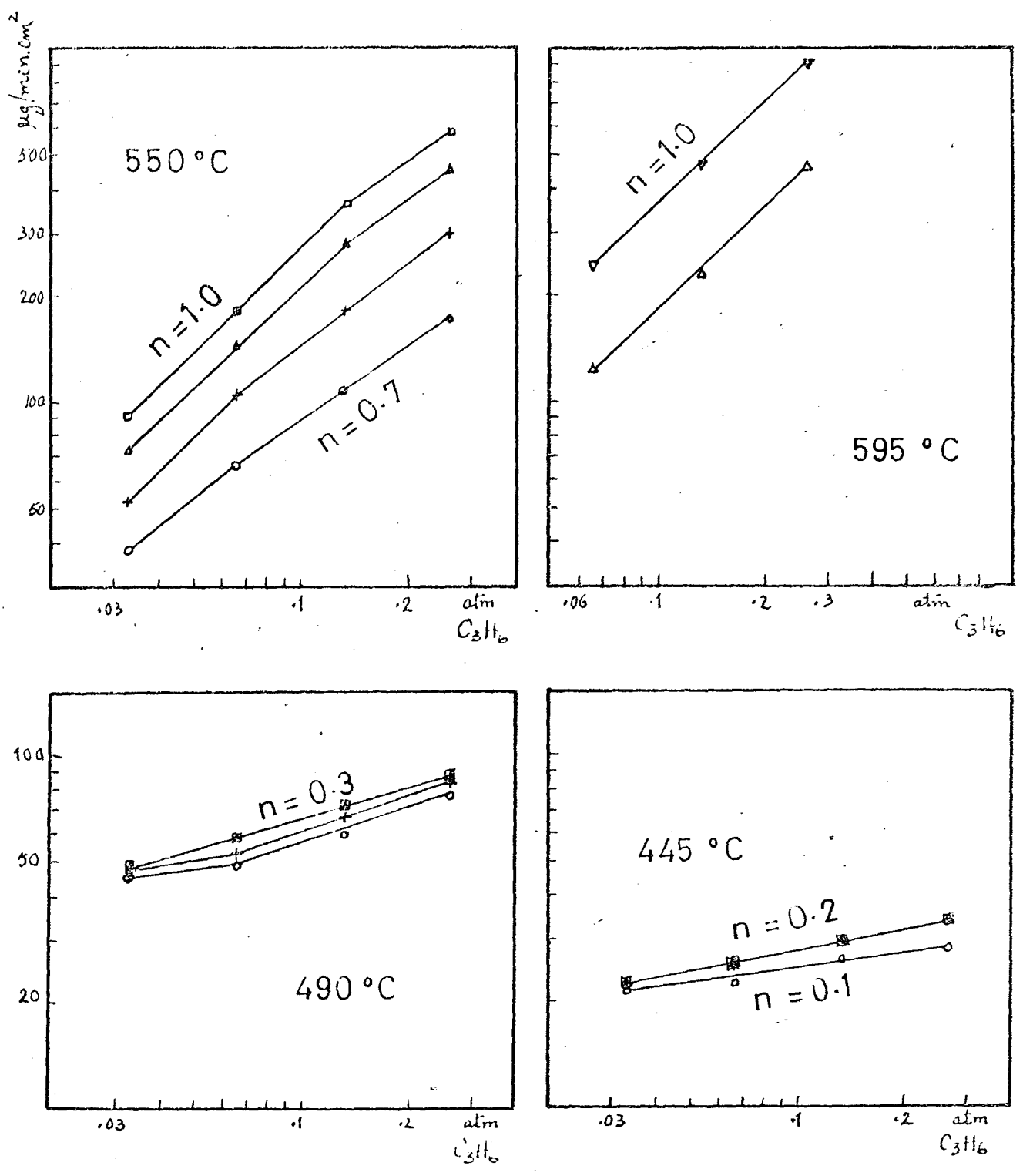


Fig. 3.2 Carbon deposition on nickel foils.

Orders of reaction in propylene.

○ $P_{\text{H}_2} = .033 \text{ atm}$; + $P_{\text{H}_2} = .066 \text{ atm}$; $\Delta P_{\text{H}_2} = .132 \text{ atm}$

□ $P_{\text{H}_2} = .198 \text{ atm}$; $\nabla P_{\text{H}_2} = .264 \text{ atm}$

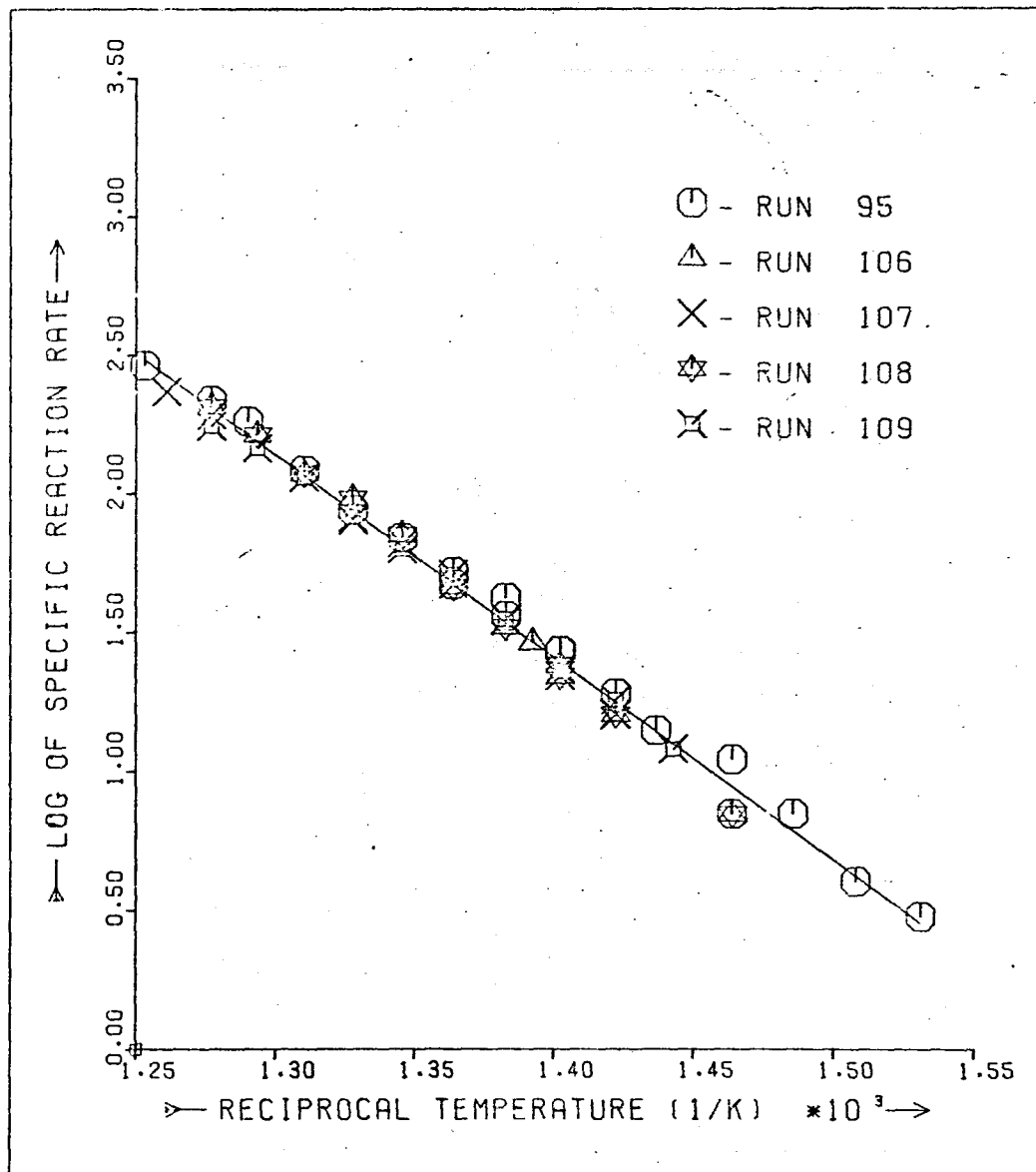


Fig. 3.3 Arrhenius plot for carbon deposition on nickel foils at low temperatures (< 820 K)

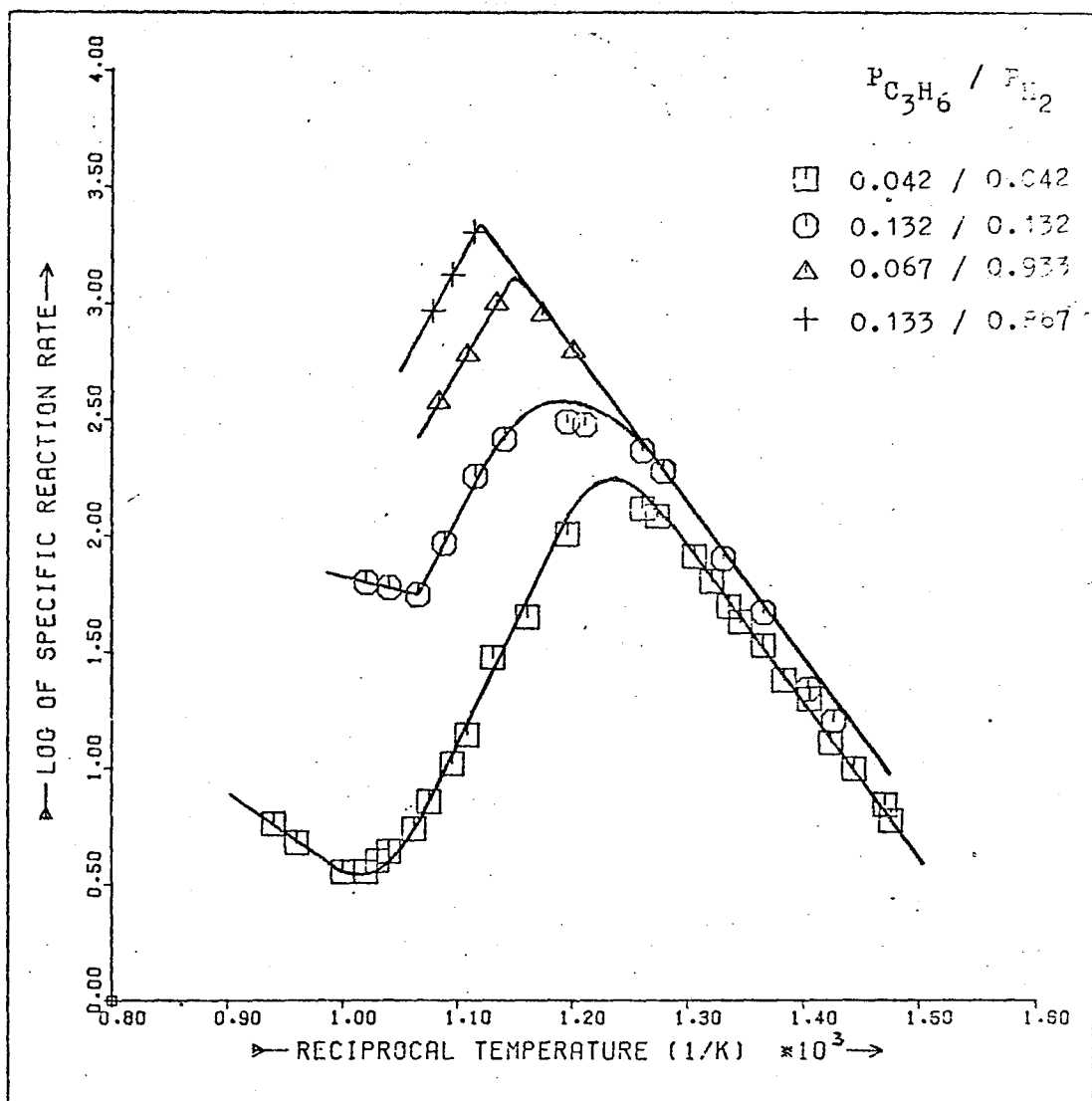


Fig. 3.4 Carbon deposition on nickel foils :
Complex temperature dependencies.

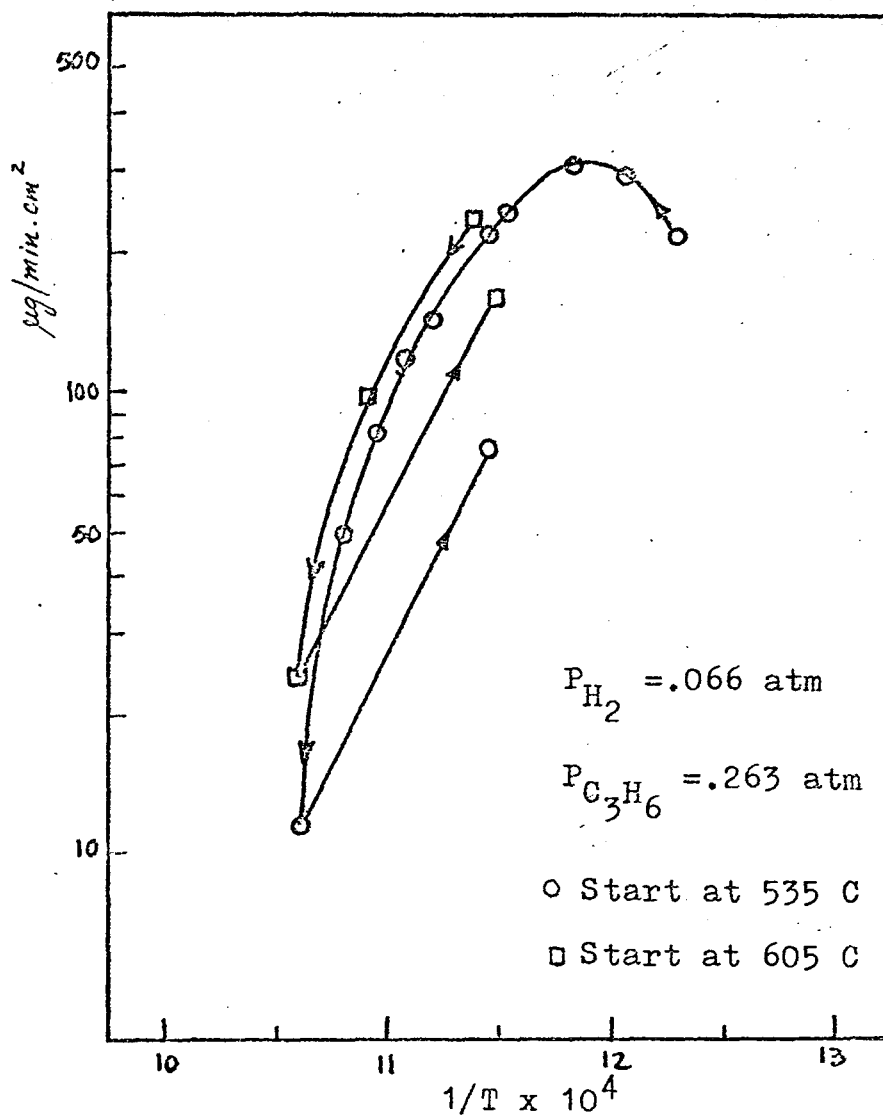


Fig. 3.5 Arrhenius plot for carbon formation, showing deactivation effects.

and certainly when $P(\text{H}_2) \approx 0.9$ atm. the slope for the intermediate temperature region yielded an apparent activation energy in the range -40 to -48 kcal/mole and the Arrhenius plot was reversible, in the sense that temperatures could be scanned up and down, original rates being always reached at each point. Even in the cases where deactivation had occurred, an apparent activation energy in the range -40 to -46 kcal/mole was observed when scanning temperatures up (Fig.3.5).

At temperatures higher than 670-700°C, rates of reaction were found to increase again with temperature. Carbon deposition was also observed to occur over the walls of the reactor and the catalyst was quickly deactivated.

In run 144, deposition was initiated at 745°C and the rate of carbon lay down was found to fall rapidly from the initial value of 46 $\mu\text{g}/\text{min}\cdot\text{cm}^2$ to 2 $\mu\text{g}/\text{min}\cdot\text{cm}^2$. When the temperature was decreased to 620°C the rate increased to 19 $\mu\text{g}/\text{min}\cdot\text{cm}^2$, and at 565°C the observed rate was 51 $\mu\text{g}/\text{min}\cdot\text{cm}^2$.

Run 318, at the same temperature, was started without hydrogen in the feed; the rate of coking was very low (0.2 $\mu\text{g}/\text{min}\cdot\text{cm}^2$) and remained constant even when the temperature was lowered to 497°C. However, upon admission of hydrogen at this temperature ($P(\text{H}_2) = 0.132$ atm), the rate of carbon formation increased to 65 $\mu\text{g}/\text{min}\cdot\text{cm}^2$.

3.2.1.4 Effect of Hydrogen

a) Low temperatures (< 540°C)

Long induction periods were observed before carbon deposition would start when no hydrogen was present in the feed gas, mainly at low partial pressures of C_3H_6 . The rate of deposition eventually obtained was lower than when hydrogen was present (cf. runs 26 and

36). The length of the induction period was found to be very much dependent on the pretreatment given to the foil, but no systematic studies of this effect were undertaken. It was observed that the extent of coking was limited to about 3 mg/cm^2 , above which the deposition would come to a complete stop (cf. Table 3.5).

Examination of the samples showed that they were evenly coated with carbon films (Fig. 3.12). Admission of hydrogen would re-start deposition, but the carbon formed was of a different, sooty, structure (Fig. 3.12).

The effect of temperature upon carbon deposition in the absence of hydrogen was studied in runs 36 and 299 (Fig. 3.7) and found to be very similar to the effect observed in the presence of hydrogen: - At low temperatures an activation energy of about 31 kcal/mole was determined, but the Arrhenius plot would start tailing off as the temperature of 540°C was approached. The rate of deposition was independent of the pressure of propylene up to about 470°C . However, increasing the temperature above 540°C had drastic effects, and the rates of deposition became negligible ($< 1 \mu\text{g/min.cm}^2$), as seen in Fig.3.6.

b) High temperatures ($> 540^\circ\text{C}$)

In the absence of hydrogen carbon deposition was found to be either non-existent or to occur up to a limited extent, very close to the solubility of carbon in nickel. A shiny graphitic deposit was observed coating the nickel foil (runs 275, 292, 297; Cf. Fig.3.12). This graphitic deposit was found to prevent further deposition if the temperature was decreased to below 540°C . However, deposition would re-start if hydrogen was admitted to the system (run 292). These results are summarized in Table 3.6.

Table 3.5 Effect of Hydrogen on Carbon Deposition at
Temperatures below 540 °C

Run	Temp °C	P _{C₃H₆} atm	P _{H₂} atm	I.T. min	Rate (*)	Observations
10	494	.132	.066	-	104	
	494	.132	0		40	
11	494	.066	0	8	37	Carbon film, no soot
23	492	.132	0	23		
36	492	.066	0	45	37	Cf. Figs. 3.6 & 3.7
293	520	.132	0	48	65	Film.Extent=3.3 mg/cm ²
	520	.132	.066		151	Restarted after H ₂ in
299	500	.132	0		56	Extent=2.9 mg/cm ²

(*) Rates of deposition expressed as $\mu\text{g}/\text{min}\cdot\text{cm}^2$

I.T. = Induction time before deposition started

Table 3.6 Effect of Hydrogen on Carbon Deposition at
Temperatures above 540 °C

Run	Temp °C	P _{C₃H₆} atm	P _{H₂} atm	Observations
275	600	.132	0	Shiny graphitic film, 50 μg (*)
276	600	.132	0	No deposition observed
291	600	.132	0	Foil pre-treated in H ₂ , 2 hr. 600°C
			.192	Deposition started
			0	Deposition stopped
292	600	.132	0	30 μg deposit (*)
	490			No deposition, no reaction (@)
			.080	Deposition started
			0	Deposition stopped
297	600	.132	0	Shiny graphitic film, 40 μg (*)
298	550	.132	0	Initial deposition (20 μg/min.cm ²) dropping quickly to <1 μg/min.cm ²)
314	600	.070	.137	Deposition rate = 33 μg/min.cm ²
			0	Deposition stops
	440			Still no deposition
			.137	Deposition starts, 38 μg/min.cm ²
			0	Deposition stops

(*) Solubility of C in the Ni foils used = 54-58 μg (150)

(@) Checked by gas chromatography

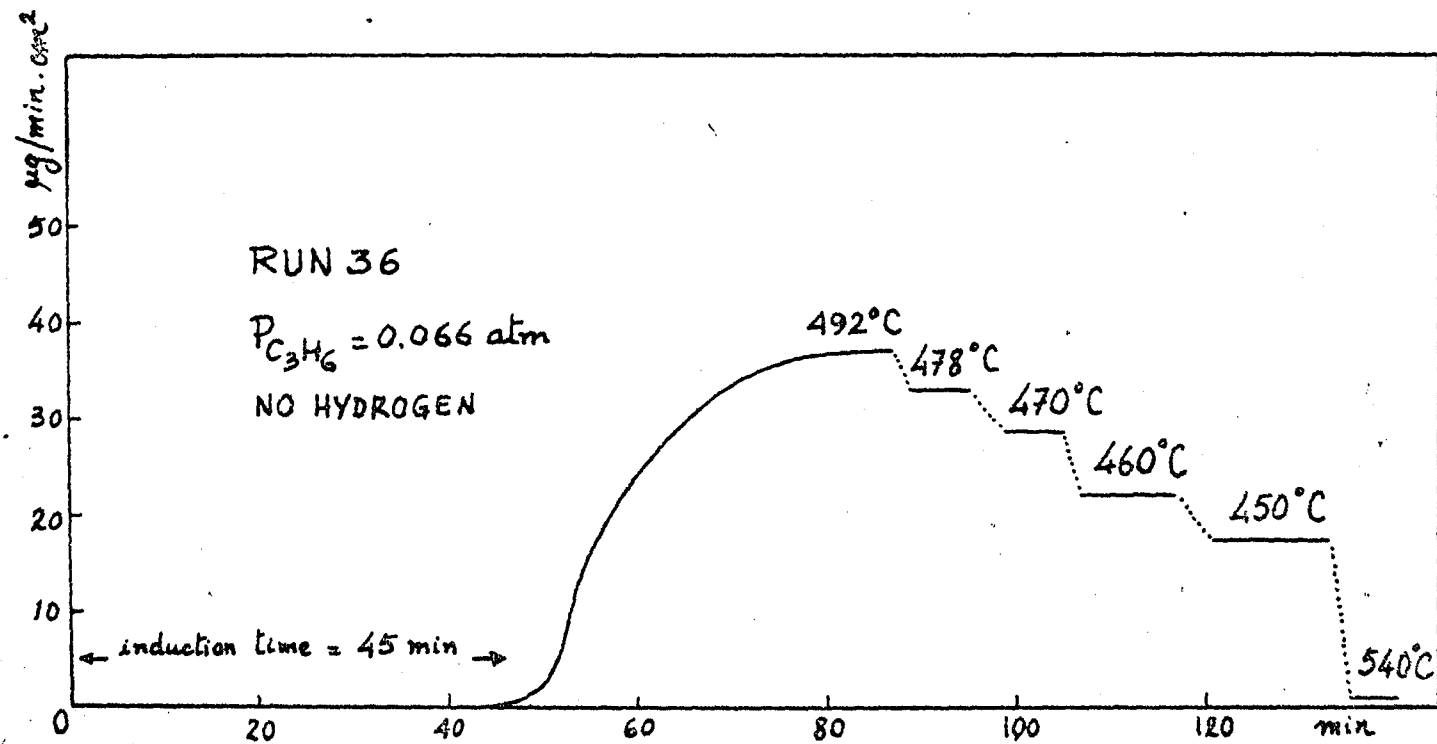


Fig. 3.6 Carbon deposition in the absence of hydrogen

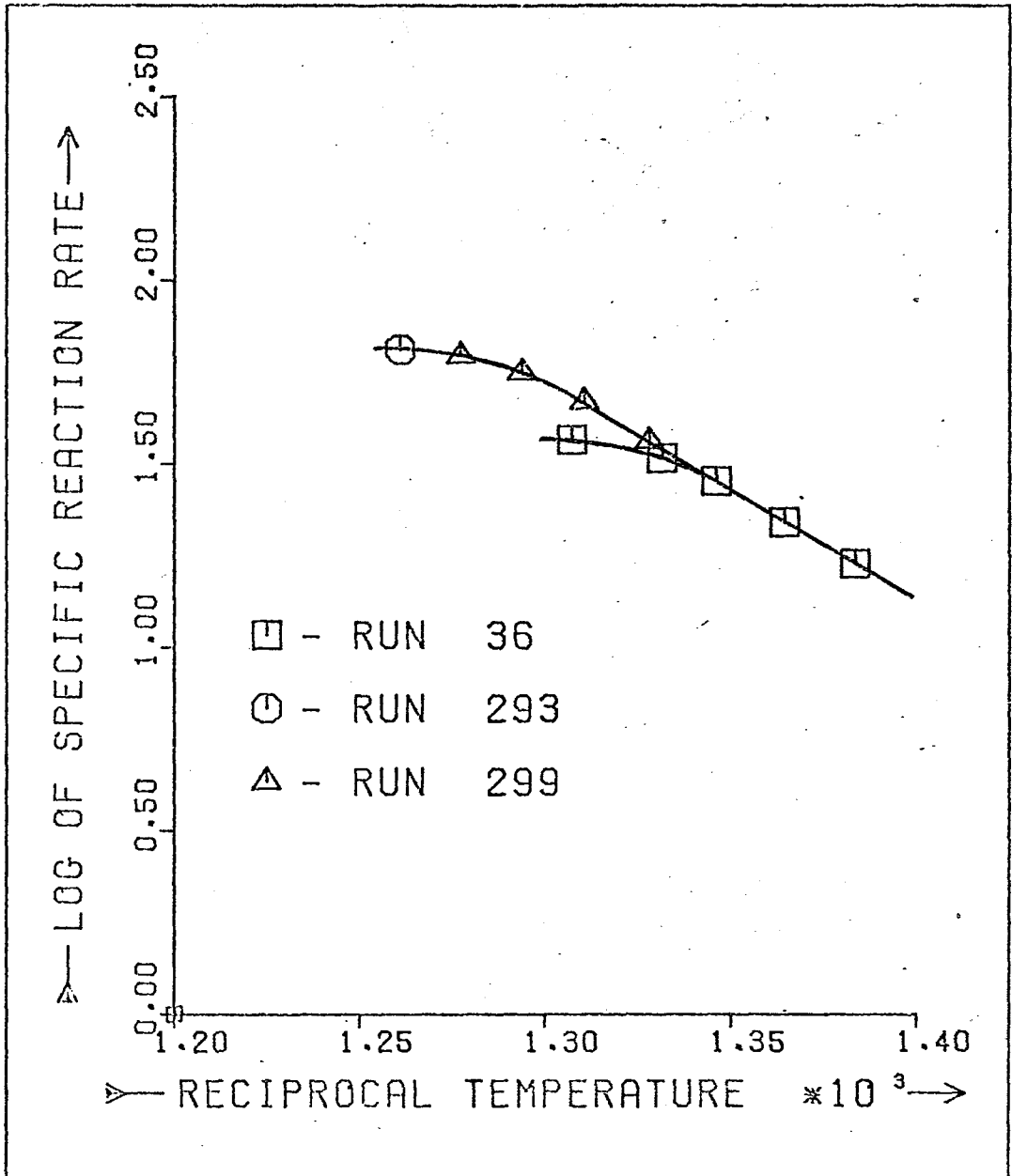


Fig. 3.7 Arrhenius plot for carbon deposition in the absence of hydrogen.

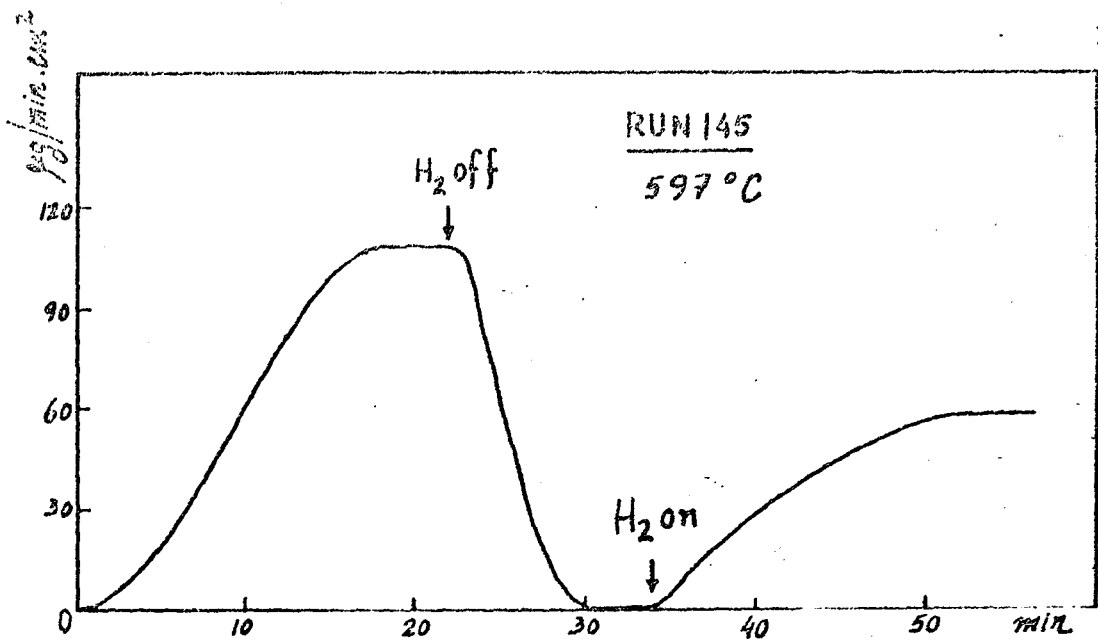


Fig. 3.8 Effect of hydrogen on carbon deposition.

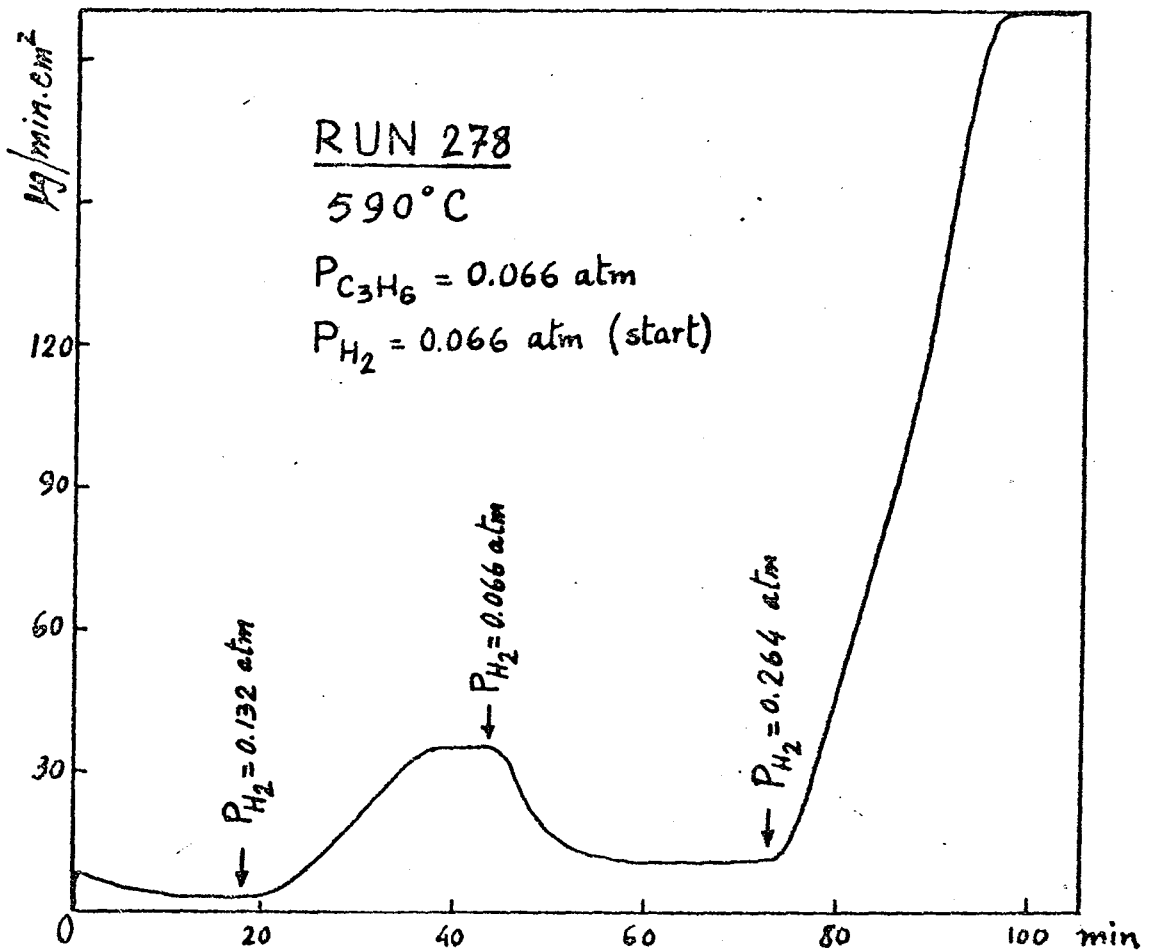


Fig. 3.9 Deactivation effects at high temperatures caused by low hydrogen pressures.

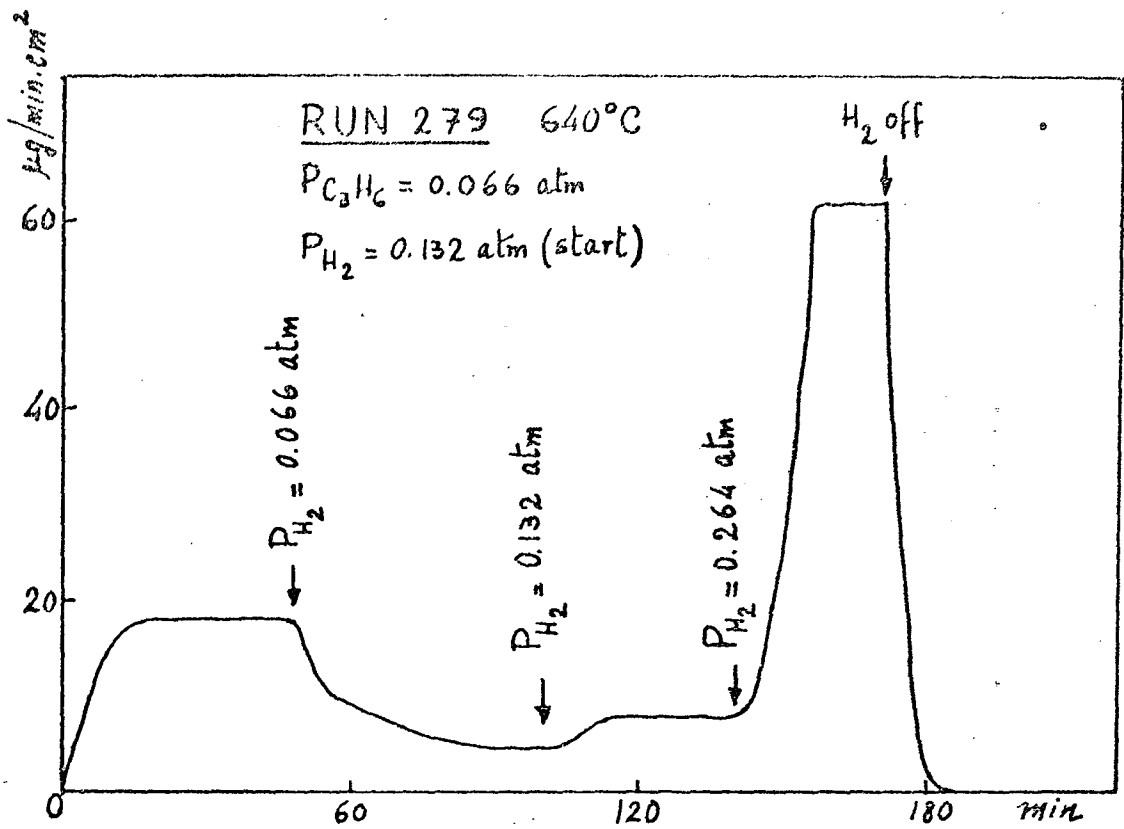


Fig. 3.10 Hydrogen effects at high temperatures.

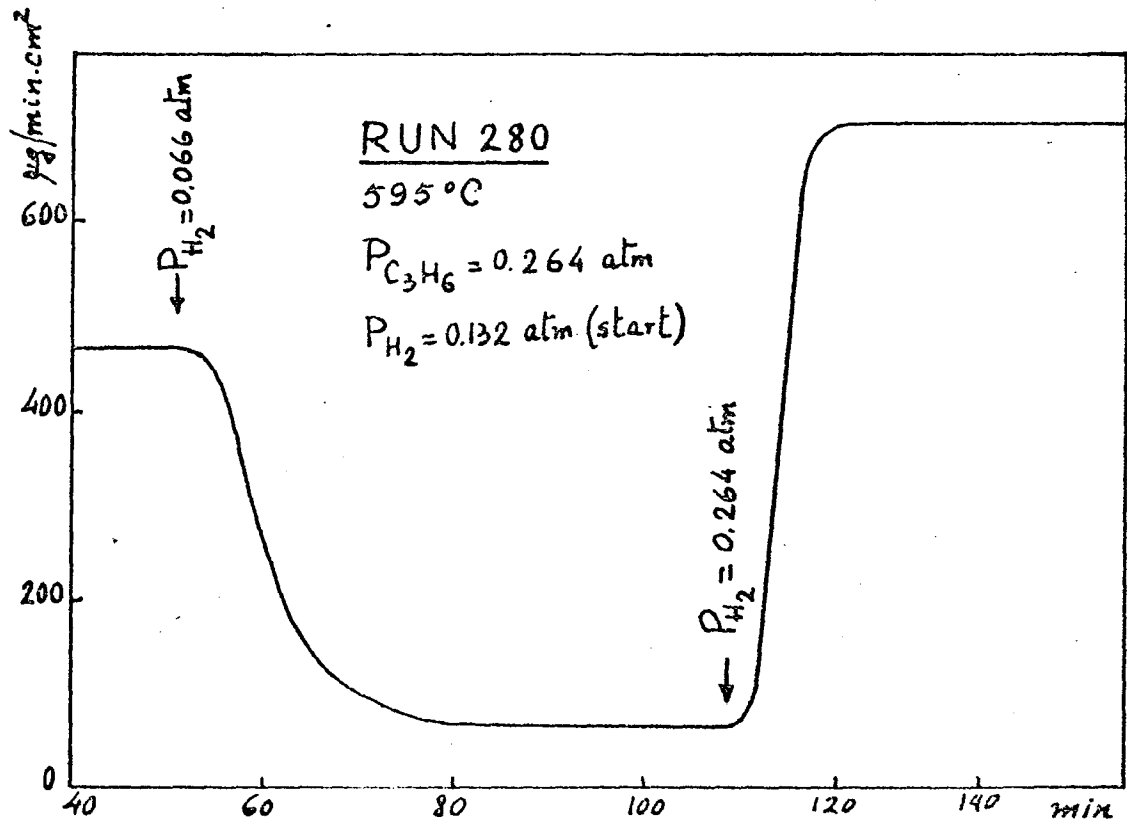


Fig. 3.11 Hydrogen effects at high temperatures.



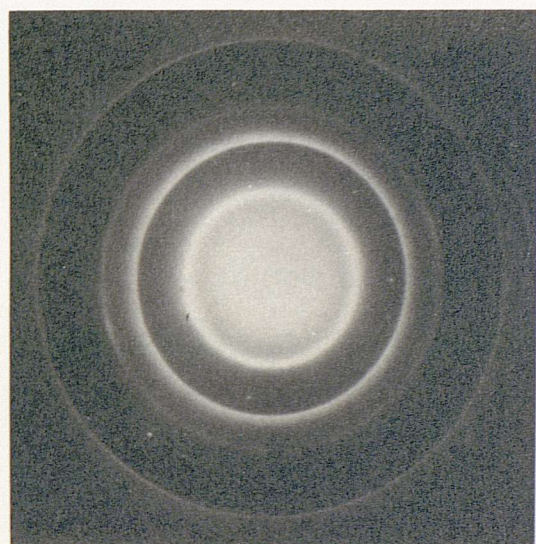
A - RUN 11 (S.E.M.) x 1500



B - RUN 20 (S.E.M.) x 1500



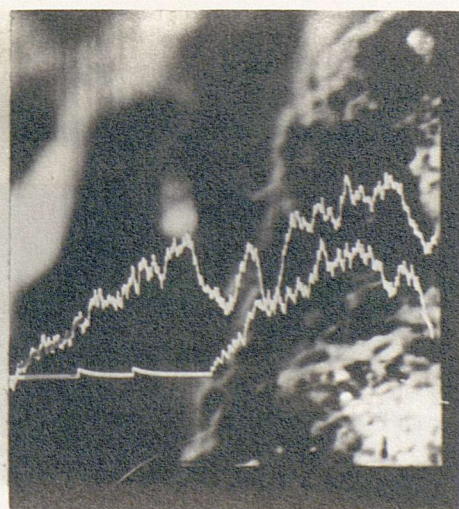
C - RUN 275 (T.E.M.) x 28000



D - RUN 275 (S.A.D.P.)



E - RUN 49 (S.E.M.) x 17000



F - RUN 203 PROBE, Ni, Al
Ni : Lower Trace

FIG. 3.12

Furthermore, if carbon deposition was initiated in the presence of hydrogen and then the hydrogen turned off, the deposition would become negligible; re-admission of hydrogen would re-start deposition, albeit at a lower rate (Fig. 3.8). It was also observed that, at these temperatures, high hydrogen partial pressures were required to maintain steady rates of deposition; otherwise, partial deactivation occurred (Figs. 3.9 - 3.11). When rates of deposition were steady, a first order dependency in the pressure of hydrogen was determined.

Very large deposits could be obtained under constant rate of deposition if the pressure of hydrogen was high (98 mg in run 281).

Pre-treatment of the nickel foils with hydrogen was not found to induce carbon formation at high temperatures in the absence of hydrogen as a reactant (run 291).

3.2.2 Carbon Deposition on Supported Nickel Catalysts

3.2.2.1 Description

The decomposition of propylene on supported catalysts was characterized by constant rates of carbon lay-down until quite large deposits were obtained. Decrease of deposition rates was eventually observed. Experimental conditions and results are shown in Table 3.7 and Fig. 3.13.

In contrast with the deposition over nickel foils, hydrogen was found to have no effect whatever on the kinetics of the process (Cf. Table 3.7, runs 325 and 326), and induction periods were never observed.

3.2.2.2 Kinetic Results

In the range 350-450°C, an activation energy of about 30 kcal/

Table 3.7 Carbon Formation on Supported Nickel Catalysts.
Experimental Conditions and Results

Run	Catalyst & load	T°C	P _{C₃H₆}	P _{H₂}	Flow rate	Rate	
	mg		atm	atm	cc/min	mg/min	
40	ICI 46-1	294	491	.115	.069	245	1.87
41	"	111	489	.115	.069	245	2.00
43	"	280	605	.132	-	230	2.50
44	"	136	600	.125	-	245	1.95
203	Ni/Al ₂ O ₃	160	500	.122	.061	245	8.
207	"	27	450	.132	-	230	1.90
208	"	29	500	.132	-	230	2.00
209	"	30	500	.132	-	345	2.00
						230	2.00
210	"	28	550	.132	-	230	1.94
211	"	26	450	.040	-	380	0.67
213	"	158	500	.071	-	323	4.5
						215	4.5
214	"	23	350	.132	-	345	0.09
						230	0.09
215	"	24	400	.044	-	345	0.45
216	"	23	450	.044	-	345	0.66
217	"	10	500	.044	-	345	0.57
218	"	18	650	.044	-	345	0.68
219	"	15	650	.044	-	345	
220	"	15	600	.044	-	345	0.68
221	"	15	450	.044	-	345	0.65
222	"	15	400	.044	-	345	0.32
224	Ni/kieselguhr	11	400	.066	-	227	0.88

Table 3.7 (Continued)

Run	Catalyst & load mg	T°C	P _{C₃H₆} atm	P _{H₂} atm	Flow rate cc/min	Rate mg/min
225	Ni/kieselguhr 11	400	.066	-	227	0.88
236	Ni/Al ₂ O ₃ 183	600	.197	-	124	1.9
256	" 17	600	.500	-	240	8.0
257	" 17	640	.500	-	240	7.4
258	" 17	580	.500	-	240	8.0
259	" 17	580	.500	-	440	8.6
261	" 161	500	.132	-	230	4.0
262	" 187	500	.132	-	230	6.8
265	" 28	600	.132	.132	270	2.0
266	" 17	550	.132	.132	270	2.0
267	ICI 46-1 23	550	.132	.132	270	1.9
268	" 20	400	.132	.132	270	0.74
271	Ni/kieselguhr 15	400	.132	-	270	1.43
272	" 16	600	.132	-	270	1.90
273	Ni/Al ₂ O ₃ 16	550	.132	-	345	1.71
274	" 15	650	.132	-	270	1.55
277	" 23	350	.044	-	345	0.09
325	" 26	400	.132	.132	270	0.667
				-		0.70
326	" 26	590	.132	.132	270	2.75
				-		2.00
				.132		2.00
327	" 32	600	.132	.132	270	2.00
328	" 32	600	.132	.132	270	2.16
329	" 32	600	.132	.132	270	2.55

Table 3.7 (Continued)

Run	Catalyst & load mg	T°C	P _{C₃H₆} atm	P _{H₂} atm	Flow rate cc/min	Rate mg/min	
330	Ni/Al ₂ O ₃	32	600	.132	.132	270	1.80
331	"	32	600	.132	.132	270	2.07
332	"	32	550	.132	.132	270	2.50
333	"	32	600	.132	.132	270	2.50
335	ICI 46-1	33	400	.132	.132	270	0.09
344	Ni/Al ₂ O ₃	5.3	400	.132	.132	270	0.10

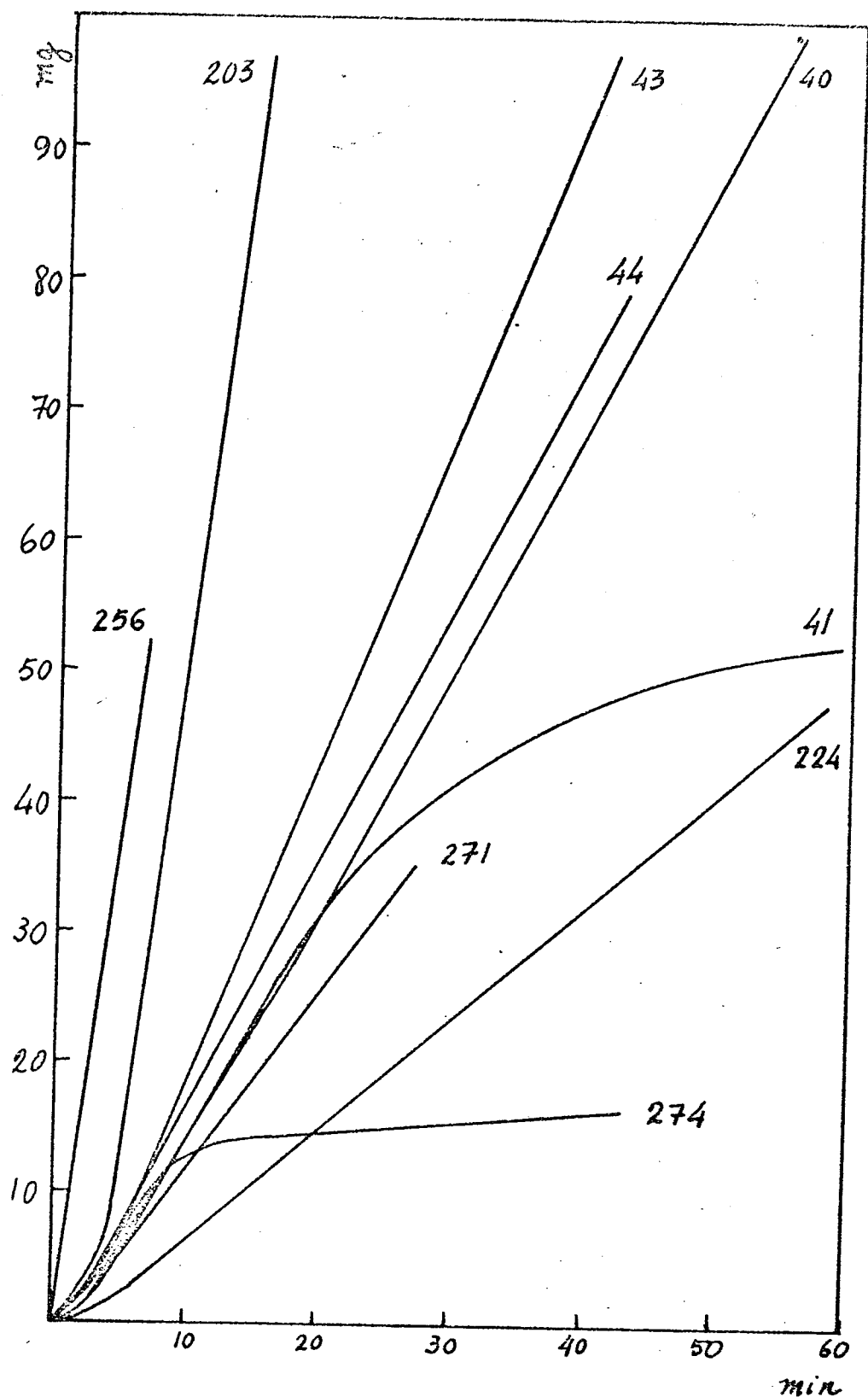


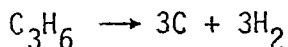
Fig. 3.13 Carbon deposition on supported nickel catalysts.

mole was determined for deposition over the nickel-alumina catalyst, and the reaction was of zero order (Fig.3.14). At higher temperatures, the reaction was found to be controlled by mass transfer, becoming of first order and practically temperature independent.

Analysis of the gas effluent at low temperatures (400°C) showed that hydrogen was being produced, no other products being detected. At 600°C, small amounts of CH₄ were also found.

Complete mass balances could be established although the errors involved could be too high. In fact, very low conversions were obtained (3-5%) and the errors involved in the complete gas chromatographic analysis were of the same order of magnitude. Therefore, it was decided to simplify the calculations, neglecting the change in volume with reaction. Since the total flow rates of the feed and effluent gases were measured by rotameters, calibrated (by soap bubble-meter) with an accuracy not greater than 3%, this procedure seems to be justified.

The results are presented in Table 3.8 and show that the decomposition of propylene, at least at low temperatures, could be explained in terms of the scheme:



When hydrogen was present in the feed, some methane was detected among the products, even at 400°C, as can be seen in Table 3.9.

3.2.2.3 Film Diffusion

Above 450°C, carbon deposition over the supported nickel catalysts was clearly limited by diffusion of the reactant from the gas phase to the surface of the catalyst. Apart from the kinetic

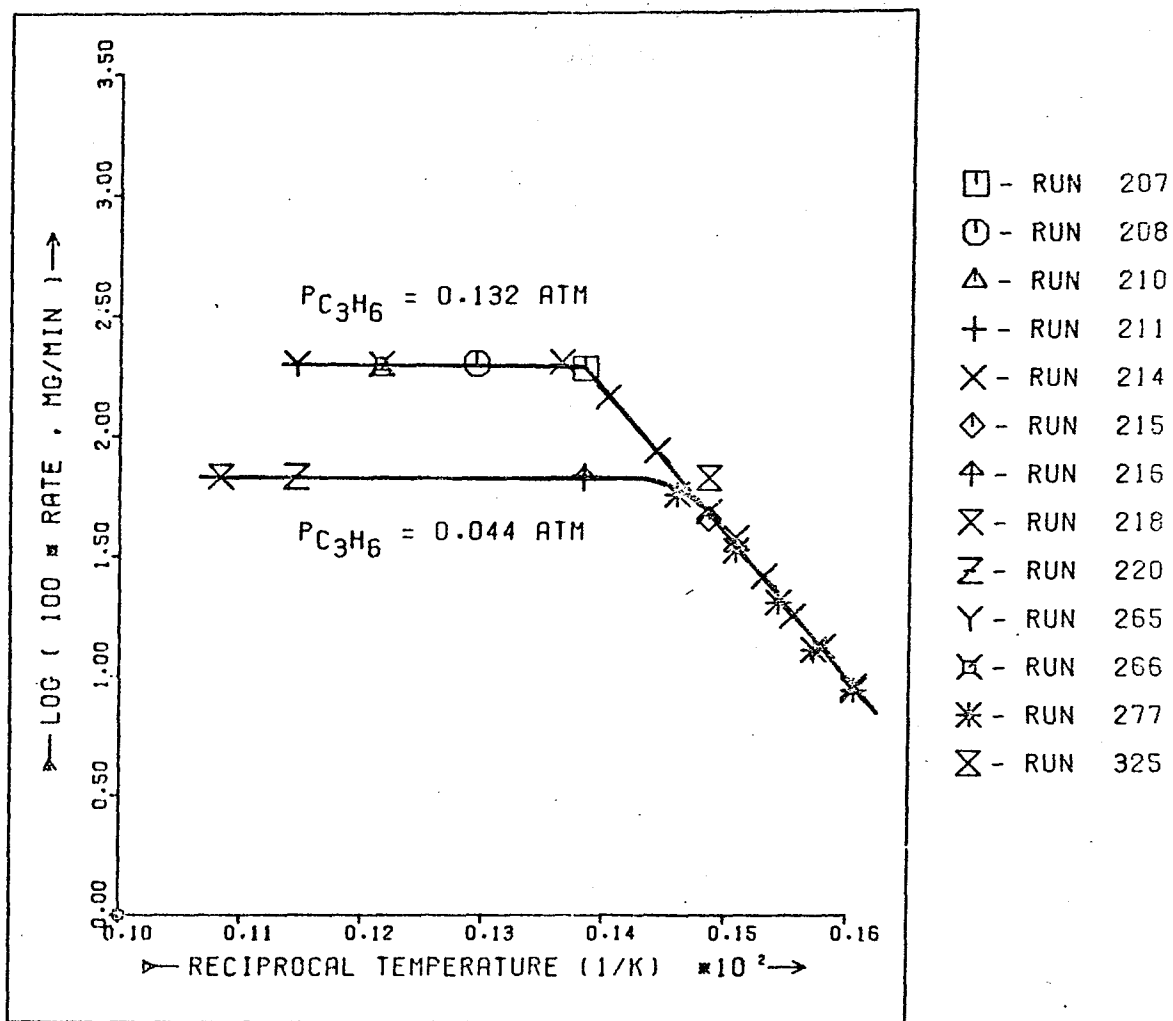


Fig. 3.14 Arrhenius plot for carbon formation on supported nickel catalysts.

Table 3.8 Decomposition of Propylene over Nickel Catalysts

Feed : C₃H₆/N₂

Run	T°C	Flow Rate mole/hr	Rate(C) mg/min	Gas Analysis mole fraction	Products out	
					H ₂ mole/hr x 10 ³	C
214	420	0.57±3%	0.87±5%	H ₂ =0.0080±5% CH ₄ =0	4.6±.3	4.3±.2
271	400	0.67±3%	1.43±5%	H ₂ =0.0100±5% CH ₄ =0	6.7±.5	7.1±.3
272	600	0.67±3%	1.90±5%	H ₂ =0.0150±5% CH ₄ =0.001±20%	10.±.8 1.4±.2 <u>11.±1.</u>	9.5±.5 0.7±.1 <u>10.2±.6</u>
273	550	0.67±3%	1.70±5%	H ₂ =0.0126±5% CH ₄ =0.001±20%	8.5±.7 1.4±.2 <u>9.9±.9</u>	8.5±.4 .7±.1 <u>9.2±.5</u>
274	650	0.67±3%	1.55±5%	H ₂ =0.0120±5% CH ₄ =0.001±20%	8.1±.7 1.4±.2 <u>9.5±.9</u>	7.8±.4 .7±.1 <u>8.5±.5</u>

Table 3.9 Decomposition of Propylene over Nickel Catalysts

Feed : $C_3H_6/H_2/N_2$

Run	T°C	Flow rate mole/hr	Rate(C) mg/min	CH ₄ out mole frac. ⁿ	Production rate mole/hr x 10 ³ C CH ₄	
265	600	0.67±3%	2.00±5%	.004±10%	10.0±.5	2.7±.3
266	550	0.69±3%	2.00±5%	.003±10%	10.0±.5	1.9±.2
267	550	0.67±3%	2.00±5%	.003±10%	10.0±.5	1.9±.2
268	400	0.67±3%	0.74±5%	.001±20%	3.7±.2	0.7±.1

Table 3.10 Decomposition of Propylene over Ni/Al₂O₃

Catalyst in Fixed-Bed Reactor

Run	T°C	Load mg	P _{C₃H₆} atm	Flow Rates C ₃ H ₆ total mole/hr		Analysis mole frac. ⁿ	Rate(C) * mg/min
284	600	20	0.10	.054	.52	H ₂ = .015 CH ₄ = .001	1.66
285	400	20	0.10	.054	.52	H ₂ = .0027 CH ₄ = 0	0.28
286	550	20	0.11	.054	.48	H ₂ = .055 CH ₄ = .001	5.38

* Rate of carbon formation calculated from mass balances:

$$\text{Rate(C)} = 200 \times (\text{total flow rate}) \times (\text{mole frac.}^n \text{ H}_2 + \text{mole frac.}^n \text{ CH}_4)$$

observations mentioned (temperature independency and first order), deposition rates were found to be nearly independent of the mass of catalyst sample. In some instances (runs 203, 213, 236) catalyst pellets were suspended from the microbalance. After coking, these pellets were cut in half and observed both under the optical microscope and the stereoscan electron microscope:

Carbon was found to be deposited near the external surface of the catalyst. All these observations suggest that the concentration of reactant at the catalyst surface was much lower than in the bulk. Such a concentration gradient could be established across the boundary layer as a result of a very fast surface reaction, film diffusion becoming rate controlling. The usual way of avoiding these mass transfer problems is to increase the total flow rate through the reactor. This was attempted (Cf. Table 3.7) but without success, since experimental limitations prevented the use of very large flow rates (which would cause too much noise in the microbalance).

The onset of diffusion limitations was also confirmed by calculation:

For the case of suspended pellets, the concentration gradient across the boundary layer can be calculated from the mass transfer coefficient obtained by application of the well known expression for a single particle(155):

$$(a) \quad \frac{k_m \cdot d_p}{D} = 2 \times (1 + 0.276 \text{Re}^{\frac{1}{2}} \cdot \text{Sc}^{\frac{1}{3}})$$

where

k_m = mass transfer coefficient

d_p = equivalent particle diameter

D = diffusivity of C_3H_6 in the reactant mixture

Re = Reynolds number = $d_p \cdot G / \mu$

Sc = Schmidt number = $\mu / \rho \cdot D$

μ = viscosity of gas

ρ = specific gravity of gas

G = mass velocity

For run 203, the following data were obtained:

Catalyst : Ni/Al₂O₃, cylindrical pellet, 4.7 x 4.7mm, 171.2 mg

A = external area = 1cm²

V = volume = 80mm³

Observed rate = 8mg/min of coke deposited = 0.243 cm³.atm.sec⁻¹
of C₃H₆ converted

Feed flow rate = 245cm³/min

Feed composition, mole fraction:

$$C_3H_6 = 0.122, H_2 = 0.061, N_2 = 0.817$$

The following properties were estimated by standard procedures at 800K (Cf. for example references 8 and 156):

$$\mu = 3.5 \times 10^{-4} \text{ g/sec.cm}$$

$$\rho = 4.1 \times 10^{-4} \text{ g/cm}^3$$

$$D = 0.69 \text{ cm}^2/\text{sec}$$

Then:

$$d_p = (6V/\pi)^{\frac{1}{3}} = 0.533 \text{ cm}$$

$$G = 0.0049 \text{ g/sec.cm}^2$$

$$Sc = 1.23$$

$$Re = 7.6$$

and, from (a), $k_m = 4.70 \text{ cm/sec}$. Since rate = $k_m \cdot A \cdot \Delta P$ (where ΔP is the partial pressure gradient in atm) it follows that $\Delta P/P = 0.5$

for $P = 0.122$ atm of C_3H_6 .

$\Delta P/P$ is then greater than 0.1 and, if 10% accuracy is required, the film gradient cannot be neglected (157).

For the case of catalyst particles in a silica basket suspended from the microbalance, calculations become more difficult since there is no way to determine the flow pattern. But qualitatively, at least, this case seems to be even worse than the case of the single pellet.

3.2.2.4 Fixed-Bed Experiments

In order to avoid these limitations, a few runs were carried out in the tubular fixed-bed reactor described in section 2.2.2. These results are shown in Table 3.10, rates of carbon deposition being calculated by mass balances. Although a larger number of experiments would be needed to establish a complete picture of the temperature dependency for carbon deposition, the results obtained suggest that a maximum in rate would be observed at around $550^\circ C$, as in the case of nickel foils.

3.2.2.5 Surface Area Measurements

All catalysts were characterized by nitrogen adsorption and carbon monoxide chemisorption as explained in Chapter 2. The results are shown in Table 2.5.

The total surface area of the Ni/Al_2O_3 catalyst was also measured before and after coking, the same value being obtained, namely, $14m^2/g$ (Cf. Table 3.11). This seems to indicate that no pore-mouth blocking occurs, at least with moderate coke deposits.

Table 3.11 B.E.T. Surface Area of Ni/Al₂O₃ Catalyst

Run	Catalyst pellet	Total S.A. m ² /g	Coke S.A. m ² /g	Catalyst Specific S.A. m ² /g
A25	before coking	2.32	-	14
A26	after coking	2.78	0.49	14

Coking conditions : 500 °C , P_{C₃H₆} = 0.13 atm

Pellet : 161 mg

Coke deposited : 3.65 mg

Deposition rate : 2.3 mg/min

3.2.3 Other Carbon Deposition Studies

In order to establish the catalytic nature of the decomposition of propylene over nickel, several runs were carried out with nickel foils previously poisoned or coated.

Poisoning was achieved by vaporizing about 1cm^3 of ethanethiol in the reactor. To coat the foil surface, the specimens were immersed in a colloidal suspension of graphite (Acheson dag n^o.580).

One of the samples was immersed in nickel nitrate melt, heated up to 450°C to decompose the nitrate and reduced in hydrogen flow for 1 hour at 600°C . This procedure is similar to the method of preparation of the catalyst $\text{Ni}/\text{Al}_2\text{O}_3$.

The results are presented in Table 3.12 and show that no carbon deposition occurred over the sulphur poisoned sample or over the graphite coatings.

Carbon deposition was however observed over the foil with fresh nickel deposited, even in the absence of hydrogen.

Deposition was also attempted over a number of carbon samples:

- Activated carbon ($565\text{ m}^2/\text{g}$), in particles of 14-40 mesh;
- Graphite rod (density = $1.9^{\pm}0.1$);
- Carbons obtained over nickel foils in previous runs.

The results are presented in Table 3.13 and show that carbon deposition did not occur over the activated carbon and graphite rod samples; indeed, the small weight uptake observed in these runs was due to deposition on the silica basket used, as was determined by comparison with a blank and also by weighing separately the basket and the samples, before and after reaction.

In contrast with this, fast deposition of carbon was observed over the samples collected from previously used nickel foils, and the rates observed were of the same order of magnitude of the rates observed over nickel foils.

Table 3.12 Carbon Deposition over Various Substrates

Run	T°C	P(C ₃ H ₆) atm	Substrate	Carbon formed
313	630	0.13	Ni foil coated with Ni nitrate melt, calcined & reduced in H ₂ . Fresh Ni=9 mg	180 μg/min dropping to 50 μg/min + H ₂ : 300 μg/min H ₂ off: decrease
315	500	0.13	Ni foil coated with graphite dag	Induction period & speed-up to 208 μg/min *
316 & 317	500	0.13	Ni foil half-coated with graphite dag (with H ₂ = 0.13 atm)	Sooty carbon on uncoated half
319	600	0.13	Ni foil half-coated with graphite dag (with H ₂ = 0.13 atm)	Sooty carbon on uncoated half
323	550	0.13	Coked foil from run 322, poisoned with ethanethiol (with H ₂ = 0.13 atm)	No deposition

* Coating peeled off and carbon formed directly on the uncovered surface of the foil.

Table 3.13 Carbon Formation over Various Carbon Samples

Run	T°C	P _{H₂}	P _{C₃H₆}	Substrate	Rate, $\mu\text{g}/\text{min}$
301	550	.13	.13	4.9 mg coke from run 290	650.
		0			0
		.13			510.
302	550	.13	.13	9.2 mg activated carbon	3.8
		0		14-40 mesh, 565 m ² /g	3.3
305	550	.13	.13	82 mg graphite rod, 3 mm	3.4
		0		diameter, 141 mm long	0.9
		.13	.26	density = 1.9 \pm .1 g/cc	1.6 *
343	590	.52	.13	100 mg coke from run 342	1.11
blank	550	.13	.13	Silica basket, empty	10

* At the end, find basket coked, graphite sample not.

Table 3.14 Carbon Formation on Alumina Samples

Run	T°C	P _{C₃H₆} atm	α-Al ₂ O ₃ sample	Rate μg/min	Gas analysis
294	650	.13	127 mg, pellet	2	traces: H ₂ , CH ₄
295	600	.13	76 mg, BSS 40/60	3→1.2	
		+H ₂		2	
296	600	.13	135 mg pellet + Ni foil, 3.12 cm ²	total 90	H ₂ =5x10 ⁻⁶ mole/min *

* At the end, find foil coated with shiny graphitic film

In order to establish the effect of the support on carbon deposition, several runs were carried out with α - Al_2O_3 (as used in the first step of the preparation of the $\text{Ni}/\text{Al}_2\text{O}_3$ catalysts). The results are presented in Table 3.14 and show that at high temperatures (600°C) some carbon deposition is observed over the alumina support. In one case, a pellet of alumina was suspended from the micro balance together with a nickel foil. At the end, the foil was found to be coated with the same graphitic deposit characteristic of runs carried out at high temperature in the absence of hydrogen, on top of which some disordered carbon was growing, but only in the face of the foil near to the alumina pellet.

3.2.4 Characterization of the Carbon Deposits

3.2.4.1 Carbon from Nickel Foils

Coked nickel foils were examined in the scanning electron microscope (S.E.M.) and by X-ray diffraction. The presence or absence of hydrogen in the course of the deposition was found to affect the structure of the carbons obtained. Stereoscan pictures showed that deposits obtained in the presence of hydrogen were more disordered and sooty (Fig. 3.12 A and B). At high temperatures ($> 540^\circ\text{C}$) polycrystalline graphite films were obtained in the absence of hydrogen, as shown in the transmission electron micrograph (T.E.M.) of Fig. 3.12C. Selected area diffraction patterns (S.A.D.P.) were also obtained (Fig. 3.12D): the diffuse rings follow the graphite pattern.

Severe disruption of the surface of the foil is shown in Fig. 3.12E, after removing the carbon by gasification with H_2O . X-ray diffraction analysis revealed the presence of graphite, and some interstitial uptake of carbon by the nickel was also evidenced by

Table 3.15 X-Ray Diffraction of Coked Nickel Foils

Diffraction angles (2θ)				
Ni foil (blank)	ASTM Ni	Run 11	Run 20	ASTM Ni _x C
76.40	76.37	76.22	76.18	75.44
92.96	92.94	92.75	92.75	92.42
			92.50	
98.48	98.44	98.35	98.20	98.06
			98.00	

Table 3.16 Elemental Analysis of Carbon Deposits from Nickel Foils (C,H)

Run	C %	H ₂ %	Balance to 100%	C:H atomic ratio
12	96.36	0.94	2.70	8.6:1
15	95.30	1.38	3.32	5.8:1
20	95.98	1.19	2.83	6.7:1
28	97.05	1.21	1.74	6.7:1

the diffraction peaks falling between the theoretical values for pure nickel and nickel carbide. This is shown in Table 3.15.

Elemental microanalysis of the carbons obtained in some runs is shown in Table 3.16. Comparison with the experimental conditions used for deposition of carbon did not show any trend in these results.

The balance to 100% was attributed to the presence of nickel in the deposits and confirmed by wet chemistry. In fact, analysis of several carbon deposits revealed the presence of nickel in concentrations of about $1.6 \pm 0.4\%$ in weight. The results, as plotted in Fig. 3.15, clearly show the existence of a linear relationship between the amount of nickel determined and the weight of coke deposited.

The carbon deposit obtained in run 300 was also characterized by nitrogen adsorption at 77K. Two determinations were made, showing good reproducibility. The adsorption-desorption isotherm (corrected for buoyancy effects) is represented in Fig. 3.16, showing a narrow hysteresis loop. The corresponding pore size distribution, as calculated by the method described in (152), is represented in Fig. 3.17, showing a peak for pores of 19\AA . The calculated parameters of the pore structure are shown in Table 3.17. The BET surface area of the carbon was taken as $109 \pm 7 \text{ m}^2/\text{g}$.

3.2.4.2 Carbon from Supported Catalysts

Several samples of carbon were collected from the outer part of thick deposits obtained on supported nickel catalysts and were analysed. The results, shown in Table 3.18, reveal the presence in the carbon of both nickel and support material. The same samples were analysed by X-ray diffraction. The phases identified were nickel and graphite for run 183, and nickel, graphite and α -alumina for the others.

Table 3.17 Characterization of Carbon from Nickel Foil
by Nitrogen Adsorption (from run 300)

Run	BET m^2/g	Pore volume V_p cm^3/g	Cum. V_p cm^3/g	Apparent density	Porosity	Cum.SA m^2/g
A27	103	0.17	0.18	1.56	0.3	
A28	116	0.17	0.18	1.62	0.3	202

N.B. Pore volume calculated from the Gurvitsch rule .

Table 3.18 Analysis of Deposits Obtained over Supported
Catalysts

Run	Catalyst	C wt %	Ni wt %	Support wt %
183	Ni/kieselguhr	94.2 \pm .2	2.42 \pm .1	3.4 \pm .3
204	Ni/Al ₂ O ₃	80.8 \pm .5	2.70 \pm .1	16.5 \pm .6
203	"	80.2 \pm .3	2.98 \pm .1	16.8 \pm .4
192	"	85.8 \pm .2	1.73 \pm .1	12.5 \pm .3

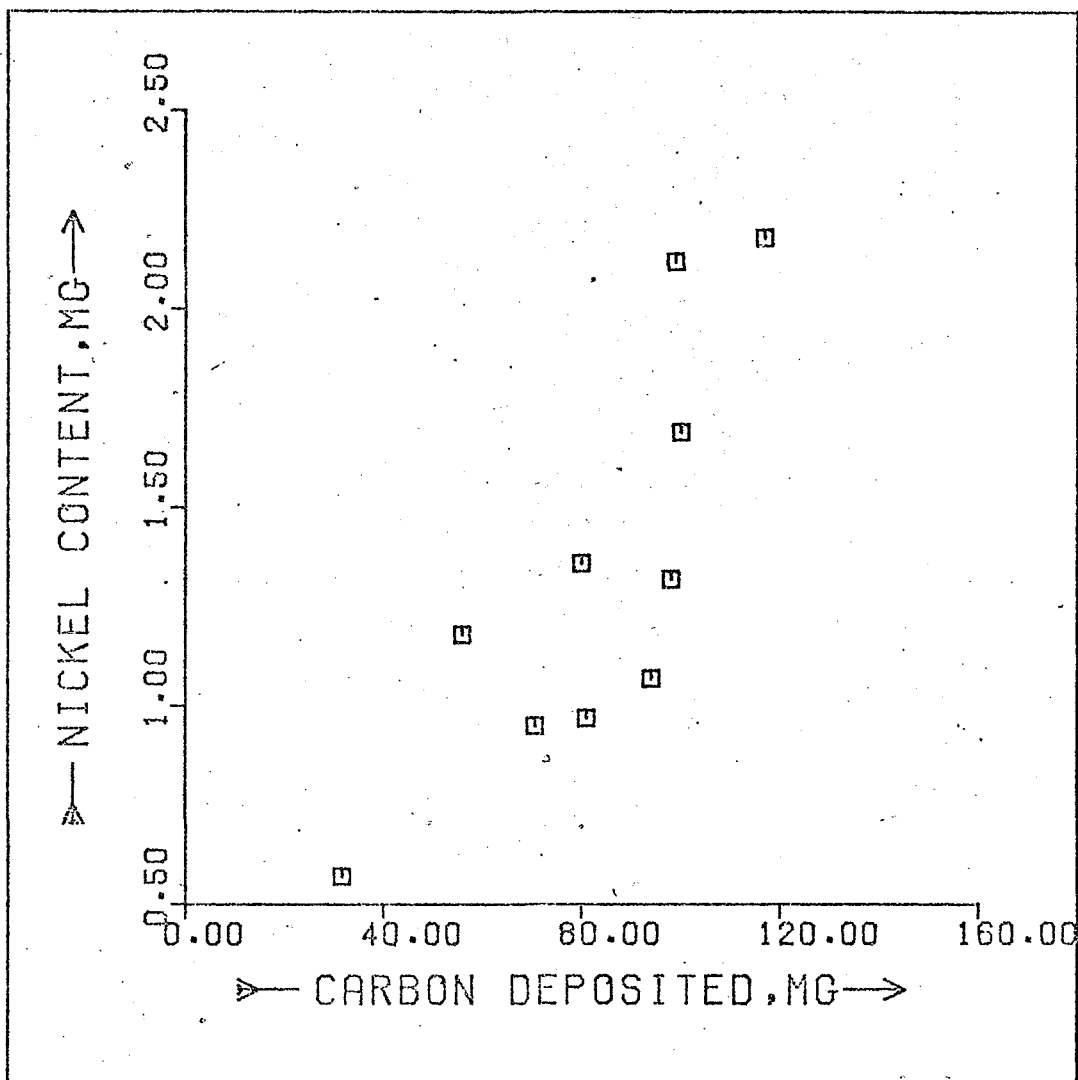


Fig. 3.15 Amount of nickel in carbon deposited over nickel foils.

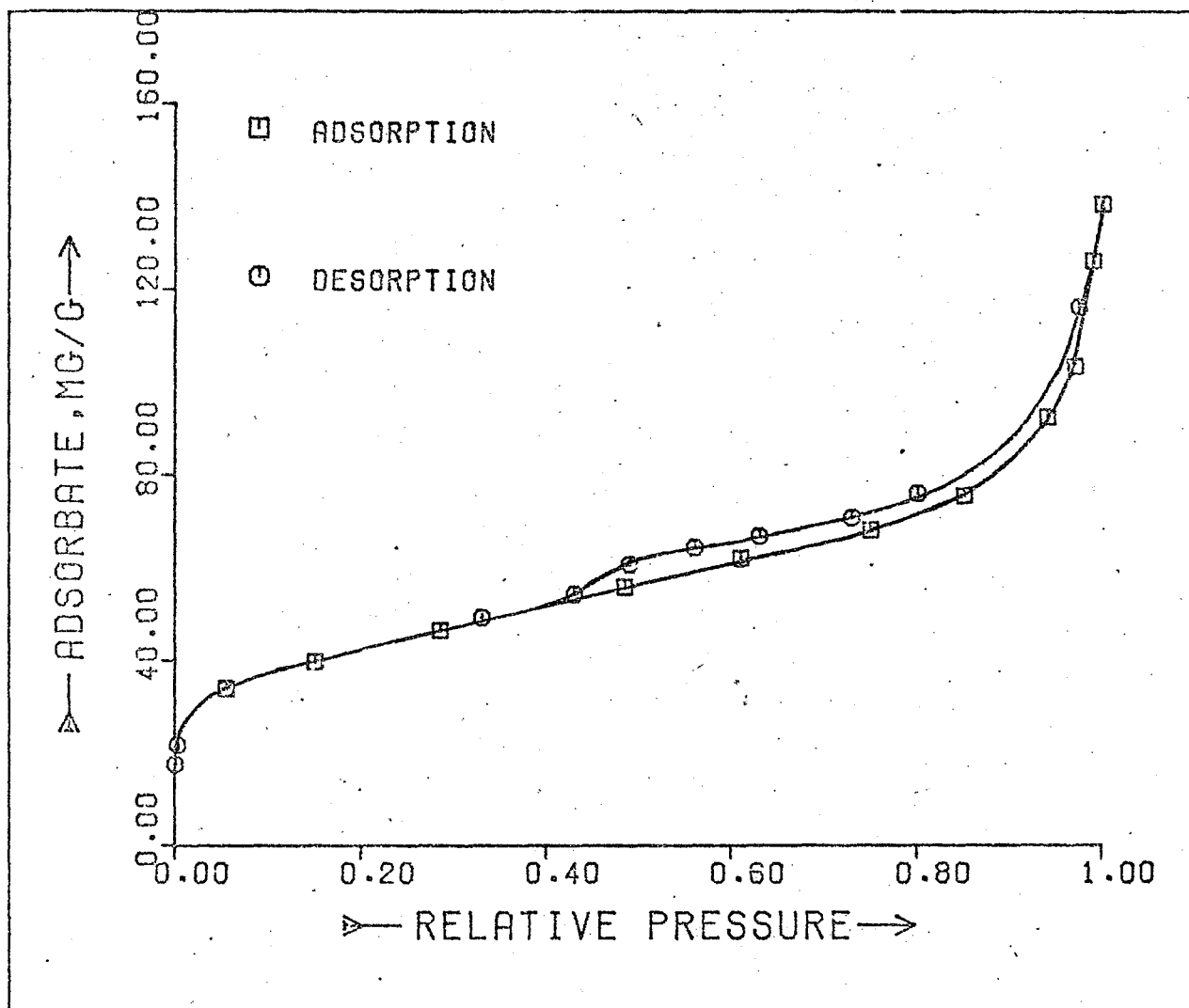


Fig. 3.16 Nitrogen adsorption isotherm for carbon deposited on nickel foil (Run 300)

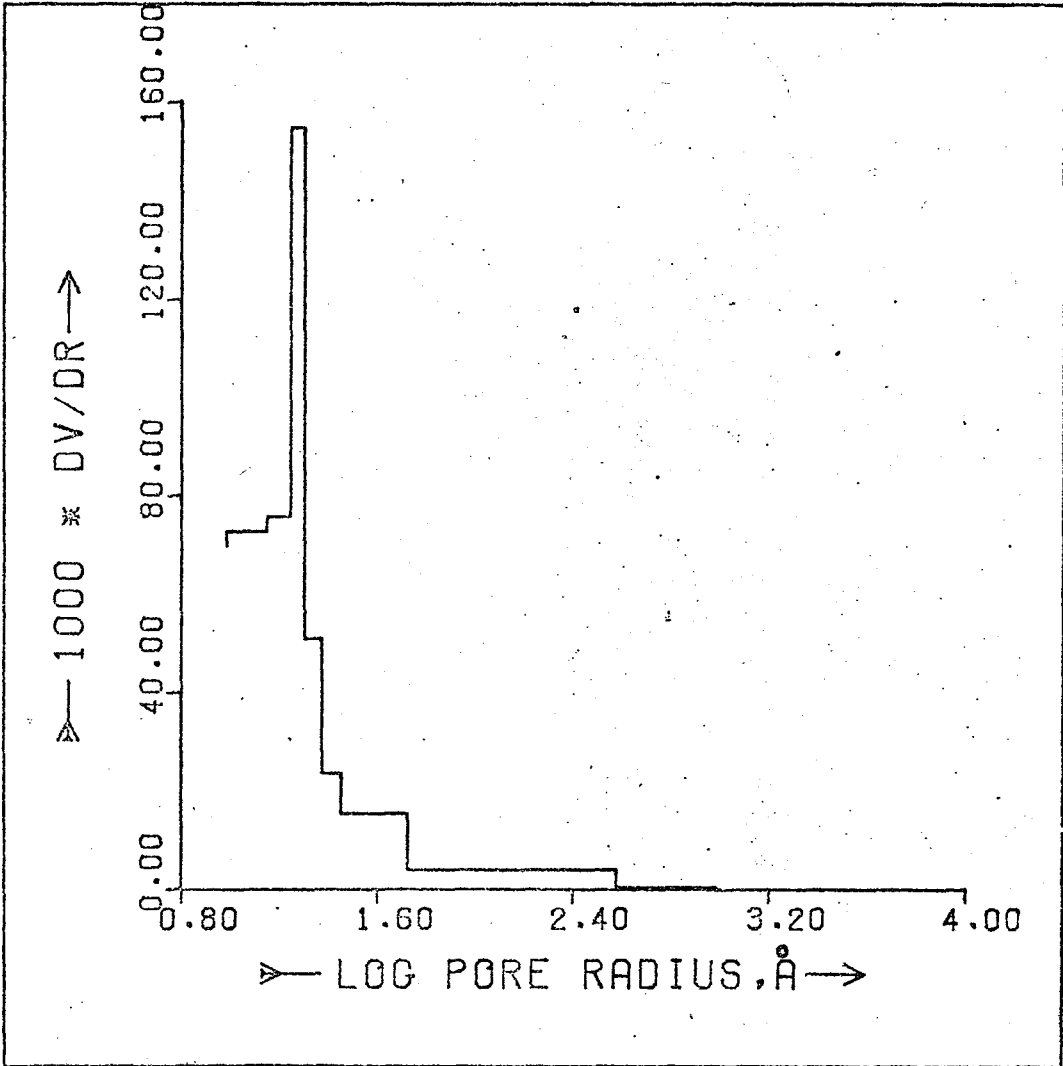


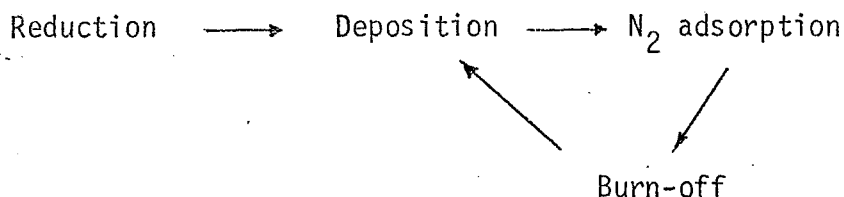
Fig. 3.17 Pore size distribution for carbon deposited on nickel foil (Run 300)

Two weak lines in the Debye-Scherrer photographs were left unidentified, but could not be due to either NiO or Ni(OH)₂.

Two catalyst pellets were coked (runs 203 and 236), sectioned and analysed by electron probe both across the section and along the external cylindrical surface. The coke deposit was about 100-200 μm thick, and penetration of the beam, even in such a light material as coke, would hardly exceed 10 μm . The results showed clearly that both Ni and Al reach the surface of the carbon deposits (Fig.3.12F).

Some carbon deposits obtained on Ni/Al₂O₃ catalysts were characterized by nitrogen adsorption. A complete isotherm for the deposit obtained in run 259 is presented in Fig.3.18 and the calculated values for pore volume, surface area, average pore radius, apparent density and porosity are shown in Table 3.19.

The surface area of carbons obtained on fresh catalyst samples was found to be $133 \pm 3 \text{ m}^2/\text{g}$. It is interesting to note that a higher surface area ($191 \text{ m}^2/\text{g}$) was obtained for carbon deposited (run 259) on a catalyst that had been previously used in a series of 25 runs, involving carbon deposition and its subsequent gasification with water vapour. In the series of runs shown in Table 3.20 the same sample of catalyst was used throughout. The sequence of experiments was:



It was observed that after 5 runs, the surface area of carbon increased from about $135 \text{ m}^2/\text{g}$ to $167 \text{ m}^2/\text{g}$. This might be related to the breakdown of the catalyst particles which was found to occur

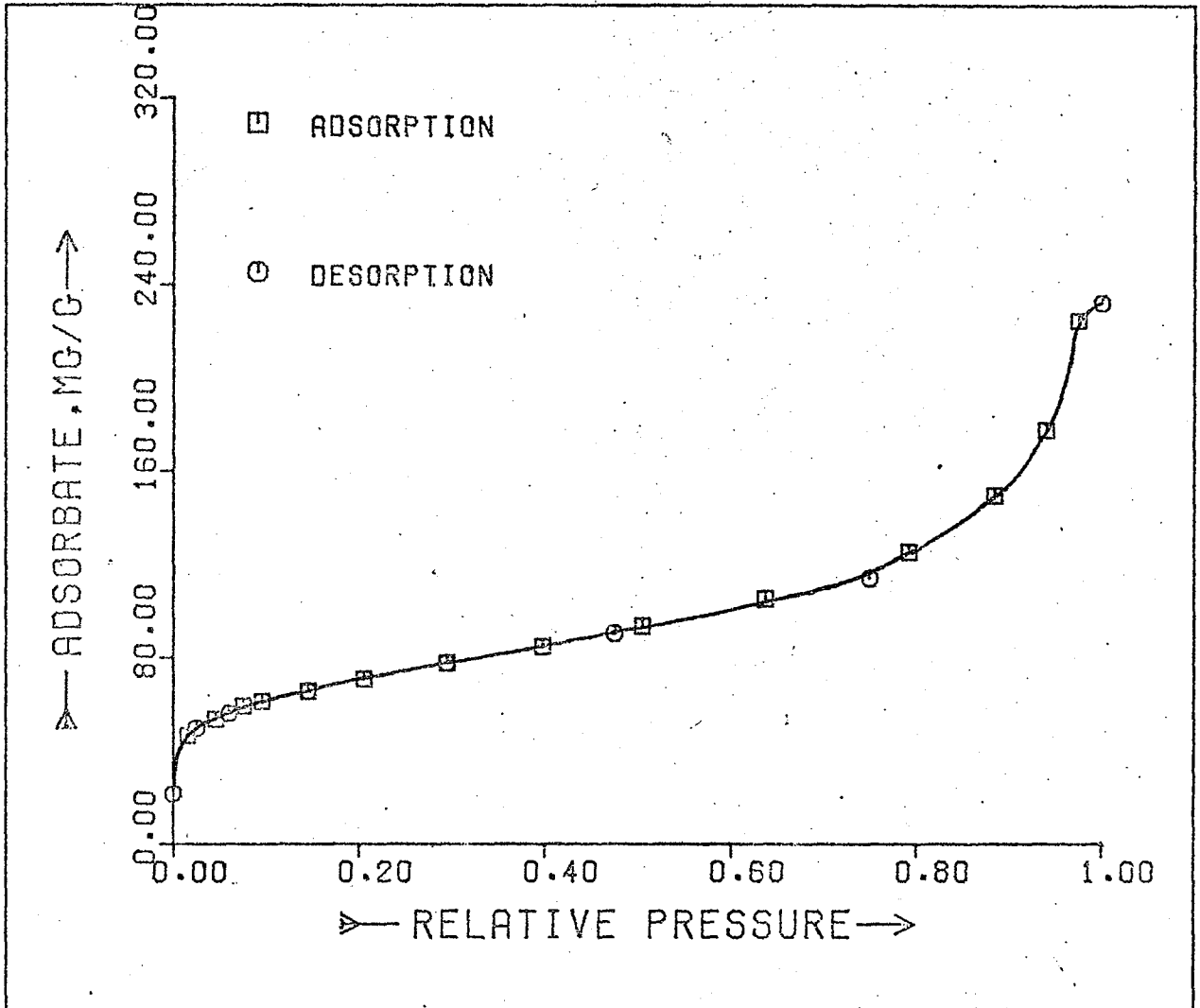


Fig. 3.18 Nitrogen adsorption isotherm for carbon deposited on Ni/Al₂O₃ catalyst (Run 259)

Table 3.19 Characterization of Carbon from Supported Catalysts by Nitrogen Adsorption (run 259)

BET S.A. m ² /g	Pore volume cm ³ /g	Avg.pore radius Å	Apparent density	Porosity
191	0.29	30	1.37	0.4

N.B. Pore volume from Gurvitsch rule.

Average pore radius by Wheeler's model = $2V_p/S$

Table 3.20 BET Surface Areas of Carbon Deposits
Obtained over Ni/Al₂O₃ Catalyst

Run	Deposition Conditions					BET S.A. m ² /g	Rate(-C) *
	T ^o C	P _{C₃H₆} atm	Flow rate cc/min	Rate mg/min	Deposit mg		
A9	580	0.5	440	7.7	42	131	1.57
A10	580	0.5	400	8.1	67	136	1.66
A11	580	0.5	440	8.3	101	129	1.75
A12	500	0.12	250	2.33	43	133	1.45
A13	After partial burn-off				6.65	135	-
A14	500	0.5	440	4.75	44	167	1.83
A15	500	0.12	250	1.91	42	161	1.61

Catalyst : 14 mg, 40-60 mesh BSS, s.a.=14 m²/g, same sample

* Rate of burn-off at 600^oC , P_{H₂O} = 0.3 atm

after a number of deposition-burnoff cycles had been carried out. The experimental procedure involved the calculation of the total area of the samples (carbon + catalyst) followed by deduction of the area due to the catalyst itself (estimated on the basis of its specific surface area previously determined, namely $14\text{m}^2/\text{g}$). Since the breakdown of catalyst particles is not expected to affect very much its own surface area as determined by nitrogen adsorption, (in fact the same area was obtained by N_2 adsorption on a $4.7 \times 4.7\text{mm}$ pellet and on small particles of $0.2 - 0.3 \text{ mm}$) it must be the structure of the carbon itself that is affected by the size of the substrate particles over which it grows. This explanation is in line with the fact that coke obtained over nickel foils was found to have lower surface area ($109 \pm 7 \text{ m}^2/\text{g}$).

3.3 GASIFICATION OF CARBON DEPOSITS BY WATER VAPOUR

3.3.1 Carbon Gasification from Nickel Foil

3.3.1.1 Description

Gasification of carbon deposited on nickel foils with water vapour starts to become significant at temperatures above 500°C . The reaction was found to depend on the amount of carbon present, but was independent of the water vapour pressure. The conditions used in the deposition runs were found to affect the rates of gasification to some extent, so that some degree of irreproducibility was inevitable.

Nearly all gasification runs were characterised by an initial period of constant rate of weight loss, followed by a gradual drop in rate, as burn-off increased. In some cases, there was an initial acceleration leading to a steady rate of gasification which then lasted for at least 50% of the burn-off. At low temperatures,

Table 3.21 Gasification with Steam of Carbon Deposited
over Nickel Foils. Conditions and Results.

Run	Coke mg	P _{H₂O} atm	Temp. °C	Area cm ²	Rate mg/min	k · 10 ³ min ⁻¹ .cm ⁻²
46	10.9	0.072	600	2.83	0.55	17.8
50	15.6	0.047	600	2.86	0.60	13.4
51	16.3	0.047	596	2.85	0.52	11.2
52	15.9	0.047	594	2.84	0.60	13.3
53	16.1	0.047	607	2.91	0.75	16.0
54	16.1	0.047	596	2.91	0.57	12.3
55	17.5	0.047	596	2.90	0.92	18.1
56	15.9	0.047	595	2.92	0.78	16.8
80	29.5	0.25	595	2.88	1.07	12.6
81	17.8	0.25	595	2.88	0.75	14.6
82	15.0	0.25	610	2.88	0.57	13.3
84	11.5	0.25	600	2.87	0.60	18.2
88	17.0	0.25	592	2.89	0.50	10.2
89	11.0	0.25	600	1.53	0.20	11.9
92	19.4	0.25	594	2.85	0.68	12.3
93	17.8	0.25	610	2.87	1.12	22.0
94	21.8	0.25	612	2.88	1.43	22.8
95	18.0	0.25	597	2.88	0.98	18.8
96	43.6	0.25	597	2.88	1.46	11.7
97	22.3	0.25	596	2.88	0.92	14.3
114	26.7	0.25	630	2.86	2.10	27.5
115	28.0	0.25	650	2.87	3.05	37.9
116	27.5	0.25	640	2.88	2.74	34.6
117	27.2	0.25	590	2.87	0.83	10.7

Table 3.21 (Continued)

Run	Coke mg	P_{H_2O} atm	Temp. $^{\circ}C$	Area cm^2	Rate mg/min	$k \cdot 10^3$ $min^{-1}.cm^{-2}$
118	28.4	0.25	660	2.88	3.55	43.4
119	26.1	0.25	620	2.87	1.45	19.4
121	27.9	0.25	670	2.85	3.34	42.0
122	27.2	0.25	670	2.84	3.62	46.9
135	30.8	.10/.36	630	2.97	2.73	29.8
306	29.5	0.25	600	3.13	1.05	11.4
307	30.6	0.25	548	3.13	0.26	2.8
			568		0.60	6.3
			610		1.60	16.7
308	32.2	0.25	650	3.05	3.75	38.2
309	36.0	.05-.27	550	3.04	0.36	3.3
		0.27	700		8.00	73.1
* 324/322	4.8	0.25	650	3.08	-	
			840		0.37	25.3
334/300	34.	0.25	600	3.17	1.20	11.1

* Nickel poisoned with ethanethiol.

N.B. $k = \text{rate} / (\text{coke}) \cdot (\text{area})$

Area = geometric area of nickel foil

some residual carbon was left on the nickel foil, but total gasification occurred on increasing the temperature.

The total flow rate was always near 1 mole/hr, water vapour being produced in the pick-up system described in the experimental chapter, operating either at 73°C or at 89°C. All experimental conditions are summarized in Table 3.21. Conditions used in the deposition runs have already been presented in Table 3.1. Gasification curves are shown in Fig.3.19. A detailed account of the experimental results is presented in the next sections.

3.3.1.2 Kinetic Results

All runs were carried out at the total pressure of 1 atm. Water vapour pressure was varied from 0.047 to 0.360 atm without any effect upon the rate of gasification (Fig.3.20). The rate of gasification was found to be approximately proportional to the amount of carbon initially present on the foil (Fig.3.21) and to the area of the nickel foil used as the substrate, as seen from comparison of runs 89 and 306 (Table 3.21).

Based on these observations, all experimental results were correlated by the expression:

$$r = k.w.A = F.w.A. \exp (-E/RT)$$

using a least-squares fitting technique, where:

r = initial rate of gasification, mg/min

w = initial weight of coke, mg

A = area of the nickel foil, cm^2

k = rate constant, $\text{min}^{-1} \text{cm}^{-2}$

F = pre-exponential factor

E = activation energy, kcal/mole

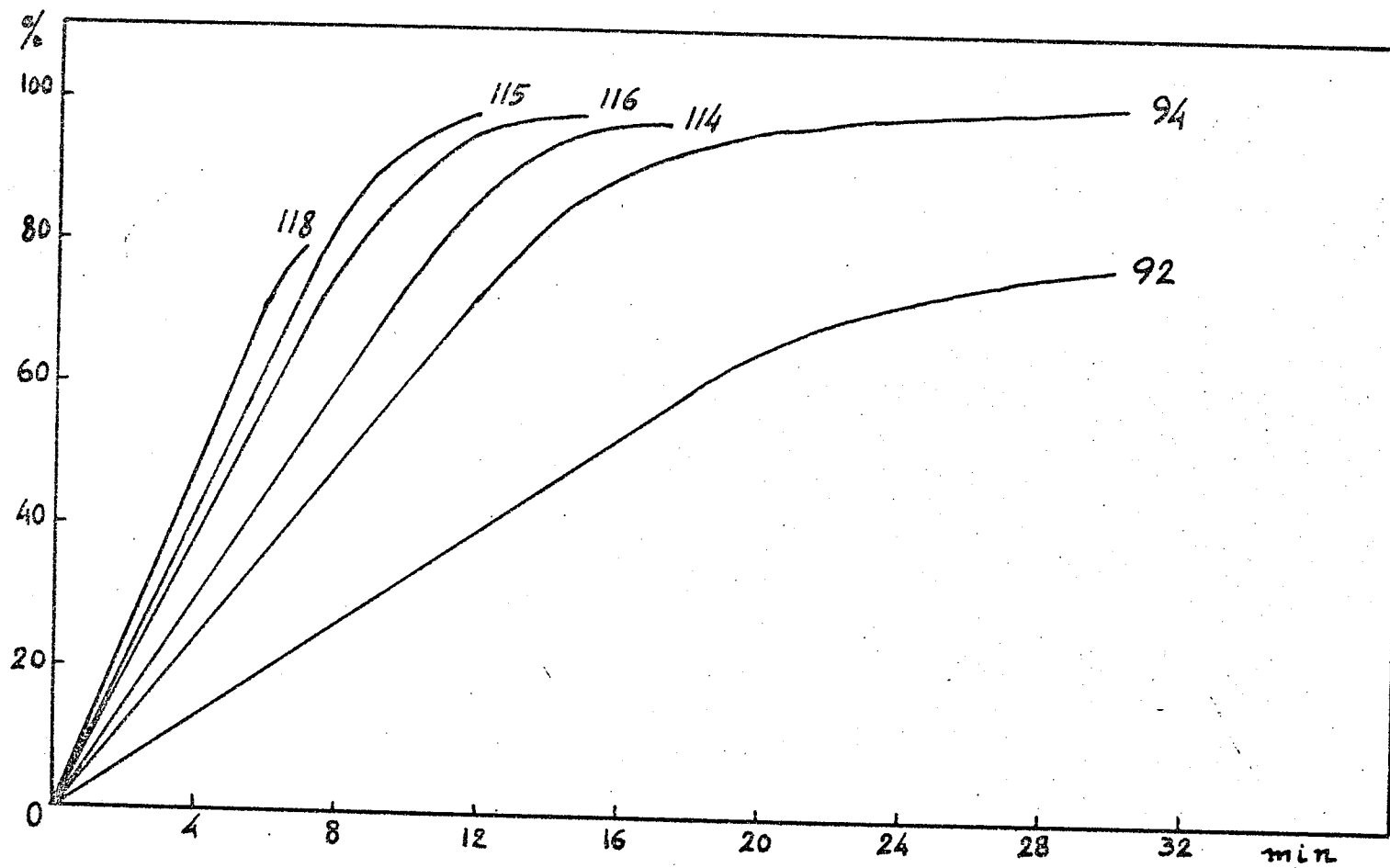


Fig. 3.19 Gasification of carbon from nickel foil , by steam.

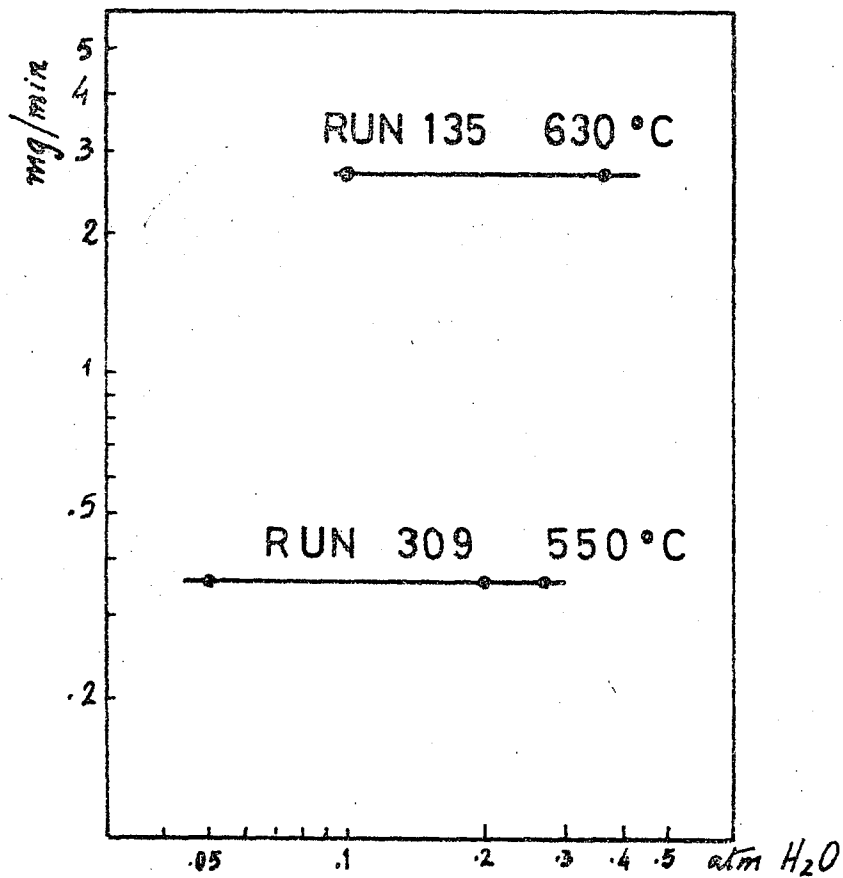


Fig. 3.20 Carbon gasification from nickel foil.
Reaction order in H₂O

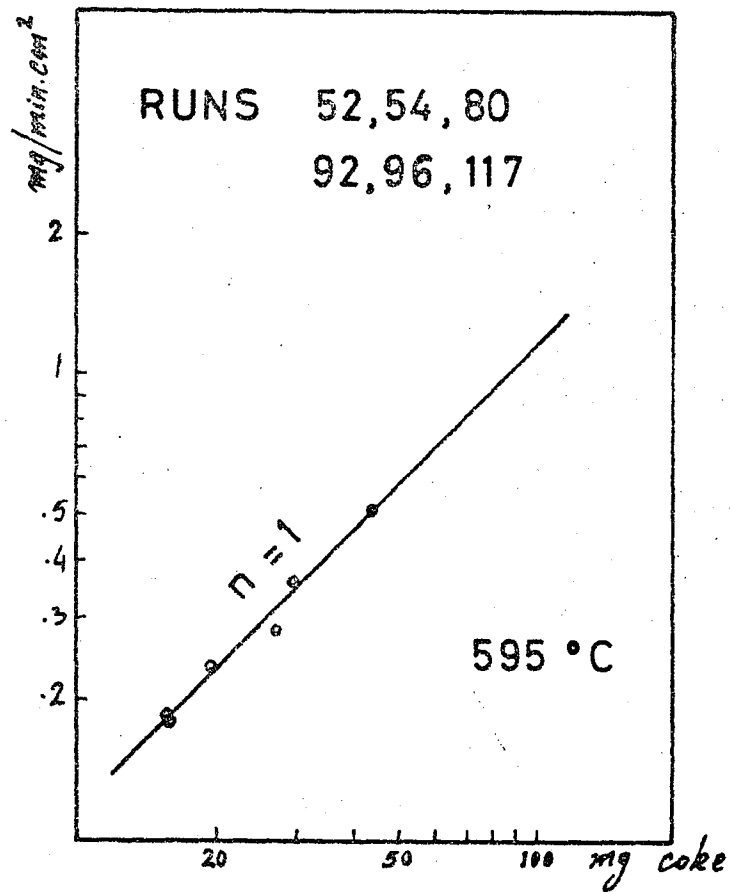


Fig. 3.21 Gasification by H₂O. Dependency on the initial weight of C.

The average deviation between experimental and calculated values was 14%. An Arrhenius plot for the rate constant k is presented in Fig. 3.22, the activation energy being 32 ± 2 kcal/mole over the temperature range studied (548 - 700°C).

3.3.1.3 Test of Diffusion Limitations

In order to check for the absence of pore diffusion limitations, the Weisz and Prater criterion (158) was applied:

$$\frac{Rn}{CDe} \cdot \frac{dw}{dt} < 1$$

where $\frac{dw}{dt}$ = measured rate of reaction, mole/sec.cm²

C = reactant concentration, mole/cm³

De = effective diffusivity, cm²/sec

R = characteristic dimension, cm

n = 1 for plane, n = 2 for cylinder

n = 3 for sphere

As an example, this criterion will be applied to run 119, where gasification at 620°C proceeded with a rate of 1.4 mg/min:

$$dw/dt = 1.4 \text{ mg/min} = 4/3 \times 10^{-6} \text{ mole water/sec.cm}^2$$

R = 0.01cm (thickness of coked foil)

$$C = 0.25 \text{ cm}^3 \text{ water/cm}^3 = 10^{-5} \text{ mole/cm}^3$$

De was estimated by the procedure outlined by Satterfield (8) from the value of diffusivity for CO₂ in electrode graphite (63)

$De = 0.013 \text{ cm}^2/\text{sec}$ (1 atm, 294K). For CO₂ at 620°C, if diffusion

occurs in the transition regime between bulk and Knudsen diffusion,

$$De = 0.013 (893/294) = 0.039 \text{ cm}^2/\text{sec}, \text{ and, for H}_2\text{O, } De = 0.039 \times$$

$$\sqrt{44/18} = 0.061 \text{ cm}^2/\text{sec}.$$

Therefore,

$$\frac{0.01}{0.061 \times 10^{-5}} \times \frac{4}{3} \times 10^{-6} \approx 0.02 < 1$$

showing that diffusion limitations should be negligible.

It has been pointed out (8, 9) that the Weisz and Prater criterion can lead to gross miscalculations when applied to cases where reaction rates are strongly inhibited by one of the products as, for example, with a Langmuir-Hinshelwood equation of the type:

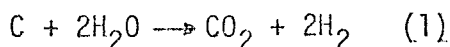
$$r = \frac{k_1 P_A}{1 + k_2 P_B + k_3 P_A}$$

However, in the present work gasification of carbon was catalysed by Ni, and it has been pointed out (70) that the reaction products in the catalysed gasification of carbon by CO_2 or H_2O tend to accelerate rather than retard the burn-off.

This was confirmed at 600°C (run 306) by admission of hydrogen (0.13 atm) without any appreciable change in the rate of gasification. In these circumstances, there is no reason to preclude the application of the Weisz and Prater criterion, and the reaction is not diffusion controlled.

3.3.1.4 Stoichiometry

Carbon gasification by water vapour in the temperature range studied was found to proceed according to the overall reaction scheme:



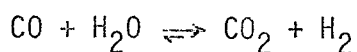
The composition of the gas phase was analysed by gas-chromatography, CO_2 and H_2 being found; traces of CO were occasionally

detected. Quantitative analysis of the gas products was usually established using the ratio of H_2 evolution to carbon burn-off, as a result of the greater sensitivity for H_2 detection:

$$Q = \frac{\text{rate of } H_2 \text{ production}}{\text{rate of C burn-off}}$$

The ratio Q was found to be always close to 2.

The primary reaction products might be CO and H_2 (63) but the water gas shift reaction would convert the CO into CO_2 :



This equilibrium is displaced towards CO_2 formation at temperatures lower than 1000K, and the presence of excess H_2O will tend to make the CO concentration negligible in the gas products.

As an example, the calculations for run 307 ($610^\circ C$) are presented, based on the data of Table 3.22. The equilibrium constant at $610^\circ C$ is $K_p = 2.39$ (1), and calculation of the partial pressure of CO in equilibrium with the above mixture yields:

$$P_{CO} = \frac{0.008 \times 0.016}{0.25 \times 2.39} = 0.0002 \text{ atm}$$

which is one order of magnitude lower than the detectable amount.

3.3.1.5 Catalysed vs. Uncatalysed Gasification

The results obtained in the present system were compared with similar data from the literature for the uncatalysed reaction. At $870^\circ C$ and 0.9 atm of H_2O , Goring et al (159) reported a rate of $1.63 \cdot 10^{-3}$ (lb atom C gasified)/(min)(lb atom C) for the gasification of a low temperature char. By extrapolation of the present data to these conditions, a rate of 3.4 min^{-1} is obtained, which is 3 orders

Table 3.22 Gasification of Carbon with Steam. StoichiometryRun 307 , at 610 °C :

Rate of burn-off = 1.60 mg/min = 0.0080 mole/hr

Nitrogen Flow Rate (inlet) = 0.75 mole/hr

Water Condensate (outlet) = 0.26 mole/hr

Effluent analysis (dry) :

(mole fraction)

$$H_2 = 0.021$$

$$CO_2 = 0.010$$

$$N_2 = 0.969$$

Effluent (dry) flow rate = 0.77 mole/hr

Rate of hydrogen production = 0.77 x 0.021 = 0.016 mole/hr

Rate of CO₂ production = 0.010 x 0.77 = 0.008 "Effluent composition (partial pressures) :

Carbon dioxide = 0.008/(0.26+0.77) = 0.008 atm

Hydrogen = 0.016/(0.26+0.77) = 0.016 "

Water = 0.26/(0.26+0.77) = 0.25 "

Stoichiometry Ratio : $Q = r(+H_2)/r(-C) = 0.016/0.008 = 2.$

of magnitude higher than the uncatalysed reaction. A rate of 2.1×10^{18} atoms C/sec.g = $2.5 \times 10^{-3} \text{ min}^{-1}$ was calculated from the data of Ergun et al (64) for the gasification of a metallurgical coke at 870°C . This is again three orders of magnitude lower than the value extrapolated from the present work.

This difference in rates could be ascribed, at least in part, to differences in the carbons used. In order to test the catalytic activity of the nickel, some poisoning studies were undertaken (Run 322).

Carbon was deposited over a nickel foil in the usual manner, and then about 1 cc of ethanethiol was vaporized in the reactor, in order to poison the nickel. Gasification of the carbon was then attempted under standard conditions ($\text{PH}_2\text{O} = 0.25 \text{ atm}$, 600°C) without any success. In fact, the temperature had to be raised to 840°C , when the rate of gasification recorded was 0.078 mg/min.mg . Extrapolation to this temperature shows the rates of gasification in the presence of unpoisoned nickel to be about 23 times higher.

A sample of very pure graphite flake (synthetic) was also treated under standard conditions (600°C , $\text{PH}_2\text{O} = 0.25 \text{ atm}$) for 1 hr without any gasification being detected. The temperature was progressively increased, and the first signs of some weight loss were recorded only at 900°C .

The conclusion emerges that the uncatalysed gasification of carbon is not significant in the presence of a nickel catalyst.

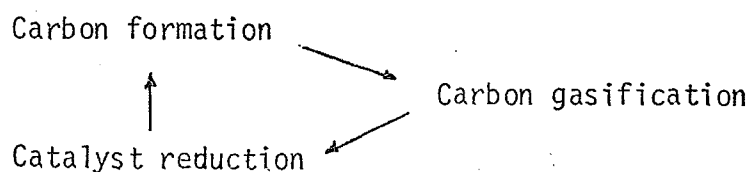
3.3.2 Carbon Gasification from Supported Catalysts

Carbon burn-off by water vapour from supported catalysts was studied in the range of temperatures from 550 to 750°C .

Table 3.23 Gasification with Steam of Carbon Deposited
on Supported Nickel Catalysts. ($P_{H_2O} = .3 \text{ atm}$)

Run	Catalyst & Load mg	Coke mg	Temp. °C	Rate mg/min	Series No.	
176	ICI 46-1	55.7	22.8	600	1.84	
194	Ni/Al ₂ O ₃	52.0	40.0	600	1.21	
196	"	52.0	37.4	600	1.25	
227	"	14.8	18.0	640	1.50	227
228	"	"	23.0	620	1.41	"
229	"	"	17.4	580	0.64	"
230	"	"	46.5	650	1.67	"
231	"	"	34.0	680	2.22	"
232	"	"	46.5	640	1.97	"
234	"	16.7	35	620	1.25	234
240	"	"	101.5	650	1.90	"
241	"	"	20.3	600	1.00	"
245	"	"	14.0	600	1.00	"
246	"	"	45.6	600	1.11	"
247	"	"	7.0	600	1.22	"
248	"	"	70.0	600	1.16	"
255	"	"	92.0	700	3.33	"
257	"	"	75.0	750	4.60	"
258	"	"	90.0	820	6.65	"
328	"	31.5	24.0	600	1.06	328
329	"	"	25.0	600	0.91	"
330	"	"	34.0	650	1.83	"
331	"	"	31.6	620	1.16	"
332	"	"	36.8	550	0.52	"
333	"	"	33.6	570	0.72	"

Several series of runs were performed, using the same catalyst sample throughout each series; the sequence was:



The results are presented in Table 3.23 and conditions used to obtain the carbon deposits can be seen in Table 3.7 (carbon from C_3H_6) and Table 3.31 (carbon from C_3H_6 in the presence of H_2O).

From these results, rates of gasification appear to be independent of the amounts of coke and catalyst present, and were correlated by the simple expression

$$r = F \cdot \exp(-E/RT)$$

where

r = rate of gasification, mg/min

F = pre-exponential factor, mg/min

E = activation energy, kcal/mole

The average deviation was only 9% and the statistical analysis of the residuals did not show any significant dependency on the two other variables, weight of coke and weight of catalyst (Fig.3.23).

The temperature dependency for series 227, 234 and 328 is shown in Fig.3.24, the activation energy determined being 18 ± 1 kcal/mole over the range $550 - 750^\circ C$. Comparison with the results described in section 3.3.1 suggests that diffusion limitations were of importance in this system.

The stoichiometry in this case was also found to be in agreement with the scheme

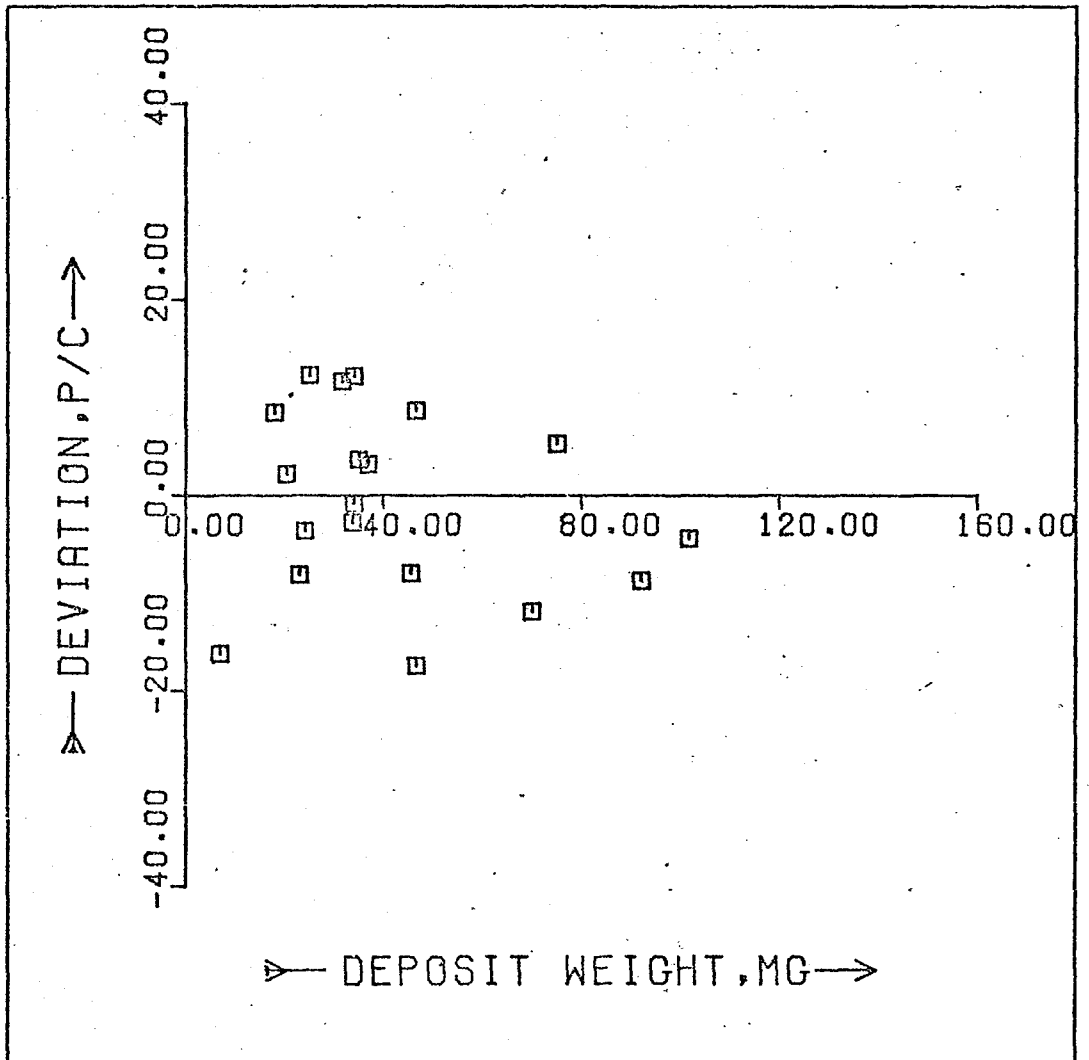


Fig. 3.23 Statistical Analysis of the Residuals.
Carbon gasification, by steam, from
nickel - alumina catalyst.

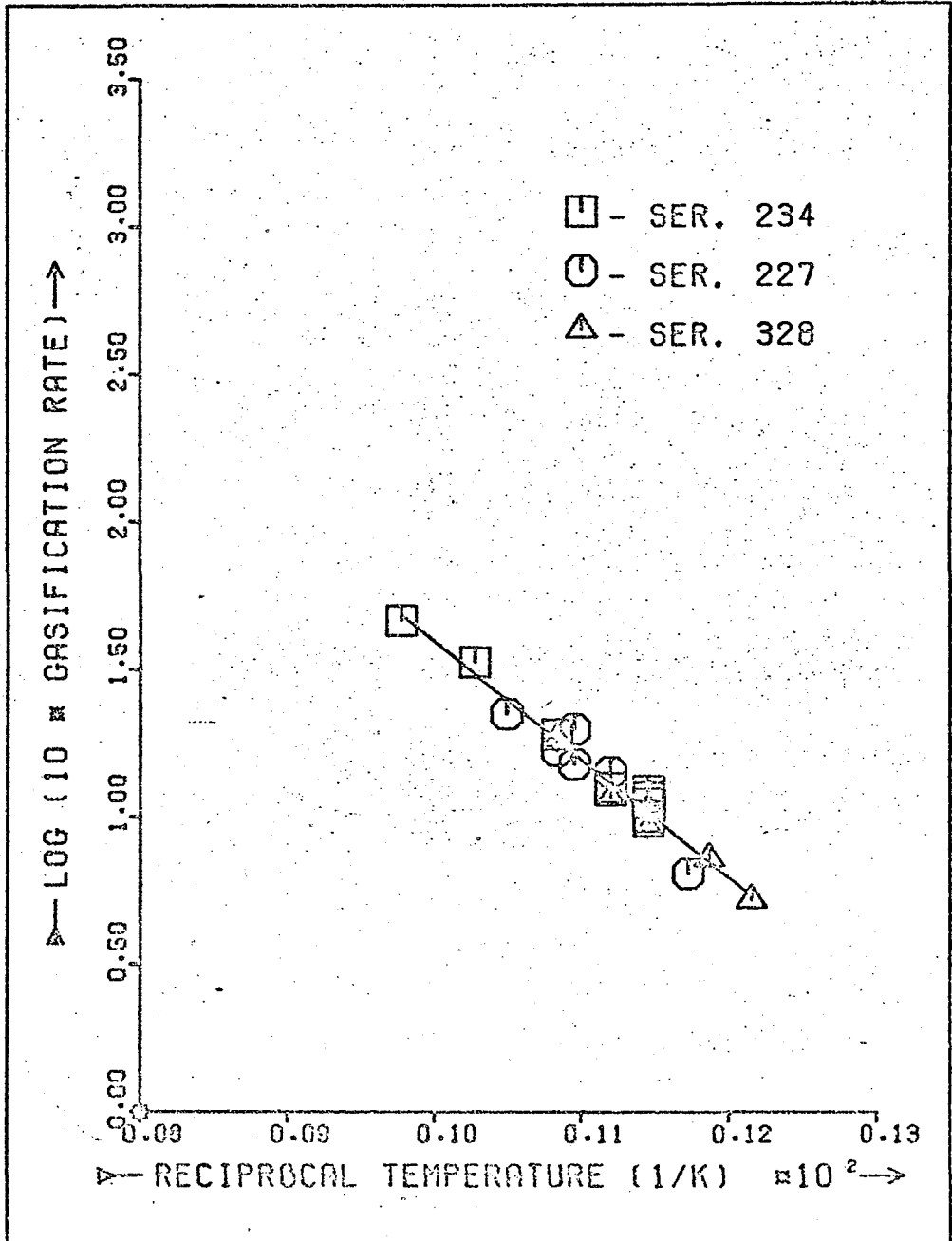


Fig. 3.24 Arrhenius plot for the gasification with steam of carbon deposited on supported nickel catalysts.

Table 3.24 Gasification of Carbon with Steam. Stoichiometry

Run *	T°C	r (-C) mole/hr	x (H ₂)	Flow rate mole/hr	r (+H ₂) mole/hr	$Q = \frac{r(H_2)}{r(-C)}$
191	597	.0090	.024	.75	.018	2.0
240	650	.0095	.027	.77	.021	2.2

N.B. x (H₂) = mole fraction of H₂ in dry effluent.

r (-C) = rate of carbon burn-off

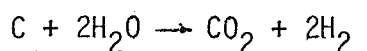
r (H₂) = rate of hydrogen production = x(H₂).Flow rate

Table 3.25 Comparison of Carbon Surface Area before and after Burn-off

Run *	Coke mg	S.A. m ²	sp. S.A. m ² /g	Burn-off %	S.A. m ²	sp. S.A. m ² /g
A12/A13	43.	5.7	133	85	0.89	135
300/334	37.1	4.1±.4	109±7	38	2.15	107

* Runs 191 , 240 , A12/A13 : Nickel-alumina catalyst.

Run 300/334 : Nickel foil



as seen in Table 3.24.

3.3.3 Surface Area Measurements

The surface area of the carbon deposits was determined before and after partial burn-off with steam, since "activation" of carbons by partial gasification has been reported in some systems (169). The results are presented in Table 3.25 and show that the specific surface area of the coke remained approximately unchanged throughout the gasification, using both nickel foil and nickel-alumina catalyst.

3.4 GASIFICATION OF CARBON DEPOSITS BY HYDROGEN

3.4.1 Carbon Gasification from Nickel Foil

3.4.1.1 Description

Gasification of carbon deposited on Ni foils with H_2 is much slower than with H_2O . The reaction shows features very similar to those of the $\text{C-H}_2\text{O}$ reaction, the main difference being the 2nd order kinetics observed for hydrogen. The only product of reaction identified was methane.

Experimental results are presented in Table 3.26 and the corresponding conditions of deposition can be obtained from Table 3.1.

3.4.1.2 Kinetic Results

The partial pressure of hydrogen was varied from 0.375 to 1.0 atm and the rate of gasification was found to follow 2nd order kinetics, as shown in Fig.3.25. As with gasification by water vapour, the rate of reaction was approximately proportional to the amount of carbon originally present on the foil, as seen in Fig.3.26.

Table 3.26 Gasification with Hydrogen of Carbon Deposited
over Nickel Foils. Conditions and Results .

Run	Coke mg	P _{H₂} atm	Temp. °C	Area cm ²	Rate mg/min	k . 10 ³ min ⁻¹ .cm ⁻² .atm ⁻²
263	31.0	1.00	650	3.06	1.64	17.3
			640		1.39	14.7
			630		1.15	12.1
			620		0.89	9.4
			610		0.77	8.1
			600		0.58	6.1
264	25.4	.375	650	2.82	0.17	16.5
		.500			0.32	18.0
		1.00			1.21	16.9
269	15.0	.500	650	2.93	0.20	18.1
		1.00			0.79	18.0
270	15.8	.500	665	2.94	0.26	22.4
320	44.3	1.00	650	3.10	-	
*			750		-	
			850		0.111	0.81

* Nickel poisoned with ethanethiol

N.B. $k = \text{rate} / (\text{coke}) \cdot (\text{area}) \cdot (P_{H_2})^2$

Area = geometric area of nickel foil

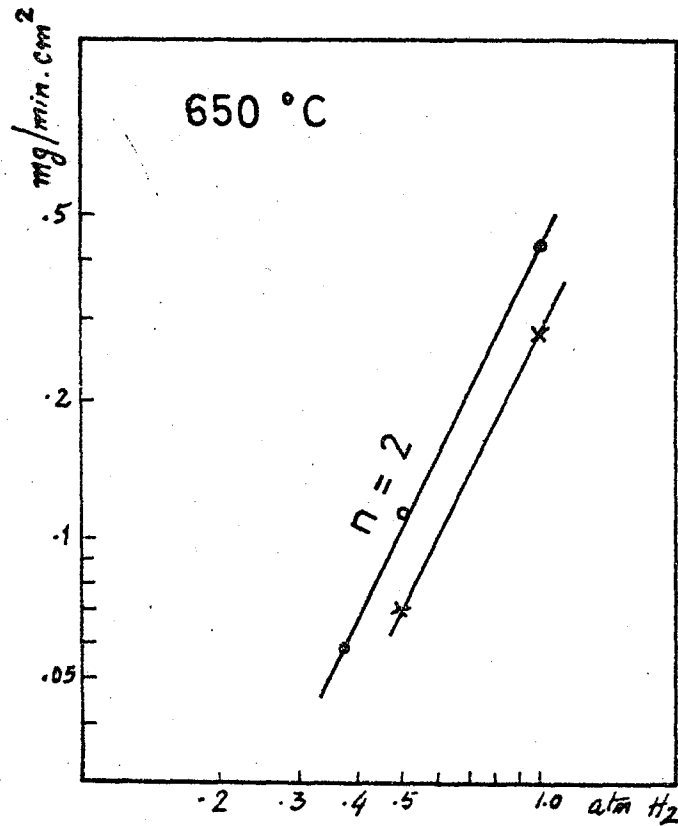


Fig. 3.25 Gasification, by hydrogen, of carbon deposited on Ni foil. Order in H_2

RUNS
 △ 263
 ○ 264
 × 269

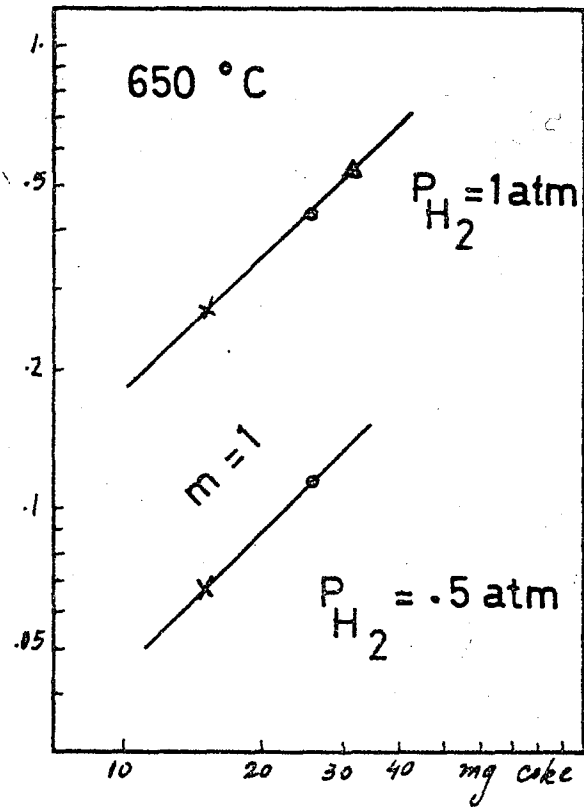


Fig. 3.26 Gasification, by hydrogen, of carbon deposited on Ni foil. Dependency in C weight.

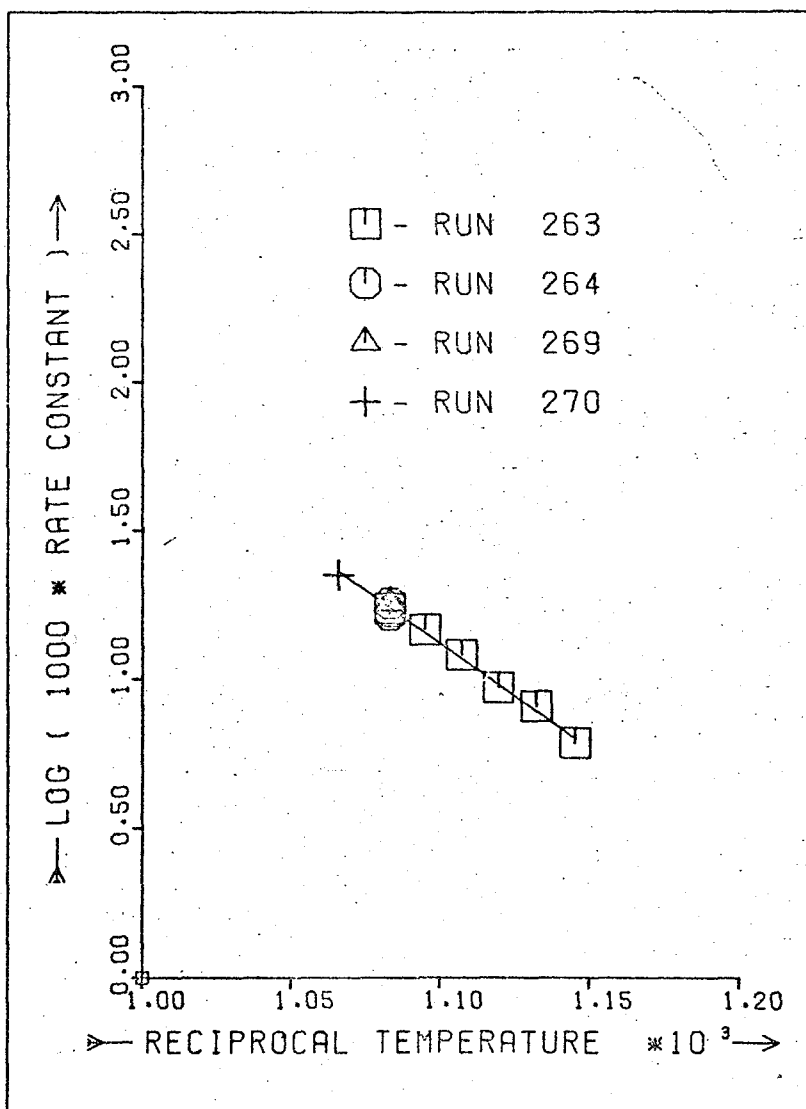


Fig. 3.27 Arrhenius plot for carbon gasification from Ni foil. Gasification by hydrogen

On the basis of these observations, a rate constant was calculated as

$$k = r/w \cdot (P_{H_2})^2 \cdot A$$

The fitting of the experimental data involved an average error of 3%.

k = rate constant, $\text{min}^{-1} \text{cm}^{-2} \text{atm}^{-2}$

r = burn-off rate, mg/min

w = weight of carbon deposit, mg

P_{H_2} = H_2 partial pressure, atm

A = Geometric area of nickel foil, cm^2

The activation energy measured from the Arrhenius plot of Fig. 3.27 was found to be 32.4 ± 0.9 kcal/mole over the range 600 - 665°C.

Diffusion limitations were considered to be absent by comparison with the gasification by steam (Cf. 3.3.1.3), since in the case of hydrogen experimental rates are much lower and the effective diffusivity is certainly higher.

Methane has been reported to have no inhibiting effect upon gasification rates (69).

3.4.1.3 Catalysed vs. Uncatalysed Gasification

Zielke and Goring (69) studied the gasification of a low temperature char with hydrogen at 816°C and pressures from 2 to 30 atm. Extrapolation of their data to 1 atm shows a rate of gasification of $7.5 \times 10^{-5} \text{min}^{-1}$, which can be compared with 0.68min^{-1} , as extrapolated from run 263, 4 orders of magnitude higher.

In order to check the catalytic activity of nickel in the present system, gasification of a coke deposit was attempted after

poisoning the nickel with ethanethiol (run 320). No gasification was observed with 1 atm of hydrogen at 650°C and 750°C. At 850°C, the rate constant obtained was only 0.81×10^{-3} . Extrapolation of the rate constant obtained with unpoisoned deposits gives 362×10^{-3} at 850°C, which is 450 times higher.

Tomita et al (76,77) have also studied the nickel catalysed gasification of carbons. For an active carbon they reported a difference of 6 orders of magnitude between the catalysed and uncatalysed reactions.

3.4.2 Carbon Gasification from Supported Catalysts

The reaction of hydrogen with carbons deposited on supported nickel catalysts was studied in the range of temperatures of 500 - 650°C and hydrogen partial pressures of 0.13 - 1.00 atm; experimental conditions and results are presented in Table 3.27 and the conditions used to obtain the carbon deposits can be found in Table 3.7.

The results show that the rates of gasification were independent of the amount of carbon present originally and approximately proportional to the catalyst load used. The order of reaction with respect to hydrogen was determined at 600°C (run 261) and at 650°C (run 266); 2nd order kinetics were observed, as shown in Fig.3.28. The temperature dependency of gasification rates was studied in run 262 and an activation energy of 31 ± 3 kcal/mole was determined.

On the basis of the above observations, the gasification rates determined with the Ni/Al₂O₃ catalyst were correlated by the expression

$$r = k \cdot (P_{H_2})^2 \cdot A$$

Table 3.27 Gasification with Hydrogen of Carbon Deposited
over Supported Catalysts. Conditions and Results

Run	Catalyst & load mg	Coke mg	P_{H_2} atm	Temp. °C	Rate mg/min	$k \cdot 10^3$ *	
261	Ni/Al ₂ O ₃ p. 161	37	.13	600	0.12	11.0	
			.23		0.31	9.1	
			.37		0.83	9.2	
262	" p. 187	26.6	.28	500	0.09	1.5	
				520	0.18	2.8	
				540	0.30	4.8	
				560	0.40	6.5	
265	" 27.8	28.1	.13	600	0.03	14.4	
				650	0.06	30.8	
			.37		0.43	27.6	
266	" 17.0	85.4	.30	650	0.16	26.1	
			.60		0.68	27.8	
			1.0		2.40	35.3	
267	ICI 46-1	23.3	32.0	.30	654	0.19	15.3
268	"	19.8	34.0	.30	650	0.22	20.3
325	Ni/Al ₂ O ₃	26.0	29.0	1.0	500	0.13	1.3
326	"	26.0	41.8	1.0	590	1.09	10.5
335	ICI 46-1	32.8	4.7	.30	650	0.18	10.0
344	Ni/Al ₂ O ₃	5.3	3.6	1.0	650	0.67	31.8

* $k = \text{rate}/(P_{H_2})^2 \cdot (\text{Ni area in catalyst}), \text{mg/min.cm}^2 \cdot \text{atm}^2$

p : catalyst pellet ; otherwise, the catalyst was crushed and sieved to 40-60 mesh BSS.

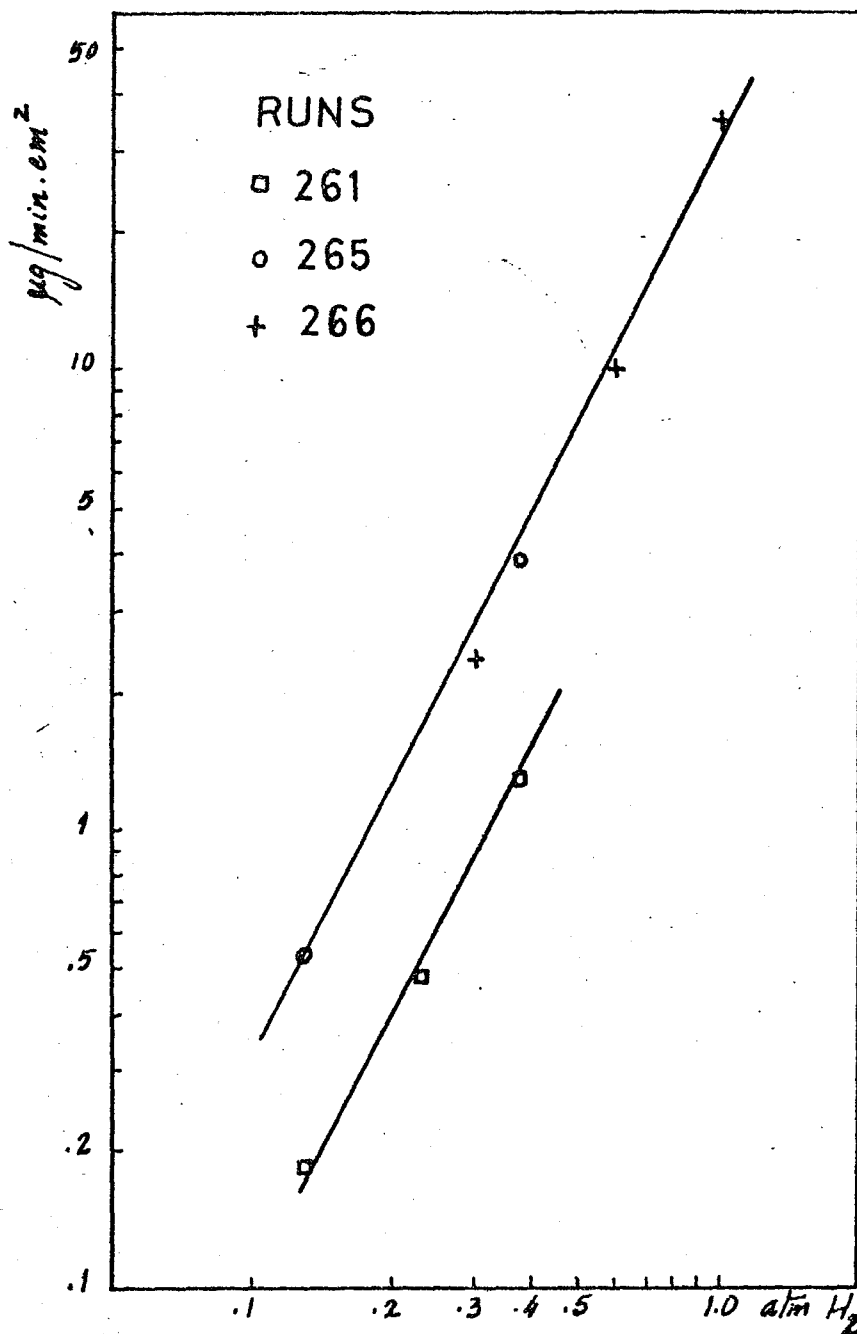


Fig. 3.28 Gasification from supported catalysts. Reaction order in hydrogen

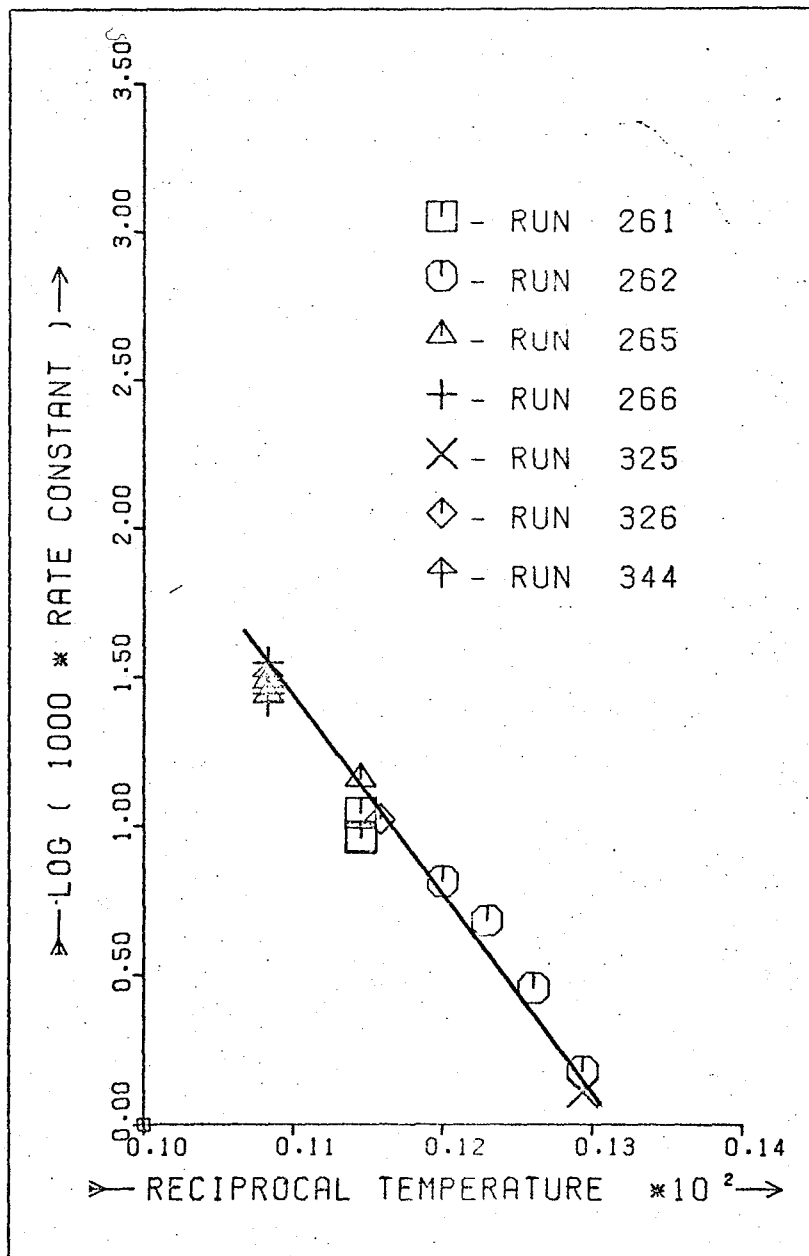


Fig. 3.29 Arrhenius plot for carbon gasification from supported catalysts. Reaction with H_2 .

Table 3.28 Gasification of Carbon by Hydrogen at 650 °C.Mass Balance for Run 268Measured Rates :

Hydrogen feed rate = 0.14 mole/hr

Effluent flow rate = 0.51 "

Rate of gasification = 0.0011 "

Effluent analysis :Hydrogen, mole fraction = 27×10^{-2} Methane , mole fraction = 26×10^{-4} MASS BALANCES (mole/hr)

	<u>Input</u>	<u>Output</u>
Hydrogen	0.14	$0.51(0.27+0.005) = 0.14$
Carbon	0.0011	$0.51(0.0026) = 0.0013$

where

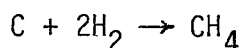
r = rate of gasification, mg/min

P_{H_2} = partial pressure of hydrogen, atm

k = rate constant, $\text{mg}\cdot\text{min}^{-1} \text{ atm}^{-2} \text{ cm}^{-2}$

A = nickel surface area of the catalyst loaded, cm^2 (see Table 2.5)

The average deviation for the fit was 17%. The Arrhenius plot for the rate constant is shown in Fig.3.29. Analysis of the effluent gases has shown the presence of methane, the reaction proceeding in accordance with the scheme

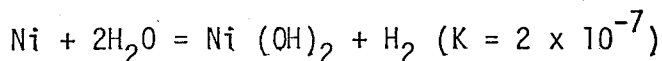
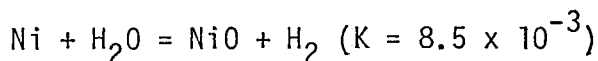


A complete mass balance is presented in Table 3.28.

3.5 STEAM-REFORMING OF PROPYLENE

3.5.1 Carbon Formation on Nickel Foil

Several experiments were carried out with propylene and water vapour in the feed, in the range of temperatures from 560 to 650°C. Hydrogen was also added in order to prevent the oxidation of the catalyst. In most cases the ratios of water to hydrogen and of water to propylene were both 6. The equilibrium constants for the oxidation of nickel were calculated at 600°C:



and the ratio $\text{H}_2 : \text{H}_2\text{O} = 1/6$ used should be more than enough to prevent oxidation of the metal. However, the measured rates of carbon deposition were not steady, and were found to decrease sharply from

the initial value. At later stages, deposition was maintained with a rate sometimes as low as 1/4 of the initial rate.

The initial rates were found to vary widely from run to run, but somewhat better reproducibility was obtained with the final rates. In some cases, temperature or partial pressures were varied in the same run, when this stage of deposition had been reached. After any change, the system was brought to the original conditions and the kinetic parameters were determined by interpolation between the two readings.

The effluent was analysed by gas chromatography: carbon dioxide was detected among the products of reaction at 640°C, but the conversions were so low that a proper mass balance could not be established. As a result, only rates of carbon deposition were measured over nickel foil. The conditions used are presented in Table 3.29 and the experimental results are described next and summarized in Figs. 3.30 and 3.31.

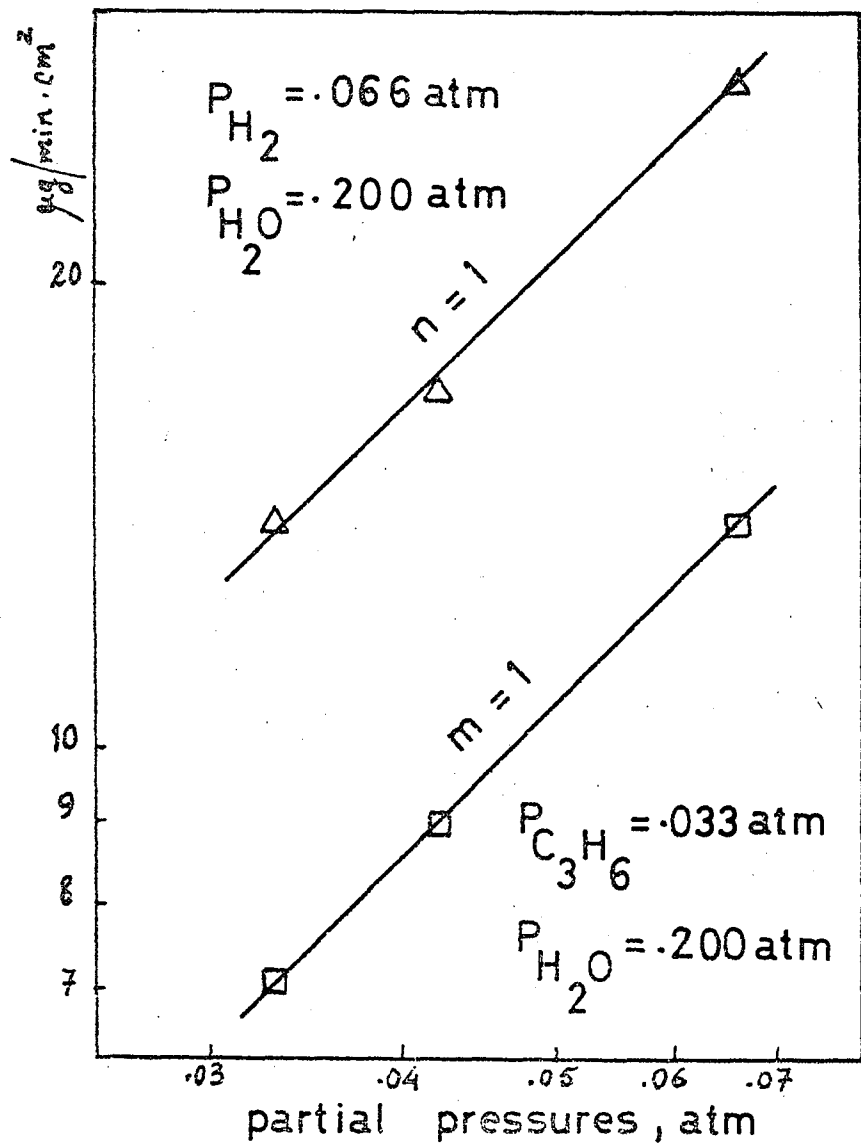
The effect of the partial pressures of the reactants upon the rates of deposition was investigated at 640°C, and is shown in Fig.3.30. Carbon deposition was not observed at 640°C in the absence of hydrogen. The reaction was found to follow first order kinetics both in propylene and hydrogen, and the order with respect to the water pressure was found to be -1.

The rate of deposition showed a negative dependency on temperature, as shown in Fig.3.31. An apparent activation energy of -43 ± 3 kcal/mole was determined by fitting an Arrhenius-type law to the results.

Table 3.29 Carbon Formation from Propylene on Nickel
Foil in Presence of Steam.
Experimental Conditions

Run	Temp °C	Partial Pressures , atm			Effects studied
		C ₃ H ₆	H ₂	H ₂ O	
124	620	0.042	0.042	0.266	Temperature
126	590	0.042	0.042	0.266	Temperature
128	557	0.042	0.042	0.266	Temperature
130	620	0.042	0.042	0.266	
131	640	0.042	0.042	0.266	
132	640	0.042	0.042	0.266	
133	640	0.042	0.042	0.266	
141	640	0.042	0.042	0.266	
142	640	0.042	0.042	0.266	Gas analysis
143	640	0.042	0.042	0.266	Effect of H ₂
146	640	0.033	0.033	0.237	Partial pressures
147	640	0.033	0.033	0.200	Partial pressures
153	600	0.042	0.042	0.266	Temperature
154	590	0.042	0.042	0.266	Temperature
155	590	0.042	0.042	0.266	

N.B. Total pressure = 1 atm



RUNS 146, 147

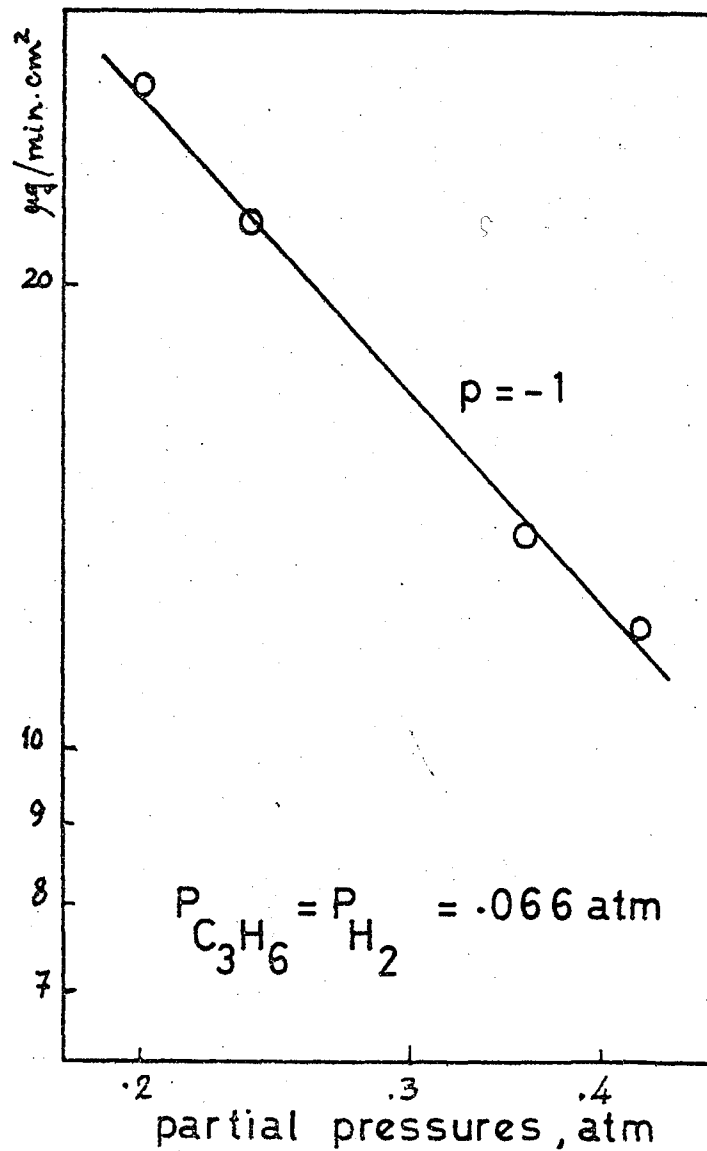


Fig. 3.30 Reaction orders : rate = $k \cdot (P_{C_3H_6})^n \cdot (P_{H_2})^m \cdot (P_{H_2O})^p$

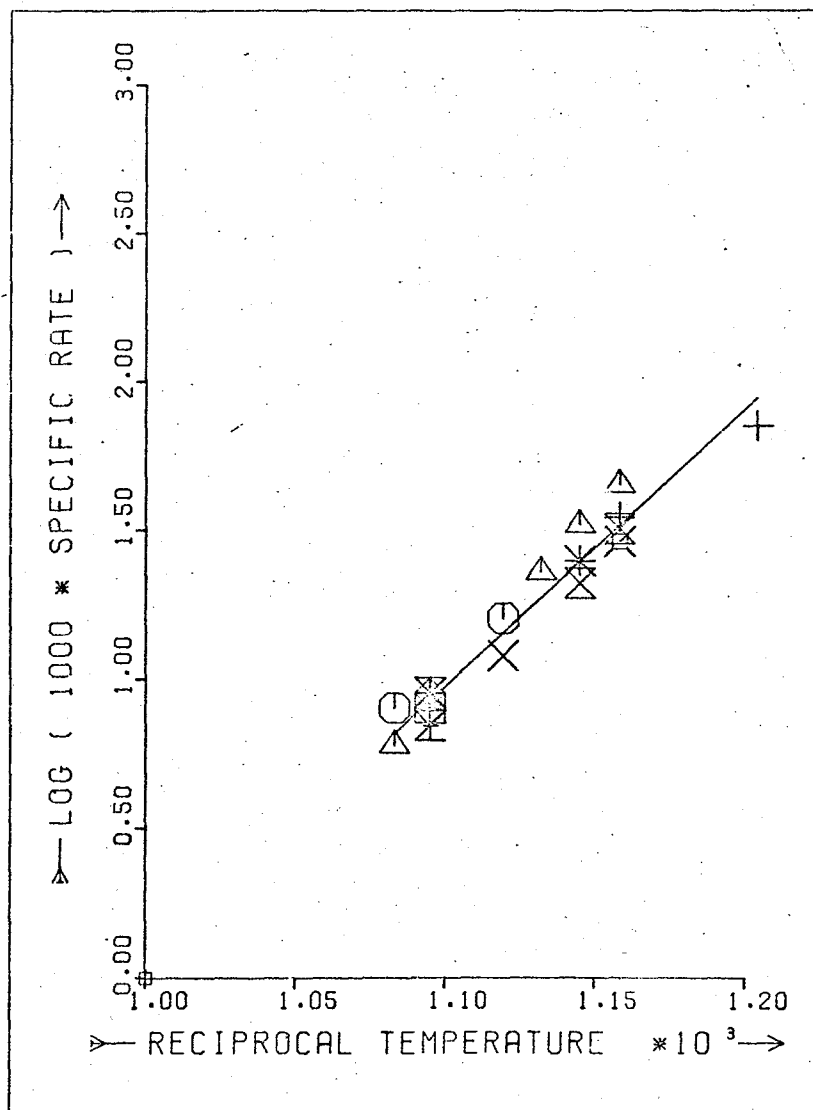


Fig. 3.31 Arrhenius plot for carbon formation on nickel foils in the presence of steam.

3.5.2 Steam-Reforming on Supported Nickel Catalysts

3.5.2.1 Preliminary Experiments

Preliminary experiments were carried out in order to determine the optimum experimental conditions.

The choice of catalyst particle size was limited to less than 1mm to avoid pore diffusion limitations (58), but very fine powders were also unsuitable, being easily blown out of the basket. The size 40-60 mesh B.S.S. (0.235 - 0.360mm) was found to be a good compromise.

The choice of a convenient catalyst load was extremely important, in order to avoid mass transfer limitations as a result of the method used to suspend the catalyst from the balance (Cf. section 3.2.2.3). Large catalyst loads (eg. 200 mg) were found to be unsuitable, as only the upper layers of catalyst were available for reaction. This is clearly shown in Table 3.30, where the rates of hydrogen production under fixed conditions of temperature and pressure are compared for different catalyst loads. Comparison with runs carried out in the fixed-bed reactor showed that a load of about 50 mg could be used in the basket without any problems.

Table 3.30 Comparison of Conversions for Different Catalyst Loads. Steam-Reforming Reaction

Run	Reactor	Load mg	Rate H ₂ prod. ⁿ mole/hr	Specific Rate mole/hr.g
162	Fixed-bed	178	0.085	0.48
169	Microbalance	53	0.026	0.49
163	Microbalance	179	0.026	0.15

Catalyst : ICI 46-1 , 600°C , $P_{C_3H_6} = 0.067$, $P_{H_2O} = 0.265$ atm

The main gaseous products of reaction were found to be hydrogen and carbon oxides; methane was detected in many cases, but always in small concentrations.

Low conversions were obtained in the differential reactor, so that the errors involved in the analysis of the gas phase could affect significantly the calculation of rates of reactant consumption. Rates of gas production however, could be calculated with an accuracy usually better than 10%. For this reason, no hydrogen was used in the feed when the steam reforming reaction was to be studied. As a consequence, rates of carbon deposition were found to decrease slightly with time.

Carbon formation occurred under most conditions, except when the alkali promoted catalyst (ICI 46-1) was used. In this case, substantial carbon formation was only observed after a number of runs were performed with the same catalyst sample, or when the steam-ratio was very low.

Preliminary experiments with alkali treated catalyst have shown that, after an initially fast drop in activity (lasting about 30 min) the catalyst performance could be considered steady (Fig.3.32). Carbon deposition at 600°C occurred at the beginning of the experiments, at very slow rates ($< 8 \mu\text{g}/\text{min}$), and would eventually become negligible ($< 1 \mu\text{g}/\text{min}$). The initial rates of deposition were not reproducible from run to run and it is thought that this deposition was due to a deficiency of steam during the start-up procedure. At higher temperatures, carbon deposition did not occur, as a result of increased rates of carbon removal : in run 174, at 650°C, the small amount of carbon deposited during the start-up was slowly burnt-off in the course of the experiment. These observations

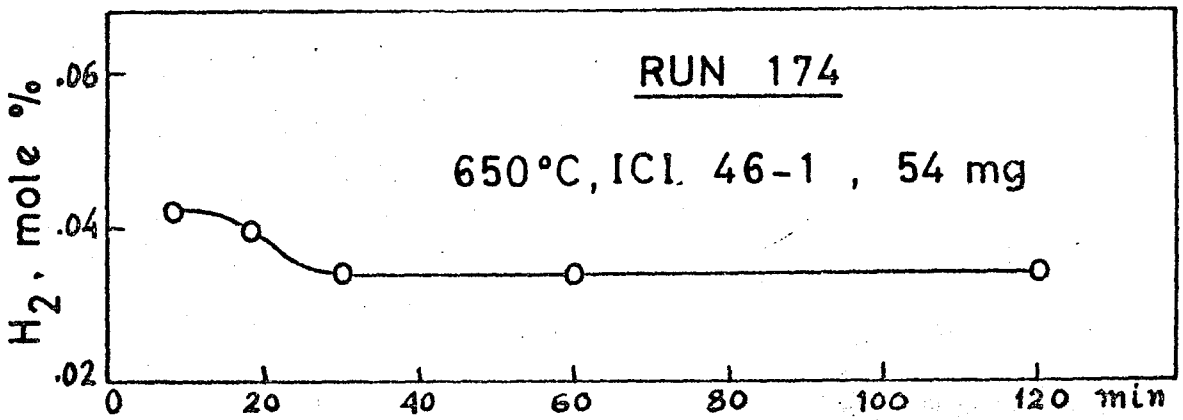


Fig. 3.32 Steam reforming of propylene : initial deactivation.

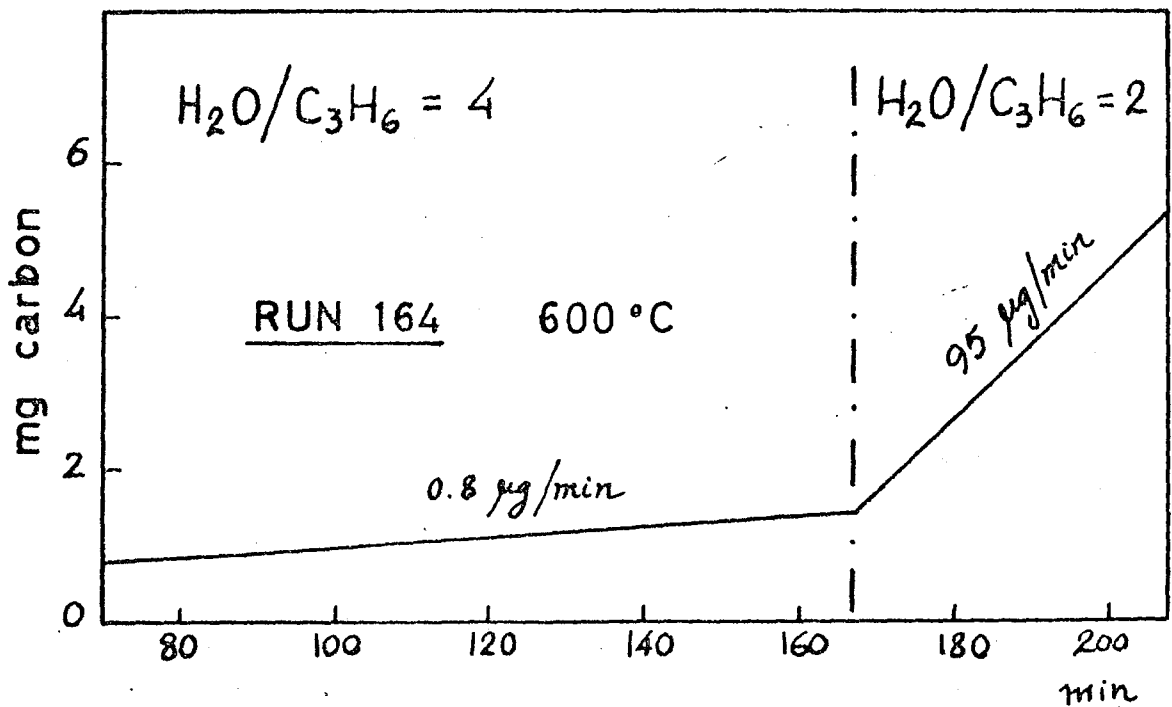


Fig. 3.33 Effect of steam ratio on carbon deposition in the steam reforming of propylene.

apply when the ratio $(\text{H}_2\text{O}) : (\text{C}_3\text{H}_6)$ was ≥ 4 . However, for lower ratios carbon deposition was considerably faster (Fig.3.33). It was also observed that carbon deposition on catalyst 46-1 became progressively easier with time on stream (each sample of catalyst being usually used for a number of runs). This is possibly due to the loss of K_2O from the catalyst (1), or to the migration of potassium from the surface to the bulk, leaving uncovered acid sites (33).

Several series of experiments were carried out with the same catalyst sample, after regeneration and reduction. The results are presented in two sections, one dealing only with carbon deposition, the other referring mainly to the steam-reforming reaction.

3.5.2.2 Carbon Formation

Carbon deposition in the presence of water vapour was studied in the range of temperatures from 400°C to 670°C . Experimental conditions and results are shown in Table 3.31 and Figs. 3.34 to 3.36. Rates of carbon deposition were found to increase with temperature up to about 550°C , and the apparent activation energy measured was 30 kcal/mole (Fig.3.35). Above 550°C , rates of carbon deposition were found to decrease when the temperature was increased, and first order dependency on the pressure of propylene was observed (Fig..3.36). The effect of water vapour was to decrease the rate of carbon deposition, an experimental order of about -1 being measured (Runs 230 and 231).

At low temperatures ($400\text{--}450^\circ\text{C}$) hydrogen showed a negative effect upon the rates of carbon deposition: At 450°C , an increase in the rate of deposition of 1.5 times was observed after turning off the hydrogen supply (run 243); at 400°C , a two-fold increase was

Table 3.31 Carbon Formation from C_3H_6/H_2O on Nickel-
-Alumina Catalyst

Run	Load mg	Temp °C	$P_{C_3H_6}$ atm	P_{H_2} atm	P_{H_2O} atm	Rate mg/min
204	161, p	593	.09	-	.59	3.7
205	162, p	640	.10	-	.54	.92
206	170, p	640	.05	-	.62	.54
226	15	600	.063	-	.250	
227		595	.063	-	.250	
228		570	.063	-	.250	
229		580	.063	-	.250	.014
			.053	.174	.210	.532
230		600	.040	-	.250	.054
			.033	.174	.205	.236
			.066	.174	.205	.590
			.066	.174	.315	.500
			.132	.174	.315	1.280
			.132	.087	.315	.930
231		650	.040	.330	.250	.452
			.080	.330	.250	.938
			.080	.225	.380	.490
232		600	.040	.330	.250	.540
		580	.040	.330	.250	.695
233	17	450	.040	.330	.250	.213
234		600	.040	.330	.250	.438
237		600	.033	.290	.300	.400
			.066	.290	.300	.775
			.099	.290	.300	1.150

Table 3.31 (Continued)

Run	Load	Temp	P _{C₃H₆}	P _{H₂}	P _{H₂O}	Rate
237			.231	.290	.300	2.300
			.132	.290	.300	1.570
238	500		.033	.270	.270	.550
			.066	.270	.270	1.000
			.132	.270	.270	1.570
			.264	.270	.270	1.960
239	550		.033	.270	.270	.675
			.066	.270	.270	1.270
			.132	.270	.270	2.400
			.264	.270	.270	3.280
240	650		.033	.270	.270	.595
			.066	.270	.270	1.000
			.132	.270	.270	2.160
			.264	.270	.270	3.900
241	500		.033	.270	.270	.500
242	600		.033	.270	.270	.360
243	450		.033	.270	.270	.250
			.066	.270	.270	.333
			.132	.270	.270	.430
			.264	.270	.270	.500
			.264	-	.270	.730
244	400		.033	.270	.270	
245	450		.033	.270	.270	.245
	400		.033	.270	.270	.020
			.033	-	.270	.040
246	600		.033	.270	.270	.645
			.033	.135	.270	.482

Table 3.31 (Continued)

Run	Load	Temp	P _{C₃H₆}	P _{H₂}	P _{H₂O}	Rate
246		600	.033	-	.270	-
			.033	.135	.270	.265
247		400	.033	-	.270	.070
248		500	.033	.270	.270	.570
249		500	.264	-	.270	3.1
250		500	.264	.270	.270	2.18
251		650	.264	.270	.270	7.2
252		630	.264	.270	.270	6.6
253		600	.264	.270	.270	6.0
254		580	.264	.270	.270	6.3
255		650	.264	.270	.270	5.5

N.B. p = pellet

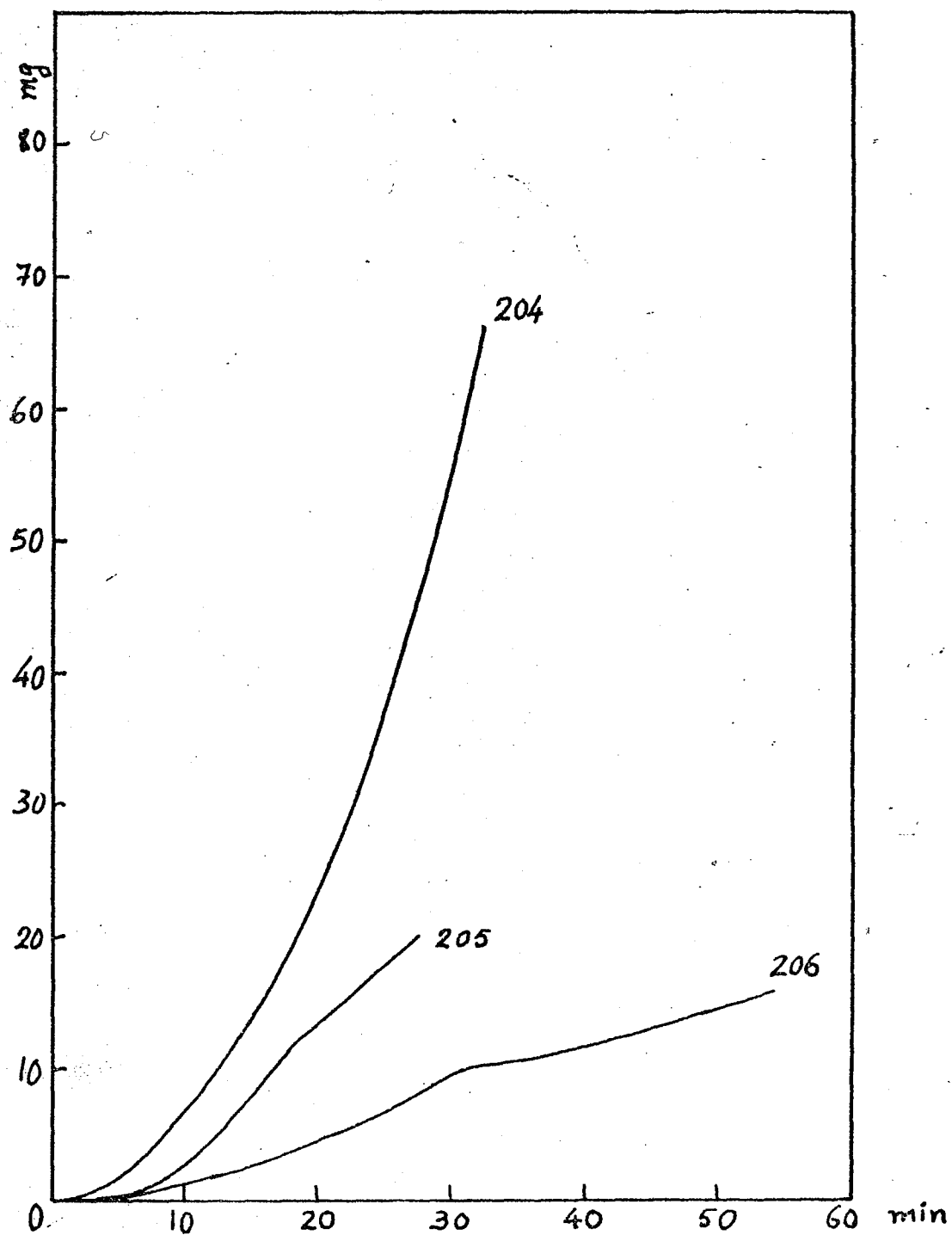


Fig. 3.34 Carbon deposition in the presence of steam on supported nickel catalysts.

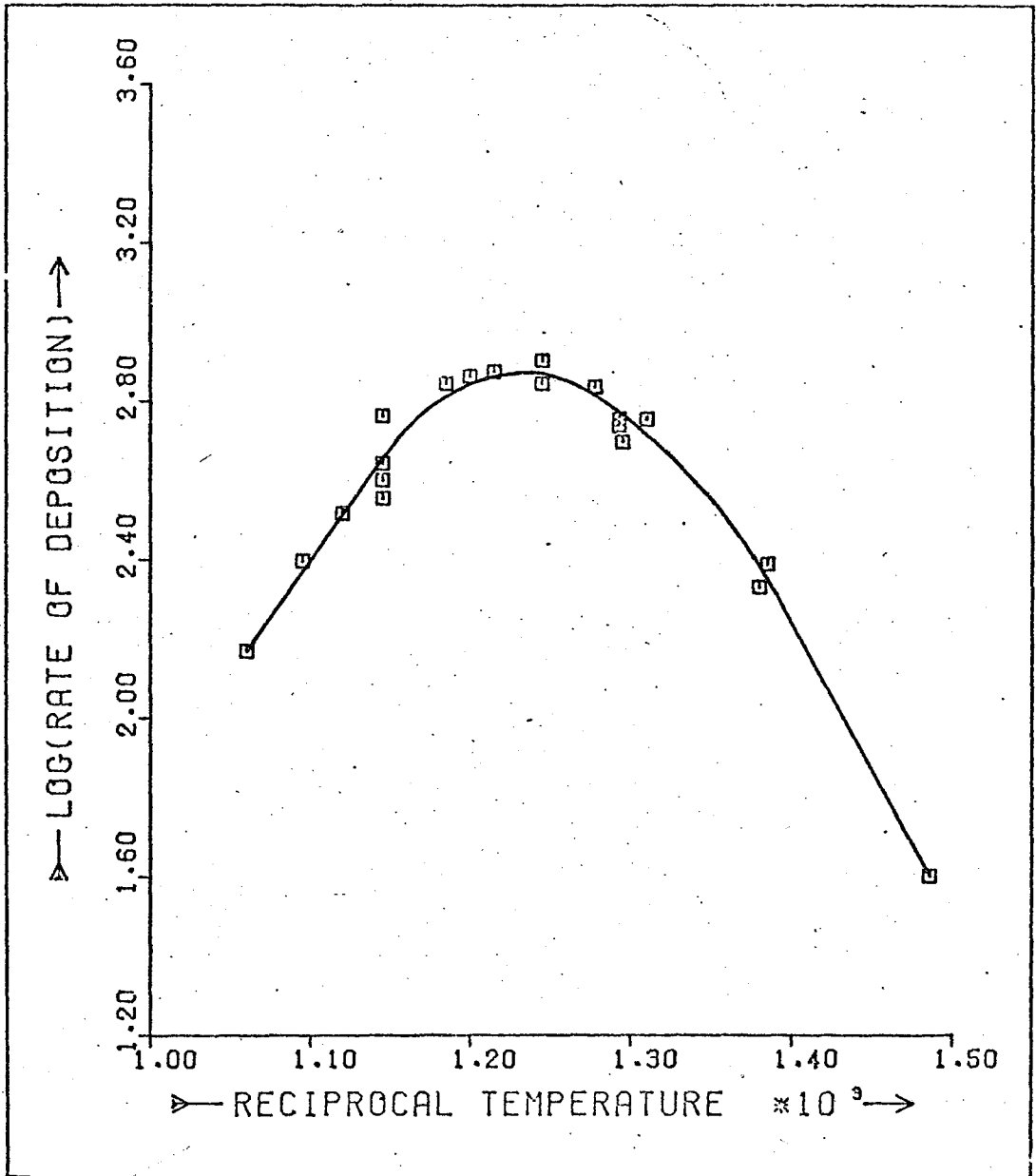


Fig. 3.35 Arrhenius plot for the rates of carbon deposition in the presence of steam.
 17 mg catalyst Ni/Al₂O₃, $P_{C_3H_6} = 0.033$ atm
 $P_{H_2} = 0.27$ atm, $P_{H_2O} = 0.27$ atm

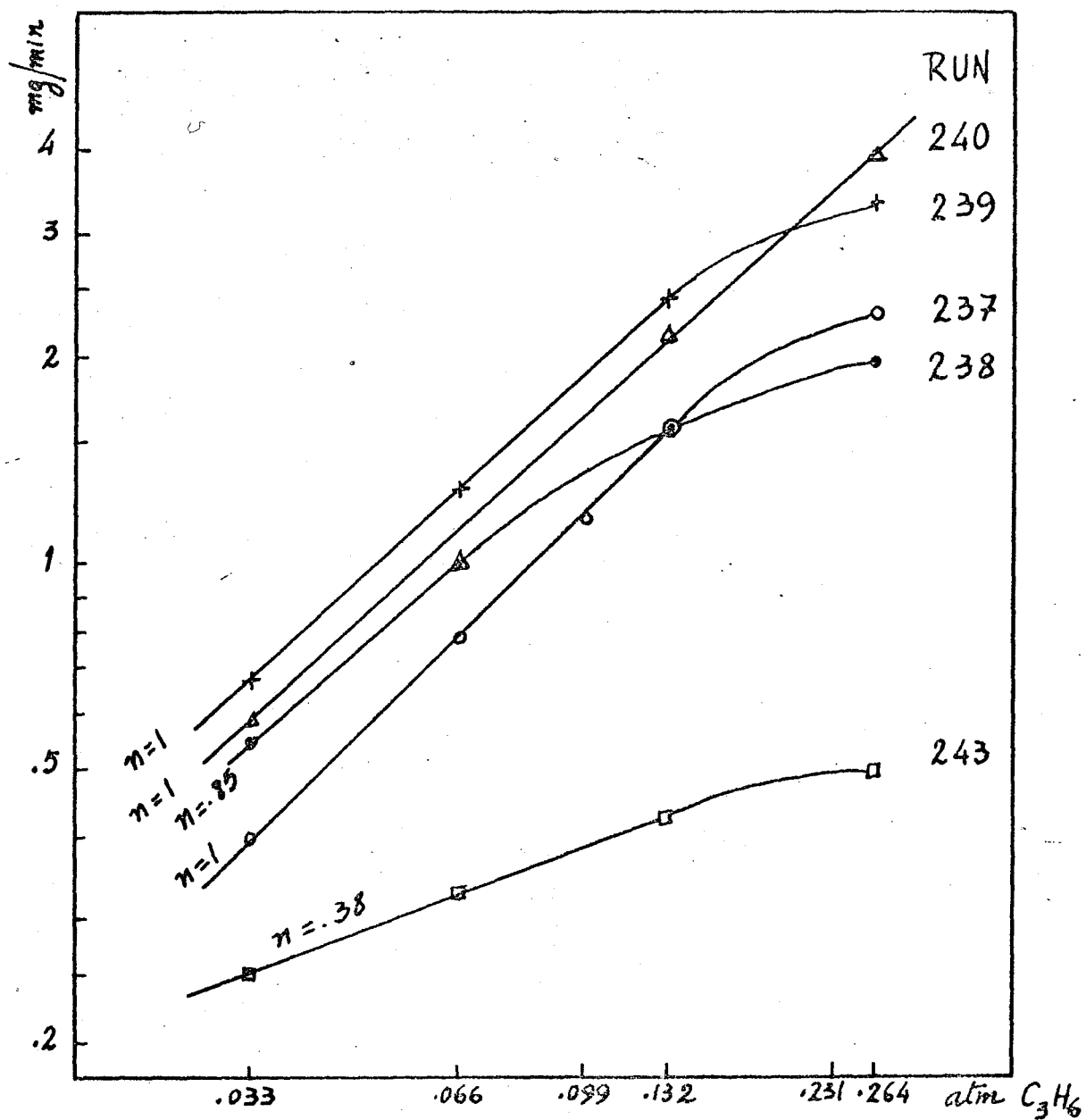


Fig. 3.36 Carbon deposition on nickel-alumina catalyst in the presence of steam. Reaction order in propylene.

measured under the same circumstances (run 244). The deposition was perfectly steady and no deactivation could be observed in the absence of hydrogen. An almost opposite effect of hydrogen was found at high temperatures (600°C): - Deactivation was observed in the absence of hydrogen (run 246) and a positive order with respect to hydrogen was determined. Deactivation became apparent by the impossibility of returning to the original rates of deposition once the hydrogen concentration in the feed had been held at very low levels. Steady rates of coking were observed for higher hydrogen pressures, and the production of carbon was found to have an order of reaction of about 0.3 - 0.4 in hydrogen.

3.5.2.3 The Steam-Reforming Reaction

The reaction of propylene with steam over supported nickel catalysts was studied in the range of temperatures from 500 to 650°C . Water vapour was always kept in excess, in order to maintain conditions thermodynamically unfavourable to carbon formation.

The kinetic features of the reaction were studied over the $\text{Ni}/\text{Al}_2\text{O}_3$ catalyst (without alkali); some comparison experiments were performed with the catalysts 46-1 and Ni/kieselguhr. Conditions used are shown in Table 3.32 and the results are presented in Table 3.33 and Fig.3.37.

Although complete mass balances could usually be established (Cf. Table 3.34), calculations based on the measured conversion of propylene were unreliable, as pointed out earlier. Since the rates of production of hydrogen and carbon dioxide could be determined with greater accuracy, the following balances were used:

Table 3.32 Steam-Reforming of Propylene

Run	Catalyst	T ^o C	P _{C₃H₆}	P _{H₂O}	TFR	R _C	R _P
175	ICI 46-1	600	.086	.343	.700	0.0	.058
177	"	600	.106	.580	.565	0.050	.043
178	"	600	.106	.580	.565	0.0	.059
179	"	600	.106	.504	.567	0.0	.053
180	"	630	.095	.508	.631	0.0	.072
185	"	620	.108	.532	.557	0.0	.063
186	"	600	.096	.587	.638	0.0	.043
183	Ni/kieselguhr	600	.097	.541	.596	.400	.228
188	Ni/Al ₂ O ₃	600	.097	.548	.610	.057	.044
190	"	600	.097	.538	.597	.057	.050
192	"	600	.100	.545	.591	.059	.050
193	"	620	.093	.537	.648	.021	.057
195	"	640	.091	.513	.645	.010	.073
199	"	620	.103	.518	.570	.020	.059
201	"	600	.091	.498	.897	.072	.043
311	"	600	.037	.280	1.045	.002	.027
311	"	600	.074	.280	1.045	.018	.043
311	"	600	.074	.400	1.061	.011	.039
311	"	600	.148	.400	1.061	.054	.063
312	"	500	.038	.283	.990	.042	.008
312	"	550	.038	.283	.990	.014	.020
312	"	580	.038	.283	.990	.006	.024
312	"	640	.038	.283	.990	0.0	.036

N.B. Partial pressures in atm

TFR = Total flow rate, mole/hr

R_C = Rate of carbon formation, mole/hr.g

R_P = Rate of propylene conversion by steam-reforming
mole/hr.g

Table 3.33 Steam-Reforming : Product Gas Composition

Run	Dry effluent composition, mole %						Effluent Flow Rate mole/hr
	H ₂	N ₂	CO	CH ₄	CO ₂	C ₃ H ₆	
188	.085	.700	.003	.001	.030	.181	.31
190	.088	.705	.003	-	.027	.177	.31
192	.089	.694	.004	.001	.026	.186	.30
193	.083	.713	.007	.001	.027	.169	.34
195	.092	.720	.007	.002	.025	.154	.35
199	.090	.690	.013	.003	.028	.176	.31
201	.053	.762	.003	-	.017	.165	.48
178	.099	.643	.008	.003	.036	.211	.27
179	.096	.677	.012	.003	.041	.171	.33
180	.120	.661	.016	.003	.056	.144	.38
185	.088	.677	.012	.001	.032	.190	.30
186	.071	.687	.004	-	.035	.201	.29
183	.197	.605	.023	.004	.040	.131	.35

Table 3.34 Steam-Reforming. Mass Balance for Run 188

<u>Feed flow rates, mole/hr</u>			<u>Effluent, mole/hr</u>	
C_3H_6	N_2	H_2O	Dry gas	Condensate
0.059	0.217	0.334	0.310	0.314

Rate of carbon formation = 0.6 mg/min = 0.003 mole/hr

BALANCES

	<u>Input, mole/hr</u>	<u>Output, mole/hr</u>
N_2	0.217	$0.310(0.700)=0.217$
O_2	0.334	$0.314+0.31(0.003+2 \times 0.030)=0.334$
H_2	$3 \times 0.059=0.177$	$0.31(0.085+2 \times 0.001+3 \times 0.181)=0.196$
	<u>0.334</u>	<u>0.314</u>
	0.511	0.510
C	$3 \times 0.059=0.177$	$0.31(0.003+0.001+3 \times 0.181)=0.179$
		<u>0.003</u>
		0.182

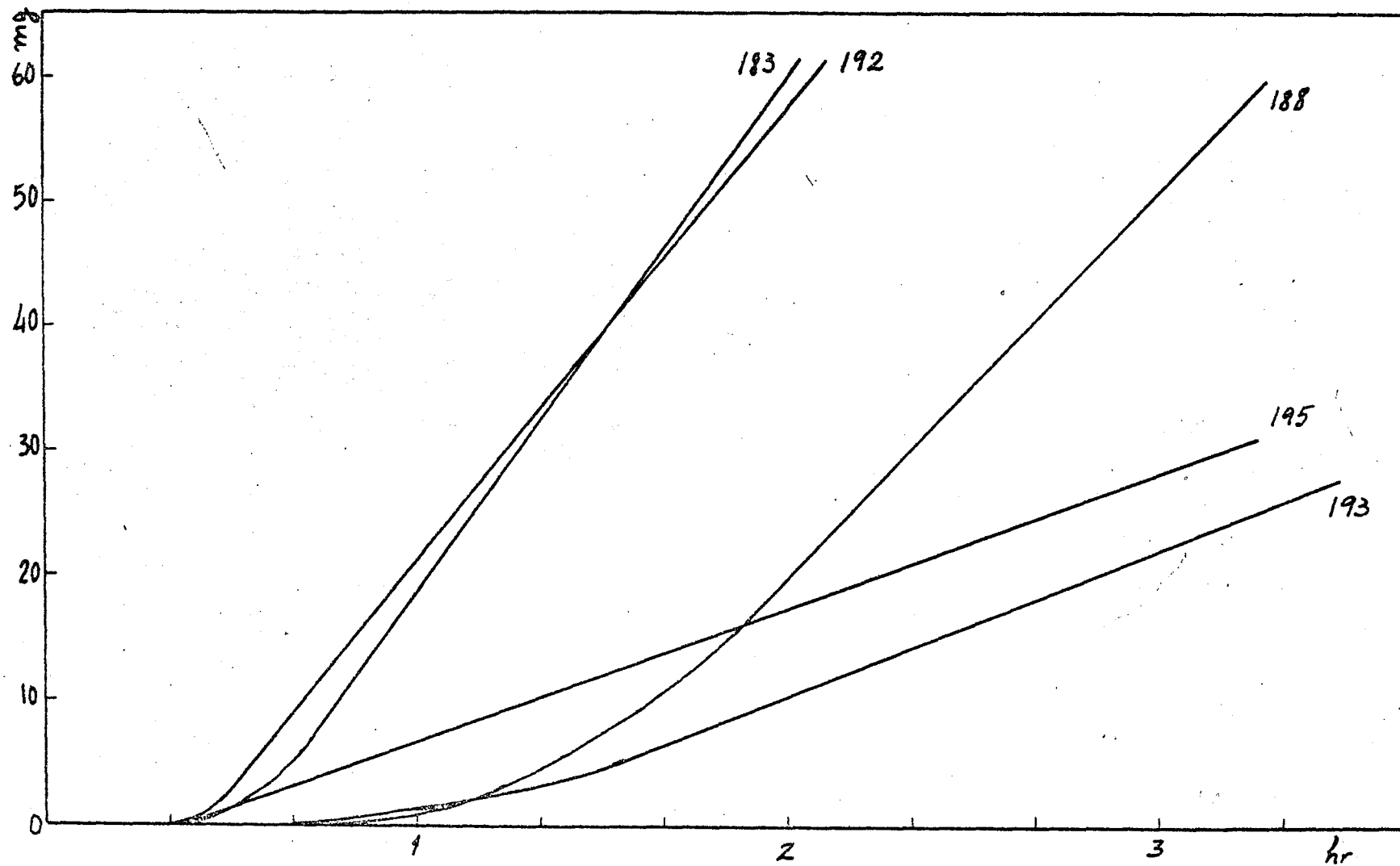


Fig. 3.37 Carbon deposition in steam reforming runs.

$$3 R_p = R_{CO} + R_{CO_2} \quad (\text{Carbon balance})$$

$$R_H = R_W + 3R_p \quad (\text{Hydrogen balance})$$

$$R_W = R_{CO} + 2R_{CO_2} \quad (\text{Oxygen balance})$$

where methane was neglected and:

R_p = rate of propylene conversion

R_W = rate of water consumption

R_H = rate of hydrogen production

R_{CO} = rate of carbon monoxide production

R_{CO_2} = rate of carbon dioxide production

From these equations, the rate of propylene conversion can be expressed as function of the rates of hydrogen and carbon dioxide production:

$$R_p = (R_H - R_{CO_2}) / 6$$

When carbon formation was a side reaction (catalysts Ni-alumina and Ni-kieselguhr), the appropriate deduction was made from the overall rate of reaction in order to obtain the rate of the steam-reforming reaction:

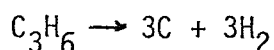
$$R_p^1 = (R_H - R_C - R_{CO_2}) / 6$$

where

R_C = rate of carbon formation (since one mole of hydrogen is produced with each mole of carbon)

R_p^1 = rate of propylene converted by steam-reforming

At 600°C, the process could be approximately described by the equations:



since methane was produced in negligible amounts and $(CO) \ll (CO_2)$. At higher temperatures, the proportion of CO in the product gas increased, but methane could still be neglected.

The experimental orders of reaction determined with catalyst nickel-alumina at 600°C were 0.64 in propylene and -0.04 in steam (Fig.3.38). A power rate law was used to calculate the rate constant for hydrogen production, plotted in Fig. 3.39:

The activation energy obtained in the range 500-640°C was 13.2 ± 0.3 kcal/mole. An activation energy of 16 ± 1 kcal/mole was determined with the rates of propylene conversion, R_p .

Comparison of the activities of the three catalysts at 600°C based on their nickel area is shown in Fig.3.40. It is observed that the alkali promoted catalyst exhibits slightly lower specific activity. A similar effect of the potassium oxide promoter on the activity of the catalyst has been reported in the literature (26).

Selectivity for hydrogen production was found to increase with temperature, as carbon deposition becomes progressively less important.

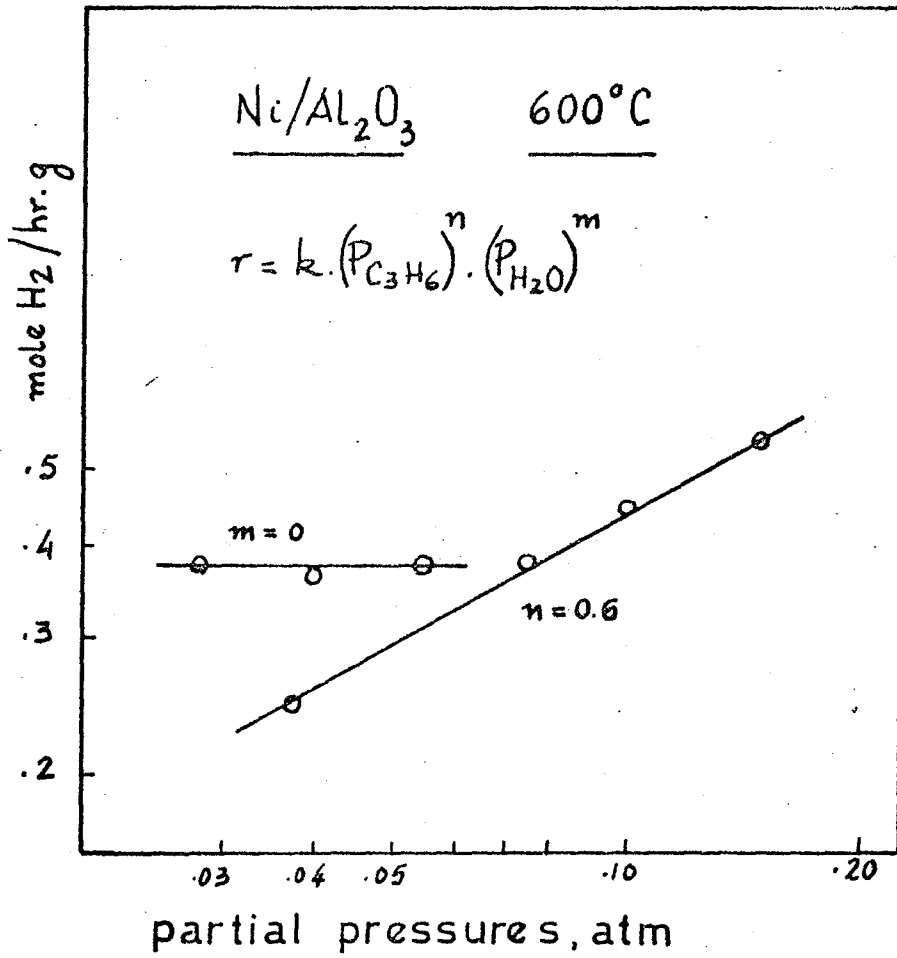


Fig. 3.38 Steam reforming : reaction orders

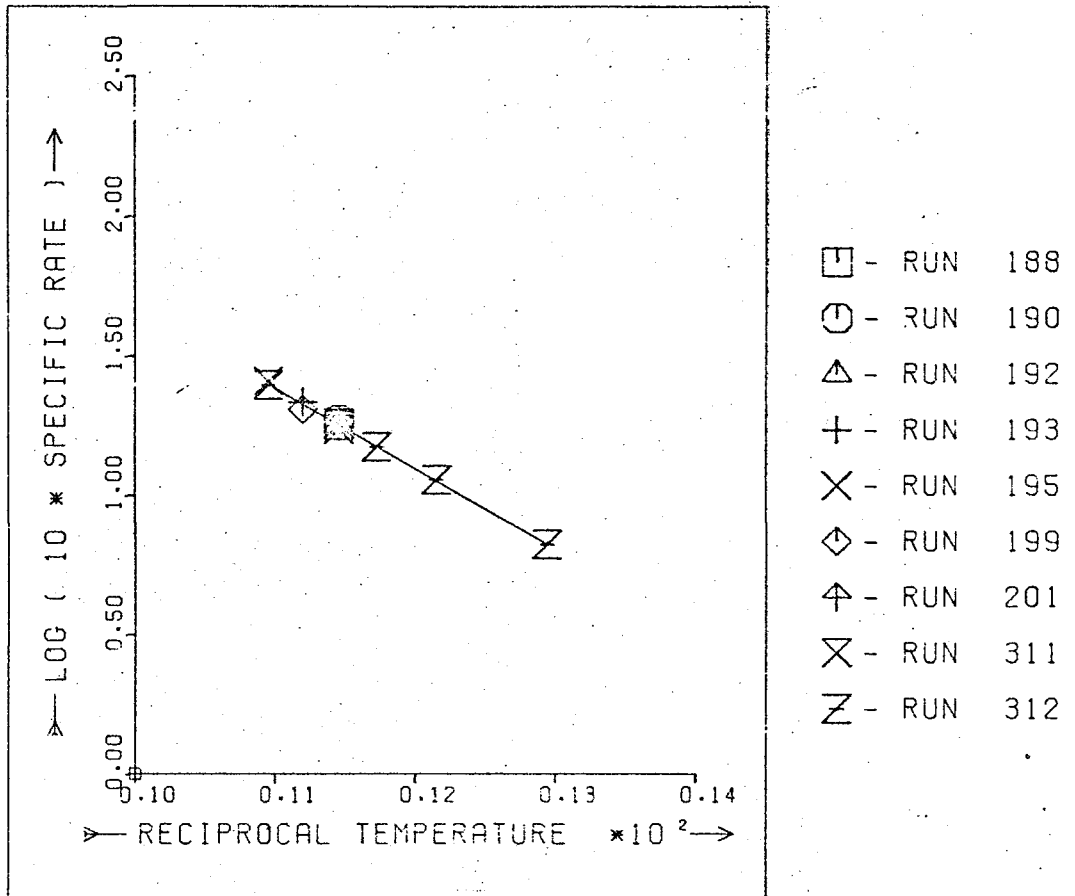


Fig. 3.39 Arrhenius plot for the rates of hydrogen production by the steam-reforming of C_3H_6

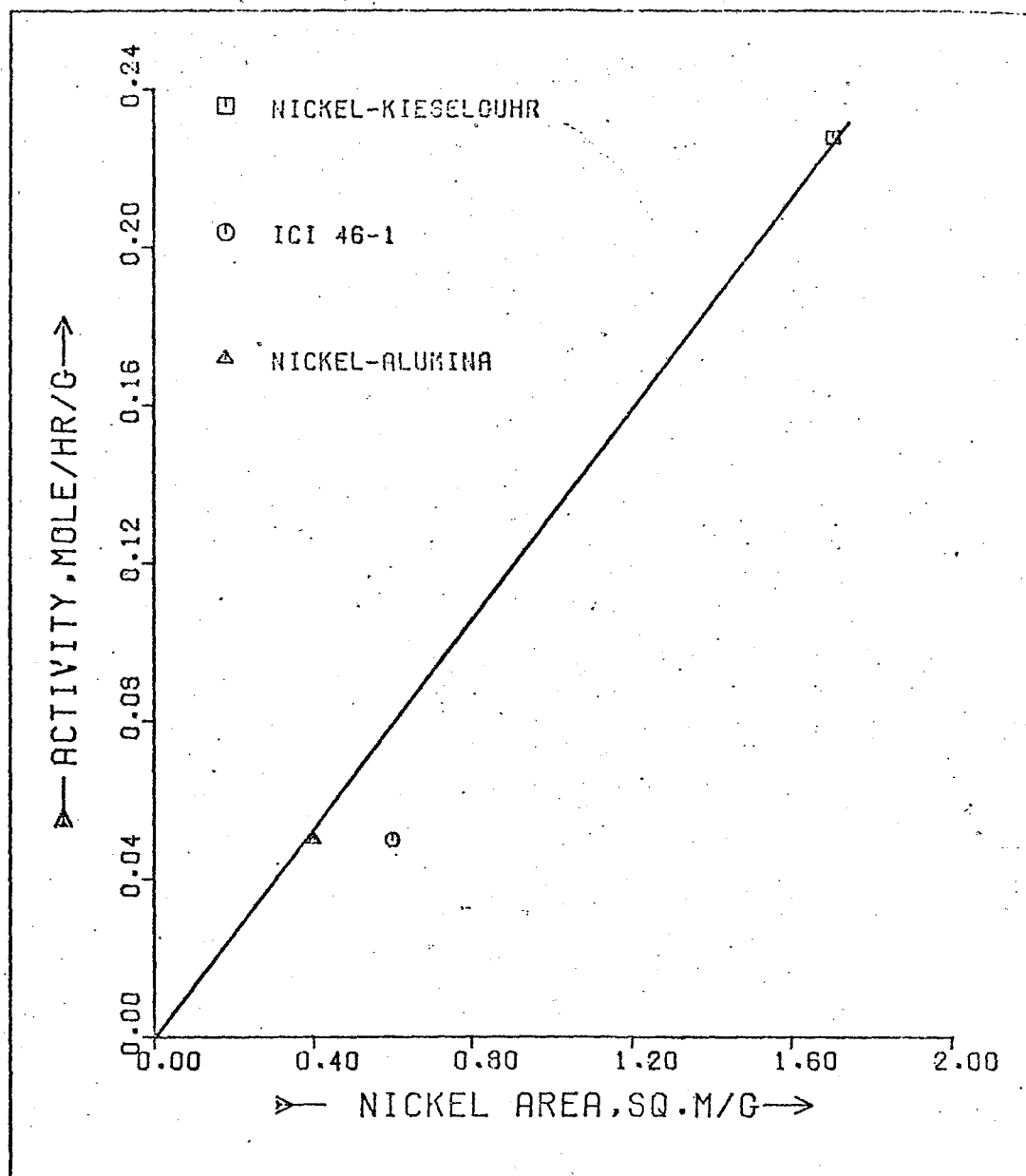


Fig. 3.40 Activity of nickel catalysts for the steam reforming of propylene.

3.6 KINETIC RESULTS : SUMMARY

3.6.1 Carbon Formation from Propylene at Low Temperatures (< 540°C)

rate = $43 \times 10^{10} \times \exp(-33300/RT)$ $\mu\text{g}/\text{min}\cdot\text{cm}^2$ based on the initial nickel area available : geometric area in the case of nickel foil, metal surface area (from CO chemisorption) for supported catalysts.

3.6.2. Carbon Gasification by Steam on Nickel Foil

rate = $1.75 \times 10^6 \times W \times \exp(-32000/RT)$ $\text{mg}/\text{min}\cdot\text{cm}^2$ where W = initial amount of carbon to be gasified; the rate is referred to the area (geometric) of the foil.

3.6.3 Carbon Gasification by Hydrogen on Nickel Foil

$$\text{rate} = 7.86 \times 10^5 \times W \times P_{\text{H}_2}^2 \times \exp(-32400/RT) \text{ mg}/\text{min}\cdot\text{cm}^2$$

where the rate is referred to the geometric area of the foil. W = initial deposit to be gasified. P_{H_2} = hydrogen partial pressure, atm.

3.6.4 Carbon Gasification by Hydrogen on Supported Catalysts

$$\text{rate} = 7.0 \times 10^5 \times P_{\text{H}_2}^2 \times \exp(-31000/RT) \text{ mg}/\text{min}\cdot\text{cm}^2$$

referred to the metal area of the catalyst, as determined by CO chemisorption.

3.6.5 Steam-Reforming of Propylene

$$R_p = 3.5 \times 10^3 \times PP^{0.64} \times PW^{-0.04} \times \exp(-16000/RT) \text{ mole}/\text{Hr}\cdot\text{g}$$

where

PP = partial pressure of propylene. PW = partial pressure of steam.

CHAPTER 4 DISCUSSION

	Page
4.1 <u>PYROLISIS</u>	210
4.1.1 Nickel foils	210
4.1.2 Comparison between nickel foil and supported nickel catalysts	223
4.1.3 A model for carbon formation	226
4.2 <u>CARBON GASIFICATION</u>	235
4.3 <u>STEAM REFORMING</u>	244

4 DISCUSSION

The results obtained for carbon formation from pyrolysis and from steam-reforming on nickel foils and supported nickel catalysts will now be compared; for ease of presentation, the discussion is split into appropriate sections.

4.1 PYROLYSIS

4.1.1 Nickel Foils

The features observed for the pyrolysis of propylene over nickel foil can be best discussed from examination of Fig. 3.4. The results are very similar to those obtained in a static system by Lobo (46) and the explanation for many of the observations appears to be the same.

Constant rates of carbon deposition were obtained for extended periods of time, under some conditions right up to the limits imposed by the equipment used. Nickel crystallites were found in the carbon deposits (Cf 3.2.4) and the deposits were found to catalyse the reaction even when separated from the original foil. Gas-phase reactions were not important below 650°C and no deposition could be observed after poisoning the foils with sulphur compounds. Graphite itself was not a catalyst for the reaction at these temperatures ($< 650^{\circ}\text{C}$).

At low temperatures, below 550°C , zero order kinetics were observed, and the activation energy for the reaction was found to be 33 kcal/mole, the rate of reaction increasing with temperature. These features seem to support the explanation advanced by Lobo et al. (131) that the diffusion of carbon through nickel is rate determining in this temperature range.

At temperatures above 650°C, it seems likely that gas-phase carbon formation is becoming important. In support of this, carbon was found to be deposited on the walls of the reactor.

At intermediate temperatures (550-650°C) some novel features of the reaction were discovered. The rate of reaction was found to decrease with increasing temperature, but positive orders of reaction were determined: first order in hydrogen and first order in propylene. The energy of activation was approximately -40 kcal/mole.

Several possibilities were considered as to why a decrease in rate should become important at these temperatures, and the first possibility that sprang to mind was that, since the rate was measured in terms of weight uptake, the decrease in rate with increase in temperature could be due to the increasing importance of carbon gasification by the hydrogen produced in the reaction. As a result, the influence of hydrogen on the reaction was studied in detail.

a) Low Temperature (<550°C)

Carbon gasification by hydrogen was found not to be important below 550°C, so that the gasification process does not influence the results obtained at low temperatures. However, some interesting features were found in this region, as summarised in Table 4.1 (I).

In the absence of hydrogen, carbon deposition was preceded by long induction periods, followed by an acceleration leading to a steady-state rate of deposition which was somewhat lower than when hydrogen was present. The extent of deposition was limited to about 3 mg/cm² and the carbon films obtained seemed to

Table 4.1 Effect of hydrogen

I - Low temperature (<math>550^{\circ}\text{C}</math>)

	Without H_2	With H_2
Induction period	Yes	No
Rate of deposition	Low	High
Extent of deposition	Limited ($\approx 3\text{mg}/\text{cm}^2$)	Unlimited ($> 40\text{mg}/\text{cm}^2$)
Type of carbon	Ordered	Sooty
Kinetics :		
Order w.r.t. C_3H_6	0	0
Activation energy	33 kcal/mole	33 kcal/mole

II - High temperature ($550-650^{\circ}\text{C}$)

	Without H_2	With H_2
Extent of deposition	C solubility in Ni	Unlimited ($> 40\text{mg}/\text{cm}^2$)
Type of carbon	Graphite poly- cristalline film	Soot

prevent further deposition. With hydrogen, induction periods were never observed and sooty carbon could be formed at constant rate over the foil, apparently without limit (within the range of the equipment used). Carbon formation was markedly accelerated by hydrogen, in agreement with the findings of Tesner (108), Lobo (132) and Nishiyama (134).

To explain the observed features of the process of carbon formation on nickel foils, the following steps have been considered:

- 1 Adsorption of the reactants on the surface;
- 2 Surface reaction, leading to adsorbed carbon species;
- 3 Diffusion of carbon through the nickel crystallites and precipitation of graphite at the grain boundaries lifting up the crystallites, which will subsequently be carried on top of the growing carbon, thus ensuring constant rates of deposition.

At low temperatures ($<550^{\circ}\text{C}$), diffusion of carbon in nickel is assumed to be rate determining, while in the range from 550 to 650°C surface reaction seems to be controlling. At still higher temperatures ($>650^{\circ}\text{C}$), carbon formation in the gas-phase becomes important.

Nucleation of the carbon may occur on the external surface or at grain boundaries, the latter being energetically more favoured. Growth of surface nuclei cannot lift metal particles out of the substrate, instead it would result in the encapsulation of the active surface, inhibiting further deposition. The presence of hydrogen may prevent this type of nucleation by keeping the surface clean of such encapsulating species. Nucleation at grain boundaries would then be enhanced and the growth of carbon there could push metal grains out of the substrate, thus ensuring

constant activity for carbon formation as observed experimentally. It has also been reported (42) that hydrogen enhances grain boundary grooving of nickel films at low temperatures (400-570°C). This process might provide an easier path for diffusing carbon species, therefore accounting for the elimination of induction periods.

Hydrogen also affects the structure of the deposit obtained, and carbons formed in its absence tend to be more ordered. This is understandable, since lower rates of deposition are obtained in the absence of hydrogen, therefore creating more suitable conditions for the growth of good graphite (93).

b) High temperature ($> 550^{\circ}\text{C}$)

In the intermediate temperature range (550-650°C), experiments with high and low pressures of hydrogen have confirmed that at least one role of hydrogen is to keep the surface clean, preventing deactivation. High pressures of hydrogen would remove any deposit on the gas-metal interface, allowing carbon formation to continue and ensuring reversibility on increasing and decreasing temperature (Fig.3.4). Under such conditions, parallel lines are obtained in the Arrhenius plots, for different gas compositions in contrast with the results previously reported by Lobo (46), where different slopes were measured in the Arrhenius plots, corresponding to different composition. This was possibly due to the use of low hydrogen pressures, which were not sufficient to keep all the surfaces clean of encapsulating species. Permanent deactivation, by encapsulation of some crystallites with carbon, would then be expected, resulting in an hysteresis effect similar to that of the Arrhenius plot shown in Fig.3.5, where the rates of deposition fall more rapidly when the temperature is increased. Indeed, they fall even if the temperature is held constant, and steady

rates are only obtained again at lower temperatures, where this deactivation effect is negligible. Therefore, if the temperature is lowered rapidly to such a region, "freezing" the deactivation, a line of about -40 kcal/mole can still be drawn in the Arrhenius plot, although the rate now obtained is lower. Reversibility is lost, as shown by the impossibility of returning to the original rate of deposition.

The same reasoning could perhaps explain the very steep branch for the intermediate temperature region observed by Lobo (130) in the case of acetylene decomposition, where the experiments were performed without hydrogen addition. The thermogravimetric method used, where heating and cooling rates were established (160), would then make the deactivation effect difficult to be recognised.

In the absence of hydrogen, carbon formation was found to proceed to the limit of solubility in nickel, and a polycrystalline graphitic film was obtained. Previous studies (138) have shown that dissolution of carbon in nickel can be followed by the precipitation of well ordered graphite, which effectively encapsulates the surface. That such a process is important under the present conditions is confirmed by the amount of carbon deposited and by the observation that carbon formation after such deposition will not re-start, even at low (440°C) temperatures. However, the introduction of hydrogen into the feed led to the deposition of sooty carbon, and two explanations seem possible:

(1) Attack of the hydrogen on the encapsulating carbon, resulting in the re-formation of a clean nickel surface and leading to renewed carbon formation;

2) Alternatively, a nickel species incorporating hydrogen might be essential for carbon formation. Recent electron diffrac-

tion studies (42) have in fact revealed that a hitherto unreported Ni-H₂-C or Ni-H₂ compound is formed at temperatures greater than 540°C. Full explanation of the effects observed cannot be attempted until the importance of such compounds in carbon formation has been established.

Carbon gasification was found to be important above 550°C and the kinetics of the reaction were determined and are summarised in Table 4.5.

Considering first the possibility that gasification is determining the inflection in the Arrhenius plots, the rates of carbon formation were corrected by the calculated rates of gasification, as shown in Fig.4.1. It is seen that, although there is a slight influence on the results, the amount of carbon gasified is insufficient to account for the decrease in rate with increasing temperature. Therefore, alternative explanations must be considered.

Some possible reasons for this effect have been presented and discussed previously : sintering, absence of formation of an intermediate carbide, effect of approaching equilibrium, poisoning and decreasing adsorption (131) as well as the change in critical size of nuclei (99). Of these, only the effect of decreasing adsorption has been found to be acceptable as a possible answer to the reversible decline in rate in the present context. The suggestion is that, above a certain temperature, the surface reaction step takes over from diffusion of carbon in the nickel as rate determining. This is to a certain extent confirmed by the observed change from zero order kinetics to second order (overall) kinetics. Now, when rates of reaction are used in the Arrhenius plots, the slope of such plot will only measure the true

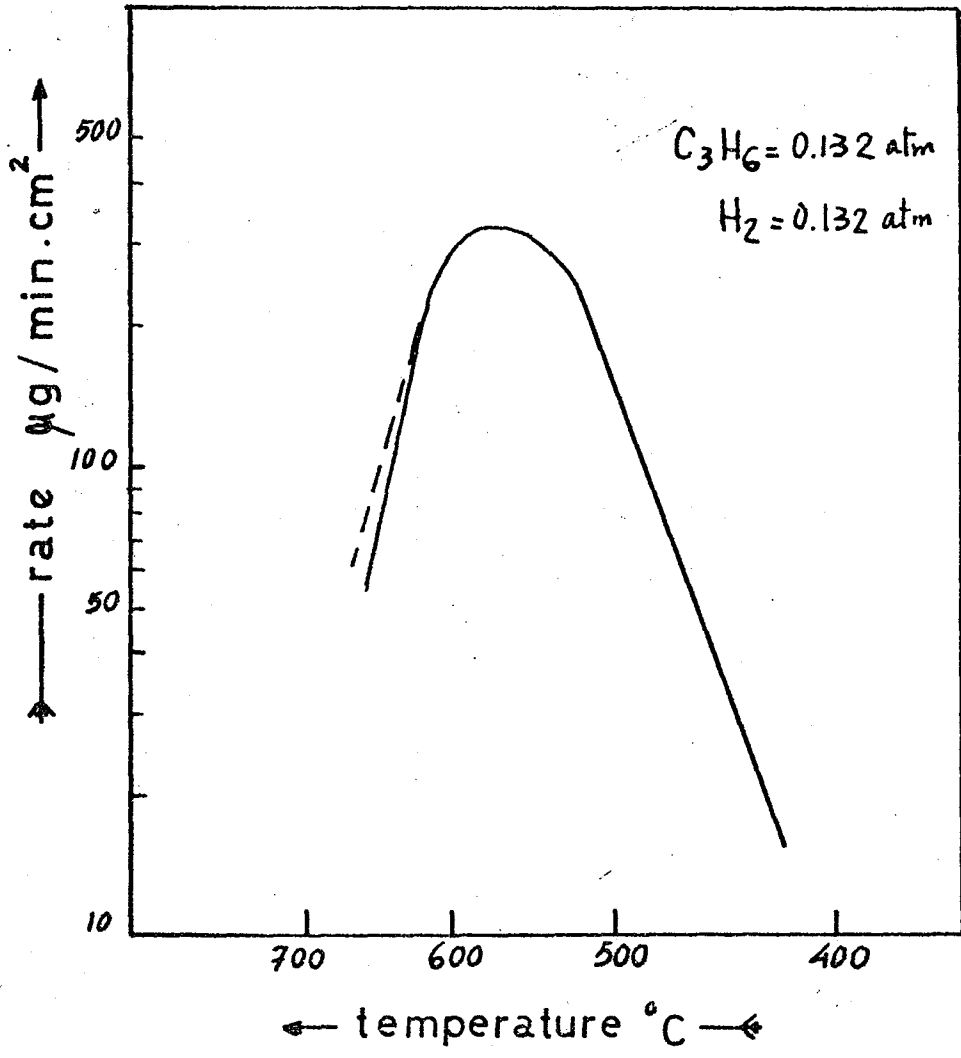
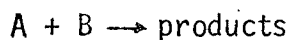


Fig. 4.1 Carbon Deposition Corrected for Gasification (run 138)

activation energy when zero order kinetics are obeyed. In all other cases, the apparent activation energy determined will correspond to the combined effects of the true activation energy for reaction and the heats of adsorption of the reactants.

Let us consider the following reaction:



with a rate equation of Langmuir-Hinshelwood type

$$r = \frac{k \cdot b_A P_A \cdot b_B P_B}{(1 + b_A P_A)(1 + b_B P_B)}$$

At low temperatures we may expect the reactants to be strongly adsorbed so that $b_A P_A \gg 1$, $b_B P_B \gg 1$ and the rate equation reduces to

$$r = k \quad (\text{zero order})$$

At higher temperatures, the reactants will become weakly adsorbed so that

$$b_A P_A \ll 1, b_B P_B \ll 1 \quad \text{and}$$

$$r = k b_A P_A b_B P_B \quad (\text{2nd order})$$

Therefore, we have for the first case

$$\frac{d \ln r}{dT} = \frac{d \ln k}{dT} = \frac{E}{RT^2}$$

$$\text{or } E_a = E$$

whereas, for the second case,

$$\frac{d \ln r}{dT} = \frac{d \ln k}{dT} + \frac{d \ln b_A}{dT} + \frac{d \ln b_B}{dT}$$

$$\text{or } \frac{E_a}{RT^2} = \frac{E}{RT^2} + \frac{\Delta H_A}{RT^2} + \frac{\Delta H_B}{RT^2}$$

since b_A and b_B are equilibrium constants for adsorption, therefore obeying the van t' Hoff relationship:

$$\frac{d \ln K}{dT} = \frac{\Delta H}{RT^2}$$

In this last case, therefore,

$$E_a = E + \Delta H_A + \Delta H_B$$

and the measured activation energy will contain terms corresponding to adsorption.

The following heats of adsorption were obtained from the literature at zero coverage (161):

Hydrogen on nickel : $\Delta H = -30$ kcal/mole

Ethylene on nickel : $\Delta H = -58$ kcal/mole

Acetylene on nickel : $\Delta H = -67$ kcal/mole

No value was found for propylene on nickel, but it is expected to be similar to those of acetylene or ethylene. Now, possible surface reactions such as dehydrogenative adsorption followed by hydrogenolysis of the residue, can be expected to be associated with activation energies in the range of 20 to 40 kcal/mole (162). The combination of this activation energy with the heats of adsorption of hydrogen and propylene will therefore result in a negative apparent activation energy. It is to be noted, however, that the change from a fully covered surface to a low coverage is not expected to occur at temperatures as high as 550°C.

This might possibly occur at temperatures of 100 or 200°C, as in the case of olefin hydrogenation discussed originally by

zur Strassen (163). The present situation may then be described in face of Fig. 4.2:

The surface reaction step is assumed to be very fast compared with diffusion of carbon in nickel below 550°C, and therefore is not rate determining. This step is associated with an activation energy E , possibly in the range of 20-40 kcal/mole. However, at some low temperature, the reactants become weakly adsorbed and the overall "activation energy" becomes apparently negative.

Diffusion of carbon in nickel is the slow step but, as temperature is increased, its Arrhenius plot intersects the descending branch correspondent to the surface reaction (affected by adsorption of reactants) and this becomes the slower step. This occurs at a temperature near to 550°C but depending on the partial pressures of the reactants, as shown in Fig 4.2. As the pressures are increased, the maximum moves to higher temperatures and this is consistent with the surface reaction step taking over as rate determining.

This explanation, based on the heats of adsorption, has been criticised mainly on the basis of the Arrhenius plots presented for acetylene (130), with a very steep branch in the intermediate temperature region. The fitting of a straight line in that temperature range would yield an "activation energy" of about -200 kcal/mole, which could not be explained in terms of the heat of adsorption of acetylene ($\Delta H = -67$ kcal/mole). This has been recognised in the present work as a deactivation effect, due to the absence of hydrogen. When such effects are avoided, the explanation based on heats of adsorption does fit the results.

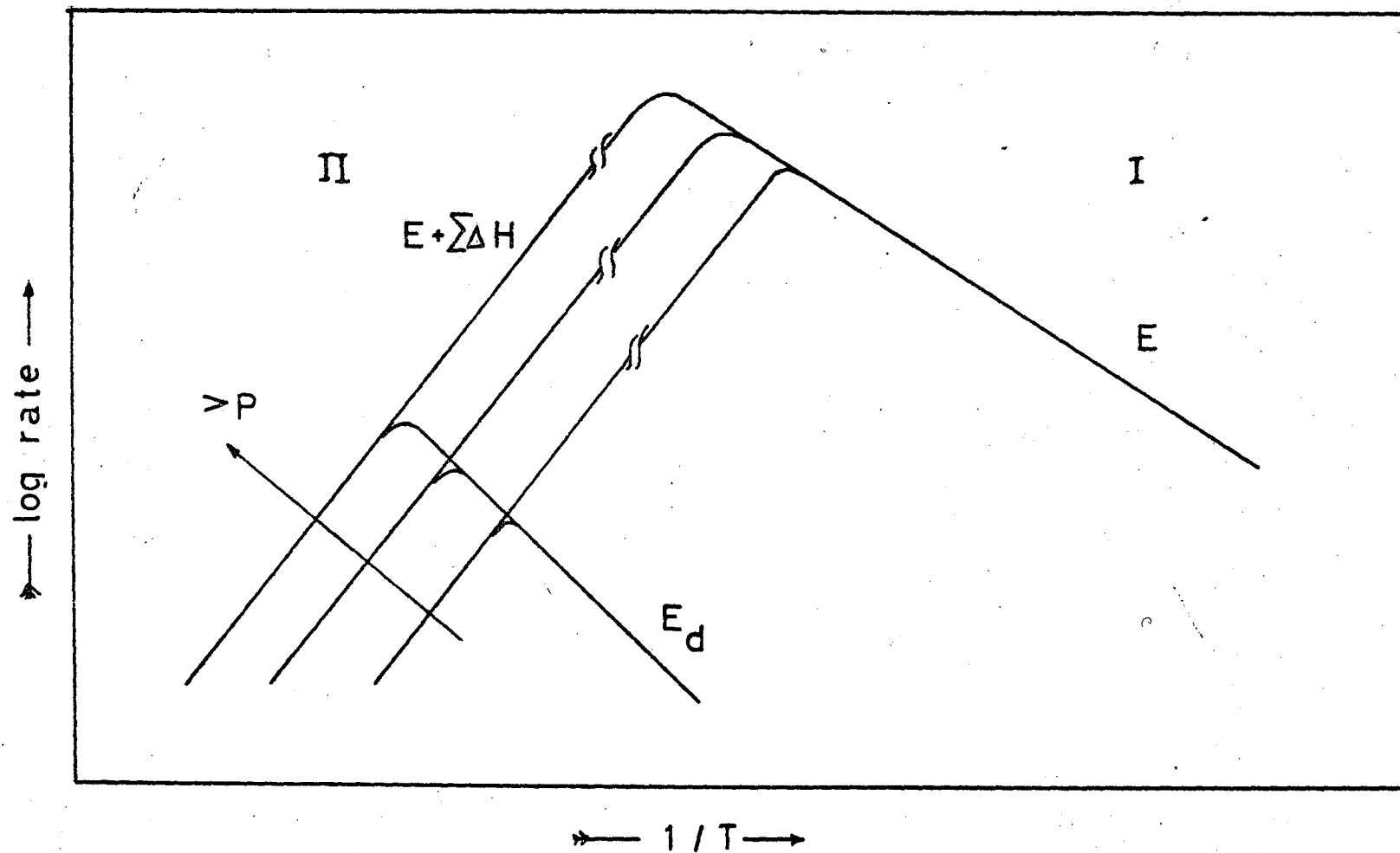


Fig. 4.2 Apparent activation energies (adapted from ref. 170)

The possibility of nickel hydride formation, as discussed earlier, must also be considered. If such compounds become necessary for carbon formation, then:

$$\text{rate (C formation)} = k \cdot P_{\text{C}_3\text{H}_6} \cdot (\text{NiH}_2)$$

If $\text{Ni} + \text{H}_2 = \text{NiH}_2$, then

$$K = \frac{(\text{NiH}_2)}{(\text{Ni}) \cdot P_{\text{H}_2}}$$

and

$$\text{rate (C formation)} = k P_{\text{C}_3\text{H}_6} \cdot K \cdot (\text{Ni}) \cdot P_{\text{H}_2}$$

(Ni) may be assumed constant and

$$\text{rate (C formation)} = k^1 \cdot P_{\text{C}_3\text{H}_6} \cdot P_{\text{H}_2} \cdot K$$

$$\text{so that } \frac{d \ln \text{rate}}{dT} = \frac{d \ln k^1}{dT} + \frac{d \ln K}{dT}$$

$$\text{and } E_a = E^1 + \Delta H (\text{hydride})$$

Therefore, an effect similar to decreased adsorption might be operative.

Both carbide and hydride formation are processes accompanied by lattice expansion, and this might provide the stress forces necessary to mechanically disrupt the surface of the foil, releasing the nickel crystallites required to maintain a constant activity. Carbide formation might then be important at low temperatures ($< 550^\circ\text{C}$) while hydride formation would take over above 550°C .

4.1.2 Comparison between Nickel Foil and Supported Nickel Catalysts

The results obtained for carbon formation on nickel foils and supported nickel catalysts may now be compared. The kinetic features of the reaction were very similar, the only difference being the complete independence of deposition rates on the presence or absence of hydrogen in the case of supported catalysts, induction periods never being observed. This different behaviour must obviously be discussed in terms of the differences in structure between nickel foils and supported catalysts. One such difference is the presence of a new material, the support. Another is the state of the metal crystallites.

It might be argued that carbon deposition on the support itself would release enough hydrogen to make its presence in the feed redundant. This would require the production of substantial amounts of hydrogen if deactivation at high temperatures were to be avoided (Cf. 3.2.1.4). In order to investigate this possibility, alumina pellets were used in conjunction with nickel foils (Cf. 3.2.3): Although some carbon was formed on the support itself, mainly at high temperatures, the amount of hydrogen released was clearly not enough to explain the difference in behaviour between foil and supported catalysts.

The different state of the metal crystallites may explain the need for the presence of hydrogen in the case of nickel foils. In fact, if nickel crystallites are to be detached from the foil, preferential carbon nucleation at grain boundaries is required and this is favoured when hydrogen is present, hence the positive effect of hydrogen on rates of carbon deposition. In the case of the supported nickel catalysts, the nickel crystallites are already

distributed over the support, and these are expected to be pushed up with the growing carbon without further assistance from hydrogen. No induction periods would be expected or are observed in this case.

Alternatively, the support might provide a catalytic function, such as cracking, which would be absent in the case of nickel foils. Nickel on its own, without hydrogen, would dehydrogenate the hydrocarbon, but without breaking the C-C bonds. Hydrogen would then be required to produce hydrogenolysis reactions, whereas in the case of supported catalysts hydrogen is made redundant.

Above approximately 450°C, the measured rates of carbon deposition on supported catalysts were limited by gas-phase diffusion, but comparison with foil was possible at lower temperatures. The same activation energy (30 kcal/mole) order of reaction (zero) and specific rates of carbon formation (Table 4.2) were obtained over foils or supported catalysts. The comparison was made on the basis of the original nickel surface area available, and shows that the same mechanism of carbon formation is operative, regardless of the support material. The reaction may therefore be classified as "facile", according to Boudart (164). It should be noted, however, that the crystallite sizes of the catalysts used are outside the critical range of particle sizes (1-5 nm) discussed by Boudart (164). The crystallite sizes of the supported catalysts used in the present work were calculated from the specific surface areas and metal content by the formula $d = 6V/A$, assuming spherical shapes, and are presented in Table 4.3.

Table 4.2 Specific Rates of Carbon Formation from
Propylene on Nickel Catalysts

($T = 400^{\circ}\text{C}$, $P_{\text{C}_3\text{H}_6} = 0.13 \text{ atm}$)

RUN	Catalyst	Weight mg	Metal Area (*)	Rate $\mu\text{g}/\text{min}$	Specific Rate $\mu\text{g}/\text{min}\cdot\text{cm}^2$
107	Ni foil	123.2	23 cm^2/g	17	6
325	Ni/ Al_2O_3	26.0	.4 m^2/g	667	6
268	ICI 46-1	19.5	.6 "	740	6
271	Ni/kieselguhr	15.1	1.7 "	1430	6

(*) For nickel foil, the geometric area was used.

For supported catalysts, the metal area was determined by CO chemisorption.

Table 4.3 Crystallite Sizes of Supported Nickel Catalysts

Catalyst	Ni content V (cm^3/g)	Metal Area A (m^2/g)	Crystallite Size $d = 6V/A$ (μm)
Ni/ Al_2O_3	0.02	0.4	0.3
ICI 46-1	0.02	0.6	0.2
Ni/kieselguhr	0.05	1.7	0.18

Diffusion limitations were met with in microbalance runs above about 450°C, and it was not possible to check the occurrence of maxima in rate as observed with foils. These mass-transfer problems were certainly a consequence of the geometry of the system, whereby samples of catalyst were suspended from the balance inside small baskets. Since total flow rates could not be increased very much, concentration gradients would be established between the gas phase and the catalyst sample, the gas by-passing the basket. However, a few runs carried out in the fixed-bed reactor suggest that a maximum in rate would also be observed for supported nickel catalysts.

Surface area measurements indicate that pore-mouth poisoning does not occur for low coke contents; for heavy deposits, however, the shape of some of the carbon formation curves (Fig.3.13) indicate that pore-mouth blocking may occur. The carbon deposits themselves are of high surface area (100-200 m²/g) and medium porosity (0.3 - 0.4).

4.1.3 A Model for Carbon Formation

The literature survey (Section 1.3) and the results of the present work show considerable evidence in support of a mechanism of carbon growth involving the diffusion of carbon through nickel. This evidence is summarized below:

- 1) Extended periods of constant growth can be observed without apparent deactivation;
- 2) Various olefins and acetylene have been found to produce carbon on nickel at very similar rates and following the same kinetics (46);
- 3) Carbon formation from acetylene on Ni, Fe, Co and Cr

showed an activation energy in good agreement with the coefficient of temperature dependence for diffusion of carbon in those metals (112);

4) Nickel particles have been observed at the top of carbon growing filaments (105);

5) Zero order kinetics were determined;

6) The rate of growth was reported to vary in inverse dependency with the particle size of the metal (112); this was quantitatively determined for iron, and also found with cobalt, although a previous report showed no correlation for the case of nickel (105).

Both Lobo et al (131) and Baker et al (105) proposed models for carbon growth in which diffusion of carbon in the metal was considered to be the rate determining step, at least in part of the temperature range (131).

For carbon formation from acetylene, Baker et al (105) proposed that a temperature gradient would develop across the metal particles and provide the driving force for diffusion of carbon. This was suggested by the fact that acetylene decomposition is highly exothermic, therefore releasing a considerable amount of heat at the exposed face of the metal particle. When this suggestion is taken together with the results of Lobo (46), however, it has to be dismissed, since a similar mechanism must be operative in the case of decomposition of olefins, and some of these reactions are in fact endothermic. The heats of these reactions were calculated by standard methods (22) at reaction temperatures, and are presented in Table 4.4. Therefore, the existence of a temperature gradient is not a general feature of the process.

Table 4.4 Standard Heats of Carbon Formation Reactions

Reaction	ΔH° kcal/mole		
	600K	800K	1000K
$\text{CH}_4 \rightarrow \text{C} + 2\text{H}_2$	19.9	20.8	21.4
$\text{C}_2\text{H}_2 \rightarrow 2\text{C} + \text{H}_2$	-53.9	-53.6	-53.3
$\text{C}_2\text{H}_4 \rightarrow 2\text{C} + 2\text{H}_2$	-10.6	- 9.8	- 9.2
$\text{C}_3\text{H}_6 \rightarrow 3\text{C} + 3\text{H}_2$	- 2.0	- 0.7	-0.03
$\text{C}_4\text{H}_8 \rightarrow 4\text{C} + 4\text{H}_2$			
1-butene	3.7	5.1	5.9
cis-butene	5.8	7.5	8.4
trans-butene	6.4	7.9	8.7
$2\text{CO} \rightarrow \text{CO}_2 + \text{C}$	-41.5	-41.2	-40.8

On the other hand, Lobo (46) considered a concentration profile in the nickel particles at steady state : The concentration of carbon in the nickel at the gas-exposed surface would be determined by the solubility limit at each temperature, while at the rear of the particle, where carbon growth occurred, the concentration of nickel would be taken always as zero. The following expression could then be derived for the rate of diffusion, N , across a slab of nickel of thickness L :

$$N = -D \frac{dC}{dx} = DS/L$$

However, as Lobo points out (46) this model would not account for the measured activation energy determined for the reaction (33 kcal/mole) since the solubility S is itself temperature dependent. Therefore, the activation energy of the process would be that for diffusion of carbon through nickel (33 kcal/mole) plus the temperature coefficient for the solubility of carbon in nickel (150), 10 kcal/mole, i.e. 43 kcal/mole. Comparison with the experimentally determined value (33 kcal/mole) leads to rejection of this model.

Now, if precipitation of carbon occurs at the rear of the particle, then there must exist some sort of supersaturation of carbon in the metal; if it were zero, as assumed by Lobo (46), no precipitation would occur. On this basis the following model was developed:

- 1) The hydrocarbon adsorbs on the metal and undergoes dehydrogenation and hydrogenolysis reactions on the surface, producing carbon atoms (since nickel is a very active dehydrogenation catalyst at the high temperatures considered).

2) Preferential nucleation of carbon occurs at grain boundaries. This had been experimentally observed in the work of Presland (95), Lobo (46) and Moayeri (42), and can be explained on thermodynamic grounds.

3) Carbon atoms are taken in solution at the surface of the nickel crystallites and diffuse through the metal, precipitating at the grain boundaries. The nickel crystallites will be lifted up from the surface of the catalyst and will be transported with the growing carbon, therefore ensuring constant rates of deposition, since no poisoning of the surface occurs. Under certain circumstances surface nucleation may also occur, and this will lead to encapsulation with carbon and subsequent deactivation of the metal.

Dissolution of amorphous carbon in nickel and its subsequent precipitation as graphite has been shown to be possible under reaction conditions (138). The work of Lobo (46), Derbyshire (99) and Moayeri (42) provides additional evidence that carbon deposits may show considerable crystallinity, at least during the initial stages of the deposition. Under the present working conditions, high supersaturation (relatively low temperatures, and high pressures) will tend to cause high rates of deposition, and the deposits are expected to be of poor crystallinity. This was in fact the case, with sooty carbons being obtained although the presence of graphitic crystallites was established. Therefore, precipitation of graphite layers may be assumed, at least at the nickel-carbon interface, with the proviso that, due to unsuitable conditions, no three-dimensional ordering occurs in the present case.

The driving force for diffusion of carbon from the deposition face to the rear of the particle is assumed to be the excess free energy of the carbon atoms relative to the graphite structure, and

the process can occur isothermally. This is analogous with the process of catalytic carbon graphitization, as reviewed by Fischbach (165), which can occur entirely in the solid state (166). These processes involve the transformation.

C (disordered) $\rightarrow C$ in Ni \rightarrow Graphite while in the present case the scheme $C_a^* \rightarrow C$ in Ni \rightarrow Graphite is considered (C_a^* = adsorbed carbon atoms)

Let

V = rate of surface reaction

V_m = experimentally measured rate of carbon formation

V_d = rate of diffusion of carbon in nickel

V_p = rate of graphite precipitation

C_d = Concentration of carbon dissolved in nickel

C_a = Concentration of carbon atoms at the surface

C_g = Concentration of graphite at the rear surface

The surface reaction is assumed to be much faster than the other steps, at least at low temperatures (< 800 K), so that $V \gg V_d$ and $C_{d_0} = C_d^e$ (1.)

where:

Subscript 0 : exposed surface of Ni particle

Subscript 1 : rear face of Ni particle

Superscript e : in equilibrium

Considering the three phases shown in Fig. 4.3, the following equilibria will be established:

$$(2.) \quad K_0 = C_{d_0}^e / C_a^e \quad (\text{dissolution})$$

$$(3.) \quad K_1 = C_g^e / C_{d_1}^e \quad (\text{precipitation})$$

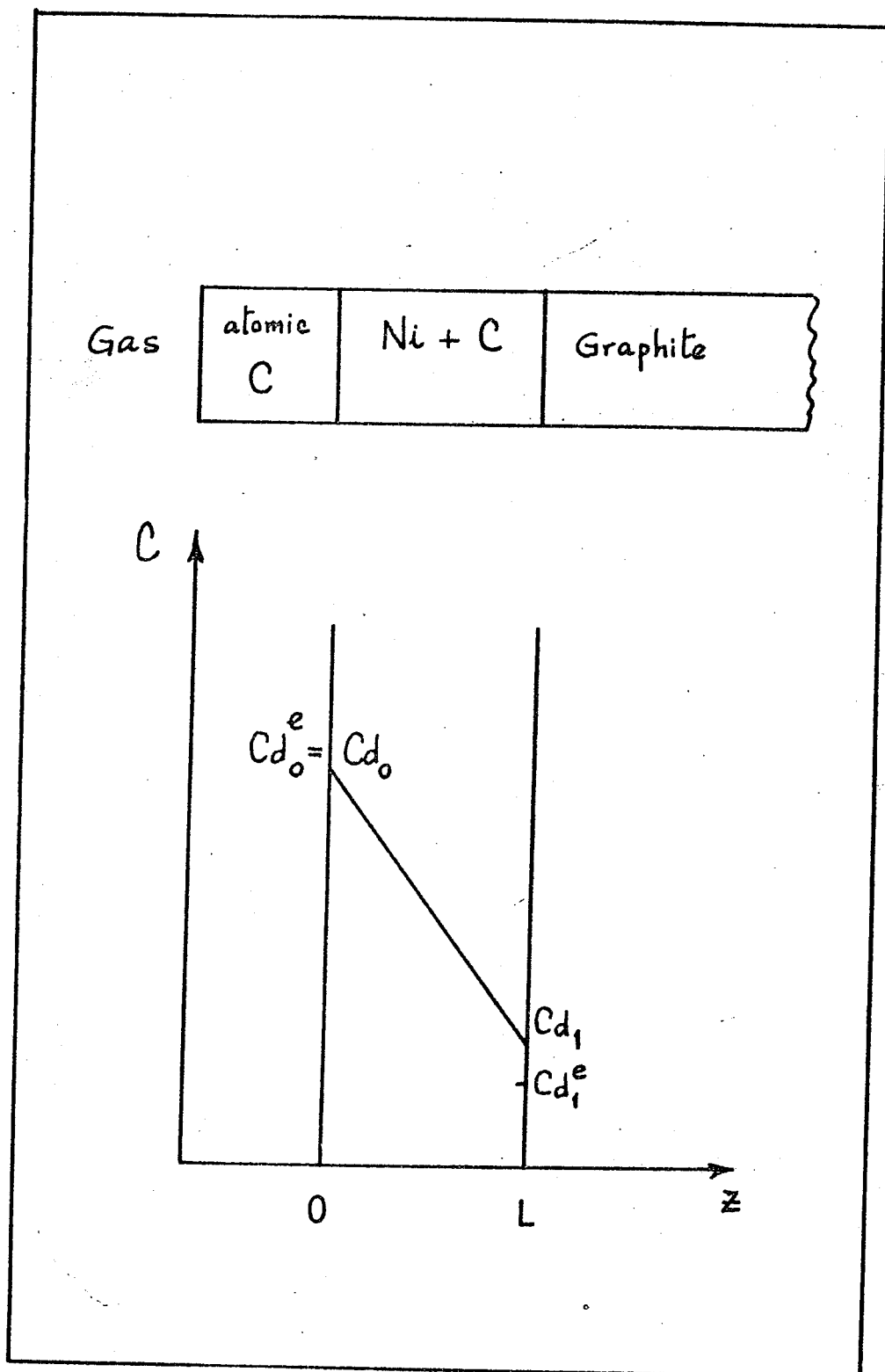


Fig. 4.3 Concentration profile of carbon in a nickel crystallite of thickness L

and

$$(4.) \quad V_d = D/L \cdot (Cd_0^e - Cd_1)$$

$$(5.) \quad V_p = k \cdot (Cd_1 - Cd_1^e)$$

where $(Cd_1 - Cd_1^e) =$ supersaturation

$$(6.) \quad V_m = V_d = V_p = V \quad (\text{processes in series})$$

from (5.) and (6.):

$$(7.) \quad Cd_1 = V_m/k + Cd_1^e$$

and from (4.) and (7.)

$$(8.) \quad V_m = \frac{D/L \cdot (Cd_0^e - Cd_1^e)}{1 + \frac{D}{L \cdot k}}$$

Provided that the precipitation is fast compared with diffusion,
 $k \gg D/L$

$$(9.) \quad V_m = \frac{D}{L} \cdot (Cd_0^e - Cd_1^e)$$

Since the observed activation energy is found to be 33kcal/mole, i.e. about the same as for diffusion of carbon in nickel (167), then the model predicts that the term $(Cd_0^e - Cd_1^e)$ shall be nearly temperature independent. The solubility of carbon in nickel can be expressed as (150):

$$\ln S = 2.48 - 4880/T \quad \text{g/100g}$$

and the diffusivity as (167):

$$D = 0.195 \exp\left(-\frac{34800}{RT}\right) \text{ cm}^2/\text{sec}$$

The average size of nickel particles in the carbon has been estimated (from gasification results, section 4.2) as 70 nm. Therefore, the simplified equation (9.) can be used to determine

the term $\Delta C = (C_{d_0}^e - C_{d_1}^e)$. At 400°C , the rate of carbon deposition was determined as $6 \mu\text{g}/\text{min}\cdot\text{cm}^2$ under conditions where the reaction is of zero order. Therefore

$$D(400^\circ\text{C}) = 10^{-12} \text{ cm}^2/\text{sec}$$

$$L = 7 \times 10^{-6} \text{ cm}$$

$$V_m = 0.1 \mu\text{g}/\text{sec}\cdot\text{cm}^2$$

$$\text{and } \Delta C = V_m \cdot L / D = 7 \times 10^5 \mu\text{g}/\text{cm}^3 = 0.7 \text{ g}/\text{cm}^3$$

This value is much larger than the solubility of carbon in nickel,

$$S(400^\circ\text{C}) = 7.6 \times 10^{-4} \text{ g}/\text{cm}^3$$

but is of the same order of magnitude of the carbon content of nickel carbide:

For Ni_3C , the carbon content is 6.4 wt% (168) or $0.62 \text{ g}/\text{cm}^3$ (approximately). It may then be proposed that $C_{d_0}^e$ corresponds closely to the concentration of carbon in a "nickel carbide" matrix while $C_{d_1}^e$ corresponds to the solubility of carbon in nickel. Under such conditions, the concentration gradient in the nickel particle will have a negligible temperature dependency. Therefore, at the front end of the nickel particle we may assume the formation of nickel carbide while, at the rear, carbide decomposition releases graphite.

This treatment may be applied to the data of Baker et al (105), for the growth of carbon filaments on nickel at 600°C :

$$\text{filament diameter} = 30 \text{ nm}$$

$$\text{rate of growth} = 90 \text{ nm}/\text{sec}$$

Therefore

$$\Delta C = \frac{90 \times 10^{-7} \times 2.26 \times 30 \times 10^{-7}}{3.9 \times 10^{-10}} = 0.16 \text{ g}/\text{cm}^3$$

since the density of graphite is 2.26, and $D(600^{\circ}\text{C}) = 3.9 \times 10^{-10} \text{ cm}^2/\text{sec}$. This is again some two orders of magnitude higher than the solubility of carbon in nickel (at 600°C , $S = 0.004 \text{ g/cm}^3$), but of the same order of magnitude of the concentration gradient determined from the present results. It should be noted, however, that under the experimental conditions used the results of Baker et al (105) cannot be interpreted entirely with this model. Not only was there no inverse correlation between rates of growth and particle size, but also, at 600°C and $5 \times 10^{-4} \text{ atm}$, the reaction must have been proceeding well into the region of chemical reaction control, i.e. in region II of the Arrhenius plot of Fig.4.2.

4.2 CARBON GASIFICATION

Gasification of the carbon deposits obtained was studied mainly to provide additional information on the mechanisms of carbon formation and of steam-reforming.

The kinetic results obtained are summarised in Table 4.5. Comparison of foil with supported catalyst is unfortunately impossible for the system $\text{C} - \text{H}_2\text{O}$, due to diffusion limitations, but these were absent in the reaction with hydrogen. The main difference observed is the dependency of gasification rates on the initial amount of carbon when nickel foil is used as the substrate for carbon formation. This can be explained in terms of the mechanism for carbon formation previously discussed, which involves the detachment of crystallites from the foil.

In the present system, carbon gasification was catalysed by nickel, as confirmed by the experimental results and comparison with literature data (3.3.1.5 and 3.4.1.3). In fact, pure graphite samples and sulphur-poisoned carbon deposits could not

Table 4.5 GASIFICATION OF CARBON DEPOSITS

 TOTAL PRESSURE = 1 ATM

TEMPERATURE RANGE 800 - 1000 K

RANGE OF WATER PARTIAL PRESSURES 0.05 - 0.36 ATM

RANGE OF HYDROGEN PARTIAL PRESSURES 0.13 - 1.0 ATM

	BY WATER	BY HYDROGEN
NICKEL FOIL	<p>$E = 32 \pm 2$ KCAL/MOLE</p> <p>ZERO ORDER</p> <p>RATE PROPORTIONAL TO INITIAL CARBON WEIGHT</p> <p>RATE CONSTANT AT 923 K= $40.8 \text{ E-03 MIN}^{-1} \cdot \text{CM}^{-2}$</p>	<p>$E = 32 \pm 1$ KCAL/MOLE</p> <p>2ND. ORDER</p> <p>RATE PROPORTIONAL TO INITIAL CARBON WEIGHT</p> <p>RATE CONSTANT AT 923 K= $17.4 \text{ E-03 MIN}^{-1} \cdot \text{CM}^{-2} \cdot \text{ATM}^{-2}$</p>
SUPPORTED NICKEL CATALYSTS	<p>$E = 18 \pm 1$ KCAL/MOLE</p> <p>PROBABLY DIFFUSION LIMITATIONS</p>	<p>$E = 31 \pm 3$ KCAL/MOLE</p> <p>2ND. ORDER</p> <p>RATE INDEPENDENT OF AMOUNT OF CARBON</p> <p>RATE CONSTANT AT 923 K= $32.7 \text{ E-03 MG} \cdot \text{MIN}^{-1} \cdot \text{CM}^{-2} \cdot \text{ATM}^{-2}$</p>

be gasified in the temperature range considered here (800-1000K).

The measured rates of gasification were constant with burn-off for long periods (up to 70% burn-off), but with foils they were proportional to the amount of carbon initially present. This is best shown in Fig.4.4. This result must then be related to the amount of nickel present in the carbon deposit. Chemical analysis revealed the presence of nickel in approximately constant concentration ($1.6 \pm .4$ wt%), inferring that the quantity of nickel contained in carbons deposited over the foils is proportional to the amount of carbon deposited. (Fig.3.15). Therefore, larger carbon deposits contain more dispersed nickel - which acts as a catalyst for gasification - and the observed rates of gasification are higher.

In Fig.4.5, rates of carbon gasification at fixed temperature and pressure were plotted, together with the amount of nickel determined, as a function of the initial weight of the deposit. Therefore, specific rates of carbon gasification may be obtained by dividing the ordinates of the two lines at each value of the abscissa, and a constant value is found.

The rate constants determined for foil and supported catalyst, in the case of hydrogen gasification, may now be compared. From Table 4.5, at 650°C ,

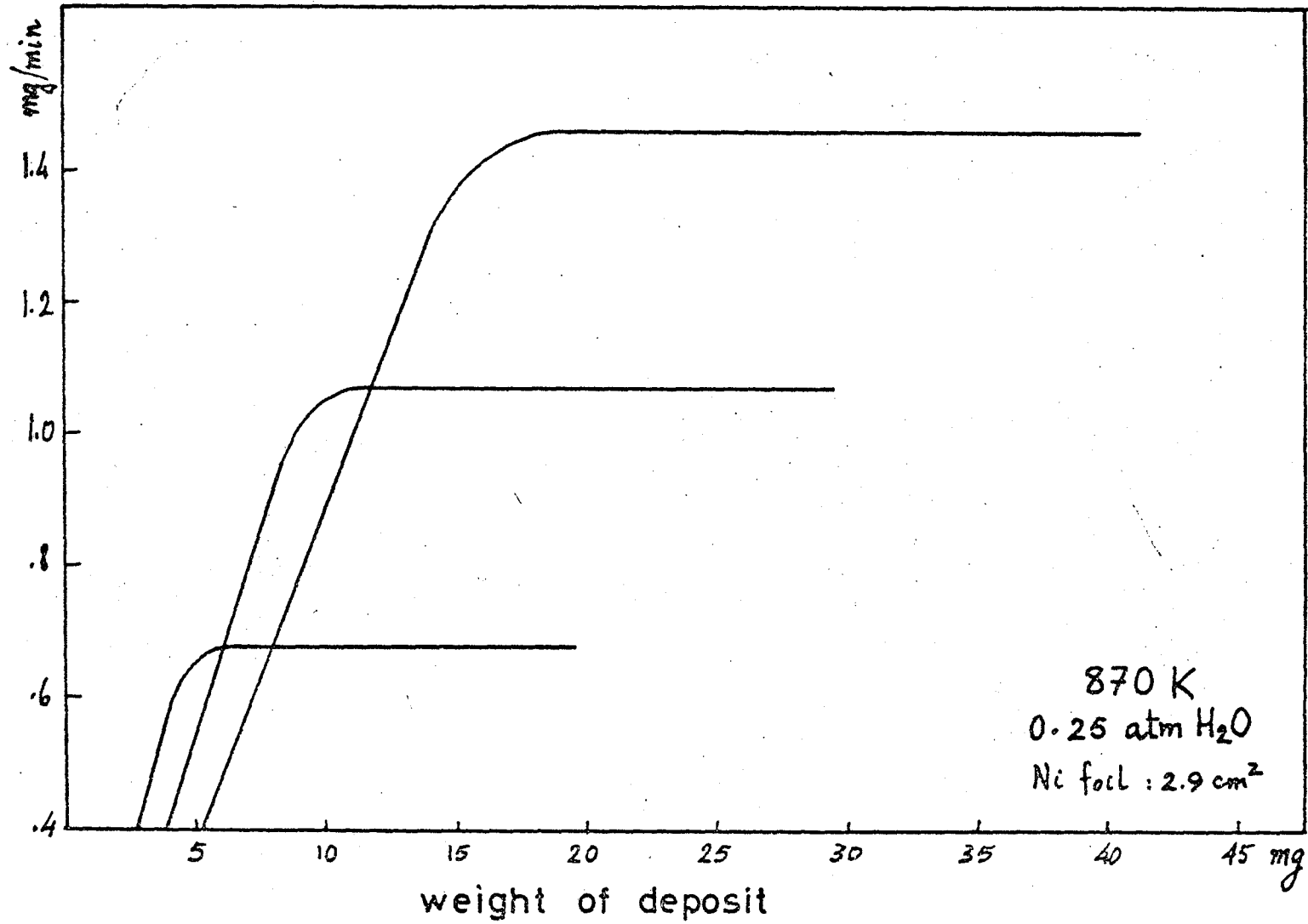
$$k_f = 17.4 \times 10^{-3} \text{ min}^{-1} \cdot \text{atm}^{-2} \cdot \text{cm}^{-2}$$

referred to the geometric area of the foil, and

$$k_s = 32.7 \times 10^{-3} \text{ mg} \cdot \text{min}^{-1} \cdot \text{atm}^{-2} \cdot \text{cm}^{-2}$$

If it is assumed that the presence of the support does not affect the gasification process, then

Fig. 4.4 Rates of burn-off



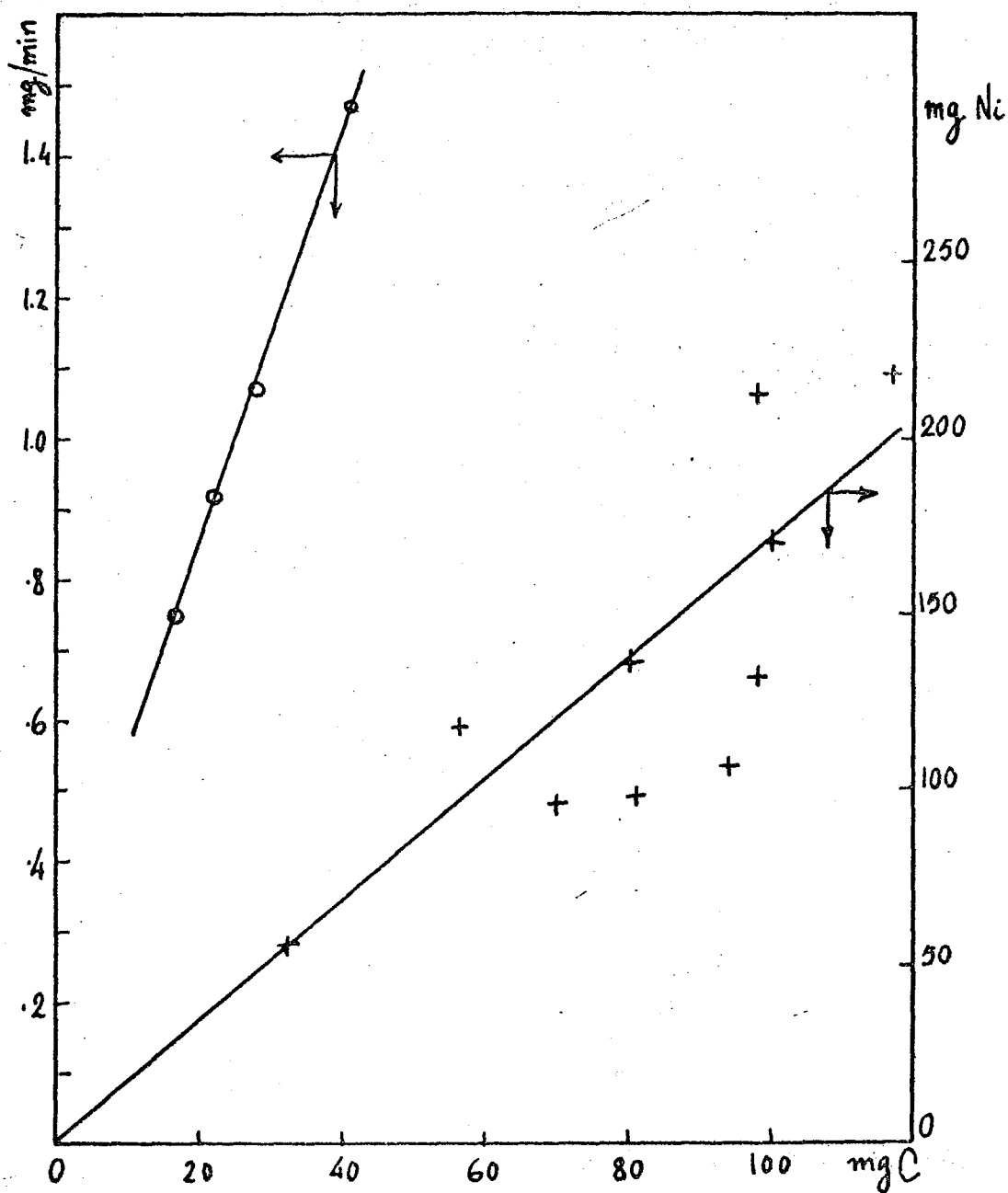


Fig. 4.5 Rates of burn-off, and amount of Ni vs. weight of carbon deposit.

(870 K, 0.25 atm H₂O, Ni foil = 2.9 cm²)

$$k_s = 3.kf/S \quad (S = \text{Ni surface area, cm}^2/\text{mg})$$

since foils of approximately 3cm^2 area were used. Then,

$$S = 0.16 \text{ m}^2 \text{ (Ni)/g(C)}$$

An attempt was made to confirm this calculation by determining the Ni surface area of the dispersion Ni-C by CO chemisorption. Although noticeable uptakes were measured in the gravimetric system, they lacked reproducibility and were certainly inaccurate.

If the calculated value for surface area, $0.16\text{m}^2/\text{g}$, is taken together with the average nickel concentration measured, 1.6 wt%, the average particle size for the nickel may now be estimated. Assuming spherical shape, $d = 6V/A = 70\text{nm}$ and this compares with the estimated crystallite size of the parent foil (46) of 100nm . However, a well defined particle size is unlikely. If nickel crystallites are detached from the foil, a nickel crystallite at the surface of the carbon may be expected to leave a trail of nickel particles in the deposit. These nickel particles may then catalyse the gasification of the carbon, the original foil itself giving only a negligible contribution to gasification, its area being too small. That the nickel left within the carbon can influence the catalyst activity is shown by results obtained on nickel films (42). Coked films are found to have greater activity for steam-reforming than the fresh catalyst, presumably as a result of increased metal area originating from the presence of metal particles in the carbon.

The case of supported catalysts is different in that there is no "production" of nickel crystallites; these are already present on the fresh catalyst, dispersed over the refractory

support. Carbon formation occurs on these crystallites which are expected to be pushed up with the growing deposit. Different amounts of carbon deposited will therefore contain the same amount of nickel (the amount originally available) and gasification rates will be independent of the initial weight of carbon, as has been shown experimentally.

Constant rates of carbon gasification have also been reported by Macak et al (35), who studied gasification by steam of carbons deposited from heptane on nickel catalysts. From their reported data, an activation energy of 28 kcal/mole can be calculated which, by comparison with the present results, seems to suggest that diffusion limitations were absent. At 650^o C, 0.4 atm of H₂O and with 100 mg of catalyst Ni/Al₂O₃, they reported a rate of carbon gasification of 14.6 mg/min. Although they quote a surface area of 10.2 m²/g for their catalyst (Ni content = 6.16 wt%), this is probably the total surface area, so that a direct comparison with the present results is not possible.

These authors took the constancy of gasification rates as a proof that the reaction was not being catalysed by the metal; they suggest that in the latter case, an increase in rate would be observed as carbon removal would increase the possibility of reactant transport to the surface of the catalyst. This explanation would require the gasification reaction to be gas diffusion controlled and does not account for the possible presence of nickel particles at the surface of the carbon deposits. So, although there is good agreement between the present work and the results reported by Macak et al (35) a completely different explanation has been suggested here, since there is no doubt that carbon gasification is nickel catalysed.

Hydrogen gasification of carbon deposits from a nickel catalyst was studied by Gilliland et al (75), and an activation energy of 36 ± 6 kcal/mole was reported in reasonable agreement with the present work. A reaction order of 0.5 was also suggested from a rather doubtful comparison between two runs, and is not supported by the present findings.

Tomita et al (77) have reported activation energies of 25 and 41 kcal/mole for the nickel catalysed and non-catalytic carbon hydrogenation respectively. With other metals (Rh, Pt) activation energies in the range 30-36 kcal/mole were measured (76).

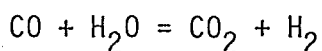
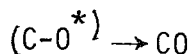
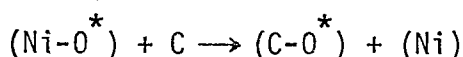
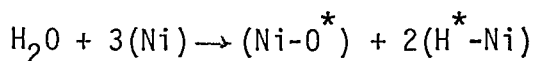
The presence of nickel particles in the carbon will possibly give rise to a spill-over effect (78). The metal can act as a dissociation centre for hydrogen, and the hydrogen atoms so produced may then migrate along the surface of the carbon; therefore, gasification will not be restricted to the regions of contact between carbon and nickel. A similar explanation has been recently suggested by McKee (171). From there on, a mechanism similar to that proposed by Zielke et al (69) for the uncatalysed gasification may be operative, the exposed edges of the graphite lattice being hydrogenated. The rate equation obtained

$$r = \frac{a(P_{H_2})^2}{1 + b(P_{H_2})}$$

predicts orders of reaction of 2 at low pressures and 1 at high pressures. The same authors (69) reported orders of reaction of 1.60 between 10 and 20 atm and 1.27 between 20 and 30 atm, at 1200K. The 2nd order kinetics determined in the present work,

at partial pressures of hydrogen up to 1 atm, support these views.

In contrast, the gasification of carbon by steam was found to be of zero order (Cf. section 3.3). The rates of gasification were sufficiently high to yield a partial pressure of hydrogen capable of maintaining the nickel in the reduced state. The metal may then act as a dissociation centre for steam:



with the water gas-shift equilibrium well displaced towards carbon dioxide production. The reaction between adsorbed oxygen and carbon can only occur at the Ni-C interface. Therefore, mobility of the metal particles is expected, and has been observed in the course of several studies (171, 172).

It is interesting to find that a mechanism of gasification by steam involving diffusion of carbon in the nickel is also capable of explaining the rates measured in the present work. If the nickel particles are saturated with carbon (and this has been assumed when discussing carbon formation) then a concentration gradient may be set up when reaction with steam, assumed to be fast, depletes the exposed surface. If diffusion in the nickel is the slow step, all carbon which arrives at the surface will react quickly and we have:

$$\text{rate} = DS/L \text{ (diffusion of C in Ni)}$$

$$S(650^\circ\text{C}) = 5.37 \times 10^{-3} \text{ g/cm}^3$$

$$D(650^{\circ}\text{C}) = 1.27 \times 10^{-9} \text{ cm}^2/\text{sec}$$

$$L = 7 \times 10^{-6} \text{ cm}$$

$$\text{rate (C diffusion)} = 0.975 \text{ } \mu\text{g}/\text{sec. cm}^2$$

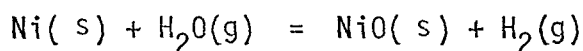
The measured rate constant for burn-off was $k_f(\text{H}_2\text{O}, 650^{\circ}\text{C}) = 40.8 \times 10^{-3} \text{ min}^{-1} \cdot \text{cm}^{-2}$, based on the geometric area of the foil ($\approx 3\text{cm}^2$). From the previous discussions, where it was found that the nickel area of carbon deposits was $0.16\text{m}^2/\text{g}$, the value must be corrected as $\text{rate (burn-off)} = 3 \times 40.8 \times 10^{-3} / (60 \times 1.6) \text{ mg}/\text{cm}^2 \cdot \text{sec} = 1.28 \text{ } \mu\text{g}/\text{cm}^2 \cdot \text{sec}$ which is indeed in good agreement with predictions from carbon diffusion.

If this is so, then zero order kinetics are expected. A similar mechanism has been proposed to explain the oxidation of carbon at the surface of polycrystalline nickel in the range 300 to 800K (173). In the case of hydrogen gasification, the reaction step is too slow and controls the process.

4.3 STEAM-REFORMING

Carbon formation was found to accompany the steam-reforming of propylene over most catalysts studied. The general features of the deposition were very similar to those observed in the absence of steam. Thus, at low temperatures ($< 800 \text{ K}$), carbon formation increased with temperature with an activation energy of about 30 kcal/mole. The observed rates of deposition were reduced in the presence of steam, and hydrogen was found to inhibit carbon deposition at 400-450 $^{\circ}\text{C}$. Above 800K, carbon deposition decreased as temperature was increased ($E_a = -43 \pm 3 \text{ kcal/mole}$ over Ni foil) and orders of +1 in propylene and -1 in steam were determined.

Hydrogen also had a positive effect on carbon deposition: On nickel foil, first order kinetics (in H_2) were measured, while on the supported catalyst the effect of hydrogen could be measured by an experimental order of +0.3 or +0.4. However, severe deactivation occurred in the absence of hydrogen, and very small rates of deposition were recorded. This last effect was mostly apparent in the series of runs summarized in Table 3.31, since the small loads of catalyst (15-17 mg) used and the lower pressures of propylene were bound to produce very little hydrogen by steam-reforming. On the other hand, the experiments of Table 3.32 were only slightly affected by the absence of hydrogen in the feed, and deactivation only occurred after considerable coke build-up. In this case, larger catalyst loads ($\approx 53\text{mg}$) and higher propylene pressures assured the production of relatively large amounts of hydrogen. Therefore, it is most probable that the deactivation effect is a result of catalyst oxidation by steam:



At 600°C , the equilibrium constant for the reaction is 8.5×10^{-3} (53). Therefore, when $(\text{H}_2\text{O})/(\text{H}_2) > 117$ oxidation may occur.

This explanation is supported by the results of run 246 (Cf. Table 3.31). Although the effluent gas was not analysed, comparison with steam reforming experiments (Tables 3.32 and 3.33) permits the calculation of the hydrogen produced by reaction of propylene with steam, showing that a partial pressure of hydrogen close to 0.002 atm would be established. The ratio of water to hydrogen would then exceed 117 and oxidation of the catalyst

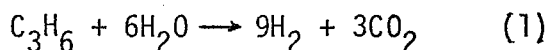
became possible.

Over nickel foils, a first order dependency on the hydrogen pressure was expected, by comparison with carbon formation from propylene pyrolysis in the absence of steam. Possible reasons for this effect were discussed in section 4.1.1. On the other hand, pyrolysis over supported catalysts was indifferent to the presence or absence of hydrogen, but the fractional order measured in the presence of steam can still be explained on kinetic grounds: In fact, the presence of hydrogen must certainly affect the adsorption equilibrium of water.

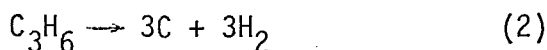
The rates of carbon formation under steam-reforming conditions were found to decrease as temperature increased (above 550°C) so that the selectivity towards steam-reforming products was improved at higher temperatures. With the alkalis catalyst, carbon formation was prevented in the presence of excess steam ($H_2O : C_3H_6 \geq 4$), although carbon formation from pyrolysis (i.e. in the absence of steam) was not inhibited at all. This is as a result of the catalytic effect of alkali in carbon gasification by steam (rates of burn-off over catalyst 46-1 being 50% higher than with catalyst nickel-alumina) and also, possibly, of the enhanced adsorption of water on the alkalis catalyst. With lower steam-ratios, however, carbonisation occurred. After several reaction cycles with the same catalyst sample, carbon formation became progressively easier, possibly as a result of loss of alkali.

The kinetic results obtained in the steam-reforming reaction may now be examined. The main products of the reaction were found to be hydrogen, carbon dioxide and carbon monoxide. Methane was also detected, but in negligible amounts, and the amount of

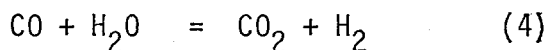
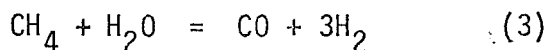
carbon dioxide was in general much higher than CO. The steam-reforming reaction at 600°C could then be expressed as



with accompanying carbon formation



It is known that the products of steam-reforming react in the gas-phase between themselves and steam (1), so that the final product gas mixture has a composition that can be approximately determined by the two equilibria:

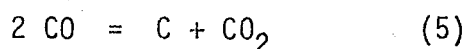


Equilibrium calculations are shown in the Appendix for the steam-reforming of propylene according to the scheme (1), at various conversion levels. The unreacted propylene is treated as an inert, and carbon formation is considered absent.

These calculations predict that, under the experimental conditions used (i.e. high temperature, excess steam and low conversions), no methane will be produced. Therefore, at low conversions, reaction (3) can be neglected. The experimental results show that, although very small, some methane is produced, but this occurs even in the absence of steam (Cf. section 3.2.2). It is probable that this methane results from the pyrolysis of propylene or from interaction of carbon with hydrogen. It is also interesting to note that the amount of CO produced is higher than the equilibrium composition. Therefore, it may be assumed

that both CO and CO₂ are primary products of the reaction, in agreement with the findings of Akers et al (50).

On the other hand, the amounts of hydrogen and carbon dioxide produced are accurately predicted by the equilibrium calculations, as shown in Fig.4.6. It is also to be noted that the ratio (CO₂)/(CO)² was, in practice, usually higher than the equilibrium constant for the Boudouard reaction:



Therefore, thermodynamics predict that no carbon can coexist in equilibrium with the product gases. The experimental fact that carbon is formed shows that carbon forming reactions are faster than carbon gasification.

The experimentally determined order of reaction in propylene (0.6) suggests that surface reaction may be the rate determining step. The results were analysed using Langmuir-Hinshelwood models, taking surface reaction as the slow step. Since excess steam was always used, a zero order dependency in water is expected, as observed. Therefore, the adsorption coefficient of water cannot be determined, and a 3 parameter model was used to test the data:

$$\text{rate} = \frac{a \cdot P_p}{1 + b \cdot P_p} \cdot \exp(-E/RT)$$

where P_p = propylene partial pressure. The associative adsorption of propylene is implicit in this equation; dissociative adsorption was not considered, since a reaction order in the range 0-0.5 would then be expected.

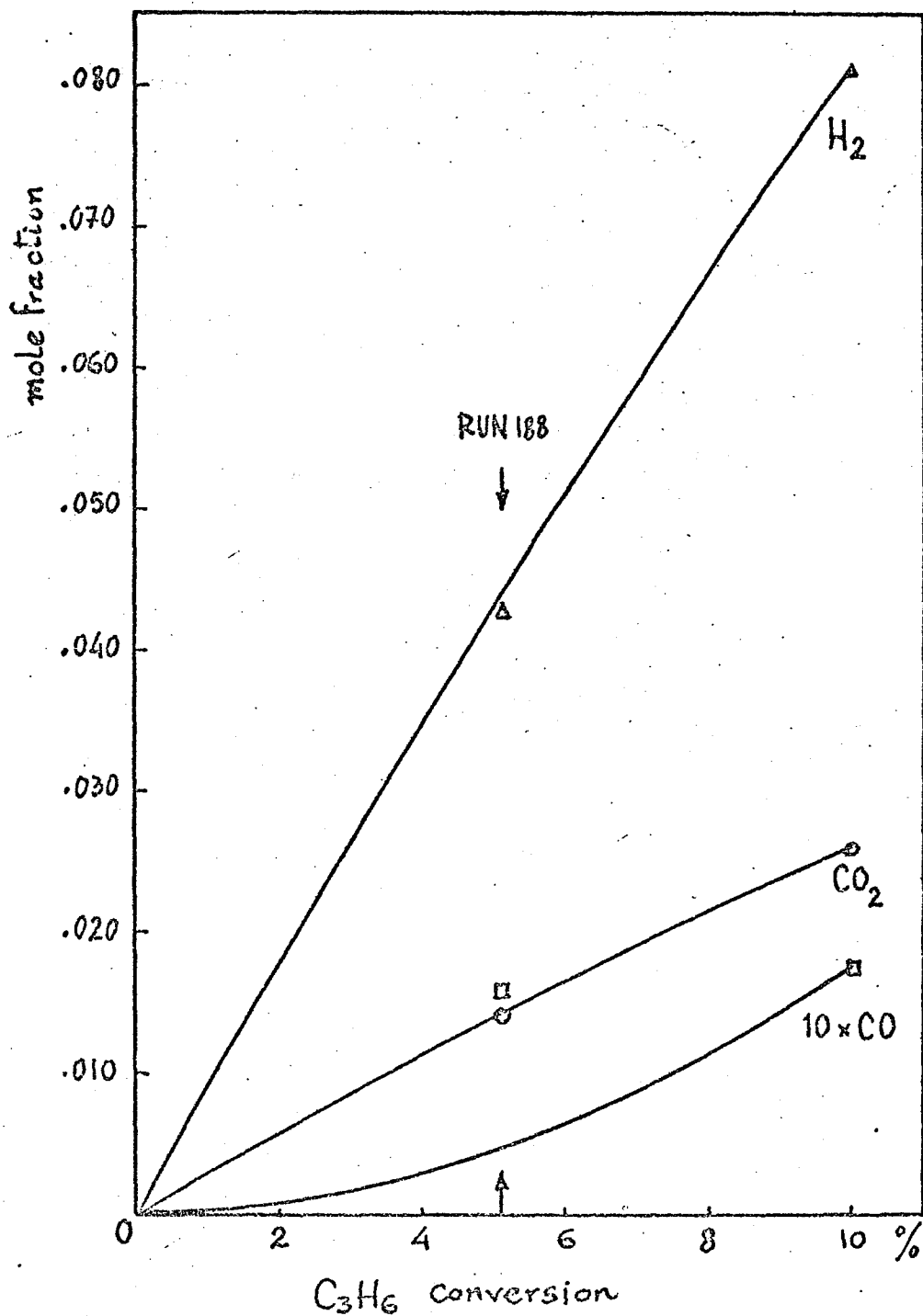


Fig. 4.6 Steam-reforming of propylene.

Equilibrium compositions & run 188.

The above model was found to fit the experimental data obtained with the nickel-alumina catalyst with an average deviation of 6%, and the following rate equation was determined:

$$R_p^1 = 6.45 \times 10^3 \times \frac{P_p}{1 + 7.71 P_p} \cdot \exp\left(-\frac{15500}{RT}\right)$$

Discrimination between different kinetic models (for example, between competitive adsorption of propylene and steam and adsorption on different sites) would only be possible with an extended range of partial pressures, outside the scope of the present work. However, the evidence presented in the literature survey (section 1.2.5.2.) favours the adsorption of steam and propylene on different sites.

The reaction model discussed by Rostrup-Nielsen (Cf. section 1.2.5.2 and ref.26), based on the mechanisms of hydro-genolysis, was also tested but did not correlate the data well.

Studies of propylene steam-reforming on nickel films were reported recently (42). Reaction orders of 0.75 and 0.6 for propylene and water, respectively, were determined, and the activation energy was 15 kcal/mole. A different steam dependency is expected; since the type of support is of paramount importance in determining water adsorption (26); the other parameters are in reasonable agreement with the present results.

CONCLUSIONS

1. Carbon formation from propylene on nickel catalysts was found to occur for extended periods of time without any significant effect on the activity of the catalyst. Nickel particles were found in the deposits and these deposits were active for further carbon formation when separated from the original catalyst. Poisoning of the nickel with sulphur compounds completely suppressed carbon formation.
2. Detailed studies carried out with nickel foils in the range 650-1050 K have shown a complex temperature dependency of deposition rates. Below 800 K, rates of deposition followed zero order kinetics, with an activation energy of 33.3 ± 4 kcal/mole. Above about 800 K, the rates of deposition decreased as temperature was increased and the reaction became of 2nd order overall; the maximum in the rate of carbon formation was found to move to higher temperatures when the reactant pressures were increased. At still higher temperatures (above 920 K) gas phase reactions became important and the rates increased again with temperature.
3. The effect of hydrogen on carbon formation was dependent on the temperature range, but it always increased the rate of deposition. Above 800 K, deactivation was observed when the hydrogen pressure was low, and deposition was prevented in the absence of hydrogen. These results were explained in terms of encapsulation of the nickel. Below 800 K, lower rates, limited deposition and induction periods were observed without hydrogen.

4. The kinetic features of the deposition were explained in terms of a model involving the diffusion of carbon in nickel. Below 800 K, this may be the rate determining step. Carbon species formed on the nickel surface enter the lattice and diffuse to the rear of the particle, where segregation of graphite occurs. The model is consistent with the formation of a nickel carbide at the exposed face of the particle. Above 800 K, the results are consistent with a surface reaction controlling the process. The decrease in rates at higher temperatures cannot result from carbon gasification and was explained in terms of decreased adsorbed. The observed "negative activation energy" (-40 kcal/mole) would then include the heats of adsorption of hydrogen and propylene.

5. Comparison of pure nickel foils with supported catalysts shows that the support material has no influence on the kinetics, and the rates of deposition correlate well with the initial area of nickel available. Hydrogen did not affect the process of carbon formation on supported catalysts and induction periods were never observed. Alternative explanations are discussed.

6. The kinetics of carbon gasification, by steam and by hydrogen, were determined. The reaction was nickel catalysed, and could be suppressed by sulphur poisoning.

7. With nickel foils, an interesting dependency of gasification rates on the initial amount of carbon was observed. This was attributed to the presence of nickel particles lifted from the foil

during deposition of carbon. Conventional analysis has confirmed this assumption, and the presence of nickel in constant concentration was determined. Gasification rates were then compared with results obtained with supported catalysts. The metal surface area of carbons obtained on nickel foils could then be calculated, and was found to be $0.16 \text{ m}^2/\text{g}$; the nickel content was $1.6 \pm 0.4 \text{ wt } \%$, and the average size of the nickel particles was estimated as 70 nm. The specific surface area of the carbon itself was found to remain unchanged by gasification.

8. The measured rates of gasification by steam could also be explained by a mechanism controlled by diffusion of carbon in the nickel. Gasification by hydrogen was found to be a 2nd order reaction, possibly involving a spill-over phenomenon.

9. The steam-reforming reaction was in general accompanied by carbon deposition on the catalyst, except when an alkali was present together with excess steam. The major gaseous products were hydrogen and carbon dioxide. The absence of significant catalyst deactivation on coking was explained in terms of the proposed mechanism for carbon formation: - If carbon diffuses in the nickel, then a clean surface will be always available for reaction.

10. The steam-reforming reaction showed an order of 0.6 in propylene, suggesting surface reaction control involving associative adsorption of propylene. Water was probably adsorbed on different sites, although no definite conclusion can be drawn from the

present work. The systematic use of excess steam does not allow for a possible discrimination among different models.

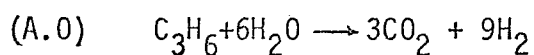
11. The microbalance flow reactor used in this investigation proved to be a powerful tool for the accurate determination of kinetic data in reactions involving the formation (or consumption) of solids over a catalyst. These advantages were best exploited when using metal foils; supported catalysts were too active and diffusion limitations were encountered, possibly as a result of channelling around the catalyst. A possible way of improving the system could involve the use of the microbalance in association with a stirred tank reactor.

A P P E N D I C E S

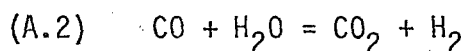
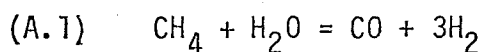
A P P E N D I X A

Calculation of the equilibrium product composition of propylene
steam-reforming at low conversions

It is assumed that propylene reacts initially with water vapour producing hydrogen and carbon dioxide:



The following equilibria are then established:



the equilibrium constants of which can be found in the literature (1).

Let:

AM = Propylene % conversion in reaction (A.0)

X1 = No. of moles of CO produced by reaction (A.1)

X2 = No. of moles of CO consumed by reaction (A.2)

a = $H_2O : C_3H_6$ feed ratio

b = $N_2 : C_3H_6$ feed ratio

K1 = equilibrium constant for (A.1)

K2 = equilibrium constant for (A.2)

Basis: 1 mole C_3H_6 initially, 1 atm. At equilibrium, and assuming that no carbon is present:

$$\begin{aligned}
 \text{Moles } C_3H_6 & : 1 - 0.01 AM \\
 \text{Moles } H_2O & : a - 0.06 AM - X1 - X2 \\
 \text{Moles } CO_2 & : 0.03 AM + X2 \\
 \text{Moles } CO^2 & : X1 - X2 \\
 \text{Moles } N_2 & : b \\
 \text{Moles } H_2 & : 0.09 AM + 3.X1 + X2 \\
 \text{Moles } CH_4 & : -X1
 \end{aligned}$$

$$\text{Total} : 1 + a + b + 2X1 + 0.05 AM$$

The equilibrium constants for (A.1) and (A.2) may then be expressed as:

$$K1 = \frac{(X1 - X2) (0.09AM + 3X1 + X2)^3}{(-X1) (a - 0.06AM - X1 - X2) (1 + a + b + 2X1 + 0.05AM)^2}$$

$$K2 = \frac{(0.03AM + X2) (0.09 AM + 3X1 + X2)}{(X1 - X2) (a - 0.06AM - X1 - X2)}$$

These equations were solved for X1 and X2 for propylene conversions of 1-10%, the feed composition being taken as in Run 188 : a = 5.66, b = 3.68. The results, at temperatures of 600, 620 and 640°C, are presented in Tables A.1 - A.3.

The hypothesis that no carbon is present at equilibrium may then be tested by considering the carbon forming reactions

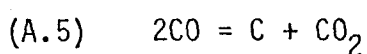
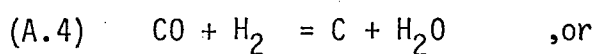
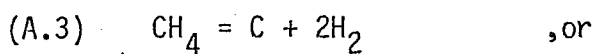


TABLE A.1 PROPYLENE STEAM-REFORMING AT 873 K . EQUILIBRIUM COMPOSITION, MOLE FRACTION

AM	X1	X2	C3H6	N2	H2O	H2	CO2	CO	CH4
1.0	-.00000	-.00019	.09528	.35419	.53560	.00864	.00287	.00002	.00000
2.0	-.00000	-.00076	.09387	.35249	.53072	.01717	.00567	.00007	.00000
3.0	-.00000	-.00171	.09247	.35081	.52257	.02558	.00842	.00016	.00000
4.0	-.00000	-.00305	.09108	.34915	.51452	.03387	.01110	.00029	.00000
5.0	-.00000	-.00477	.08971	.34750	.50659	.04204	.01371	.00045	.00000
6.0	-.00000	-.00689	.08835	.34586	.49877	.05010	.01627	.00065	.00000
7.0	-.00001	-.00939	.08700	.34425	.49106	.05805	.01877	.00088	.00000
8.0	-.00001	-.01230	.08566	.34265	.48346	.06589	.02120	.00114	.00000
9.0	-.00063	-.01560	.08434	.34106	.47596	.07362	.02358	.00144	.00000
10.0	-.00304	-.01930	.08303	.33949	.46858	.08123	.02589	.00178	.00000

TABLE A.2 PROPYLENE STEAM-REFORMING AT 893 K . EQUILIBRIUM COMPOSITION, MOLE FRACTION

AM	X1	X2	C3H6	N2	H2O	H2	CO2	CO	CH4
1.0	-.00000	-.00067	.09528	.35419	.53504	.00860	.00282	.00006	.00000
2.0	-.00000	-.00085	.09387	.35249	.53073	.01716	.00567	.00008	.00000
3.0	-.00000	-.00191	.09247	.35081	.52258	.02556	.00840	.00018	.00000
4.0	-.00000	-.00339	.09108	.34915	.51455	.03383	.01106	.00032	.00000
5.0	-.00000	-.00531	.08971	.34750	.50664	.04199	.01366	.00050	.00000
6.0	-.00000	-.00765	.08835	.34586	.49884	.05003	.01620	.00072	.00000
7.0	-.00000	-.01043	.08700	.34425	.49115	.05796	.01867	.00098	.00000
8.0	-.00001	-.01364	.08566	.34264	.48358	.06577	.02108	.00127	.00000
9.0	-.00001	-.01728	.08434	.34106	.47612	.07346	.02342	.00160	.00000
10.0	-.00002	-.02135	.08303	.33948	.46876	.08105	.02571	.00197	.00000

TABLE A.3 PROPYLENE STEAM-REFORMING AT 913 K . EQUILIBRIUM COMPOSITION, MOLE FRACTION

AM	X1	X2	C3H6	N2	H2O	H2	CO2	CO	CH4
1.0	-.00000	-.00024	.09528	.35419	.53500	.00864	.00286	.00002	.00000
2.0	-.00000	-.00094	.09387	.35249	.53074	.01715	.00566	.00009	.00000
3.0	-.00000	-.00211	.09247	.35081	.52260	.02554	.00838	.00020	.00000
4.0	-.00000	-.00376	.09108	.34915	.51459	.03380	.01103	.00036	.00000
5.0	-.00000	-.00587	.08971	.34750	.50669	.04194	.01361	.00055	.00000
6.0	-.00000	-.00846	.08835	.34586	.49892	.04996	.01612	.00079	.00000
7.0	-.00000	-.01151	.08700	.34425	.49126	.05786	.01857	.00108	.00000
8.0	-.00000	-.01504	.08566	.34264	.48371	.06564	.02095	.00140	.00000
9.0	-.00001	-.01903	.08434	.34106	.47628	.07330	.02326	.00176	.00000
10.0	-.00001	-.02349	.08303	.33948	.46896	.08086	.02551	.00217	.00000

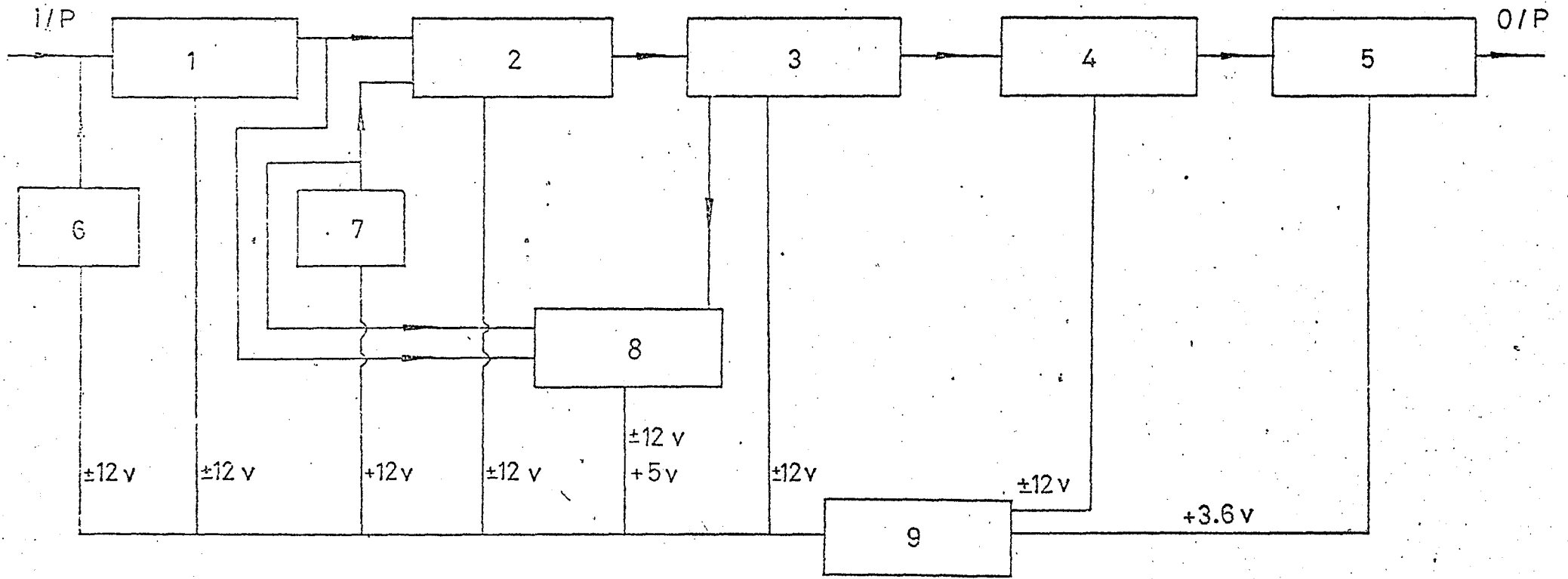
For freedom from carbon

$$P(\text{H}_2)^2/P(\text{CH}_4) > K_3$$

$$P(\text{H}_2\text{O})/P(\text{CO}) \cdot P(\text{H}_2) > K_4$$

$$P(\text{CO}_2)/P(\text{CO})^2 > K_5$$

and these conditions are satisfied for the feed composition considered, i.e. the actual steam-ratio is higher than the thermodynamic minimum.



APPENDIX B. Block diagram of the three term temperature controller

Key to Appendix B

Component	Description
1	Preamplifier
2	Difference Amplifier Proportional Band Adjustment
3	Three Term Amplifier
4	Voltage to Frequency Converter
5	Output Control Logic
6	Ambient Compensation
7	Temperature Setting
8	Indicator
9	Power Supply

REFERENCES

1. "Catalyst Handbook" - Wolfe Scientific Books (1970)
2. Maxted, E.B., Adv.Catal.3, 129 (1951)
3. Williams, A., Butler, G., Hammonds, J., J.Catal.24, 352 (1972)
4. Ruckenstein, E., Pulvermacher, B., A.I.Ch.E.J. 19, 356 (1973)
5. Schlaffer, W.G., Morgan, C.Z., Wilson, J.N., J.Phys.Chem 61, 714 (1957)
6. Wheeler, A., Adv.Catal. 3, 249 (1951)
7. Levenspiel, O., "Chemical Reaction Engineering" 2nd Ed., John Wiley (1972)
8. Satterfield, C.N., "Mass Transfer in Heterogeneous Catalysts", M.I.T. Press (1970)
9. Petersen, E.E., "Chemical Reaction Analysis" Prentice-Hall (1965)
10. Szepe, S., Levenspiel, O., "Proc. 4th. Eur.Symp. on Chemical Reaction Engineering" Brussels, 1968. Pergamon (1971)
11. Masamune, S., Smith, J.M., A.I.Ch.E.J. 12, 384 (1966)
12. Sagara, M., Masamune, S., Smith, J.M., A.I.Ch.E.J. 13 1226 (1967)
13. Murakami, Y., Kobayashi, T., Hattori, T., Masuda, M., Ind. Eng.Chem. Fund. 7, 599 (1968)
14. Richardson, J.T., Ind.Eng.Chem.Proc.Des.Dev. 11, 8 (1972)

15. Ozawa, Y., Bischoff, K.B., Ind.Eng.Chem.Proc.Des.Dev. 7, 67 (1968)
16. Rostrup-Nielsen, J.R., J.Catal., 33, 184 (1974)
17. Levenspiel, O., J. Catal., 25, 265 (1972)
18. Khang, S.J., Levenspiel, O., Ind.Eng.Chem.Fund. 12, 185 (1973)
19. Weisz, P.B., Goodwin, R.D., J.Catal., 2, 397 (1963)
20. Thomas, C.L., "Catalytic Processes and Proven Catalysts", Academic Press (1970)
21. Bridger, G.W., Wyrwas, W., Chem.Proc.Eng. 48, 101 (1967)
22. Hougen, O.A., Watson, K.M., Ragatz R.A.,
"Chemical Process Principles" Vol.II, 2nd Ed.
John Wiley (1959)
23. Lihou, D.A., Chem.Proc.Eng. 46, 487 (1965)
24. Rogers, M.C.F., Crooks, W.M., J.Appl.Chem. 16, 253 (1966)
25. Hebden, D., Percival, G., Inst. Gas Eng.J. p.229 August (1972)
26. Rostrup-Nielsen, J.R., J.Catal.31, 173 (1973)
27. Dowden, D.A., Schnell, C.R., Walker, G.T. Preprint, 4th Int.Congr.Cat., Moscow (1968)
28. Dowden, D.A., Chem.Eng.Progr.Symp. 63 (no.73) 90 (1967)
29. Andrew, S.P.S., Ind.Eng.Chem.Prod.Res.Dev. 8, 321 (1969)
30. Kearby, K.K., Ind.Eng.Chem. 42, 295 (1950)

31. Nicklin, T., Farrington, F., Burgess, K.H. Inst.Gas Eng.J. 8, 473 (1968)
32. Nicklin, T., Whittaker, R.J., Inst. Gas Eng.J. 8, 15 (1968)
33. Nicklin, T., Farrington, F., Whittaker, R.J. Inst. Gas Eng., 35th Autumn Research Meeting, London, November (1969)
34. Bhatta, K.S.M., Dixon, G.M., Ind.Eng.Chem.Prod.Res.Dev. 8,324 (1969)
35. Macak, J., Licka, S., Malecha, J., Chim.Ind.Genie Chim. 105, 517 (1972)
36. Bhatta, K.S.M., Dixon, G.M. Trans.Far.Soc. 63, 2217 (1967)
37. Igarashi, A., Muroi, K., Kato, A., Ogino, Y. Bull.Japan Petrol.Inst. 13, 221 (1971)
38. Brooks, C.S., Adv.Chem.102, 426 (1971)
39. Rostrup-Nielsen, J.R., J.Catal. 11, 220 (1968)
40. McCarroll, J.J., Edmonds, T., Pitkethly, R.C. Nature, 223, 1260 (1969)
41. Rostrup-Nielsen, J.R., J.Catal.21, 171 (1971)
42. Moayeri, M., Ph.D.Thesis, London Univ. (1974)
43. Moseley F., Stephens, R.W., Stewart, K.D., Wood, J. J. Catal. 24, 18 (1972)
44. Saito, M., Tokuno, M., Morita, Y. Kogyo Kagaku Zasshi, 74, 693 (1971)
45. Saito, M., Tokuno, M., Morita, Y. Kogyo Kagaku Zasshi, 74, 687 (1971)
46. Lobo, L.S., Ph.D.Thesis, London Univ. (1971)

47. Gordon, A.S., *Ind.Eng.Chem.* 44, 1857 (1952)
48. Bodrov, I.M., Apel'baum, L.O., Temkin, M.I., *Kinetics & Catalysis* 5, 614 (1964)
49. Kemball, C., *Proc.Roy.Soc. A* 207, 539 (1951)
50. Akers, W.W., Camp.D.P., *A.I.Ch.E.J.* 1, 471 (1955)
51. Bodrov, I.M., Apel'baum, L.O., Temkin, M.I. *Kinetics & Catalysis*, 8, 696 (1967)
52. Bodrov, I.M., Apel'baum, L.O., Temkin, M.I. *Kinetics & Catalysis*, 9, 877 (1968)
53. Ross, J.R.H., Steel, M.C.F., *J.Chem.Soc.Faraday Trans.I* 69, 101 (1973)
54. Ross, J.R.H., Private communication
55. Takemura, Y., Yamamoto, K., Morita, Y., *Int.Chem.Eng.* 7, 737 (1967)
56. Balashova, S.A., Slovokhotova, T.A., Balandin, A.A. *Kinetics & Catalysis* 7, 273 (1966)
57. Lavrov, N.V., Petrenko, I.G., *Proc.Acad.Sci (U.S.S.R.) Chem.Sect.* 158, 938 (1964)
58. Schnell, C.R., *J. Chem.Soc.(B)* 158 (1970)
59. Phillips, T.R., Mulhall, J., Turner, G. *J.Catal.* 15, 233 (1969)
60. Phillips, T.R., Yarwood, T.A., Mulhall, J., Turner, G.E., *J.Catal.* 17, 28 (1970)
61. Appleby W.G., Avery, W.H., Meerbott, W.K., *J.Am.Chem.Soc.* 69, 2279 (1947)

62. Boudart, M., A.I.Ch.E.J. 18, 465 (1972)
63. Walker, P.L., Jr., Rusinko, F., Jr., Austin, L.G., Adv. Catal. 11 133 (1959)
64. Ergun, S., Mentser, M., Chemistry and Physics of Carbon Vol.1, p.203 (P.L. Walker Jr., Ed.) Dekker, N.Y. (1966)
65. Batchelder, H.R., Busche, R.M., Armstrong, W.P., Ind. Eng.Chem. 45, 1856 (1953)
66. Fredersdorff, C.G., Inst.Gas Techn. Res. Bull. no.19 (1955)
67. Johnstone, H.F., Chen, C.Y., Scott, D.S. Ind. Eng. Chem. 44, 1564 (1952)
68. Gadsby, J., Hinshelwood, C.N., Sykes, K.W. Proc.Roy.Soc. A187, 129 (1946)
69. Zielke, C.W., Gorin, E., Ind.Eng.Chem. 47, 820 (1955)
70. Walker, P.L., Jr., Shelef, M., Anderson, R.A., Chemistry and Physics of Carbon, Vol.4, p.287 (P.L. Walker Jr., Ed.) Dekker, N.Y., (1968)
71. Tuddenham, W.M., Hill, G.R., Ind.Eng.Chem. 47, 2129 (1955)
72. Heuchamps, C., Duval, X., Letort, M., Compt. Rend., 260, 1160/1657 (1965)
73. Walker, P.L., Jr., Austin, L.G., Tietjen, J.J. Chemistry and Physics of Carbon, Vol.1 p.327, (P.L. Walker Jr., Ed.) Dekker, N.Y. (1966)
74. Vastola, F.J., Walker, P.L. Jr., J.Chim.Phys., 58, 20 (1961)
75. Gilliland, E.R., Harriott, P., Ind.Eng.Chem. 46, 2195 (1954)
76. Tomita, A., Tamai, Y., J.Catal., 27, 293 (1972)

77. Tomita, A., Sato, N., Tamai, Y., Carbon, 12, 143 (1974)
78. Boudart, M., Aldag, A.W., Vannice, M.A., J.Catal., 18, 46 (1970)
79. Germain, J.E. "Catalytic Conversion of Hydrocarbons" Academic Press (1969)
80. Parks G.S., Huffman, H.M. "Free Energy of Some Organic Compounds" Reinhold (1932)
81. Rostrup-Nielsen, J.R., J.Catal. 27, 343 (1972)
82. Lecoanet, A., Thèse de l'Université de Paris (1968)
83. Dent, F.J., Moignard, L.A., Eastwood, A.H., Blackburn, W.H., Hebden, D., Trans.Inst.Gas Eng. p.602 (1945-1946)
84. Ergun, S., Carbon 6, 141 (1968)
85. Ruland, W., Chemistry and Physics of Carbon, vol.4, p.1 (P.L. Walker Jr., Ed.) Dekker, N.Y. (1968)
86. Biscoe J., Warren, B.E., J.Appl.Phys. 13, 364 (1942)
87. Ergun, S., Chemistry and Physics of Carbon, Vol.3, p.211 (P.L. Walker Jr., Ed.) Dekker, N.Y. (1968)
88. Bokros, J.C., Chemistry and Physics of Carbon, Vol.5, p.1, (P.L. Waler Jr. Ed) Dekker, N.Y. (1969)
89. Palmer, H., Cullis, C.F., Chemistry and Physics of Carbon, Vol.1, p.266, (P.L. Walker Jr., Ed.) Dekker, N.Y., (1965)
90. Banerjee, B.C., Hirt, T.J., Walker, P.L. Jr., Nature 192 450 (1961)
91. Cullis, C.F., Presland, A., Read, I., Trimm, D., 2nd. Ind. Carbon and Graphite Conf., London (1965)

92. Walker, P.L., Jr., Rakszawski, J.F., Imperial, G.R.,
J. Phys. Chem., 63, 133 (1959)
93. Presland, A., Roscoe, C., Walker, P.L., Jr., 3rd Ind. Carbon
and Graphite Conf. London (1970) p.116
94. Blau, G., Presland, A., *ibid.*, p.121
95. Presland, A., Walker, P.L., Jr., Carbon 7, 1 (1969)
96. Robertson, S.D., Nature, 221, 1044 (1969)
97. Baird, T., Fryer, J.R., Grant, B., Carbon 12, 591 (1974)
98. Baker, R., Feates, F., Harris, P., Carbon 10, 93 (1972)
99. Derbyshire, F.J., Ph.D. Thesis, Univ. London (1974)
100. Moayeri, M., M.Sc. Thesis, Univ. London (1970)
101. Derbyshire, F.J., Trimm, D.L., 4th London Int. Carbon and
Graphite Conf. (1974)
102. Baird, T., Fryer, J., Grant, B., Nature 233 329 (1971)
- 103. Robertson, S.D., Carbon, 8, 365 (1970)
104. Robertson, S.D., Carbon, 10, 221 (1972)
105. Baker, R., Barber, M., Harris, P., Feates, F., Waite, R.,
J. Catal. 26, 51 (1972)
106. Hofer, L., Sterling, E., McCartney, J., J. Phys. Chem. 59,
1153 (1955)
107. Ruston, W., Warzee, M., Hennaut, J., Waty, J., Carbon 7,
47 (1969)
108. Tesner, P., Robinovich, E., Rafalkes, I., Arefieva, E.,
Carbon 8, 435 (1970)

109. Renshaw, G., Roscoe, C., Walker, P. L., Jr., J. Catal. 18
164 (1970)
110. Renshaw, G., Roscoe, C., Walker, P. L., Jr., J. Catal. 22
394 (1971)
111. Fryer, J., Paal, Z., Carbon, 11, 665 (1973)
112. Baker, R., Harris, P., Thomas, R., Waite, R., J. Catal. 30,
86 (1973)
113. Tamai, Y., Nishiyama, Y., Takahashi, M., Carbon 6, 593
(1968)
114. Tamai, Y., Nishiyama, Y., Takahashi, M., Carbon 7, 209
(1969)
115. Hofer, L., Catalysis Vol. 4, P.373 (P. H. Emmett, Ed.)
Reinhold (1956)
116. Anderson, R. B., Catalysis Vol. 4, P.29 (P. H. Emmett, ed.)
Reinhold (1956)
117. Davis, W. R., Slawson, R. J., Rigby, G. R. Nature 171, 756
(1953)
118. Leidheiser, H., Gwathmey, A., J.Am.Chem.Soc., 70. 1206
(1948)
119. Kehrer, V. J., Leidheiser, H., J. Phys. Chem., 58, 550
(1954)
120. Cunningham, R., Gwathmey, A., Adv. Catalysis, 9, 25 (1957)
121. Gwathmey, A., Cunningham, R., Adv. Catalysis, 10, 57 (1958)
122. Somorjai, G., J. Catal. 27, 453 (1972)
123. Grenga, H., Lawless, K., J. Appl. Phys. 43, 1508 (1972)
124. Karu A., Beer, M., J. Appl. Phys. 37, 2179 (1966)
125. Tomita, A., Yoshida, K., Nishiyama, Y., Tamai, Y., Carbon 10
601 (1972)

126. Cimino, A., Parravano, G., J. Phys.Chem. 56, 706 (1952)
127. Lafitau, H., Jacque, L., Bull. Soc.Chim. France, 4779 (1968)
128. Escoubes, M., Quinson, J., Eyraud, C., Bull. Soc.Chim. France, 2435 (1967)
129. Saito, T., Gejyo, T., Carbon 9, 93 (1971)
130. Lobo., L., Trimm, D., Nature 234. 15 (1971)
131. Lobo, L., Trimm, D., Figueiredo, J., 5th. Int. Congr. Catalysis, Palm-Beach (1972)
132. Lobo, Trimm, D., J. Catal. 29, 15 (1973)
133. Lobo, L., 3rd Symp. Iberoamericano Catal. Caracas (1972)
Acta Cientifica Venezolana, 24 (Sup. 2) 219 (1973)
134. Nishiyama, Y., Tamai, Y., J. Catal. 33, 98 (1974)
135. Walker, P. L., Jr., Rakszswaki, J., Imperial, G., J. Phys. Chem. 63, 140 (1959)
136. Haas, L., Khalafalla, S., Weston, P., U.S. Bureau of Mines, Report 7064 (1968)
137. Nagakura, S., J. Phys.Soc. Japan, 12, 482 (1957)
138. Derbyshire, F. J. Presland, A., Trimm, D., Carbon 10, 114 (1972)
139. Slovokhotova, T., Balandin, A., Nazarova, D., Vestn. MGU, No. 5, 193 (1957)
140. Slovokhotova, T., Ivanov, A., Vestn. MGU, No. 2, 125 (1951)

141. Rozhdestvenskii, V., Erofeeva, V. Neftekhimiya, 2, 204 (1965)
142. Greensfelder, B., Voge, H., Ind. Eng.Chem. 37, 514 (1945)
143. Mills, G. A., Steffgen, F. W., Catalysis Reviews, Vol. 8, P. 159 (H. Heinemann, ed.) Marcel Dekker, Inc. (1974)
144. Browning, L. C., Emmett, P. H., J. Am.Chem.Soc. 74, 1680 (1952)
145. Saito, M., Tokuno, M., Amano, I., Morita, Y., Kogyo Kagaku Zasshi, 73, 2405 (1970)
146. Balandin, A. A., Prag, M., Slovokhotova, T. A., Dokl. AN SSSR. 163, 638 (1965)
147. Balashova, S., Slovokhotova, T., Balandin, A., Izv. AN SSSR, Otd. Khim.n., 275 (1965)
148. Patrikeev, V., Odyakov, V., Balandin, A., Zh. Prikl. Khim. (Leningrad) 41, 1063 (1968)
149. Patrikeev, V., Odyakov, V., Sholin, A., Balandin, A., Zh. Prikl. Khim. (Leningrad) 41, 1297 (1968)
150. Lander, J. J., Kern, H. E., Beach, A. L., J. Appl. Phys., 23, 1305 (1952)
151. Pierce, C. J., J. Phys. Chem. 57, 149 (1953)
152. Gregg, S. J. Sing, K.S.W., "Adsorption, Surface Area and Porosity", Academic Press, N.Y. (1967)
153. Melville, H., Gowenlock, B.
"Experimental Methods in Gas Reactions"
MacMillan (1964)

154. Brooks, C. S., Christopher, G. L. M., J. Catal. 10, 211 (1968)
155. Frössling, N., Carlands Beitr. Geophys. 32, 170 (1938)
156. Perry, H. (ed.)
"Chemical Engineers Handbook", 4th Ed.
McGraw Hill Book Company
157. Yang, K. Hougen, O., Chem.Eng. Progr. 46, 146 (1950)
158. Weisz, P. B., Prater, C. D., Adv. Catalysis, 6, 143 (1954)
159. Goring, G., Curran, G., Tarbox, R., Gorin, E., Ind. Eng. Chem. 44, 1051 (1952)
160. Lobo, L. S., Trimm, D. L.
"Progress in Vacuum Microbalance Techniques"
Vo. 2 (S. Bevan, S. Gregg, N. Parkyns, eds.)
Heyden & Son (1973)
161. Hayward, D. L., Trapnell, B.M.W.
"Chemisorption" Butterworths, London (1964)
162. Bond, G. C., "Catalysis by Metals" Academic Press, N.Y. (1962)
163. Zur Strassen, H., Z. Phys.Chem. (Leipzig) A 169, 81 (1934)
164. Boudart, M., Adv. Catalysis, 20, 153 (1969)
165. Fischbach, D. B., "Chemistry and Physics of Carbon"
Vol. 7, P. 1 (P. L. Walker Jr., Ed.) Dekker, N.Y. (1971)
166. Gillot, J., Lux, B., Cornuault, P., du Chaffaut, F.,
Ber. Deut. Keram. Ges., 45, 224 (1968)

167. Diamond, S., Ph.D. Thesis, Univ. Illinois (1965)
168. Hansen, M., "Constitution of Binary Alloys" McGraw-Hill, 2nd. ed. N.Y. (1958)
169. Marsh, H., Rand, B., Carbon 9, 47 (1971)
170. Bernardo, C., Lobo, L., J. Catal., in press.
171. McKee, D. W., Carbon 12, 453 (1974)
172. Thomas, J. M., Chemistry and Physics of Carbon, Vol. 1, (P. L. Walker Jr., Ed.) Dekker, N. Y. (1966)
173. McAllister, J., White, J., J. Phys. Chem. 76, 968 (1972)